Nonlinear dynamics of lexible structures using corotational beam elements

Thanh Nam Le

Thèse

THESE INSA Rennes
sous le sceau de l'Université européenne de Bretagne
pour obtenir le titre de
DOCTEUR DE L'INSA DE RENNES
Spécialité : Spécialité : Génie Civil (Mécanique des Structures) et le titre de
DOCTOR OF PHILOSOPHY OF KTH STOCKHOLM
Spécialité : Structural Design and Bridges

présentée par
Thanh Nam LE
ECOLE DOCTORALE : *SDLM*
LABORATOIRE : *LGCGM*

Nonlinear dynamics of flexible structures using corotational beam elements

Thèse soutenue le 18.10.2013
devant le jury composé de :

Alain Combescure
Professor, INSA de Lyon (France) / Président
Reijo Kouhia
Professor, Tampere University of Technology (Finland) / Rapporteur
Bassam Izzuddin
Professor, Imperial College of London (UK) / Rapporteur
Ignacio Romero
Professor, Universidad Politécnica de Madrid (Spain) / Rapporteur
Laurent Stainier
Professor, Ecole Centrale de Nantes (France) / Rapporteur
Anna Pandolfi
Associate Professor, Polytecnico di Milano (Italy) / Examinateur
Jean-Marc Battini
Associate Professor, KTH Stockholm (Sweden) / Directeur de thèse
Mohammed Hjiaj
Professor, INSA de Rennes (France) / Directeur de thèse

Nonlinear dynamics of flexible structures using corotational beam elements

Thanh Nam Le

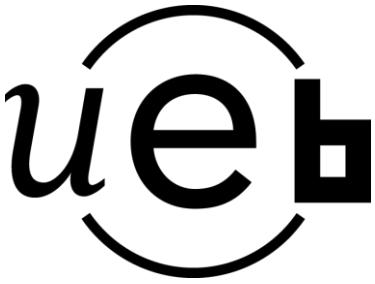

En partenariat avec

ROYAL INSTITUTE
OF TECHNOLOGY

Abstract

The purpose of this thesis is to develop corotational beam elements for the nonlinear dynamic analyse of flexible beam structures. Whereas corotational beam elements in statics are well documented, the derivation of a corotational dynamic formulation is still an issue.

In the first journal paper, an efficient dynamic corotational beam formulation is proposed for 2D analysis. The idea is to adopt the same corotational kinematic description in static and dynamic parts. The main novelty is to use cubic interpolations to derive both inertia terms and internal terms in order to capture correctly all inertia effects. This new formulation is compared with two classic formulations using constant Timoshenko and constant lumped mass matrices.

In the second journal paper, several choices of parametrization and several time stepping methods are compared. To do so, four dynamic formulations are investigated. The corotational method is used to develop expressions of the internal terms, while the dynamic terms are formulated into a total Lagrangian context. Theoretical derivations as well as practical implementations are given in detail. Their numerical accuracy and computational efficiency are then compared. Moreover, four predictors and various possibilities to simplify the tangent inertia matrix are tested.

In the third journal paper, a new consistent beam formulation is developed for 3D analysis. The novelty of the formulation lies in the use of the corotational framework to derive not only the internal force vector and the tangent stiffness matrix but also the inertia force vector and the tangent dynamic matrix. Cubic interpolations are adopted to formulate both inertia and internal local terms. In the derivation of the dynamic terms, an approximation for the local rotations is introduced and a concise expression for the global inertia force vector is obtained. Four numerical examples are considered to assess the performance of the new formulation against two other ones based on linear interpolations.

Finally, in the fourth journal paper, the previous 3D corotational beam element is extended for the nonlinear dynamics of structures with thin-walled cross-section by introducing the warping deformations and the eccentricity of the shear center. This leads to additional terms in the expressions of the inertia force vector and the tangent dynamic matrix. The element has seven degrees of freedom at each node and cubic shape functions are used to interpolate local transversal displacements and axial rotations. The performance of the formulation is assessed through five examples and comparisons with Abaqus 3D-solid analyses.

Keywords: corotational method; nonlinear dynamics; large displacements; finite rotations; time stepping method; thin-walled cross-section; beam element;

Résumé

L'objectif de ce travail de thèse est de développer des éléments poutres 2D et 3D dans le cadre corotationnel pour l'étude du comportement dynamique non-linéaire des structures à barres. Bien que la littérature contienne un certain nombre de références sur les poutres corotationnelles en statique, la formulation d'éléments poutres en dynamique dans un cadre corotationnel rigoureux reste un problème ouvert.

Dans le premier article, nous proposons une formulation corotationnelle robuste et efficace pour l'analyse dynamique non-linéaire des structures à barres planes. La principale nouveauté réside dans l'utilisation de fonctions d'interpolations cubiques à la fois pour la détermination des efforts internes mais aussi des termes d'inertie. En négligeant le carré du déplacement transversal dans le repère local, une expression analytique concise des termes dynamiques est obtenue. Cette nouvelle formulation est comparée aux deux formulations classiques utilisant la matrice masse de Timoshenko ou la matrice diagonale des masses concentrées. On peut souligner la bonne précision des résultats avec un nombre réduit d'éléments.

Le second article traite de la dynamique non-linéaire des poutres 3D pour lesquelles la paramétrisation des rotations finies et les méthodes d'intégration temporelle jouent un rôle important. Une étude bibliographique approfondie sur ces deux aspects, nous conduit à analyser et comparer quatre formulations dynamiques. Pour chacune d'entre elles, l'approche corotationnelle est utilisée pour développer les termes statiques, tandis que les termes dynamiques sont établis dans un contexte lagrangien total avec interpolations linéaires. Les calculs théoriques relatifs aux quatre formulations ainsi que la mise en œuvre pratique des différents algorithmes sont fournis en détail. La précision numérique des calculs et l'efficacité des formulations sont ensuite comparées. D'autre part, quatre prédicteurs et diverses possibilités de simplifier la matrice d'inertie tangente sont testés. La paramétrisation des rotations à l'aide de la partie vectorielle des quaternions est retenue et une simplification de la matrice tangente dynamique est proposée.

Dans le troisième article, une nouvelle formulation corotationnelle cohérente est développée pour l'analyse dynamique de poutre 3D (sans gauchissement). La nouveauté de cette formulation réside dans l'utilisation de la méthode corotationnelle pour établir l'expression non seulement du vecteur des efforts internes, de la matrice de rigidité tangente, mais aussi du vecteur des efforts d'inertie et la matrice d'inertie tangente. Ainsi, les fonctions d'interpolations cubiques sont adoptées pour tous les termes de l'équation de la dynamique. Une approximation des rotations locales est introduite permettant d'établir une expression concise du vecteur force d'inertie. Quatre exemples numériques sont considérés pour évaluer la performance de la nouvelle formulation par rapport à deux autres approches basées sur des interpolations linéaires.

Enfin, dans le quatrième article, l'élément de poutre corotationnel 3D précédent est étendu pour la dynamique non-linéaire des structures avec une section transversale à paroi mince en introduisant les déformations de gauchissement et l'excentricité du centre de cisaillement. Cette cinématique conduit à des termes supplémentaires dans les expressions du vecteur force d'inertie et la matrice d'inertie tangente. L'élément a sept degrés de liberté au niveau de chaque nœud, et les fonctions de forme cubique sont utilisées pour interpoler les déplacements transversaux locaux et les rotations axiales. La performance de la formulation est évaluée à travers cinq exemples et des comparaisons avec des analyses éléments finis 3D réalisées avec le code Abaqus.

Mots-clés : méthode corotationnelle ; dynamique non-linéaire ; grands déplacements ; grandes rotations ; méthode d'intégration temporelles ; section transversale à paroi mince ; élément de poutre ;

Preface

The research presented in this PhD thesis was carried out both at the Division of Structural Engineering and Bridges, Department of Civil and Architectural Engineering, KTH Royal Institute of Technology, SWEDEN and at the Department of Civil Engineering, INSA de Rennes, FRANCE. The project was financed by Region Bretagne (FRANCE) and also by the Division of Structural Engineering and Bridges, KTH.

First of all, I express my gratitude to my supervisors, Associate Professor Jean-Marc Battini (KTH) and Professor Mohammed Hjiaj (INSA de Rennes) for their support, their encouragement, and guidance. I want to thank for their help during the writing of the papers, and of this thesis.

Second, I would especially like to thank Professor Costin Pacoste for valuable discussions during the my period at KTH. Moreover, I would like to thank Professor Raid Karoumi (KTH) for reviewing the manuscript of this thesis.

I also thank my colleagues at the Division of Structure Engineering and Bridges (KTH), and at the Department of Civil Engineering (INSA de Rennes), who facilitated the progress of this work by many useful discussions.

Finally, I am deeply grateful to my parents and my sister for their love and support.

Rennes, August 2013

Thanh-Nam Le

Publications

This thesis is based on the work presented in the following journal papers:

Paper 1: Le, T.-N., Battini, J.-M. and Hjiaj, M., Efficient formulation for dynamics of corotational 2D beams.
Computational Mechanics, 48 (2) : 153-161, 2011.
DOI: 10.1007/s00466-011-0585-6.

Paper 2: Le, T.-N., Battini, J.-M. and Hjiaj, M., Dynamics of 3D beam elements in a corotational context: a comparative study of established and new formulations.
Finite Elements in Analysis and Design, 61 : 97-111, 2012.
DOI: 10.1016/j.finel.2012.06.007.

Paper 3: Le, T.-N., Battini, J.-M. and Hjiaj, M., A consistent 3D corotational beam element for nonlinear dynamic analysis of flexible structures.
Accepted for publication in *Computer Methods in Applied Mechanics and Engineering*, 2013.
DOI: 10.1016/j.cma.2013.11.007.

Paper 4: Le, T.-N., Battini, J.-M. and Hjiaj, M., Corotational formulation for nonlinear dynamics of beams with arbitrary thin-walled cross-sections.
Accepted for publication in *Computers & Structures*, 2013.
DOI: 10.1016/j.compstruc.2013.11.005.

Contents

Abstract i

Résumé iii

Preface v

Publications vii

Contents ix

1 Introduction 1
- 1.1 Background . . . 1
- 1.2 Aims and scope . . . 2
- 1.3 Outline of thesis . . . 3

2 2D corotational beam element 5
- 2.1 Corotational framework . . . 5
- 2.2 Local beam kinematic description . . . 7
- 2.3 Elastic force vector and tangent stiffness matrix . . . 8
- 2.4 Inertia force vector and tangent dynamic matrix . . . 8
- 2.5 Numerical example . . . 10

3 Finite rotations in dynamics 13
- 3.1 Finite rotations . . . 14
- 3.2 Time stepping method for finite rotations . . . 17
- 3.3 Comparison of dynamic formulations . . . 19
- 3.4 Numerical example . . . 20

4 3D corotational beam elements with solid cross-section 23
- 4.1 Beam kinematics . . . 24
- 4.2 Global internal force vector and tangent stiffness matrix . . . 29
- 4.3 Finite rotation parameters . . . 32
- 4.4 Local internal force vector and tangent stiffness matrix . . . 34
- 4.5 Inertia force vector and tangent dynamic matrix . . . 40
- 4.6 Numerical example . . . 41

5 3D corotational beam elements with thin-walled cross-section 45
- 5.1 Kinetic energy . . . 46
- 5.2 Beam kinematics . . . 47
- 5.3 Local beam kinematic description . . . 48
- 5.4 Internal force vector and tangent stiffness matrix . . . 49
- 5.5 Inertia force vector and tangent dynamic matrix . . . 49
- 5.6 Numerical example . . . 51

6 Conclusions and future research **55**
6.1 Conclusions 55
6.2 Future research 57

Bibliography **59**

Paper 1: Efficient formulation for dynamics of corotational 2D beams **63**

Paper 2: Dynamics of 3D beam elements in a corotational context: a comparative study of established and new formulations **81**

Paper 3: A consistent 3D corotational beam element for nonlinear dynamic analysis of flexible structures **115**

Paper 4: Corotational formulation for nonlinear dynamics of beams with arbitrary thin-walled cross-sections **151**

Résumé en français: Eléments de poutre corotationnels pour l'analyse dynamique non-linéaire des structures à barres. **189**

Chapter 1

Introduction

1.1 Background

Flexible beams are used in many applications, for instance large deployable space structures, aircrafts and wind turbines propellers, offshore platforms. These structures often undergo large displacements and finite rotations, but still with small deformations. The simulation of their nonlinear dynamic behavior is usually performed using beam finite elements. A considerable number of beam models related to this attractive topic can be found in the literature and most of these formulations are based on a classic total Lagrangian formulation or a corotational formulation.

The classic total Lagrangian formulation is based on the use of displacement and rotation variables with respect to a fixed inertial frame. Therefore, the kinetic energy takes a simple, quadratic form. This is the main reason why this method is frequently used to develop nonlinear beam models in dynamic analysis (see [52, 54] for 2D case, and [11, 30, 34, 35, 43, 55] for 3D case). However, as mentioned in [34], the nonlinear relations between global displacement and rotation variables and the strain measures introduce a complex definition of the strain energy, even in case of small strains. Furthermore, due to the fact that global displacement and rotation variables are considered, linear interpolations is the unique choice for two-noded beam formulations, which is not accurate, especially for flexible beams.

The corotational approach is also a total Lagrangian formulation, but the idea is to decompose the motion of the element into rigid body and pure deformational parts. During the rigid body motion, a local coordinate system, fixed to the element, moves and rotates with it. The deformational part is measured in this local system. Indeed, this framework has been adopted by several authors to develop efficient beam and shell elements for the nonlinear static and dynamic analysis of flexible structures [9, 14–17, 19, 24, 26, 33, 44, 46, 47, 56]. Moreover, numerous works based on the corotational approach have been carried out in the last decade by the Division of Structural Engineering and Bridges (KTH-Stockholm) and by the Structural Engineering Research Group (INSA de Rennes). Several efficient 2D and 3D beam elements have been developed in order to model large displacements of structures in statics [1, 2, 5, 8, 49]. The structures can have solid or thin-walled cross-section.

The main interest of the corotational method is that with a proper choice of the length of the element, the local displacements are small relative to the local system. Therefore, different assumptions can be made to represent the local deformations, giving rise to different possibilities for the local element formulation.

For the geometrically and materially static nonlinear analysis of beam structures with corotational approach, several local formulations have been proposed by Battini and Pacoste [8], and Alsafadie et al. [1]. The results of a comparative study of 3D beam formulations, which can be found in [1], have shown that local beam elements based on cubic interpolations are more efficient and accurate than the ones which employ linear interpolations. However, in dynamics, one has to deal with the inertia terms which by nature are complicate to formulate. This is particularly true in the corotational formulation of Bernoulli-type

beam elements. This difficulty has hampered the development of the corotational approach in nonlinear dynamics. To avoid the consistent derivation of the inertia terms, several routes have been considered.

For 2D dynamic analysis, quite a few authors [44, 46, 56] adopted the constant lumped mass matrix without any attempt to check its accuracy. Iura and Atluri [33] suggested to simply switch to a Timoshenko beam model where the mass matrix is constant and therefore the inertial terms are simple to evaluate. Behdinan et al. [9] proposed a 2D corotational dynamic formulation where cubic interpolations were used to describe the global displacements, which is not consistent with the idea of the corotational method as originally introduced by Nour-Omid and Rankin [45]. For 3D dynamic analysis, Crisfield et al. [14] suggested to use a constant Timoshenko mass matrix along with local cubic interpolations to derive the internal force vector and the corresponding tangent stiffness matrix. As pointed out by Crisfield et al. [14], this combination was not consistent but it provided reasonable results when the number of elements is large enough. Hsiao et al. [24] presented a corotational formulation for the nonlinear analysis of 3D beams. However the corotational framework adopted in [24] is different from the classic one [45]. In fact, to the author's knowledge, there is no general formulation for dynamic corotational beam elements in the literature. Hence, a consistent corotational beam formulation for 2D and 3D nonlinear dynamics is a very interesting topic for further research.

Finally, it must be noted that nonlinear 3D beam elements are not just a simple extension of 2D ones, mainly because of the complex nature of the finite rotations. More specifically, the finite rotations are non-commutative and non-additive. They cannot be treated in the same simple manner as translations and require special update and time stepping procedures. Several possibilities to parameterize the finite rotations can be found in [11, 30, 55]. Each parametrization has advantages and drawbacks, and the choice of an effective approach is still an issue.

1.2 Aims and scope

The main objective of this work is to extend the corotational beam elements in the previous works [1, 2, 5, 8, 49] by considering inertia effect and to investigate nonlinear dynamic behaviors of structures with large displacements. It should be noted that several versions of the corotational method have been proposed in the literature. The one employed in this work has been proposed by Rankin and Nour-Omid [45, 50], and then further developed by Battini and Pacoste [8].

For this purpose, the author first focuses on 2D beam elements. A general 2D corotational dynamic beam element is developed. In order to capture correctly all inertia effects, the local cubic interpolations are adopted not only to obtain the elastic terms but also to derive the inertia terms. Several numerical examples are then implemented to compare the accuracy of the new formulation against two classic formulations using linear Timoshenko mass matrix and linear lumped mass matrix. This work is presented in the first paper [37].

Before extending the previous 2D dynamic beam element to 3D, the parametrization of the finite rotations and their update procedures for nonlinear 3D beam elements are carefully investigated. For that, four dynamic beam formulations derived in a total Lagrangian context together with corotational internal force vectors and tangent stiffness matrices are compared. They are based on three different parameterizations of rotations. The first three formulations are taken from the literature. The last one is new and uses three of the four Euler parameters (quaternion) as rotational variables. For all these approaches, theoretical derivations as well as practical implementations are given in detail. The similarities and differences between them are pointed out. Six numerical examples are then implemented in order to compare these four formulations in terms of numerical accuracy and computational efficiency. Regarding efficiency, several predictors and various possibilities to simplify the tangent inertia matrix are tested. This work is presented in the second paper [38].

The next part of this PhD work concerns 3D corotational dynamic beam formulations. First, a 3D dynamic beam element is developed. The same idea as in case of 2D is used: to derive both internal and inertia

terms, the corotational method and local cubic interpolations are adopted. This approach ensures the consistency of the formulation. A proper approximation for the local rotations is adopted in the derivations of the inertia terms. To enhance the efficiency of the iterative procedure, the less significant term in the tangent dynamic matrix is ignored. Four numerical examples are then analysed with the objective to compare the performances of the new formulation against two other approaches. The first one is similar to the one presented above, but linear local interpolations, instead of cubic ones, are used to derive only the dynamic terms. The purpose is to evaluate the influence of the choice of the local interpolations on the dynamic terms. The second approach is the classic total Lagrangian formulation proposed by Simo and Vu-Quoc [53–55]. This work is presented in the third paper [39].

Finally, the previous 3D beam element is extended to model beams with arbitrary thin-walled open cross-sections. For this purpose, warping deformations and eccentricity of shear center are taken into account. In order to introduce the warping deformations, the kinematic description proposed by Gruttmann et al. [22] is adopted. Consequently, the beam element has seven degrees of freedom at each node. Regarding the static deformational terms, i.e. the internal force vector and tangent stiffness matrix, the corotational beam element developed by Battini and Pacoste [8] is adopted. However, in order to introduce the bending shear deformations, the cubic Hermitian functions are modified as suggested in the Interdependent Interpolation Element (IIE) formulation [51]. Five numerical examples are analysed to evaluate the accuracy of the formulation against Abaqus 3D-solid elements. This work is presented in the fourth paper [40].

1.3 Outline of thesis

This thesis is based on the work and results given in the four appended journal papers. To highlight their contributions and to put them in the context of an overall project, relevant aspects of each paper are summarized in the four following chapters. Moreover, to make this thesis self-contained, additional knowledge is introduced. The organisation of the thesis is as follows

Chapter 2 presents main features of the 2D beam formulation, which was developed in the first paper [37].

Chapter 3 summarizes important aspects which were dealt in the second paper [38].

Chapter 4 presents in detail 3D corotational beam kinematics, derivations of internal force vectors and tangent stiffness matrices for different parameterizations of finite rotations and several local beam elements. This presentation is taken entirely from the work of Battini [5, 6]. Then, the dynamic formulation developed in the third paper [39] is briefly introduced.

Chapter 5 gives a presentation of a corotational formulation for beams with arbitrary thin-walled cross-sections. This formulation was developed in the fourth paper [40].

Chapter 2

2D corotational beam element

The corotational approach is a well known method to derive efficient nonlinear beam finite elements [9, 14, 16, 17, 19, 24, 26, 33, 44, 46, 56]. The main idea is to decompose the motion of the element into rigid body and pure deformational parts. During the rigid body motion, a local coordinates system, fixed to the element, moves and rotates with it. The deformational part is measured in this local system. The main interest of the approach is that different assumptions can be made to represent the local deformations, giving different possibilities for the local element formulation.

Regarding the dynamic formulation of 2D corotational beams, several options are available. If linear interpolations are used for the local formulation, e.g. by taking the classical linear Timoshenko element, then inertia corotational terms are easily derived and the classical linear and constant Timoshenko mass matrix is obtained. However, linear interpolations assume that the transverse displacements are equal to zero along the element, which is not accurate, especially for flexible beams. If cubic interpolations are used for the local formulation, e.g. by taking the classic linear Bernoulli element, then the derivation of the inertia terms becomes very complicated. In [14], Crisfield et al. suggested that this derivation is impossible due to its complexity. Therefore, they used the constant Timoshenko mass matrix although they adopted local cubic interpolations to derive the elastic force vector and the tangent stiffness matrix. The same approach was adopted in [33]. In [44, 46, 56], the authors used a constant lumped mass matrix without any attempt to check its accuracy. In [9], Behdinan et al. proposed a corotational dynamic formulation. But the cubic shape functions were used to describe the global displacements, which is not consistent with the idea of the corotational method.

In the paper [37], the authors proposed a new corotational formulation. The novelty is that local cubic interpolations were used not only to obtain the elastic terms but also to derive the inertia terms. The efficiency of the formulation, compared with the two other corotational approach based on Timoshenko and lumped mass matrix, was shown through four numerical examples. The purpose of this chapter is to summarize relevant aspects of this formulation.

2.1 Corotational framework

The corotational beam kinematic for a two-noded straight element is presented in Fig. 2.1. The coordinates for the nodes 1 and 2 in the global coordinate system (x,z) are (x_1,z_1) and (x_2,z_2). The vector of global displacements is defined by

$$\mathbf{q} = \begin{bmatrix} u_1 & w_1 & \theta_1 & u_2 & w_2 & \theta_2 \end{bmatrix}^{\mathrm{T}}, \tag{2.1}$$

while the vector of local displacements is defined by

$$\overline{\mathbf{q}} = \begin{bmatrix} \overline{u} & \overline{\theta}_1 & \overline{\theta}_2 \end{bmatrix}^{\mathrm{T}}. \tag{2.2}$$

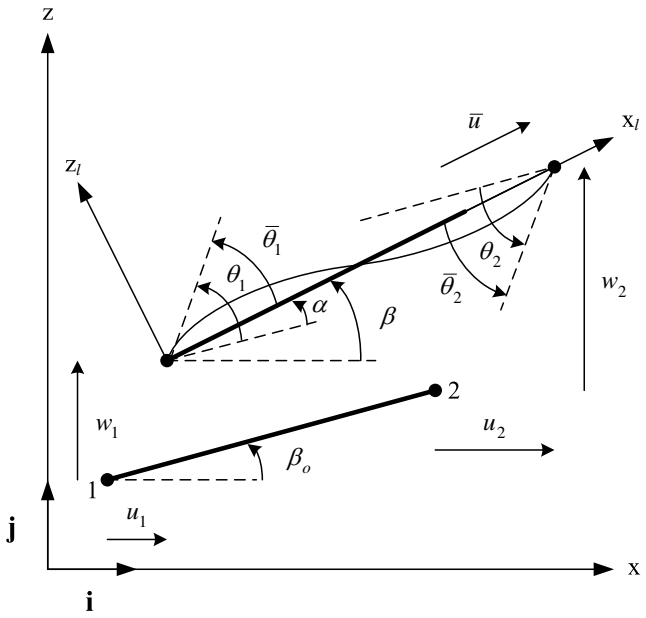

Fig. 2.1: Beam kinematics 1.

The components of $\overline{\mathbf{q}}$ can be computed according to

$$\overline{u} = l_n - l_o \,, \tag{2.3}$$

$$\overline{\theta}_1 = \theta_1 - \alpha = \theta_1 - \beta + \beta_o \,, \tag{2.4}$$

$$\overline{\theta}_2 = \theta_2 - \alpha = \theta_2 - \beta + \beta_o \,. \tag{2.5}$$

In Eq. (2.3), l_o and l_n denote the initial and current lengths of the element

$$l_o = [\,(x_2 - x_1)^2 + (z_2 - z_1)^2\,]^{1/2} \,, \tag{2.6}$$

$$l_n = [\,(x_2 + u_2 - x_1 - u_1)^2 + (z_2 + w_2 - z_1 - w_1)^2\,]^{1/2} \,. \tag{2.7}$$

The current angle of the local system with respect to the global system is denoted as β and is given by

$$c = \cos\beta = \frac{1}{l_n}(x_2 + u_2 - x_1 - u_1) \,, \tag{2.8}$$

$$s = \sin\beta = \frac{1}{l_n}(z_2 + w_2 - z_1 - w_1) \,. \tag{2.9}$$

At the initial configuration, $\beta = \beta_o$ and

$$c_o = \cos\beta_o = \frac{1}{l_n}(x_2 - x_1) \,, \tag{2.10}$$

$$s_o = \sin\beta_o = \frac{1}{l_n}(z_2 - z_1) \,. \tag{2.11}$$

The rigid rotation α is computed as

$$\sin\alpha = c_o\, s - s_o\, c \,, \tag{2.12}$$

$$\cos\alpha = c_o\, c - s_o\, s \,. \tag{2.13}$$

The local rotations $\overline{\theta}_i$ $(i = 1,2)$ are calculated using

$$\sin\overline{\theta}_i = \sin\theta_i \cos\alpha - \cos\theta_i \sin\alpha \,, \tag{2.14}$$

$$\cos\overline{\theta}_i = \cos\theta_i \cos\alpha + \sin\theta_i \sin\alpha \,. \tag{2.15}$$

Then, $\overline{\theta}_i$ is determined by

$$\begin{aligned}
&\overline{\theta}_i = \sin^{-1}(\sin\overline{\theta}_i) && \text{if } \sin\overline{\theta}_i \geq 0 \text{ and } \cos\overline{\theta}_i \geq 0 \,, \\
&\overline{\theta}_i = \cos^{-1}(\cos\overline{\theta}_i) && \text{if } \sin\overline{\theta}_i \geq 0 \text{ and } \cos\overline{\theta}_i < 0 \,, \\
&\overline{\theta}_i = \sin^{-1}(\sin\overline{\theta}_i) && \text{if } \sin\overline{\theta}_i < 0 \text{ and } \cos\overline{\theta}_i \geq 0 \,, \\
&\overline{\theta}_i = -\cos^{-1}(\cos\overline{\theta}_i) && \text{if } \sin\overline{\theta}_i < 0 \text{ and } \cos\overline{\theta}_i < 0 \,.
\end{aligned} \tag{2.16}$$

It should be noted that this procedure to derive $\overline{\theta}_i$ differs from the one in [13]. Here, the angles of rotations are not limited by π as in [13].

The connection between the variations of the local and global displacements is obtained as

$$\delta\overline{\mathbf{q}} = \mathbf{B}\,\delta\mathbf{q} \,. \tag{2.17}$$

By taking the differentiation of the expressions (2.3) to (2.5), the transformation matrix $\mathbf{B}$ is obtained as

$$\mathbf{B} = \begin{bmatrix} \mathbf{b}_1 \\ \mathbf{b}_2 \\ \mathbf{b}_3 \end{bmatrix} = \begin{bmatrix} -c & -s & 0 & c & s & 0 \\ -s/l_n & c/l_n & 1 & s/l_n & -c/l_n & 0 \\ -s/l_n & c/l_n & 0 & s/l_n & -c/l_n & 1 \end{bmatrix} \,. \tag{2.18}$$

2.2 Local beam kinematic description

The Interdependent Interpolation Element (IIE), proposed in [51], is adopted for the local beam kinematic description. The development of this beam element is based on the exact solution of the homogeneous form of the equilibrium equations for a Timoshenko beam. Consequently, the IIE element not only retains the accuracy inherent to the cubic interpolation, but also includes the bending shear deformation. The shape functions of the IIE element are given by

$$\varphi_1 = \mu\, x \left[6\,\Omega \left(1 - \frac{x}{l_o} \right) + \left(1 - \frac{x}{l_o} \right)^2 \right] \,, \tag{2.19}$$

$$\varphi_2 = \mu\, x \left[6\,\Omega \left(\frac{x}{l_o} - 1 \right) - \frac{x}{l_o} + \frac{x^2}{l_o^2} \right] \,, \tag{2.20}$$

$$\varphi_3 = \mu \left(1 + 12\,\Omega - \frac{12\,\Omega\, x}{l_o} - \frac{4\,x}{l_o} + \frac{3\,x^2}{l_o^2} \right) \,, \tag{2.21}$$

$$\varphi_4 = \mu \left(\frac{12\,\Omega\, x}{l_o} - \frac{2\,x}{l_o} + \frac{3\,x^2}{l_o^2} \right) \,, \tag{2.22}$$

where

$$\Omega = \frac{E\,I}{G\,A\,K_s\,l_o^2} \,, \quad \mu = \frac{1}{1+12\Omega} \,, \tag{2.23}$$

A, I : Section's area and second moment of area ,
K_s : Shear correction coefficient .
With $\Omega = 0$, the Hermitian shape functions of the classical Bernoulli elements are recovered.

Using this beam element, the axial displacement u, the transverse displacement w and the local rotation ϑ are calculated by

$$u = \frac{x}{l_o}\,\overline{u}\,, \tag{2.24}$$

$$w = \varphi_1\overline{\theta}_1 + \varphi_2\overline{\theta}_2\,, \tag{2.25}$$

$$\vartheta = \varphi_3\overline{\theta}_1 + \varphi_4\overline{\theta}_2\,. \tag{2.26}$$

2.3 Elastic force vector and tangent stiffness matrix

By equating the virtual work in the local and global systems, the relation between the local elastic force vector $\mathbf{f}_l$ and the global one $\mathbf{f}_g$ is obtained as

$$V = \delta\mathbf{q}^{\mathrm{T}}\mathbf{f}_g = \delta\overline{\mathbf{q}}^{\mathrm{T}}\mathbf{f}_l = \delta\mathbf{q}^{\mathrm{T}}\mathbf{B}^{\mathrm{T}}\mathbf{f}_l\,. \tag{2.27}$$

Eq. (2.27) must apply for any arbitrary $\delta\mathbf{q}$. Hence the global elastic force vector $\mathbf{f}_g$ is given by

$$\mathbf{f}_g = \mathbf{B}^{\mathrm{T}}\mathbf{f}_l\,, \quad \text{with} \quad \mathbf{f}_l = \begin{bmatrix} N & M_1 & M_2 \end{bmatrix}^{\mathrm{T}}\,. \tag{2.28}$$

The global tangent stiffness matrix is defined by

$$\delta\mathbf{f}_g = \mathbf{K}_g\,\delta\mathbf{q}\,. \tag{2.29}$$

By taking the differentiation of Eq. (2.28), the global stiffness matrix is obtained as

$$\mathbf{K}_g = \mathbf{B}^{\mathrm{T}}\mathbf{K}_l\,\mathbf{B} + \frac{\mathbf{z}\,\mathbf{z}^{\mathrm{T}}}{l_n}N + \frac{1}{l_n^2}(\mathbf{r}\,\mathbf{z}^{\mathrm{T}} + \mathbf{z}\,\mathbf{r}^{\mathrm{T}})(M_1 + M_2)\,, \tag{2.30}$$

where

$$\mathbf{r} = \begin{bmatrix} -c & -s & 0 & c & s & 0 \end{bmatrix}^{\mathrm{T}}\,, \tag{2.31}$$

$$\mathbf{z} = \begin{bmatrix} s & -c & 0 & -s & c & 0 \end{bmatrix}^{\mathrm{T}}\,. \tag{2.32}$$

The local elastic force vector $\mathbf{f}_l$ and local tangent stiffness matrix $\mathbf{K}_l$, which is defined by $\delta\mathbf{f}_l = \mathbf{K}_l\,\delta\overline{\mathbf{q}}$, depend on the definition of the local formulation.

The shape functions of the IIE were used together with a shallow arch beam theory. The shallow arch longitudinal and shear strains are given by

$$\varepsilon = \frac{1}{l_o}\int_{l_o}\left[\frac{\partial u}{\partial x} + \frac{1}{2}\left(\frac{\partial w}{\partial x}\right)^2\right]\mathrm{d}x - \frac{\partial^2 w}{\partial x^2}\,z\,, \tag{2.33}$$

$$\gamma = \frac{\partial w}{\partial x} + \vartheta\,. \tag{2.34}$$

The expressions of $\mathbf{f}_l$, $\mathbf{K}_l$ were then derived using Maple. The code was given in [37].

2.4 Inertia force vector and tangent dynamic matrix

The kinetic energy K of an element is given as

$$K = \frac{1}{2}\rho\left\{\int_{l_o} A(\dot{u}_{\mathrm{G}}^2 + \dot{w}_{\mathrm{G}}^2)\mathrm{d}l + \int_{l_o} I\,\dot{\theta}^2\mathrm{d}l\right\}\,, \tag{2.35}$$

where

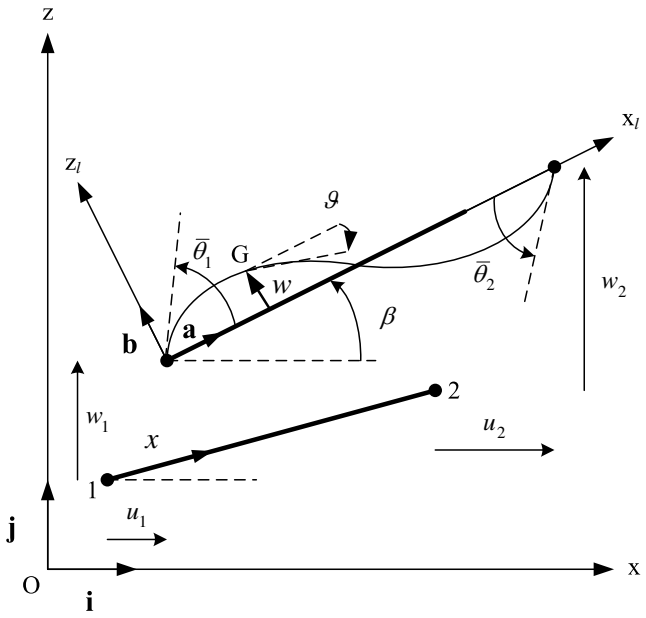

Fig. 2.2: Beam kinematics 2.

- ρ : Mass per unit volume,
- u_{G} , w_{G}: Global displacements of the cross-section centroid,
- θ : Global rotation of the section.

The global position of the cross-section centroid is given by (see Fig. 2.2)

$$\mathrm{OG} = (x_1 + u_1)\,\mathbf{i} + (z_1 + w_1)\,\mathbf{j} + \frac{l_n}{l_o} x\,\mathbf{a} + w\,\mathbf{b}\,, \tag{2.36}$$

The velocities of the centroid are then calculated by taking time derivative of the previous expression

$$\dot{u}_{\mathrm{G}} = \dot{u}_1 + \frac{x}{l_o}(\dot{u}_2 - \dot{u}_1) - \dot{w}\sin\beta - w\dot{\beta}\cos\beta\,, \tag{2.37}$$

$$\dot{w}_{\mathrm{G}} = \dot{w}_1 + \frac{x}{l_o}(\dot{w}_2 - \dot{w}_1) + \dot{w}\cos\beta - w\dot{\beta}\sin\beta\,, \tag{2.38}$$

The global rotation of the cross-section is given by

$$\dot{\theta} = \dot{\vartheta} + \dot{\alpha} = \dot{\vartheta} + \dot{\beta}\,. \tag{2.39}$$

The quantities $w, \dot{w}, \dot{\vartheta}$ are interpolated from the nodal quantities using Eqs. (2.25) and (2.26). However, Ω is taken to 0 as suggested in [51]. Extensive numerical studies performed have shown that this simplification does not modify the numerical results.

The exact expression of the kinetic energy K is then obtained by substituting Eqs. (2.37)-(2.39) into Eq. (2.35).

Moreover, the kinetic energy can be written as

$$K = \frac{1}{2}\,\dot{\mathbf{q}}^{\mathrm{T}}\,\mathbf{M}\,\dot{\mathbf{q}} = \frac{1}{2}\dot{\mathbf{q}}^{\mathrm{T}}\,\mathbf{T}^{\mathrm{T}}\,\mathbf{M}_l\,\mathbf{T}\,\dot{\mathbf{q}}\,, \tag{2.40}$$

where $\mathbf{T}$ is rotation matrix. Hence, the expression of the local matrix $\mathbf{M}_l$ can be derived. At this point, two simplifications are introduced in the expression of the local mass matrix. The local displacement w is assumed small and therefore the terms containing w^2 are neglected. Furthermore, the approximation $l_n = l_o$ is considered (small axial deformation assumption). With these simplifications, the local mass matrix is only function of $\overline{\theta}_1$ and $\overline{\theta}_2$.

The inertia force vector is calculated from the kinetic energy by using the Lagrange's equation of motion

$$\mathbf{f}_K = \frac{\mathrm{d}}{\mathrm{d}t}\left[\frac{\partial K}{\partial \dot{\mathbf{q}}}\right] - \left[\frac{\partial K}{\partial \mathbf{q}}\right] . \tag{2.41}$$

With the expression of the kinetic energy, $\mathbf{f}_K$ is obtained as

$$\begin{aligned}\mathbf{f}_K = \mathbf{M}\,\ddot{\mathbf{q}} + \left\{\mathbf{M}_\beta\left(\frac{\mathbf{z}^{\mathrm{T}}}{l_n}\dot{\mathbf{q}}\right) + \mathbf{M}_{\overline{\theta}_1}(\mathbf{b}_2^{\mathrm{T}}\dot{\mathbf{q}}) + \mathbf{M}_{\overline{\theta}_2}(\mathbf{b}_3^{\mathrm{T}}\dot{\mathbf{q}})\right\}\dot{\mathbf{q}} \\ - \left(\frac{1}{2}\dot{\mathbf{q}}^{\mathrm{T}}\mathbf{M}_\beta\dot{\mathbf{q}}\right)\frac{\mathbf{z}}{l_n} - \left(\frac{1}{2}\dot{\mathbf{q}}^{\mathrm{T}}\mathbf{M}_{\overline{\theta}_1}\dot{\mathbf{q}}\right)\mathbf{b}_2 - \left(\frac{1}{2}\dot{\mathbf{q}}^{\mathrm{T}}\mathbf{M}_{\overline{\theta}_2}\dot{\mathbf{q}}\right)\mathbf{b}_3 ,\end{aligned} \tag{2.42}$$

where $\mathbf{M}_\beta = \dfrac{\partial \mathbf{M}}{\partial \beta}$, $\mathbf{M}_{\overline{\theta}_1} = \dfrac{\partial \mathbf{M}}{\partial \overline{\theta}_1}$, $\mathbf{M}_{\overline{\theta}_2} = \dfrac{\partial \mathbf{M}}{\partial \overline{\theta}_2}$.

From the expression of the inertia force vector given in Eq. (2.42), the following differentiations are calculated

$$\mathbf{C}_K = \frac{\partial \mathbf{f}_K}{\partial \dot{\mathbf{q}}} , \tag{2.43}$$

$$\mathbf{K}_K = \frac{\partial \mathbf{f}_K}{\partial \mathbf{q}} . \tag{2.44}$$

For the expressions of $\mathbf{C}_K$ and $\mathbf{K}_K$, the interested reader is referred to [37].

2.5 Numerical example - Cantilever beam

The example, described in Fig. 2.3, is a cantilever beam of length $L = 10$ m with uniform cross-section and subjected to a sinusoidal tip force $P = P_o \sin(wt)$ at the free end. The amplitude of the load P_o is taken equal to 10 MN and its frequency w is 50 rad/s. The cross-section depth and width are $a = 0.25$ m and $e = 0.5$ m, respectively. The elastic modulus of the beam E is 210 GPa and the mass per unit volume is $\rho = 7850$ kg/m^3.

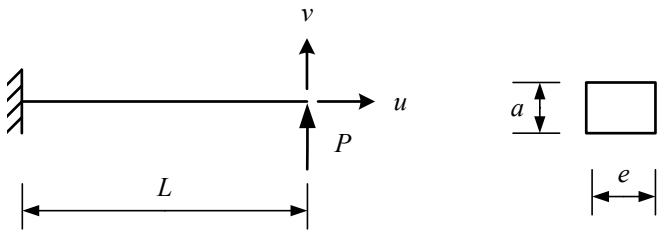

Fig. 2.3: Cantilever beam : geometrical data.

The nonlinear dynamic behavior of the beam was analysed using three different beam formulations: the new one, and the two formulations usually found in the literature, i.e. the lumped mass matrix and the Timoshenko mass matrix. For all dynamic formulations, the elastic force vector and tangent stiffness

matrix were derived using the IIE shape functions in order to account for shear deformability. The three dynamic formulations were compared with a reference solution. This solution was obtained with a large number of elements and was identical for the three considered dynamic formulations. The reference solution was also checked with Abaqus (total Lagrangian formulation) and the same results were obtained.

In this example, the reference solution was obtained with 48 elements. The results given by three formulations considering only 3 elements, with the time step size $\Delta t = 10^{-4}$ s, were shown in Figs. 2.4 and 2.5. For the presentation of the results, the following colors were used in all figures:

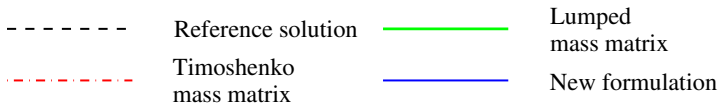

It can be observed that the proposed formulation gave results that were in very agreement with the reference solution with only three elements. However, the results obtained with the lumped and Timoshenko approaches did not agree well with the reference solution over the whole time domain.

This example shows that the new formulation, based on local cubic interpolations, is more efficient than two other formulations, which are based on local linear interpolations (Timoshenko mass matrix) and lumped mass matrix. This advantage is due to a better representation of the local displacements in the inertia terms.

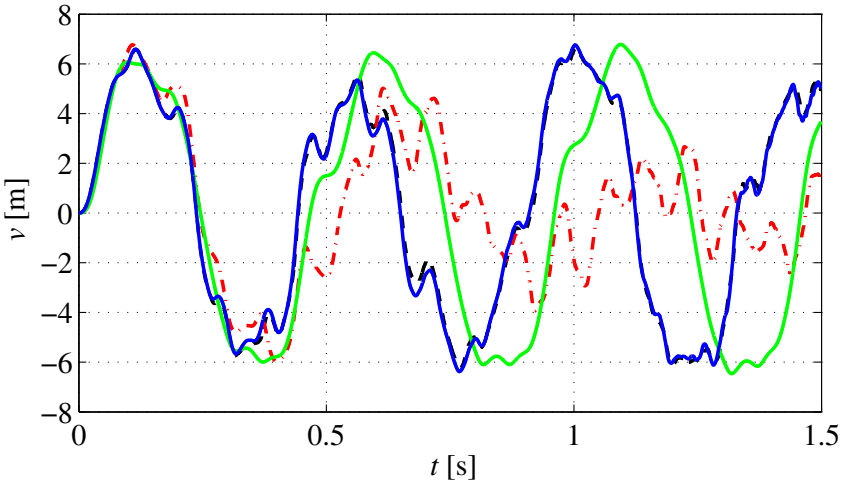

Fig. 2.4: Cantilever beam - Vertical displacement history.

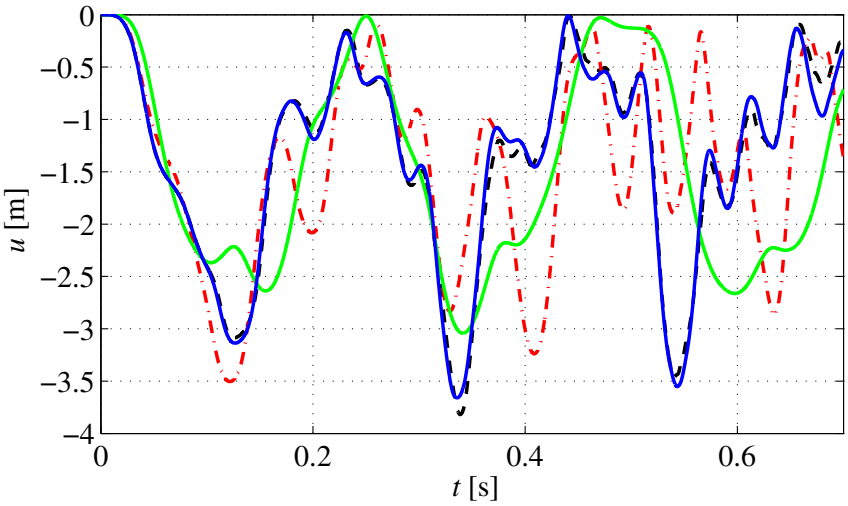

Fig. 2.5: Cantilever beam - Horizontal displacement history.

Chapter 3

Finite rotations in dynamics

The extension of a 2D beam formulation to 3D is not an easy task. The difficulty is mainly due to the complex nature of the finite rotations. More specifically, the finite rotations are non-commutative and non-additive, thus they cannot be treated in a simple manner as the translational displacements. As a consequence, the standard Newmark time stepping method cannot be directly applied to the finite rotations. This method must be reformulated according to the parametrization of the finite rotations.

Several aspects of the finite rotations in dynamics were investigated in [38]. The first one concerned the parametrization of the finite rotations. In the computational mechanics, many possibilities to parameterize finite rotations can be found [3, 11, 13, 21, 36]. Rotation tensor, rotational vector and Euler parameters were studied. These parameterizations are popular in the finite element method, however, each of them has certain deficiencies. The rotation tensor, with nine components to handle, requires special update procedure. In contrast, only three parameters are needed for the rotational vector, and the Euler parameters. Furthermore, the rotations become additive and can be updated in the same manner as the translations. However, the amplitude of the finite rotations represented by these parameterizations are limited by 2π for the rotational vector, and by π for the Euler parameters. To avoid this inconvenience, Cardona and Geradin [11], Ibrahimbegović [28] and Battini [7] introduced the notion of the incremental rotational vector and the incremental Euler parameters. Then, additive updates still apply but this time only within each increment. The amplitudes of the rotations are just limited within each increment, which is not a problem.

The second aspect was related to the Newmark time stepping methods for the finite rotations and the efficiency of the iterative procedure. Two Newmark algorithms have been used in the literature. In the first one, proposed by Simo and Vu-Quoc [55], the Newmark equations were written using the material incremental rotational vector, the material angular velocity and the material acceleration. This approach was adopted in [14, 32, 34, 35]. Ibrahimbegović and Mikdad [30] reformulated this method using spatial forms. In the second approach, introduced by Cardona and Geradin [11], the standard Newmark algorithm was applied to the incremental rotational vector and its time derivatives. Hence, the update procedure of the rotational quantities took a similar form as the displacements. In the works of Forsell [18] and Mäkinen [43], this approach was adopted using the total rotational vectors. Regarding the efficiency of the iterative procedure, several predictors and possibilities to simplify the tangent inertia matrix were also tested.

In order to compare these parameterizations and the Newmark methods for the finite rotations, four nonlinear dynamic formulations were investigated in [38]. For all of these formulations, theoretical derivations and practical implementations were given in detail. The similarities and differences between them were also pointed out. Moreover, to assess the four formulations in terms of numerical accuracy and computational efficiency, six nonlinear dynamic examples were analyzed.

The objective of this chapter is to present a short summary of these aspects and one example is reproduced. The organisation of the chapter is as follows. Section 3.1 presents three parameterizations of the finite rotations. The Newmark time stepping methods are introduced in Section 3.2. The four dynamic

formulations are summarized in Section 3.3. Finally, one numerical example is investigated in Section 3.4.

3.1 Finite rotations

Parametrization of the finite rotations

The coordinate of a fixed vector $\mathbf{x}_o$ that is rotated into the position $\mathbf{x}$ (see Fig. 3.1) is given by the relation

$$\mathbf{x} = \mathbf{R}\,\mathbf{x}_o\,. \tag{3.1}$$

The rotation matrix $\mathbf{R}$ is an element of the $SO(3)$ group. Its coordinate representation is a 3x3 orthogonal

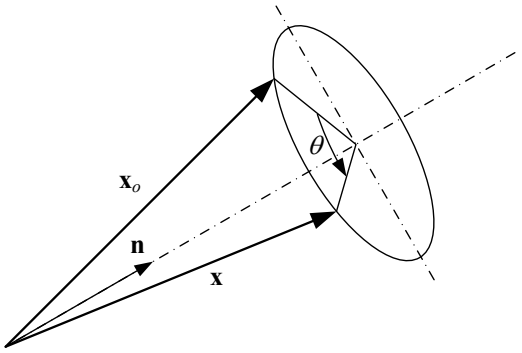

Fig. 3.1: Finite rotation of a vector.

matrix involving nine components. However, due to its orthonormality, the rotation matrix $\mathbf{R}$ can be parameterized using only three independent parameters. One possibility is to use the rotational vector defined by

$$\boldsymbol{\theta} = \theta\,\mathbf{n}, \tag{3.2}$$

where $\mathbf{n}$ is an unit vector defining the axis of the rotation and $\theta = (\boldsymbol{\theta}^{\mathrm{T}}\boldsymbol{\theta})^{1/2}$ is the angle of the rotation.

The relation between the rotation matrix and the rotational vector is given by the Rodrigues' formula

$$\mathbf{R} = \mathbf{I} + \frac{\sin\theta}{\theta}\widetilde{\boldsymbol{\theta}} + \frac{1-\cos\theta}{\theta^2}\widetilde{\boldsymbol{\theta}}\,\widetilde{\boldsymbol{\theta}}, \tag{3.3}$$

where $\widetilde{\boldsymbol{\theta}}$ is the skew matrix associated to the vector $\boldsymbol{\theta}$.

If the trigonometric functions in the above equation are expanded in Taylor series, $\mathbf{R}$ can be written as

$$\mathbf{R} = \mathbf{I} + \widetilde{\boldsymbol{\theta}} + \frac{1}{2}\widetilde{\boldsymbol{\theta}}^2 + \cdots = \exp(\widetilde{\boldsymbol{\theta}})\,. \tag{3.4}$$

Another possibility to parameterize the rotation matrix is to use the Euler parameters (quaternion), which by introducing the scaling factor 2 gives

$$\mathbf{q} = 2\sin\frac{\theta}{2}\,\mathbf{n}. \tag{3.5}$$

In terms of $\mathbf{q}$, the rotational tensor $\mathbf{R}$ is given by

$$\mathbf{R}(\mathbf{q}) = (2q_o^2 - 1)\mathbf{I} + \frac{1}{2}\mathbf{q}\mathbf{q}^{\mathrm{T}} + q_o\widetilde{\mathbf{q}}, \tag{3.6}$$

with $q_o = (1 - \mathbf{q}^{\mathrm{T}}\mathbf{q}/4)^{1/2}$.

It can be observed that this parametrization requires only three parameters $\mathbf{q}$ (see Eq. (3.5)) instead of four$(\mathbf{q}, q_o)$ as usually found in the literature.

Variation of the rotation parameters

The admissible variation $\delta\mathbf{R}$ of the rotation matrix $\mathbf{R}$ is calculated by

$$\begin{aligned}\delta\mathbf{R} = \frac{\mathrm{d}}{\mathrm{d}\varepsilon}\left[\mathbf{R}_\varepsilon\right]_{\varepsilon=0} &= \frac{\mathrm{d}}{\mathrm{d}\varepsilon}\left(\exp(\varepsilon\,\widetilde{\delta\mathbf{w}})\,\mathbf{R}\right)_{\varepsilon=0} = \widetilde{\delta\mathbf{w}}\mathbf{R} \\ &= \frac{\mathrm{d}}{\mathrm{d}\varepsilon}\left(\mathbf{R}\exp(\varepsilon\,\widetilde{\delta\boldsymbol{\omega}})\right)_{\varepsilon=0} = \mathbf{R}\widetilde{\delta\boldsymbol{\omega}}\,. \end{aligned} \tag{3.7}$$

Physically, $\delta\mathbf{w}$ and $\delta\boldsymbol{\omega}$ represent infinitesimal spatial and material rotations superposed onto the rotation $\mathbf{R}$. $\delta\mathbf{w}$, which is also denoted as spatial spin variables, is related to small variation of the rotational vector through

$$\delta\mathbf{w} = \mathbf{T}_s(\boldsymbol{\theta})\,\delta\boldsymbol{\theta}\,, \tag{3.8}$$

with

$$\mathbf{T}_s(\boldsymbol{\theta}) = \mathbf{I} + \frac{1-\cos\theta}{\theta^2}\widetilde{\boldsymbol{\theta}} + \frac{\theta-\sin\theta}{\theta^3}\widetilde{\boldsymbol{\theta}}\,\widetilde{\boldsymbol{\theta}}\,. \tag{3.9}$$

In connection with the operator $\mathbf{T}_s$, it should also be noted that

$$\det(\mathbf{T}_s) = \frac{2(1-\cos\theta)}{\theta^2}\,, \tag{3.10}$$

which shows that the corresponding mapping ceases to be a bijection for $\theta = 2k\pi$ $(k = 1, 2, ...)$ [28, 48].

The inverse relation of Eq. (3.8) is defined as

$$\delta\boldsymbol{\theta} = \mathbf{T}_s^{-1}(\boldsymbol{\theta})\,\delta\mathbf{w}\,, \tag{3.11}$$

with

$$\mathbf{T}_s^{-1}(\boldsymbol{\theta}) = \frac{(\theta/2)}{\tan(\theta/2)}\mathbf{I} + \left(1 - \frac{(\theta/2)}{\tan(\theta/2)}\right)\frac{\boldsymbol{\theta}\boldsymbol{\theta}^{\mathrm{T}}}{\theta^2} - \frac{1}{2}\widetilde{\boldsymbol{\theta}}\,. \tag{3.12}$$

The relation between the spatial spin variables and a small variation of the Euler parameters is given by

$$\delta\mathbf{w} = \mathbf{T}_q(\mathbf{q})\,\delta\mathbf{q}\,, \tag{3.13}$$

with

$$\mathbf{T}_q(\mathbf{q}) = q_o\mathbf{I} + \frac{\mathbf{q}\mathbf{q}^{\mathrm{T}}}{4\,q_o} + \frac{\widetilde{\mathbf{q}}}{2}\,. \tag{3.14}$$

It should be noted that the operator $\mathbf{T}_q(\mathbf{q})$ is undefined for $q_o = 0$, which corresponds to $\theta = k\pi$.

Similar relations connecting the material spin variables $\delta\boldsymbol{\omega}$ and $\delta\boldsymbol{\theta}$, $\delta\mathbf{q}$ can also be obtained by noting that $\delta\mathbf{w} = \mathbf{R}\,\delta\boldsymbol{\omega}$. This issue, however will not be dealt with in this thesis.

Update procedures of finite rotations

Due to the fact that the finite rotations are not elements of a linear space, the two successive rotations are not commutative. Therefore, the update procedure of the finite rotations after each Newton-Raphson iteration depends on the choice of the parametrization of finite rotations, and needs to be carefully treated.

If the spatial spin variables are used to parameterize finite rotations, the update of the rotation matrix at i^{th} iteration of step $(n+1)$ is performed according to

$$\mathbf{R}_{n+1}^{i} = \exp(\widetilde{\Delta\mathbf{w}})\mathbf{R}_{n+1}^{i-1}\,, \tag{3.15}$$

where $\Delta\mathbf{w}$ are the iterative spatial spin variables.

If the rotational vector or the Euler parameters are used as parameters (see [6, 47]), then the rotations become additive and are simply updated at each iteration using

$$\boldsymbol{\theta}^{i} = \boldsymbol{\theta}^{i-1} + \Delta\boldsymbol{\theta}\,, \tag{3.16}$$

$$\mathbf{q}^{i} = \mathbf{q}^{i-1} + \Delta\mathbf{q}\,. \tag{3.17}$$

However, the relations in Eqs. (3.8) and (3.13) cease to be bijections respectively for $\theta = 2\pi$ and for $\theta = \pi$. Consequently, the angle of rotation is limited to 2π with the parametrization using the rotational vector and π in case of the Euler parameters. In many dynamic analysis, angles of rotations can become larger than these limitations.

In order to overcome this inconvenience, Cardona and Geradin [11], Ibrahimbegović [28] and Battini [7] proposed to perform Eqs. (3.8) and (3.13) only within an increment, and introduced the concept of incremental rotational vector and incremental Euler parameters. Then, the update procedure at the step $(n+1)$ is performed in the following way: at the beginning of the step, the incremental rotational vector and the incremental Euler parameters are set equal to zero ($\boldsymbol{\theta}_{n+1}^{0} = \mathbf{q}_{n+1}^{0} = \mathbf{0}_{[3\text{x}1]}$). At iteration i, they are updated using

$$\boldsymbol{\theta}_{n+1}^{i} = \boldsymbol{\theta}_{n+1}^{i-1} + \Delta\boldsymbol{\theta}\,, \tag{3.18}$$

$$\mathbf{q}_{n+1}^{i} = \mathbf{q}_{n+1}^{i-1} + \Delta\mathbf{q}\,, \tag{3.19}$$

and the rotation matrix is updated using

$$\mathbf{R}_{n+1}^{i} = \exp(\widetilde{\boldsymbol{\theta}_{n+1}^{i}})\,\mathbf{R}_{n}\,, \tag{3.20}$$

$$\mathbf{R}_{n+1}^{i} = \mathbf{R}(\mathbf{q}_{n+1}^{i})\,\mathbf{R}_{n}\,, \tag{3.21}$$

where $\boldsymbol{\theta}_{n+1}^{i}, \mathbf{q}_{n+1}^{i}$ are the spatial incremental rotational vector and the spatial incremental Euler parameters, respectively.

Hence, additive updates still apply within each increment. The amplitude of the rotations are just limited in each increment, which is not a problem.

Angular velocities and accelerations

In order to simulate dynamic behavior of beam structures, angular velocities and accelerations must be calculated. Considering Eq. (3.7), the angular velocity can be expressed in spatial form as

$$\widetilde{\mathbf{w}} = \dot{\mathbf{R}}\,\mathbf{R}^{\mathrm{T}}\,, \tag{3.22}$$

or in material form as

$$\widetilde{\boldsymbol{\omega}} = \mathbf{R}^{\mathrm{T}}\,\dot{\mathbf{R}}\,. \tag{3.23}$$

Due to the fact that the rotation matrix is an orthogonal matrix, the mutual relations between the corresponding axial vectors can be written as

$$\dot{\mathbf{w}} = \mathbf{R}\,\dot{\boldsymbol{\omega}}\,, \tag{3.24}$$

$$\dot{\boldsymbol{\omega}} = \mathbf{R}^{\mathrm{T}}\,\dot{\mathbf{w}}\,. \tag{3.25}$$

By taking the time derivatives of Eqs. (3.22) and (3.23), the angular accelerations in spatial and material form are given by

$$\widetilde{\ddot{\mathbf{w}}} = \ddot{\mathbf{R}}\,\mathbf{R}^{\mathrm{T}} + \dot{\mathbf{R}}\,\dot{\mathbf{R}}^{\mathrm{T}}\,, \tag{3.26}$$

$$\widetilde{\ddot{\boldsymbol{\omega}}} = \mathbf{R}^{\mathrm{T}}\,\ddot{\mathbf{R}} + \dot{\mathbf{R}}^{\mathrm{T}}\,\dot{\mathbf{R}}\,. \tag{3.27}$$

The relations between the two forms of angular acceleration are given by

$$\ddot{\mathbf{w}} = \mathbf{R}\,\ddot{\boldsymbol{\omega}}\,, \tag{3.28}$$

$$\ddot{\boldsymbol{\omega}} = \mathbf{R}^{\mathrm{T}}\,\ddot{\mathbf{w}}\,. \tag{3.29}$$

The spatial angular velocity can be directly calculated from the rotational vector and from the Euler parameters by

$$\dot{\mathbf{w}} = \mathbf{T}_s(\boldsymbol{\theta})\,\dot{\boldsymbol{\theta}} = \mathbf{T}_q(\mathbf{q})\,\dot{\mathbf{q}}\,. \tag{3.30}$$

By taking the time derivative of the previous equation, the spatial angular acceleration is calculated by

$$\ddot{\mathbf{w}} = \mathbf{T}_s(\boldsymbol{\theta})\,\ddot{\boldsymbol{\theta}} + \dot{\mathbf{T}}_s(\boldsymbol{\theta})\,\dot{\boldsymbol{\theta}} = \mathbf{T}_q(\mathbf{q})\,\ddot{\mathbf{q}} + \dot{\mathbf{T}}_q(\mathbf{q})\,\dot{\mathbf{q}}\,. \tag{3.31}$$

The expressions of $\dot{\mathbf{T}}_s(\boldsymbol{\theta})\,\dot{\boldsymbol{\theta}}$ and $\dot{\mathbf{T}}_q(\mathbf{q})\,\dot{\mathbf{q}}$ are given by

$$\dot{\mathbf{T}}_s(\boldsymbol{\theta})\,\dot{\boldsymbol{\theta}} = \left\{ c_1\,\dot{\boldsymbol{\theta}}\boldsymbol{\theta}^{\mathrm{T}} + c_2\,\widetilde{\boldsymbol{\theta}}\dot{\boldsymbol{\theta}}\boldsymbol{\theta}^{\mathrm{T}} + c_3\,(\boldsymbol{\theta}^{\mathrm{T}}\dot{\boldsymbol{\theta}})\,\boldsymbol{\theta}\boldsymbol{\theta}^{\mathrm{T}} + c_5\,\left[\boldsymbol{\theta}\dot{\boldsymbol{\theta}}^{\mathrm{T}} + (\boldsymbol{\theta}^{\mathrm{T}}\dot{\boldsymbol{\theta}})\mathbf{I}\right] \right\} \dot{\boldsymbol{\theta}}\,, \tag{3.32}$$

where

$$c_1 = \frac{\theta\,\cos\theta - \sin\theta}{\theta^3}\,, \qquad c_2 = \frac{\theta\sin\theta + 2\cos\theta - 2}{\theta^4}\,,$$

$$c_3 = \frac{3\sin\theta - 2\theta - \theta\,\cos\theta}{\theta^5}\,, \qquad c_5 = \frac{\theta - \sin\theta}{\theta^3}\,,$$

and

$$\dot{\mathbf{T}}_q(\mathbf{q})\dot{\mathbf{q}} = \left(\dot{\mathbf{q}}^{\mathrm{T}}\dot{\mathbf{q}} + \frac{(\mathbf{q}^{\mathrm{T}}\dot{\mathbf{q}})^2}{4\,q_o^2} \right) \frac{\mathbf{q}}{4\,q_o}\,. \tag{3.33}$$

Note that the material angular velocity and acceleration can also be obtained by similar formulations. This issue, however will not be dealt with in this thesis.

3.2 Time stepping method for finite rotations

Newmark time integration method

The standard relations of the Newmark time integration method for displacements are

$$\mathbf{u}_{n+1} = \mathbf{u}_n + h\dot{\mathbf{u}}_n + h^2\left[(\frac{1}{2} - \beta)\ddot{\mathbf{u}}_n + \beta\,\ddot{\mathbf{u}}_{n+1} \right]\,, \tag{3.34}$$

$$\dot{\mathbf{u}}_{n+1} = \dot{\mathbf{u}}_n + h\left[(1-\gamma)\ddot{\mathbf{u}}_n + \gamma\ddot{\mathbf{u}}_{n+1} \right]\,. \tag{3.35}$$

Due to the non-additive property of finite rotations, the update procedure for rotational quantities needs to be carefully treated. In [55], Simo and Vu-Quoc have proposed to directly apply the classic Newmark updates to material angular velocity, material acceleration and material incremental rotational vector. The algorithm is given by

$$\boldsymbol{\Theta}_{n+1} = h\dot{\boldsymbol{\omega}}_n + h^2\left[(\frac{1}{2}-\beta)\ddot{\boldsymbol{\omega}}_n + \beta\,\ddot{\boldsymbol{\omega}}_{n+1}\right], \tag{3.36}$$

$$\dot{\boldsymbol{\omega}}_{n+1} = \dot{\boldsymbol{\omega}}_n + h\left[(1-\gamma)\ddot{\boldsymbol{\omega}}_n + \gamma\ddot{\boldsymbol{\omega}}_{n+1}\right]. \tag{3.37}$$

This Newmark time integration method is adopted in [14, 32, 34, 35, 58]. Ibrahimbegović and Mikdad [30] reformulated this method using spatial forms

$$\boldsymbol{\theta}_{n+1} = h\dot{\mathbf{w}}_n + h^2\left[(\frac{1}{2}-\beta)\ddot{\mathbf{w}}_n + \beta\,\boldsymbol{\Lambda}_{n+1}^{\mathrm{T}}\ddot{\mathbf{w}}_{n+1}\right], \tag{3.38}$$

$$\dot{\mathbf{w}}_{n+1} = \boldsymbol{\Lambda}_{n+1}\left[\dot{\mathbf{w}}_n + h(1-\gamma)\ddot{\mathbf{w}}_n\right] + h\gamma\ddot{\mathbf{w}}_{n+1}, \tag{3.39}$$

where $\boldsymbol{\Lambda}_{n+1} = \exp(\widetilde{\boldsymbol{\theta}_{n+1}})$.

As pointed out by Mäkinen [42], the Newmark update procedures, given by Eqs. (3.36) and (3.37), involve vectors that do not belong to the same tangent space. Indeed, the vectors $\dot{\boldsymbol{\omega}}_{n+1}$ and $\ddot{\boldsymbol{\omega}}_{n+1}$ lie in a tangent space different from the one containing vectors $\boldsymbol{\Theta}_{n+1}$, $\dot{\boldsymbol{\omega}}_n$ and $\ddot{\boldsymbol{\omega}}_n$. Hence, these update procedures are not formally correct.

Cardona and Geradin, in [11], have proposed a different way to use Newmark time integration method for finite rotations. The time derivatives of the incremental rotational vector are used instead of angular velocity and acceleration. Hence, the additive property of the spatial incremental rotational vector can be used and the classic Newmark update procedure for translations is also applied to the rotational variables. In this case, the algorithm is given by

$$\boldsymbol{\theta}_{n+1} = h\dot{\boldsymbol{\theta}}_n + h^2\left[(\frac{1}{2}-\beta)\ddot{\boldsymbol{\theta}}_n + \beta\,\ddot{\boldsymbol{\theta}}_{n+1}\right], \tag{3.40}$$

$$\dot{\boldsymbol{\theta}}_{n+1} = \dot{\boldsymbol{\theta}}_n + h\left[(1-\gamma)\ddot{\boldsymbol{\theta}}_n + \gamma\ddot{\boldsymbol{\theta}}_{n+1}\right]. \tag{3.41}$$

Predictors for the iterative procedure

In the nonlinear dynamic analysis of structures, displacements (rotations), velocities and accelerations need to be computed at each time step. For these three unknowns, Newmark time stepping method gives only two relations. Thus one unknown must be predicted as the initial value for the solution at the time t_{n+1}. A poor predictor can increase the number of iterations and in some cases makes the procedure fail to converge.

In [38], four predictors, found in the literature, were implemented and tested:

- The first predictor (Pred. 1), called as "Unchanged displacements", is used by Simo and Vu-Quoc [55]. The displacements and the rotations at t_n are taken as predictor for the solution at t_{n+1}.
- The second one (Pred. 2), referred to "Null accelerations", is used by Cardona and Geradin [11], Mäkinen [42], Chung and Hulbert [12]. Zero translational and rotational accelerations are taken as predictor for the solution at t_{n+1}.
- The third one (Pred. 3), called as "Unchanged accelerations", used by Forsell [18], proposes to take the translational and rotational accelerations at t_n as predictor for the solution at t_{n+1}.

- The last predictor (Pred. 4), proposed by Crisfield [13], uses the tangent operator at t_n to predict initial values at t_{n+1}. This predictor was first presented in [13] for the case of a linear inertia force vector and then extended in [38] for an arbitrary nonlinear inertia force vector. At t_{n+1}, the nodal displacement vector $\mathbf{d}$ is initialized as follows

$$\mathbf{d}_{n+1}^{0} = \mathbf{d}_n + \Delta\mathbf{d}\,. \tag{3.42}$$

For the HHT α method, $\Delta\mathbf{d}$ is calculated by

$$\begin{aligned}\mathbf{K}_{\text{Total},n}\Delta\mathbf{d} =&(1+\alpha)\mathbf{f}_{\text{ext},n+1} - \mathbf{f}_{g,n} - \mathbf{f}_{k,n} - \alpha\mathbf{f}_{\text{ext},n} \\ &+\mathbf{C}_{k,n}\left(\frac{\gamma}{\beta}\dot{\mathbf{d}}_n - \frac{h(2\beta-\gamma)}{2\beta}\ddot{\mathbf{d}}_n\right) + \frac{\mathbf{M}_n}{\beta h^2}\left(h\dot{\mathbf{d}}_n + \frac{h^2}{2}\ddot{\mathbf{d}}_n\right),\end{aligned} \tag{3.43}$$

where

$$\mathbf{K}_{\text{Total},n} = (1+\alpha)\mathbf{K}_{\text{Static},n} + \mathbf{K}_{\text{Dyn},n}\,.$$

Tangent dynamic matrix

The nonlinear equation of motion is solved using the Newton-Raphson iterative procedure. Thus, the linearization of the inertia force vector need to be derived

$$\Delta\mathbf{f}_k = \mathbf{M}\Delta\ddot{\mathbf{d}} + \mathbf{C}_k\Delta\dot{\mathbf{d}} + \mathbf{K}_k\Delta\mathbf{d}\,, \tag{3.44}$$

where $\mathbf{K}_k$, $\mathbf{C}_k$ and $\mathbf{M}$ respectively denote centrifugal matrix, gyroscopic matrix and mass matrix.

In several case, the full linearization of the inertia force is difficult to obtain. In order to overcome this problem and to reduce the CPU time, Geradin and Cardona [11, 21] recommended to keep only the mass matrix and to neglect the gyroscopic and centrifugal matrices, as follow

$$\Delta\mathbf{f}_k \approx \mathbf{M}\Delta\ddot{\mathbf{d}}\,. \tag{3.45}$$

In [38], another simplification was proposed and the following three alternatives were tested: the exact tangent inertia matrix (i.e. mass, gyroscopic and centrifugal terms), only the mass matrix (as proposed in [11, 21]) and the mass and gyroscopic terms (the new proposal). The new proposal is given by

$$\Delta\mathbf{f}_k \approx \mathbf{M}\Delta\ddot{\mathbf{d}} + \mathbf{C}_k\Delta\dot{\mathbf{d}}\,. \tag{3.46}$$

3.3 Comparison of dynamic formulations

Four nonlinear dynamic formulations of 3D beam elements, based on several parameterizations and Newmark time integration methods for finite rotations (see Table 3.3), were compared in [38]. For all of them, the inertia force vector and tangent inertia matrix were derived in a total Lagrangian context and computed using two Gauss points. The first formulation was proposed by Simo and Vu-Quoc [55] and used spatial spin variables. A modification of the computation of the rotational quantities at the Gauss points was introduced in order to get a higher efficiency. The second formulation, based on the incremental rotational vector, was developed by Ibrahimbegović and Mikdad in [30]. The third one, also based on the incremental rotational vector, was proposed by Cardona and Geradin [11]. It was reformulated using the spatial form of the incremental rotational vector instead of the material one. The fourth formulation employed three of the four Euler parameters (quaternion) as rotational variables. This idea was introduced by Battini [7] for static analysis and then developed in [38] for dynamics.

Regarding the static deformational terms, i.e. the internal force vector and tangent stiffness matrix, the corotational beam elements developed by Battini and Pacoste [7, 8] were employed. For the deformational static part, the corotational formulation with the local element *t3d* proposed in [8] was adopted. The expressions of the static deformational terms will be given in detail in Chapter 4.

Table 3.1: Four nonlinear dynamic formulations.

Formulation	Rotational variables	Newmark time integration method
Simo & Vu-Quoc [55]	Spatial spin variables	Simo & Vu-Quoc
Ibrahimbegović & Mikdad [30]	Incremental rotational vector	
Cardona & Geradin [11]		Cardona & Geradin
New formulation [38]	Incremental Euler parameters	

3.4 Numerical example - Free-free flexible beam with disks

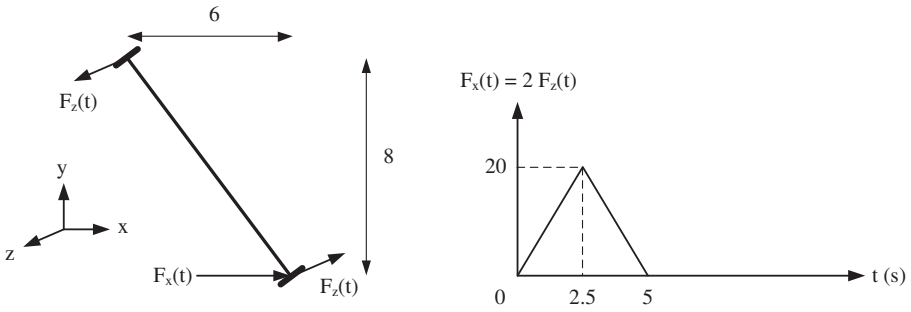

Fig. 3.2: Free-free flexible beam with disks and loading.

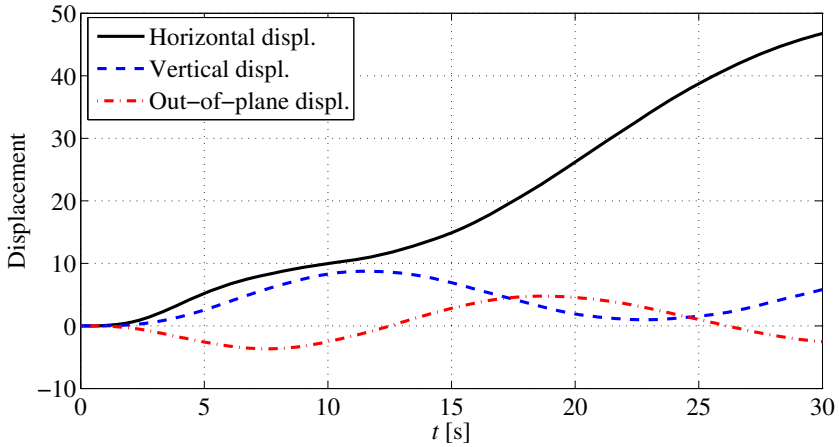

Fig. 3.3: Free-free flexible beam with disks. End responses time-history.

This example, proposed by Ibrahimbegović and Mikdad [30], analyzes the flight of a flexible beam with rigid disks attached to it. The initial configuration is given in Fig. 3.2. The mass per unit length of the beam and the inertia dyadic of the cross section in initial configuration are $A_\rho = 1$, $\mathbf{J}_\rho = \mathrm{diag}(20, 10, 10)$, respectively. The other material properties are $EA = GA = 10^4$, $EI = GJ = 500$. The disks have a point

mass $M = 10.0$ and an inertia matrix $\mathbf{J}_\rho = \text{diag}(200.0, 100.0, 100.0)$. The system is set into motion by applying a couple of out-of-plane force $F_z(t)$ and an in-plane force $F_x(t)$ with $F_x(t) = 2F_z(t)$. The beam was discretized using 10 beam elements and the disks were modeled with one-node element.

The example was analyzed using the four dynamic formulations. The nonlinear equation of motion was solved using the HHT α method with $\alpha = -0.01$. The following convergence criterion was adopted: the norm of the residual vector must be less than the prescribed tolerance $\varepsilon_f = 10^{-5}$. The time-step size $\Delta t = 0.10$ s was chosen and time histories for the displacements of the beam's lower right end were presented in Fig. 3.3. Since all formulations provided the same numerical results, the curves presented could be obtained with any of the formulations discussed.

Choice of the predictor

The four predictors described in Section 3.2 were compared with several time-step sizes. The exact tangent inertia matrices were used. The total numbers of iterations for the whole time history and for each formulation were given in Table 3.2.

Table 3.2: Number of iterations.

		Pred. 1	Pred. 2	Pred. 3	Pred. 4
Spat. Spin. Var.	$\Delta t = 0.25$ s	479	363	363	357
	$\Delta t = 0.10$ s	1181	902	901	878
Inc. Rot. V. 1	$\Delta t = 0.25$ s	479	363	363	357
	$\Delta t = 0.10$ s	1181	902	901	877
Inc. Rot. V. 2	$\Delta t = 0.25$ s	479	363	363	357
	$\Delta t = 0.10$ s	1181	902	897	877
Inc. Euler	$\Delta t = 0.25$ s	479	363	363	357
	$\Delta t = 0.10$ s	1181	902	897	877

Pred. 1 converged in all the cases, but required the largest number of iterations. In fact, this predictor assumes that the configuration of the structure does not change during a time step which does not happen in almost all cases.

In fact, for all the formulations, the best alternative was to use Pred. 4. The number of iterations was significantly smaller than for Pred. 1. This can be explained by the fact that Pred. 4 assumes linearity of the system during the time step. This is often a good approximation, especially with small time steps. In the sequel, only Pred. 4 was used in the numerical calculations.

Exact versus simplified dynamic tangent matrix and comparison of the four formulations

For each formulation, the exact tangent inertia matrix, the simplified matrix proposed by the author (Simpl. 1) and the one proposed by Geradin and Cardona (Simpl. 2) were tested. Table 3.3 showed the CPU time and the total number of iterations (in parentheses) for each formulation.

From the numerical results, it can be concluded that:

- For the first two formulations, Simpl. 2 was the slowest alternative. It increased the total number of iterations by about 25% to 38% compared with the exact matrix. In fact, for these formulations,

Table 3.3: Numerical performances.

	Spat. Spin. Var.	Inc. Rot. V. 1	Inc. Rot. V. 2	Inc. Euler
Exact	19.5 (878)	21.9 (877)	25.1 (877)	22.5 (877)
Simpl. 1	19.2 (885)	20.2 (882)	20.0 (881)	18.6 (881)
Simpl. 2	22.8 (1150)	23.8 (1140)	21.8 (1144)	21.1 (1154)

the tangent matrices do not require a lot of CPU time, so the CPU time gained by the simplification cannot compensate for the CPU time needed for the extra iterations. From the results, it was quite difficult to make a choice between the exact dynamic tangent matrix and the first simplification. The difference in terms of CPU time cost between these two matrices were small. The author recommended to use the exact tangent matrix with these two formulations.

- For the last two formulations, the best alternative was to use Simpl. 1 which reduced the CPU time by about 25% when compared to the exact matrix and by about 15% when compared to Simpl. 2.
- The formulation using the spatial Euler parameters with Simpl. 1 was the fastest.

Influence of the time-step size

The previous results showed that the formulation using the spatial Euler parameters with Simpl. 1 was the fastest. However, the example was solved with only one time-step size. To have a more complete view, the example was repeated with different time steps. The formulations Spat. Spin. Var. and Inc. Rot. V. 1 were implemented with the exact tangent inertia matrix. The other two formulations were implemented using Simpl. 1.

The results were presented in Table 3.4. They showed that the choice of time-step size did not affect the hierarchy between the formulations.

Table 3.4: Numerical performances with various time-step size.

	Spat. Spin. Var.	Inc. Rot. V. 1	Inc. Rot. V. 2	Inc. Euler
$\Delta t = 0.1$ s	19.5 (878)	21.9 (877)	20.0 (881)	18.6 (881)
$\Delta t = 0.5$ s	5.7 (239)	5.9 (237)	5.3 (239)	4.9 (239)

Chapter 4

3D corotational beam elements with solid cross-section

The purpose of this chapter is to present a 3D corotational element for dynamic analysis of beams with solid cross-sections. The corotational framework used in this chapter is the classic one proposed by Nour-Omid and Rankin [45, 50]. The main idea of the corotational method is to decompose the motion of the element into rigid body and pure deformational parts. During the rigid body motion, a local coordinates system, attached to the element, moves and rotates with it. The deformational part is measured in this local system. The main interest of the approach is that different assumptions can be made to represent the local deformations, giving rise to different possibilities for the local element formulation.

Several local formulations were proposed by Battini and Pacoste [8], and Alsafadie et al. [1] for the geometrically and materially static nonlinear analysis of beam structures with the corotational approach. The results of a comparative study of 3D beam formulations, which can be found in [1], showed that local beam elements based on cubic interpolations were more efficient and accurate than the ones which employ linear interpolations.

For 2D dynamics, Le et al. [37] developed a consistent 2D corotational beam element for nonlinear dynamics. Cubic interpolations were used to describe the local displacements and to derive both inertia and internal terms. Numerical results demonstrated that the formulation was more efficient than the classic formulations (i.e. with the constant Timoshenko and the constant lumped mass matrices).

For 3D dynamics, the possibility to use cubic interpolations to derive inertia terms is still an issue. Crisfield et al. [14] suggested to use a constant Timoshenko mass matrix along with local cubic interpolations to derive the internal force vector and the corresponding tangent stiffness matrix. As pointed out by Crisfield et al. [14], this combination is not consistent but it provides reasonable results when the number of elements is large enough. Hsiao et al. [24] presented a corotational formulation for the nonlinear analysis of 3D beams. However the corotational framework adopted in [24] was different from the classic one as proposed by Nour-Omid and Rankin [45] and adopted in [37]. Therefore, it is interesting to extend the consistent 2D corotational dynamic formulation presented in [37] to 3D beam structures. Such a beam element has been proposed in [39]. The novelty of this element is that the corotational framework has been used to derive not only the internal force vector and the tangent stiffness matrix but also the inertia force vector and the tangent dynamic matrix. The same cubic interpolations have been adopted to formulate both inertia and internal local terms. In doing so, the complex expressions of the inertia terms have been significantly simplified by adopting a proper approximation for the local rotations. To enhance the efficiency of the iterative procedure, the less significant term in the tangent dynamic matrix has been ignored. Four numerical examples have been investigated with the objective to compare the performances of the new formulation against two other approaches. The first approach is similar to the one presented above, but linear local interpolations, instead of cubic ones, are used to derive only the dynamic terms.

The purpose is to evaluate the influence of the choice of the local interpolations on the dynamic terms. The second approach is the classic total Lagrangian formulation proposed by Simo and Vu-Quoc [53–55].

The organisation of the chapter is as follows. Section 4.1 gives a complete presentation of the corotational beam kinematics in 3D. In Section 4.2 and 4.3, the global internal force vector and the tangent stiffness matrix are derived for different parameterizations of finite rotations. The local beam formulation is then given in Section 4.4. The content of Sections 4.1-4.4 are entirely taken from the work of Battini [5, 6]. They are reproduced here in order to make this thesis self-contained. Section 4.5 briefly presents the expressions of the inertia force vector and the tangent dynamic matrix. Finally, in Section 4.6, one example, reproduced from [39], is investigated.

4.1 Beam kinematics

In this work, the corotational framework introduced by Nour-Omid and Rankin [45], and further developed by Pacoste and Eriksson [49] and Battini and Pacoste [8] is fully adopted.

The definition of the corotational two node beam element involves several coordinate systems, see Fig. 4.1. First a global reference system is defined by the triad of unit orthogonal vectors $\mathbf{e}_j$ $(j = 1,2,3)$. Next, a local system which continuously rotates and translates with the element is selected. The orthonormal basis vectors of the local system are denoted by $\mathbf{r}_j$ $(j = 1,2,3)$. In the initial (undeformed) configuration, the local system is defined by the orthonormal triad $\mathbf{e}_j^o$. In addition, $\mathbf{t}_j^1$ and $\mathbf{t}_j^2$ $(j = 1,2,3)$, denote two unit triads rigidly attached to nodes 1 and 2.

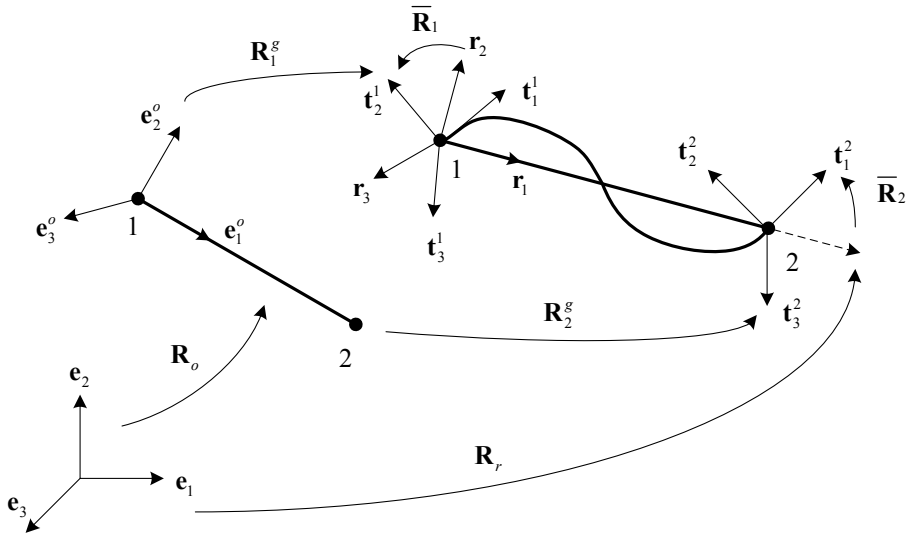

Fig. 4.1: Beam kinematics and the coordinate systems.

According to the main idea of the corotational formulation, the motion of the element from the initial to the final deformed configuration is split into a rigid body component and a deformational part. The rigid body motion consists of a rigid translation and rotation of the local element frame. The origin of the local system is taken at node 1 and thus the rigid translation is defined by $\mathbf{u}_1^g$, the translation at node 1. Here and in the sequel, superscript g indicates quantities expressed in the global reference system. The rigid rotation is such that the new orientation of the local reference system is defined by an orthogonal matrix $\mathbf{R}_r$, given by

$$\mathbf{R}_r = [\,\mathbf{r}_1\ \mathbf{r}_2\ \mathbf{r}_3\,]\,. \tag{4.1}$$

The first coordinate axis of the local system is defined by the line connecting nodes 1 and 2 of the element. Consequently, $\mathbf{r}_1$ is given by

$$\mathbf{r}_1 = \frac{\mathbf{x}_2^g + \mathbf{u}_2^g - \mathbf{x}_1^g - \mathbf{u}_1^g}{l_n}, \tag{4.2}$$

with $\mathbf{x}_i^g$ $(i = 1,2)$ denoting the nodal coordinates in the initial undeformed configuration and l_n denoting the current length of the beam, i.e.

$$l_n = \|\mathbf{x}_2^g + \mathbf{u}_2^g - \mathbf{x}_1^g - \mathbf{u}_1^g\|. \tag{4.3}$$

The remaining two axes are determined with the help of an auxiliary vector $\mathbf{p}$. In the initial configuration $\mathbf{p}$ is directed along the local $\mathbf{e}_2^o$ direction, whereas in the deformed configuration its orientation is obtained from

$$\mathbf{p} = \frac{1}{2}(\mathbf{p}_1 + \mathbf{p}_2), \qquad \mathbf{p}_i = \mathbf{R}_i^g \mathbf{R}_o [0\ 1\ 0]^{\mathrm{T}} \qquad (i = 1,2), \tag{4.4}$$

where $\mathbf{R}_i^g$ is the orthogonal matrix used to specify the orientation of the nodal triad $\mathbf{t}_j^i$, and $\mathbf{R}_o$ specifies the orientation of the local frame in the initial configuration, i.e. $\mathbf{R}_o = [\mathbf{e}_1^o\ \mathbf{e}_2^o\ \mathbf{e}_3^o]$. The unit vectors $\mathbf{r}_2$ and $\mathbf{r}_3$ are then computed by the following vector products

$$\mathbf{r}_3 = \frac{\mathbf{r}_1 \times \mathbf{p}}{\|\mathbf{r}_1 \times \mathbf{p}\|}, \qquad \mathbf{r}_2 = \mathbf{r}_3 \times \mathbf{r}_1, \tag{4.5}$$

and the orthogonal matrix $\mathbf{R}_r$ in Eq. (4.1) is completely determined.

The rigid motion previously described, is accompanied by local deformational displacements and rotations with respect to the local element axes. In this context, due to the particular choice of the local system, the local translations at node 1 are zero. Moreover, at node 2, the only non zero component is the translation along $\mathbf{r}_1$. This can easily be evaluated according to

$$\overline{u} = l_n - l_o, \tag{4.6}$$

with l_o denoting the length of the beam in the original undeformed configuration. Here and in the sequel, an overbar denotes a deformational kinematic quantity.

The global rotations at node i can be expressed in terms of the rigid rotation of the local axes, defined by $\mathbf{R}_r$, followed by a local rotation relative to these axes. The latter is defined by the orthogonal matrix $\overline{\mathbf{R}}_i$. Consequently, the orientation of the nodal triad $\mathbf{t}_j^i$ can be obtained by means of the product $\mathbf{R}_r \overline{\mathbf{R}}_i$. On the other hand, (see Fig. 4.1) this orientation can also be obtained through the product $\mathbf{R}_i^g \mathbf{R}_o$, which gives

$$\overline{\mathbf{R}}_i = \mathbf{R}_r^{\mathrm{T}} \mathbf{R}_i^g \mathbf{R}_o \qquad (i = 1,2). \tag{4.7}$$

The local rotations are then evaluated from

$$\overline{\boldsymbol{\theta}}_i = \log\left(\overline{\mathbf{R}}_i\right) \qquad (i = 1,2). \tag{4.8}$$

With respect to the moving frame, local (deformational) displacements $\mathbf{d}_l$ are defined by extracting the rigid body modes from the global displacements $\mathbf{d}_g^g$. Due to the choice of the local coordinate system, the local nodal displacement vector $\mathbf{d}_l$ has only seven components and is given by

$$\mathbf{d}_l = \left[\overline{u}\ \ \overline{\boldsymbol{\theta}}_1^{\mathrm{T}}\ \ \overline{\boldsymbol{\theta}}_2^{\mathrm{T}}\right]^{\mathrm{T}}. \tag{4.9}$$

The variation of the local nodal displacement vector is

$$\delta\mathbf{d}_l = \left[\delta\overline{u}\ \ \delta\overline{\boldsymbol{\theta}}_1^{\mathrm{T}}\ \ \delta\overline{\boldsymbol{\theta}}_2^{\mathrm{T}}\right]^{\mathrm{T}}, \tag{4.10}$$

and the global counterpart is given by

$$\delta\mathbf{d}_g = \left[\delta\mathbf{u}_1^{g\mathrm{T}}\ \ \delta\mathbf{w}_1^{g\mathrm{T}}\ \ \delta\mathbf{u}_2^{g\mathrm{T}}\ \ \delta\mathbf{w}_2^{g\mathrm{T}}\right]^{\mathrm{T}}, \tag{4.11}$$

with $\delta\mathbf{w}_i^g$ $(i=1,2)$ denoting spatial spin variables as defined in Eq. (3.7).

The connection between the variations of local and global displacements is defined by a transformation matrix $\mathbf{B}$

$$\delta\mathbf{d}_l = \mathbf{B}\,\delta\mathbf{d}_g\,. \tag{4.12}$$

The expression of $\mathbf{B}$ is derived using a sequence of two changes of variables, as described in the following subsections.

Change of variables $\delta\overline{\boldsymbol{\theta}} \longrightarrow \delta\overline{\mathbf{w}}$

The general procedure for evaluating the transformation matrix $\mathbf{B}$ involves the variations of Eqs. (4.6) and (4.7). Referring to Eq. (4.7), admissible variations $\delta\overline{\mathbf{R}}_i$ $(i=1,2)$ are computed (see Eq. (3.7)) according to

$$\delta\overline{\mathbf{R}}_i = \widetilde{\delta\overline{\mathbf{w}}_i}\,\overline{\mathbf{R}}_i\,, \tag{4.13}$$

with $\delta\overline{\mathbf{w}}_i$ denoted spatial spin variables.

The local rotational vector $\delta\overline{\boldsymbol{\theta}}_i$ is defined in Eq. (4.8). Using Eqs. (3.11), (4.8) and (4.13), the change of variables from $\delta\overline{\boldsymbol{\theta}}_i$ to $\delta\overline{\mathbf{w}}_i$ is given by

$$\delta\overline{\boldsymbol{\theta}} = \mathbf{T}_s^{-1}(\overline{\boldsymbol{\theta}})\,\delta\overline{\mathbf{w}}\,, \tag{4.14}$$

which, by introducing the notation

$$\delta\mathbf{d}_a = \left[\,\delta\overline{u}\;\;\delta\overline{\mathbf{w}}_1^{\mathrm{T}}\;\;\delta\overline{\mathbf{w}}_2^{\mathrm{T}}\,\right]^{\mathrm{T}}, \tag{4.15}$$

gives

$$\delta\mathbf{d}_l = \mathbf{B}_a\,\delta\mathbf{d}_a\,, \qquad \mathbf{B}_a = \begin{bmatrix} 1 & \mathbf{0}_{[1\times3]} & \mathbf{0}_{[1\times3]} \\ \mathbf{0}_{[3\times1]} & \mathbf{T}_s^{-1}(\overline{\boldsymbol{\theta}}_1) & \mathbf{0} \\ \mathbf{0}_{[3\times1]} & \mathbf{0} & \mathbf{T}_s^{-1}(\overline{\boldsymbol{\theta}}_2) \end{bmatrix}. \tag{4.16}$$

Here and in the sequel $\mathbf{0}_{[\mathrm{i}\times\mathrm{j}]}$ denotes an i $\times$ j zero matrix. For a 3x3 zero matrix the notation $\mathbf{0}$ is however used.

Change of variables $\delta\mathbf{d}_a \longrightarrow \delta\mathbf{d}_g$

The second step of the variable change involves $\delta\mathbf{d}_a$ and $\delta\mathbf{d}_g$, as defined in Eqs. (4.15) and (4.11), respectively.

Referring first to the local axial translation $\overline{u}$, the variations of Eq. (4.6) give

$$\delta\overline{u} = \delta l_n = \mathbf{r}\,\delta\mathbf{d}_g\,, \qquad \mathbf{r} = \left[\,-\mathbf{r}_1^{\mathrm{T}}\;\;\mathbf{0}_{[1\times3]}\;\;\mathbf{r}_1^{\mathrm{T}}\;\;\mathbf{0}_{[1\times3]}\,\right]. \tag{4.17}$$

For the rotational terms, the variations of Eq. (4.7) are needed

$$\delta\overline{\mathbf{R}}_i = \delta\mathbf{R}_r^{\mathrm{T}}\,\mathbf{R}_i^g\,\mathbf{R}_o + \mathbf{R}_r^{\mathrm{T}}\,\delta\mathbf{R}_i^g\,\mathbf{R}_o\,, \tag{4.18}$$

where $\delta\overline{\mathbf{R}}_i$ is defined in Eq. (4.13) whereas $\delta\mathbf{R}_i^g$ and $\delta\mathbf{R}_r$ are computed using the spatial form of Eq. (3.7), i.e.

$$\delta\mathbf{R}_i^g = \widetilde{\delta\mathbf{w}_i^g}\,\mathbf{R}_i^g\,, \qquad \delta\mathbf{R}_r = \widetilde{\delta\mathbf{w}_r^g}\,\mathbf{R}_r\,. \tag{4.19}$$

$\delta\mathbf{R}_r^{\mathrm{T}}$ is calculated from the orthogonality condition $\mathbf{R}_r\,\mathbf{R}_r^{\mathrm{T}} = \mathbf{I}$ which, by differentiation and introduction of Eq. (4.19) gives

$$\delta\mathbf{R}_r\,\mathbf{R}_r^{\mathrm{T}} + \mathbf{R}_r\,\delta\mathbf{R}_r^{\mathrm{T}} = 0\,, \tag{4.20}$$

$$\widetilde{\delta\mathbf{w}_r^g}\,\mathbf{R}_r\,\mathbf{R}_r^{\mathrm{T}} + \mathbf{R}_r\,\delta\mathbf{R}_r^{\mathrm{T}} = 0\,, \tag{4.21}$$

and then

$$\delta\mathbf{R}_r^{\mathrm{T}} = -\mathbf{R}_r^{\mathrm{T}}\,\widetilde{\delta\mathbf{w}_r^g}\,. \tag{4.22}$$

Using Eqs. (4.13), (4.19) and (4.22), Eq. (4.18) can be rewritten as

$$\begin{aligned}\widetilde{\delta\overline{\mathbf{w}}_i}\,\overline{\mathbf{R}}_i &= -\mathbf{R}_r^{\mathrm{T}}\,\widetilde{\delta\mathbf{w}_r^g}\,\mathbf{R}_i^g\,\mathbf{R}_o + \mathbf{R}_r^{\mathrm{T}}\,\widetilde{\delta\mathbf{w}_i^g}\,\mathbf{R}_i^g\,\mathbf{R}_o \\ &= -\mathbf{R}_r^{\mathrm{T}}\,\widetilde{\delta\mathbf{w}_r^g}\,\mathbf{R}_r\,\mathbf{R}_r^{\mathrm{T}}\,\mathbf{R}_i^g\,\mathbf{R}_o + \mathbf{R}_r^{\mathrm{T}}\,\widetilde{\delta\mathbf{w}_i^g}\,\mathbf{R}_r\,\mathbf{R}_r^{\mathrm{T}}\,\mathbf{R}_i^g\,\mathbf{R}_o \\ &= (\widetilde{\delta\mathbf{w}_i^e} - \widetilde{\delta\mathbf{w}_r^e})\,\overline{\mathbf{R}}_i\,,\end{aligned} \tag{4.23}$$

where use has been made of Eq. (4.7) and of the fact that $\mathbf{R}_r$ transforms a vector and a tensor from global to local coordinates according to

$$\mathbf{x}^e = \mathbf{R}_r^{\mathrm{T}}\,\mathbf{x}^g\,, \qquad \widetilde{\mathbf{x}}^e = \mathbf{R}_r^{\mathrm{T}}\,\widetilde{\mathbf{x}}^g\,\mathbf{R}_r\,. \tag{4.24}$$

Thus, Eq. (4.23) gives

$$\delta\overline{\mathbf{w}}_i = \delta\mathbf{w}_i^e - \delta\mathbf{w}_r^e \qquad (i=1,2)\,. \tag{4.25}$$

Further, let

$$\delta\mathbf{d}_g^e = \mathbf{E}^{\mathrm{T}}\,\delta\mathbf{d}_g\,, \qquad \mathbf{E} = \begin{bmatrix} \mathbf{R}_r & \mathbf{0} & \mathbf{0} & \mathbf{0} \\ \mathbf{0} & \mathbf{R}_r & \mathbf{0} & \mathbf{0} \\ \mathbf{0} & \mathbf{0} & \mathbf{R}_r & \mathbf{0} \\ \mathbf{0} & \mathbf{0} & \mathbf{0} & \mathbf{R}_r \end{bmatrix}. \tag{4.26}$$

Then, using the chain rule, $\delta\overline{\mathbf{w}}_i$ is evaluated as

$$\delta\overline{\mathbf{w}}_i = \frac{\partial\overline{\mathbf{w}}_i}{\partial\mathbf{d}_g^e}\,\frac{\partial\mathbf{d}_g^e}{\partial\mathbf{d}_g}\,\delta\mathbf{d}_g = \frac{\partial\overline{\mathbf{w}}_i}{\partial\mathbf{d}_g^e}\,\mathbf{E}^{\mathrm{T}}\,\delta\mathbf{d}_g \qquad (i=1,2)\,. \tag{4.27}$$

Substituting from Eq. (4.25) gives

$$\begin{bmatrix} \delta\overline{\mathbf{w}}_1 \\ \delta\overline{\mathbf{w}}_2 \end{bmatrix} = \left(\begin{bmatrix} \mathbf{0} & \mathbf{I} & \mathbf{0} & \mathbf{0} \\ \mathbf{0} & \mathbf{0} & \mathbf{0} & \mathbf{I} \end{bmatrix} - \begin{bmatrix} \mathbf{G}^{\mathrm{T}} \\ \mathbf{G}^{\mathrm{T}} \end{bmatrix} \right) \mathbf{E}^{\mathrm{T}}\,\delta\mathbf{d}_g = \mathbf{P}\mathbf{E}^{\mathrm{T}}\,\delta\mathbf{d}_g\,, \tag{4.28}$$

where the matrix $\mathbf{G}$ is defined by

$$\mathbf{G}^{\mathrm{T}} = \frac{\partial\mathbf{w}_r^e}{\partial\mathbf{d}_g^e}\,. \tag{4.29}$$

Hence, from Eqs. (4.17) and (4.28), the connection between $\delta\mathbf{d}_a$ and $\delta\mathbf{d}_g$ is given by

$$\delta\mathbf{d}_a = \mathbf{B}_g\,\delta\mathbf{d}_g\,, \qquad \mathbf{B}_g = \begin{bmatrix} \mathbf{r} \\ \mathbf{P}\mathbf{E}^{\mathrm{T}} \end{bmatrix}. \tag{4.30}$$

Expression of G

The expression of $\mathbf{G}$ is obtained from Eq. (4.19) which can be rewritten as

$$\widetilde{\delta\mathbf{w}_r^g} = \delta\mathbf{R}_r\,\mathbf{R}_r^{\mathrm{T}}\,. \tag{4.31}$$

and after the transformation (4.24) as

$$\widetilde{\delta\mathbf{w}_r}^{\,e} = \mathbf{R}_r^{\mathrm{T}}\,\delta\mathbf{R}_r\,. \tag{4.32}$$

From Eq. (4.1) and the above equation, it can easily be found that

$$\delta \mathbf{w}_r^e = \begin{bmatrix} \delta w_{r_1}^e \\ \delta w_{r_2}^e \\ \delta w_{r_3}^e \end{bmatrix} = \begin{bmatrix} -\mathbf{r}_2^{\mathrm{T}}\, \delta \mathbf{r}_3 \\ -\mathbf{r}_3^{\mathrm{T}}\, \delta \mathbf{r}_1 \\ \mathbf{r}_2^{\mathrm{T}}\, \delta \mathbf{r}_1 \end{bmatrix} . \tag{4.33}$$

Introducing the notation $\mathbf{u}_i^g = \left[u_{i1}^g \; u_{i2}^g \; u_{i3}^g \right]^{\mathrm{T}}$ $(i = 1,2)$, differentiation of Eq. (4.2) gives

$$\delta \mathbf{r}_1^g = \frac{1}{l_n} \left[\mathbf{I} - \mathbf{r}_1 \mathbf{r}_1^{\mathrm{T}} \right] \begin{bmatrix} \delta u_{21}^g - \delta u_{11}^g \\ \delta u_{22}^g - \delta u_{12}^g \\ \delta u_{23}^g - \delta u_{13}^g \end{bmatrix} , \tag{4.34}$$

and after transformation (4.24) in the local coordinate system, it is obtained

$$\delta \mathbf{r}_1^e = \frac{1}{l_n} \begin{bmatrix} \delta u_{21}^e - \delta u_{11}^e \\ \delta u_{22}^e - \delta u_{12}^e \\ \delta u_{23}^e - \delta u_{13}^e \end{bmatrix} . \tag{4.35}$$

Hence, since the local expressions of $\mathbf{r}_2$ and $\mathbf{r}_3$ are $[0\;1\;0]^{\mathrm{T}}$ and $[0\;0\;1]^{\mathrm{T}}$, Eq. (4.33) gives

$$\delta w_{r_2}^e = \frac{1}{l_n} \left(\delta u_{13}^e - \delta u_{23}^e \right) , \tag{4.36}$$

$$\delta w_{r_3}^e = \frac{1}{l_n} \left(\delta u_{22}^e - \delta u_{12}^e \right) . \tag{4.37}$$

The evaluation of $\delta w_{r_1}^e$ is more complicated and can be performed as follows. Differentiation of Eq. (4.4) gives

$$\begin{aligned} \delta \mathbf{p} &= \frac{1}{2} (\delta \mathbf{R}_1^g + \delta \mathbf{R}_2^g)\, \mathbf{R}_o\, [0\;1\;0]^{\mathrm{T}} \\ &= \frac{1}{2} (\widetilde{\delta \mathbf{w}_1^g}\, \mathbf{R}_1^g + \widetilde{\delta \mathbf{w}_2^g}\, \mathbf{R}_2^g)\, \mathbf{R}_o\, [0\;1\;0]^{\mathrm{T}} \\ &= \frac{1}{2} (\widetilde{\delta \mathbf{w}_1^g}\, \mathbf{p}_1 + \widetilde{\delta \mathbf{w}_2^g}\, \mathbf{p}_2) . \end{aligned} \tag{4.38}$$

The local expressions of the vectors $\mathbf{p}$, $\mathbf{p}_1$ and $\mathbf{p}_2$ are denoted by

$$\mathbf{R}_r^{\mathrm{T}} \mathbf{p} = \begin{bmatrix} p_1 \\ p_2 \\ 0 \end{bmatrix} , \qquad \mathbf{R}_r^{\mathrm{T}} \mathbf{p}_1 = \begin{bmatrix} p_{11} \\ p_{12} \\ p_{13} \end{bmatrix} , \qquad \mathbf{R}_r^{\mathrm{T}} \mathbf{p}_2 = \begin{bmatrix} p_{21} \\ p_{22} \\ p_{23} \end{bmatrix} . \tag{4.39}$$

The last coordinate of $\mathbf{R}_r^{\mathrm{T}} \mathbf{p}$ is zero since $\mathbf{p}$ is perpendicular to $\mathbf{r}_3$.

The local expression of $\delta \mathbf{p}$ can be deduced from Eq. (4.38) as

$$\delta\mathbf{p}^e = \frac{1}{2}\widetilde{\delta\mathbf{w}_1^e}\begin{bmatrix} p_{11} \\ p_{12} \\ p_{13} \end{bmatrix} + \frac{1}{2}\widetilde{\delta\mathbf{w}_2^e}\begin{bmatrix} p_{21} \\ p_{22} \\ p_{23} \end{bmatrix}, \tag{4.40}$$

which after calculation gives

$$\delta\mathbf{p}^e = \frac{1}{2}\begin{bmatrix} -\,p_{12}\,\delta w_{13}^e & +\,p_{13}\,\delta w_{12}^e & -\,p_{22}\,\delta w_{23}^e & +\,p_{23}\,\delta w_{22}^e \\ +\,p_{11}\,\delta w_{13}^e & -\,p_{13}\,\delta w_{11}^e & +\,p_{21}\,\delta w_{23}^e & -\,p_{23}\,\delta w_{21}^e \\ -\,p_{11}\,\delta w_{12}^e & +\,p_{12}\,\delta w_{11}^e & -\,p_{21}\,\delta w_{22}^e & +\,p_{22}\,\delta w_{21}^e \end{bmatrix}. \tag{4.41}$$

The following notations are introduced

$$\eta = \frac{p_1}{p_2}, \qquad \eta_{11} = \frac{p_{11}}{p_2}, \qquad \eta_{12} = \frac{p_{12}}{p_2}, \qquad \eta_{21} = \frac{p_{21}}{p_2}, \qquad \eta_{22} = \frac{p_{22}}{p_2}. \tag{4.42}$$

The differentiation of $\mathbf{r}_3$ is calculated from its definition (4.5). By noting that $\|\mathbf{r}_1 \times \mathbf{p}\| = p_2$, the first line of Eq. (4.33) can be rewritten as

$$\delta w_{r_1}^e = -\frac{\mathbf{r}_2^{\mathrm{T}}}{p_2}\,\delta\mathbf{r}_1^e \times \mathbf{p} - \frac{\mathbf{r}_2^{\mathrm{T}}}{p_2}\,\mathbf{r}_1 \times \delta\mathbf{p}^e - \delta\left(\frac{1}{p_2}\right)\mathbf{r}_2^{\mathrm{T}}\left(\mathbf{r}_1 \times \mathbf{p}\right). \tag{4.43}$$

The last term in the above equation is zero. The two other terms can be evaluated from Eqs. (4.35), (4.39) and (4.41). The result, after some work, is

$$\delta w_{r_1}^e = \frac{\eta}{l_n}\left(\delta w_1^e - \delta w_2^e\right) - \frac{\eta_{11}}{2}\,\delta w_{12}^e + \frac{\eta_{12}}{2}\,\delta w_{11}^e - \frac{\eta_{21}}{2}\,\delta w_{22}^e + \frac{\eta_{22}}{2}\,\delta w_{21}^e. \tag{4.44}$$

Finally, the expression for the matrix $\mathbf{G}$ is

$$\mathbf{G}^{\mathrm{T}} = \begin{bmatrix} 0 & 0 & \frac{\eta}{l_n} & \frac{\eta_{12}}{2} & -\frac{\eta_{11}}{2} & 0 & 0 & 0 & -\frac{\eta}{l_n} & \frac{\eta_{22}}{2} & -\frac{\eta_{21}}{2} & 0 \\ 0 & 0 & \frac{1}{l_n} & 0 & 0 & 0 & 0 & 0 & -\frac{1}{l_n} & 0 & 0 & 0 \\ 0 & -\frac{1}{l_n} & 0 & 0 & 0 & 0 & 0 & \frac{1}{l_n} & 0 & 0 & 0 & 0 \end{bmatrix}. \tag{4.45}$$

4.2 Global internal force vector and tangent stiffness matrix

The expression of the internal force vector in global coordinates $\mathbf{f}_g$, can be obtained by equating the internal virtual work in both the global and local systems

$$V = \delta\mathbf{d}_l^{\mathrm{T}}\,\mathbf{f}_l = \delta\mathbf{d}_g^{\mathrm{T}}\,\mathbf{f}_g. \tag{4.46}$$

Substituting Eq. (4.12) into the previous, provides the result of interest

$$\mathbf{f}_g = \mathbf{B}^{\mathrm{T}}\,\mathbf{f}_l. \tag{4.47}$$

The local internal force vector is defined as

$$\mathbf{f}_l = \begin{bmatrix} n & \mathbf{m}_1^{\mathrm{T}} & \mathbf{m}_2^{\mathrm{T}} \end{bmatrix}^{\mathrm{T}}, \tag{4.48}$$

where n denotes the axial force whereas $\mathbf{m}_1$ and $\mathbf{m}_2$ denote the moments at nodes 1 and 2, respectively.

The expression of the tangent stiffness matrix in global coordinates $\mathbf{K}_g$, is obtained by taking the variations of Eq. (4.47), which gives

$$\mathbf{K}_g = \mathbf{B}^{\mathrm{T}}\,\mathbf{K}_l\,\mathbf{B} + \left.\frac{\partial(\mathbf{B}^{\mathrm{T}}\mathbf{f}_l)}{\partial \mathbf{d}_g}\right|_{\mathbf{f}_l}. \tag{4.49}$$

In Eqs. (4.47) and (4.49), $\mathbf{B}$ and $\partial(\mathbf{B}^{\mathrm{T}}\mathbf{f}_l)/\partial\mathbf{d}_g$ play the role of transformation matrices required in order to re-express $\mathbf{f}_l$ and $\mathbf{K}_l$ in global coordinates. These matrices, which actually define the corotational framework, depend on the nonlinear functions in Eq. (4.46) and thus on the choice of the local coordinate system. However, they are independent of the particular strain definition used in order to derive $\mathbf{f}_l$ and $\mathbf{K}_l$. Consequently, various corotational elements defined using different local strain assumptions but the same type of local coordinate system will share the same transformation matrices, i.e. the corotational formulation is "element independent" [45]. Using this property, various local assumptions can be placed at the core of the corotational formulation and tested for efficiency and accuracy.

As shown in Section 4.2, the change of variables from $\mathbf{d}_l$ to $\mathbf{d}_g$ must be performed in two steps, therefore the transformations in Eqs. (4.47) and (4.49) are also derived using these two steps, as described in the following.

A virtual work equation gives

$$\mathbf{f}_a = \mathbf{B}_a^{\mathrm{T}}\,\mathbf{f}_l\,, \tag{4.50}$$

with $\mathbf{f}_a$ denoting the internal force vector consistent with $\delta\mathbf{d}_a$. The corresponding transformation for the local tangent stiffness matrices, i.e. $\mathbf{K}_l$ and $\mathbf{K}_a$, is obtained by taking the variation of Eq. (4.50)

$$\delta\mathbf{f}_a = \mathbf{B}_a^{\mathrm{T}}\,\delta\mathbf{f}_l + \delta\mathbf{B}_a^{\mathrm{T}}\,\mathbf{f}_l\,, \tag{4.51}$$

where, by definition

$$\delta\mathbf{f}_l = \mathbf{K}_l\,\delta\mathbf{d}_l\,, \qquad \delta\mathbf{f}_a = \mathbf{K}_a\,\delta\mathbf{d}_a\,. \tag{4.52}$$

Using Eqs. (4.16), (4.51) and (4.52) gives the required transformation

$$\mathbf{K}_a = \mathbf{B}_a^{\mathrm{T}}\,\mathbf{K}_l\,\mathbf{B}_a + \mathbf{K}_h\,, \qquad \mathbf{K}_h = \begin{bmatrix} 0 & \mathbf{0}_{[1\times3]} & \mathbf{0}_{[1\times3]} \\ \mathbf{0}_{[3\times1]} & \mathbf{K}_{h1} & \mathbf{0} \\ \mathbf{0}_{[3\times1]} & \mathbf{0} & \mathbf{K}_{h2} \end{bmatrix}. \tag{4.53}$$

The expressions of $\mathbf{K}_{h1}$ and $\mathbf{K}_{h2}$ are computed from

$$\frac{\partial}{\partial\overline{\mathbf{w}}}\left[\mathbf{T}_s^{-\mathrm{T}}\mathbf{x}\right] = \frac{\partial}{\partial\overline{\boldsymbol{\theta}}}\left[\mathbf{T}_s^{-\mathrm{T}}\mathbf{x}\right]\frac{\partial\overline{\boldsymbol{\theta}}}{\partial\overline{\mathbf{w}}} = \frac{\partial}{\partial\overline{\boldsymbol{\theta}}}\left[\mathbf{T}_s^{-\mathrm{T}}\mathbf{x}\right]\mathbf{T}_s^{-1}\,, \tag{4.54}$$

with the vector $\mathbf{x}$ maintained constant during differentiation. Using Eq. (3.7) gives after some algebra

$$\frac{\partial}{\partial\overline{\mathbf{w}}}\left[\mathbf{T}_s^{-\mathrm{T}}\mathbf{x}\right] = \left[\eta\left[\overline{\boldsymbol{\theta}}\,\mathbf{x}^{\mathrm{T}} - 2\,\mathbf{x}\overline{\boldsymbol{\theta}}^{\mathrm{T}} + (\overline{\boldsymbol{\theta}}^{\mathrm{T}}\cdot\mathbf{x})\,\mathbf{I}\right] + \mu\,\widetilde{\overline{\boldsymbol{\theta}}}^{2}\left[\mathbf{x}\overline{\boldsymbol{\theta}}^{\mathrm{T}}\right] - \frac{1}{2}\widetilde{\mathbf{x}}\right]\mathbf{T}_s^{-1}(\overline{\boldsymbol{\theta}})\,, \tag{4.55}$$

with the coefficients η and μ given by

$$\eta = \frac{2\sin\overline{\theta} - \overline{\theta}\,(1+\cos\overline{\theta})}{2\,\overline{\theta}^{2}\sin\overline{\theta}}\,, \quad \mu = \frac{\overline{\theta}\,(\overline{\theta}+\sin\overline{\theta}) - 8\sin^{2}(\overline{\theta}/2)}{4\,\overline{\theta}^{4}\sin^{2}(\overline{\theta}/2)}\,. \tag{4.56}$$

Thus, $\mathbf{K}_{hi}$ $(i=1,2)$ are evaluated from Eq. (4.55) with $\overline{\boldsymbol{\theta}} = \overline{\boldsymbol{\theta}}_i$ and $\mathbf{x} = \mathbf{m}_i$, with $\mathbf{m}_i$ as defined in Eq. (4.48).

Using Eq. (4.30), the internal force vector in global coordinates is computed as

$$\mathbf{f}_g = \mathbf{B}_g^{\mathrm{T}}\,\mathbf{f}_a\,. \tag{4.57}$$

Note that, according to the sequence of variable changes previously defined, the matrix $\mathbf{B}$ in Eq. (4.46) is explicitly given by the product $\mathbf{B}_a\mathbf{B}_g$.

Differentiation of Eq. (4.57) gives

$$\delta\mathbf{f}_g = \mathbf{B}_g^{\mathrm{T}}\mathbf{K}_a\mathbf{B}_g\,\delta\mathbf{d}_g + \delta\mathbf{r}^{\mathrm{T}} f_{a_1} + \delta(\mathbf{E}\mathbf{P}^{\mathrm{T}})\,\mathbf{m}\,, \tag{4.58}$$

with

$$\mathbf{m} = \begin{bmatrix} f_{a_2} & f_{a_3} & f_{a_4} & f_{a_5} & f_{a_6} & f_{a_7} \end{bmatrix}^{\mathrm{T}}, \tag{4.59}$$

where f_{a_i} $(i = 1..7)$ denotes the i^{th} component of the vector $\mathbf{f}_a$.

From Eqs. (4.17) and (4.34), it can easily be derived that

$$\delta\mathbf{r}^{\mathrm{T}} = \mathbf{D}\,\delta\mathbf{d}_g\,, \qquad \mathbf{D} = \begin{bmatrix} \mathbf{D}_3 & \mathbf{0} & -\mathbf{D}_3 & \mathbf{0} \\ \mathbf{0} & \mathbf{0} & \mathbf{0} & \mathbf{0} \\ -\mathbf{D}_3 & \mathbf{0} & \mathbf{D}_3 & \mathbf{0} \\ \mathbf{0} & \mathbf{0} & \mathbf{0} & \mathbf{0} \end{bmatrix}, \qquad \mathbf{D}_3 = \frac{1}{l_n}(\mathbf{I} - \mathbf{r}_1\,\mathbf{r}_1^{\mathrm{T}})\,. \tag{4.60}$$

The last term in expression (4.58) is evaluated from

$$\delta(\mathbf{E}\mathbf{P}^{\mathrm{T}})\,\mathbf{m} = \delta\mathbf{E}\mathbf{P}^{\mathrm{T}}\mathbf{m} + \mathbf{E}\,\delta\mathbf{P}^{\mathrm{T}}\mathbf{m}\,. \tag{4.61}$$

By introducing

$$\mathbf{P}^{\mathrm{T}}\mathbf{m} = \begin{bmatrix} \mathbf{n}_1 \\ \mathbf{m}_1 \\ \mathbf{n}_2 \\ \mathbf{m}_2 \end{bmatrix}, \tag{4.62}$$

and using Eqs. (4.26) and (4.32), the first term in Eq. (4.61) can be expressed as

$$\delta\mathbf{E}\mathbf{P}^{\mathrm{T}}\mathbf{m} = \begin{bmatrix} \mathbf{R}_r\,\widetilde{\delta\mathbf{w}_r^e} & \mathbf{0} & \mathbf{0} & \mathbf{0} \\ \mathbf{0} & \mathbf{R}_r\,\widetilde{\delta\mathbf{w}_r^e} & \mathbf{0} & \mathbf{0} \\ \mathbf{0} & \mathbf{0} & \mathbf{R}_r\,\widetilde{\delta\mathbf{w}_r^e} & \mathbf{0} \\ \mathbf{0} & \mathbf{0} & \mathbf{0} & \mathbf{R}_r\,\widetilde{\delta\mathbf{w}_r^e} \end{bmatrix} \begin{bmatrix} \mathbf{n}_1 \\ \mathbf{m}_1 \\ \mathbf{n}_2 \\ \mathbf{m}_2 \end{bmatrix} = \mathbf{E} \begin{bmatrix} \widetilde{\delta\mathbf{w}_r^e}\,\mathbf{n}_1 \\ \widetilde{\delta\mathbf{w}_r^e}\,\mathbf{m}_1 \\ \widetilde{\delta\mathbf{w}_r^e}\,\mathbf{n}_2 \\ \widetilde{\delta\mathbf{w}_r^e}\,\mathbf{m}_2 \end{bmatrix}. \tag{4.63}$$

which, using the relation

$$\widetilde{\mathbf{a}}\,\mathbf{b} = -\widetilde{\mathbf{b}}\,\mathbf{a}\,, \tag{4.64}$$

gives

$$\delta\mathbf{E}\mathbf{P}^{\mathrm{T}}\mathbf{m} = -\mathbf{E}\mathbf{Q}\,\delta\mathbf{w}_r^e\,, \qquad \mathbf{Q} = \begin{bmatrix} \widetilde{\mathbf{n}}_1 \\ \widetilde{\mathbf{m}}_1 \\ \widetilde{\mathbf{n}}_2 \\ \widetilde{\mathbf{m}}_2 \end{bmatrix}. \tag{4.65}$$

Then, by using Eq. (4.45), it is obtained

$$\delta\mathbf{E}\mathbf{P}^{\mathrm{T}}\mathbf{m} = -\mathbf{E}\mathbf{Q}\mathbf{G}^{\mathrm{T}}\mathbf{E}^{\mathrm{T}}\,\delta\mathbf{d}_g\,. \tag{4.66}$$

The calculation of the second term of Eq. (4.61) requires the value of $\delta\mathbf{P}^{\mathrm{T}}$ which can be obtained by introducing the matrix $\mathbf{A}$ such as

$$\mathbf{A}^{\mathrm{T}} = \begin{bmatrix} 0 & 0 & 0 & 0 & 0 & 0 & 0 & 0 & 0 & 0 & 0 & 0 \\ 0 & 0 & 0 & 0 & 0 & 0 & 0 & 0 & -l_n & 0 & 0 & 0 \\ 0 & 0 & 0 & 0 & 0 & 0 & 0 & l_n & 0 & 0 & 0 & 0 \end{bmatrix}, \tag{4.67}$$

and by noting that

$$\mathbf{A}^{\mathrm{T}}\mathbf{G} = \mathbf{I}. \tag{4.68}$$

Differentiation of the above equation gives

$$\delta\mathbf{A}^{\mathrm{T}}\mathbf{G} + \mathbf{A}^{\mathrm{T}}\delta\mathbf{G} = \mathbf{0}, \tag{4.69}$$

and hence

$$\delta\mathbf{G} = -\mathbf{A}^{-\mathrm{T}}\delta\mathbf{A}^{\mathrm{T}}\mathbf{G} = -\mathbf{G}\,\delta\mathbf{A}^{\mathrm{T}}\mathbf{G}. \tag{4.70}$$

Further, using the definition of $\mathbf{P}$ in Eq. (4.28) gives

$$\delta\mathbf{P} = -\mathbf{C}\,\delta\mathbf{G}^{\mathrm{T}}, \qquad \mathbf{C} = \begin{bmatrix} \mathbf{I} \\ \mathbf{I} \end{bmatrix}, \tag{4.71}$$

which can be rewritten as

$$\delta\mathbf{P}^{\mathrm{T}} = -\delta\mathbf{G}\,\mathbf{C}^{\mathrm{T}} = \mathbf{G}\,\delta\mathbf{A}^{\mathrm{T}}\mathbf{G}\,\mathbf{C}^{\mathrm{T}}. \tag{4.72}$$

Then, the second term of Eq. (4.61) becomes

$$\mathbf{E}\,\delta\mathbf{P}^{\mathrm{T}}\mathbf{m} = \mathbf{E}\mathbf{G}\,\delta\mathbf{A}^{\mathrm{T}}\mathbf{G}\,\mathbf{C}^{\mathrm{T}}\mathbf{m}, \tag{4.73}$$

which can be simplified after symbolic matrix multiplications as

$$\mathbf{E}\,\delta\mathbf{P}^{\mathrm{T}}\mathbf{m} = \mathbf{E}\mathbf{G}\mathbf{a}\,\delta l_n, \tag{4.74}$$

with

$$\mathbf{a} = \begin{bmatrix} 0 \\ \dfrac{\eta}{l_n}\left(f_{a_2} + f_{a_5}\right) - \dfrac{1}{l_n}\left(f_{a_3} + f_{a_6}\right) \\ \dfrac{1}{l_n}\left(f_{a_4} + f_{a_7}\right) \end{bmatrix}. \tag{4.75}$$

Introducing Eq. (4.17) in Eq. (4.74) gives

$$\mathbf{E}\,\delta\mathbf{P}^{\mathrm{T}}\mathbf{m} = \mathbf{E}\mathbf{G}\mathbf{a}\mathbf{r}\,\delta\mathbf{d}_g. \tag{4.76}$$

Finally, from Eqs. (4.58), (4.61), (4.66) and (4.76) the expression of the global tangent stiffness matrix is

$$\mathbf{K}_g = \mathbf{B}_g^{\mathrm{T}}\mathbf{K}_a\mathbf{B}_g + \mathbf{K}_m, \qquad \mathbf{K}_m = \mathbf{D}\,f_{a_1} - \mathbf{E}\mathbf{Q}\mathbf{G}^{\mathrm{T}}\mathbf{E}^{\mathrm{T}} + \mathbf{E}\mathbf{G}\mathbf{a}\mathbf{r}. \tag{4.77}$$

4.3 Finite rotation parameters

When the spin variables are chosen to represent the finite rotations, the global internal force vector and the tangent stiffness matrix are calculated as given in previous section. When another parametrization of the finite rotations is used, a change of variables is required. In this section, such changes of variables for spatial incremental rotational vector and spatial incremental Euler parameters are presented. These two parameterizations were presented in Section 3.1 and used for the second and the third formulations in [38].

Spatial incremental rotational vector

Let $\mathbf{d}_r^g$ denote the following vector of global nodal displacements

$$\mathbf{d}_r^g = \left[\mathbf{u}_1^{g\mathrm{T}}\ \ \boldsymbol{\theta}_1^{g\mathrm{T}}\ \ \mathbf{u}_2^{g\mathrm{T}}\ \ \boldsymbol{\theta}_2^{g\mathrm{T}}\right]^{\mathrm{T}}, \tag{4.78}$$

where $\boldsymbol{\theta}_i^g$ denotes the spatial incremental rotational vector at node i. The change to the new kinematic variables in $\mathbf{d}_r^g$ requires the connection between $\delta\mathbf{d}_g$ as defined in Eq. (4.11) and $\delta\mathbf{d}_r^g$. This connection can easily be constructed using Eq. (3.8)

$$\delta\mathbf{d}_g = \mathbf{B}_r\,\delta\mathbf{d}_r^g\,, \qquad \mathbf{B}_r = \begin{bmatrix} \mathbf{I} & \mathbf{0} & \mathbf{0} & \mathbf{0} \\ \mathbf{0} & \mathbf{T}_s(\boldsymbol{\theta}_1^g) & \mathbf{0} & \mathbf{0} \\ \mathbf{0} & \mathbf{0} & \mathbf{I} & \mathbf{0} \\ \mathbf{0} & \mathbf{0} & \mathbf{0} & \mathbf{T}_s(\boldsymbol{\theta}_2^g) \end{bmatrix}. \tag{4.79}$$

The global internal force vector $\mathbf{f}_r$ and tangent stiffness matrix $\mathbf{K}_r$, consistent with $\mathbf{d}_r^g$, are then given by

$$\mathbf{f}_r = \mathbf{B}_r^{\mathrm{T}}\mathbf{f}_g\,, \qquad \mathbf{K}_r = \mathbf{B}_r^{\mathrm{T}}\mathbf{K}_g\mathbf{B}_r + \mathbf{K}_v\,, \tag{4.80}$$

where

$$\mathbf{K}_v = \begin{bmatrix} \mathbf{0} & \mathbf{0} & \mathbf{0} & \mathbf{0} \\ \mathbf{0} & \mathbf{K}_{v1} & \mathbf{0} & \mathbf{0} \\ \mathbf{0} & \mathbf{0} & \mathbf{0} & \mathbf{0} \\ \mathbf{0} & \mathbf{0} & \mathbf{0} & \mathbf{K}_{v2} \end{bmatrix}. \tag{4.81}$$

The expressions of $\mathbf{K}_{v1}$ and $\mathbf{K}_{v2}$ are obtained from

$$\begin{aligned} \frac{\partial}{\partial\boldsymbol{\theta}}[\mathbf{T}_s^{\mathrm{T}}\mathbf{x}] = &-\left(\frac{\sin\theta}{\theta} - \left(\frac{\sin(\theta/2)}{(\theta/2)}\right)^2\right)(\mathbf{n}\times\mathbf{x})\,\mathbf{n}^{\mathrm{T}} + \frac{1}{2}\left(\frac{\sin(\theta/2)}{(\theta/2)}\right)^2\widetilde{\mathbf{x}} \\ &+\left(\cos\theta - \frac{\sin\theta}{\theta}\right)\frac{1}{\theta}\left[\mathbf{x}\mathbf{n}^{\mathrm{T}} - (\mathbf{n}^{\mathrm{T}}\mathbf{x})\mathbf{n}\mathbf{n}^{\mathrm{T}}\right] \\ &+\left(1 - \frac{\sin\theta}{\theta}\right)\frac{1}{\theta}\left[\mathbf{n}\mathbf{x}^{\mathrm{T}} - 2\,(\mathbf{n}^{\mathrm{T}}\mathbf{x})\mathbf{n}\mathbf{n}^{\mathrm{T}} + (\mathbf{n}^{\mathrm{T}}\mathbf{x})\,\mathbf{I}\right], \end{aligned} \tag{4.82}$$

with the vector $\mathbf{x}$ maintained constant during the differentiation.

Thus, $\mathbf{K}_{v1}$ and $\mathbf{K}_{v2}$ are evaluated from Eq. (4.82) with $\boldsymbol{\theta} = \boldsymbol{\theta}_1^g$ and $\boldsymbol{\theta} = \boldsymbol{\theta}_2^g$, respectively and $\mathbf{x} = \begin{bmatrix} f_{g_4} & f_{g_5} & f_{g_6} \end{bmatrix}^{\mathrm{T}}$, $\mathbf{x} = \begin{bmatrix} f_{g_{10}} & f_{g_{11}} & f_{g_{12}} \end{bmatrix}^{\mathrm{T}}$, respectively.

Spatial incremental Euler parameters

The transformation matrices required in this second case are constructed on the basis of Eq. (3.13) which provides the connection between $\delta\mathbf{w}^g$ and $\delta\mathbf{q}^g$. Following a procedure entirely similar to that used in the preceding subsection, the vector $\mathbf{d}_r^g$ is now defined as

$$\mathbf{d}_r^g = \left[\mathbf{u}_1^{g\mathrm{T}}\ \ \mathbf{q}_1^{g\mathrm{T}}\ \ \mathbf{u}_2^{g\mathrm{T}}\ \ \mathbf{q}_2^{g\mathrm{T}}\right]^{\mathrm{T}}, \tag{4.83}$$

where $\mathbf{q}_i^g$ denotes the incremental Euler parameters at node i. The transformation equations for the internal force vector and the tangent stiffness matrix are formally identical to Eqs. (4.79)-(4.81), by replacing $\mathbf{T}_s(\boldsymbol{\theta}_i^g)$ with $\mathbf{T}_q(\mathbf{q}_i^g)$.

In this case, the matrices $\mathbf{K}_{vi}$ are evaluated with $\mathbf{q} = \mathbf{q}_i^g$ $(i = 1,2)$ and $\mathbf{x} = \begin{bmatrix} f_{g_4} & f_{g_5} & f_{g_6} \end{bmatrix}^{\mathrm{T}}$, $\mathbf{x} = \begin{bmatrix} f_{g_{10}} & f_{g_{11}} & f_{g_{12}} \end{bmatrix}^{\mathrm{T}}$, respectively, from

$$\mathbf{K}_{vi} = \frac{1}{16\,q_o^3}\,\mathbf{H}. \tag{4.84}$$

The components of $\mathbf{H}$ are

$$\begin{aligned}
&A = (q_1 x_1 + q_2 x_2 + q_3 x_3), \quad H_{11} = (4q_o^2 + q_1^2)A,\\
&H_{22} = (4q_o^2 + q_2^2)A, \quad H_{33} = (4q_o^2 + q_3^2)A,\\
&H_{12} = 4q_o^2(q_1 x_2 - q_2 x_1 - q_o x_3) + q_1 q_2 A,\\
&H_{13} = 4q_o^2(q_1 x_3 - q_3 x_1 + q_o x_2) + q_1 q_3 A,\\
&H_{21} = 4q_o^2(q_2 x_1 - q_1 x_2 + q_o x_3) + q_2 q_1 A,\\
&H_{23} = 4q_o^2(q_2 x_3 - q_3 x_2 - q_o x_1) + q_2 q_3 A,\\
&H_{31} = 4q_o^2(q_3 x_1 - q_1 x_3 - q_o x_2) + q_3 q_1 A,\\
&H_{32} = 4q_o^2(q_3 x_2 - q_2 x_3 + q_o x_1) + q_3 q_2 A,
\end{aligned} \tag{4.85}$$

where x_j $(j = 1,2,3)$ are components of $\mathbf{x}$.

4.4 Local internal force vector and tangent stiffness matrix

The purpose of this section is to define the internal force vector $\mathbf{f}_l$ and tangent stiffness matrix $\mathbf{K}_l$ in local coordinates.

Assuming elastic material behavior, $\mathbf{f}_l$ and $\mathbf{K}_l$ can be derived from the strain energy Φ expressed as a function of the local displacements $\mathbf{d}_l$, through successive differentiations

$$\mathbf{f}_l = \frac{\partial \Phi}{\partial \mathbf{d}_l}, \qquad \mathbf{K}_l = \frac{\partial^2 \Phi}{\partial \mathbf{d}_l^2}. \tag{4.86}$$

As a general rule, all kinematic quantities are referred to the local element frame $\mathbf{r}_i$ $(i = 1,2,3)$, as defined in Eqs. (4.2), (4.4) and (4.5). The origin of the local system is taken at node 1 with $\mathbf{r}_1$ directed along the line of centroids. However $\mathbf{r}_2$ and $\mathbf{r}_3$ are not necessarily directed along the principal axes of the cross-section.

With respect to the local system, the Green-Lagrange strain components which contribute to the strain energy of the beam are given by

$$\begin{aligned}
\varepsilon_{11} &= u_{1,x} + \frac{1}{2}u_{1,x}^2 + \frac{1}{2}u_{2,x}^2 + \frac{1}{2}u_{3,x}^2,\\
2\varepsilon_{12} &= u_{1,y} + u_{2,x} + u_{1,x}u_{1,y} + u_{2,x}u_{2,y} + u_{3,x}u_{3,y},\\
2\varepsilon_{13} &= u_{1,z} + u_{3,x} + u_{1,x}u_{1,z} + u_{2,x}u_{2,z} + u_{3,x}u_{3,z},
\end{aligned} \tag{4.87}$$

where u_1, u_2, u_3 are the local (deformational) displacements of the current point P. In the above equation, a comma followed by an index denotes differentiation with respect to the corresponding variable.

The kinematic model proposed by Gruttmann et al. [22] is adopted, see Fig. 4.2. This kinematic description can be used for an arbitrary cross-section, therefore the local beam kinematics given here stands also for beam with arbitrary thin-walled cross-section presented in Chapter 5.

Let $\mathbf{x}_{\mathrm{P}}^o(x,y,z)$ denote the position vector of point P in the initial (i.e. rotated but still undeformed) configuration and let $\mathbf{x}_{\mathrm{P}}(x,y,z)$ denote the position vector of P in the current configuration (see Fig. 4.2). These two vectors are given by

$$\begin{aligned}
\mathbf{x}_{\mathrm{P}}^o(x,y,z) &= \mathbf{x}_{\mathrm{G}}^o(x) + y\,\mathbf{r}_2 + z\,\mathbf{r}_3,\\
\mathbf{x}_{\mathrm{P}}(x,y,z) &= \mathbf{x}_{\mathrm{G}}(x) + y\,\mathbf{a}_2(x) + z\,\mathbf{a}_3(x) + \alpha(x)\,\overline{\omega}(y,z)\,\mathbf{a}_1(x),
\end{aligned} \tag{4.88}$$

with $\mathbf{x}_{\mathrm{G}}^o$ and $\mathbf{x}_{\mathrm{G}}$ denoting the position vectors of G in the initial and current configurations, respectively.

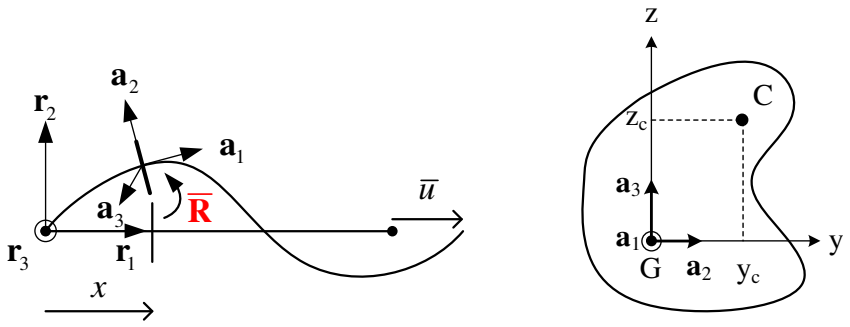

Fig. 4.2: Local beam configuration.

The warping function $\overline{\omega}(y,z)$ is defined within the Saint-Venant torsion theory and refers to the centroid G, i.e.

$$\overline{\omega} = \omega - y_c z + z_c y\,, \tag{4.89}$$

where ω refers to the shear center C with coordinates $y_c\,, z_c$. Note that in connection with ω, the following normality conditions hold

$$\int_A \omega\,\mathrm{d}A = 0\,, \quad \int_A \omega\, y\,\mathrm{d}A = 0\,, \quad \int_A \omega\, z\,\mathrm{d}A = 0\,. \tag{4.90}$$

The orthonormal triad $\mathbf{a}_i$ $(i = 1,2,3)$ which specifies the orientation of the current cross-section, is given by

$$\mathbf{a}_i = \overline{\mathbf{R}}\,\mathbf{r}_i\,, \tag{4.91}$$

where the orthogonal matrix $\overline{\mathbf{R}}$ defines a rotation relative to the local element axes, see Eq. (4.7). Using Eq. (3.4), a second order approximation of $\overline{\mathbf{R}}$ can be constructed as

$$\overline{\mathbf{R}} = \mathbf{I} + \widetilde{\overline{\boldsymbol{\theta}}} + \frac{1}{2}\widetilde{\overline{\boldsymbol{\theta}}}^2\,, \qquad \widetilde{\overline{\boldsymbol{\theta}}} = \begin{bmatrix} 0 & -\overline{\theta}_3 & \overline{\theta}_2 \\ \overline{\theta}_3 & 0 & -\overline{\theta}_1 \\ -\overline{\theta}_2 & \overline{\theta}_1 & 0 \end{bmatrix}. \tag{4.92}$$

Introducing Eq. (4.90) into Eq. (4.88), a second order approximation of the displacement vector $\overline{\mathbf{u}}_\mathrm{P} = [u_1\ u_2\ u_3]^\mathrm{T} = \mathbf{x}_\mathrm{P} - \mathbf{x}_\mathrm{P}^o$ can be evaluated as

$$\begin{aligned} u_1 &= \overline{u}_1 - y\,\overline{\theta}_3 + z\,\overline{\theta}_2 + \frac{1}{2}y\,\overline{\theta}_1\,\overline{\theta}_2 + \frac{1}{2}z\,\overline{\theta}_1\,\overline{\theta}_3 + \overline{\omega}\,\alpha\,, \\ u_2 &= \overline{u}_2 - z\,\overline{\theta}_1 - \frac{1}{2}y\,(\overline{\theta}_1^2 + \overline{\theta}_3^2) + \frac{1}{2}z\,\overline{\theta}_2\,\overline{\theta}_3 + \overline{\omega}\,\alpha\,\overline{\theta}_3\,, \\ u_3 &= \overline{u}_3 + y\,\overline{\theta}_1 - \frac{1}{2}z\,(\overline{\theta}_1^2 + \overline{\theta}_2^2) + \frac{1}{2}y\,\overline{\theta}_2\,\overline{\theta}_3 - \overline{\omega}\,\alpha\,\overline{\theta}_2\,, \end{aligned} \tag{4.93}$$

where $\overline{u}_1, \overline{u}_2, \overline{u}_3$ are the displacements of the centroid G, i.e. the components of the vector $\mathbf{x}_\mathrm{G} - \mathbf{x}_\mathrm{G}^o$.

Using Eqs. (4.89), (4.90) and (4.93), a second order approximation of the Green-Lagrange strains defined in Eq. (4.86) can be evaluated. At this level, two additional simplifications are introduced. First, the term $1/2\,\overline{u}_{1,x}^2$ in the expression of ε_{11} is neglected. Second, the nonlinear strain components generated by warping are omitted since warping effects are rationally taken into account in a linearised way only [23].

Using these simplifications gives

$$\begin{aligned} \varepsilon_{11} &= \varepsilon_c + y k_2 + z k_3 + \frac{1}{2} r^2 \overline{\theta}_{1,x}^2 + \omega \alpha_{,x} \,, \\ 2\varepsilon_{12} &= \gamma_{12} + \bar{\omega}_{,y} \alpha - z k_1 \,, \\ 2\varepsilon_{13} &= \gamma_{13} + \bar{\omega}_{,z} \alpha + y k_1 \,, \end{aligned} \tag{4.94}$$

with

$$\begin{aligned} r^2 &= y^2 + z^2 \,, \\ \varepsilon_c &= u_{1,x} + \frac{1}{2}\left(u_{2,x}^2 + u_{3,x}^2\right) \,, \\ k_2 &= -\overline{\theta}_{3,x} + \frac{1}{2}\left(\overline{\theta}_{1,x}\overline{\theta}_2 + \overline{\theta}_1\overline{\theta}_{2,x}\right) + u_{3,x}\overline{\theta}_{1,x} + z_c\alpha_{,x} \,, \\ k_3 &= \overline{\theta}_{2,x} + \frac{1}{2}\left(\overline{\theta}_{1,x}\overline{\theta}_3 + \overline{\theta}_1\overline{\theta}_{3,x}\right) - u_{2,x}\overline{\theta}_{1,x} - y_c\alpha_{,x} \,, \\ k_1 &= \overline{\theta}_{1,x} + \frac{1}{2}\left(\overline{\theta}_{2,x}\overline{\theta}_3 - \overline{\theta}_2\overline{\theta}_{3,x}\right) \,, \\ \gamma_{12} &= u_{2,x} - \overline{\theta}_3 + \frac{1}{2}\overline{\theta}_1\overline{\theta}_2 + u_{3,x}\overline{\theta}_1 - u_{1,x}\overline{\theta}_3 \,, \\ \gamma_{13} &= u_{3,x} + \overline{\theta}_2 + \frac{1}{2}\overline{\theta}_1\overline{\theta}_3 - u_{2,x}\overline{\theta}_1 + u_{1,x}\overline{\theta}_2 \,. \end{aligned} \tag{4.95}$$

The strain energy can then be evaluated from

$$\Phi = \int_{l_o} \Phi_A \mathrm{d}x = \int_{l_o} \left(\frac{1}{2} E \int_A \varepsilon_{11}^2 \mathrm{d}A + \frac{1}{2} G \int_A \left[(2\varepsilon_{12})^2 + (2\varepsilon_{13})^2 \right] \mathrm{d}A \right) \mathrm{d}x. \tag{4.96}$$

Integration through the cross-section gives

$$\begin{aligned} \int_A \varepsilon_{11}^2 \,\mathrm{d}A = A\,\varepsilon_c^2 + I_{yy}k_2^2 + I_{zz}k_3^2 + \frac{1}{4}I_{rr}\overline{\theta}_{1,x}^4 + I_\omega\,\alpha_{,x}^2 + I_o\,\varepsilon_c\,\overline{\theta}_{1,x}^2 \\ + 2\,I_{yz}k_2k_3 + I_{yr}k_2\,\overline{\theta}_{1,x}^2 + I_{zr}k_3\,\overline{\theta}_{1,x}^2 + I_{\omega r}\,\alpha_{,x}\,\overline{\theta}_{1,x}^2 \,, \end{aligned} \tag{4.97}$$

$$\begin{aligned} \int_A \left[(2\varepsilon_{12})^2 + (2\varepsilon_{13})^2 \right] \mathrm{d}A = A\,(\gamma_{12}^2 + \gamma_{13}^2) + I_o\,k_1^2 + (I_o - J)\,\alpha^2 \\ - 2\,(I_o - J)\,\alpha\,k_1 \,, \end{aligned} \tag{4.98}$$

where J denotes the Saint-Venant torsion modulus

$$J = \int_A \left[y(\bar{\omega}_{,z} + y) - z(\bar{\omega}_{,y} - z) \right] \mathrm{d}A \,, \tag{4.99}$$

and the other section quantities are defined by

$$\begin{aligned} I_{yy} &= \int_A y^2 \,\mathrm{d}A \,, & I_{zz} &= \int_A z^2 \,\mathrm{d}A \,, & I_{yz} &= \int_A yz \,\mathrm{d}A \,, \\ I_{yr} &= \int_A y r^2 \,\mathrm{d}A \,, & I_{zr} &= \int_A z r^2 \,\mathrm{d}A \,, & I_{rr} &= \int_A (y^2 + z^2)^2 \,\mathrm{d}A \,, \\ I_\omega &= \int_A \omega^2 \,\mathrm{d}A \,, & I_{\omega r} &= \int_A \omega r^2 \,\mathrm{d}A \,, & I_o &= \int_A (y^2 + z^2) \,\mathrm{d}A \,. \end{aligned} \tag{4.100}$$

In deriving Eqs. (4.98) and (4.99), the following relations have been used (cf. the proof in [22])

$$\int_A \bar{\omega}_{,y} \,\mathrm{d}A = \int_A \bar{\omega}_{,z} \,\mathrm{d}A = 0 \,, \tag{4.101}$$

$$\int_A \left(\bar{\omega}_{,y}^2 + \bar{\omega}_{,z}^2\right) \mathrm{d}A = -\int_A \left(\bar{\omega}_{,z}\, y - \bar{\omega}_{,y}\, z\right) \mathrm{d}A = I_o - J\,. \tag{4.102}$$

If the Bernoulli assumption is adopted, the bending shear strains γ_{12} and γ_{13} in Eq. (4.95) are neglected, which gives

$$\overline{\theta}_2 = -u_{3,x} + \frac{1}{2}\, u_{2,x}\, \overline{\theta}_1 + u_{1,x}\, u_{3,x}\,, \qquad \overline{\theta}_3 = u_{2,x} + \frac{1}{2}\, u_{3,x}\, \overline{\theta}_1 - u_{1,x}\, u_{2,x}\,. \tag{4.103}$$

By introducing the above equations into Eq. (4.95), the bending curvatures and torsional twist can be rewritten as

$$\begin{aligned} k_1 &= \overline{\theta}_{1,x} + \frac{1}{2}\left(u_{3,x}\, u_{2,xx} - u_{2,x}\, u_{3,xx}\right), \\ k_2 &= -u_{2,xx} + u_{1,xx}\, u_{2,x} + u_{1,x}\, u_{2,xx} - u_{3,xx}\, \overline{\theta}_1 + z_c\, \alpha_{,x}\,, \\ k_3 &= -u_{3,xx} + u_{1,xx}\, u_{3,x} + u_{1,x}\, u_{3,xx} + u_{2,xx}\, \overline{\theta}_1 - y_c\, \alpha_{,x}\,. \end{aligned} \tag{4.104}$$

Since the bending shear stresses are neglected, it appears logical to neglect the bi-shear F_ω also. Thus

$$F_\omega = \frac{\partial \Phi_A}{\partial \alpha} = 0\,, \tag{4.105}$$

where Φ_A is defined in Eq. (4.96). Introducing (4.97) and (4.98) into the above expression, gives

$$\alpha = k_1\,. \tag{4.106}$$

The integral (4.98) is then simplified under the form

$$\int_A \left[(2\varepsilon_{12})^2 + (2\varepsilon_{13})^2\right] \mathrm{d}A = J\, k_1^2\,. \tag{4.107}$$

In order to avoid membrane locking, ε_{11} in Eq.(4.94) is rewritten as

$$\varepsilon_{11} = \varepsilon_{av} + y\, k_2 + z\, k_3 + \frac{1}{2}\left(r^2 - \frac{I_o}{A}\right) \overline{\theta}_{1,x}^2 + \omega\, \alpha_{,x}\,, \tag{4.108}$$

where the "average" value ε_{av} is given by

$$\varepsilon_{av} = \frac{1}{l_o} \int_{l_o} \left[u_{1,x} + \frac{1}{2}\left(u_{2,x}^2 + u_{3,x}^2 + \frac{I_o}{A}\, \overline{\theta}_{1,x}^2\right)\right] \mathrm{d}x\,. \tag{4.109}$$

This gives

$$\begin{aligned} \int_A \varepsilon_{11}^2\, \mathrm{d}A = {} & A\, \varepsilon_{av}^2 + I_{yy}\, k_2^2 + I_{zz}\, k_3^2 + \frac{1}{4}\left(I_{rr} - \frac{I_o^2}{A}\right) \overline{\theta}_{1,x}^4 + I_\omega\, \alpha_{,x}^2 \\ & + 2\, I_{yz}\, k_2\, k_3 + I_{yr}\, k_2\, \overline{\theta}_{1,x}^2 + I_{zr}\, k_3\, \overline{\theta}_{1,x}^2 + I_{\omega r}\, \alpha_{,x}\, \overline{\theta}_{1,x}^2\,. \end{aligned} \tag{4.110}$$

Beams with solid cross-sections

For such beams, the cross-section is assumed to be bi-symmetric, with $\mathbf{r}_2$ and $\mathbf{r}_3$ directed along the principal axes of the cross-section. These assumptions give

$$I_{yz} = I_{yr} = I_{zr} = I_{\omega r} = y_c = z_c = 0\,. \tag{4.111}$$

The warping stresses are neglected and consequently the bi-shear F_ω and the bi-moment M_ω are set to zero

$$F_\omega = \frac{\partial \Phi_A}{\partial \alpha} = 0\,, \qquad M_\omega = \frac{\partial \Phi_A}{\partial \alpha_{,x}} = 0\,. \tag{4.112}$$

Introducing Eqs. (4.97) and (4.98) in the above expressions, gives

$$\alpha = k_1\,, \qquad I_\omega\,\alpha_{,x} = 0\,, \tag{4.113}$$

which are further substituted in the corresponding expressions of the strain energy.

In the second paper [38], the Timoshenko element *t3d*, based on Eqs. (4.95), (4.97) and (4.98), was used. The element adopts linear interpolations for all variables and a one point Gauss rule to avoid the shear locking. In numerical examples in the paper, the section quantity I_{rr} was neglected. Extensive numerical testing showed that this simplification has no effect on the accuracy of the results.

In the third paper [39], the Bernoulli element *b3d*, based on Eqs. (4.104), (4.107), (4.109) and (4.110), was used. This element adopts linear interpolations for the axial displacement and axial rotation, cubic interpolations for the transverse displacements. Then, due to the particular choice of the local degrees of freedom, one has

$$\begin{bmatrix} \overline{u}_1 \\ \overline{u}_2 \\ \overline{u}_3 \\ \overline{\theta}_1 \\ \overline{\theta}_2 \\ \overline{\theta}_3 \end{bmatrix} = \begin{bmatrix} N_2 & 0 & 0 & 0 & 0 & 0 & 0 \\ 0 & 0 & 0 & N_3 & 0 & 0 & N_4 \\ 0 & 0 & -N_3 & 0 & 0 & -N_4 & 0 \\ 0 & N_1 & 0 & 0 & N_2 & 0 & 0 \\ 0 & 0 & N_5 & 0 & 0 & N_6 & 0 \\ 0 & 0 & 0 & N_5 & 0 & 0 & N_6 \end{bmatrix} \mathbf{d}_l\,, \tag{4.114}$$

with

$$N_1 = 1 - \frac{x}{l_o}\,, \quad N_2 = 1 - N_1\,, \quad N_3 = x\left(1 - \frac{x}{l_o}\right)^2\,,$$
$$N_4 = -\left(1 - \frac{x}{l_o}\right)\frac{x^2}{l_o}\,, \quad N_5 = \left(1 - \frac{3x}{l_o}\right)\left(1 - \frac{x}{l_o}\right)\,, \quad N_6 = \left(\frac{3x}{l_o} - 2\right)\frac{x}{l_o}\,.$$

Let $\mathbf{u}_l = [\,0\ \ \overline{u}_2\ \ \overline{u}_3\,]^{\mathrm{T}}$ denotes the local transverse displacement vector. This vector is calculated by

$$\mathbf{u}_l = \mathbf{P}_1 \begin{bmatrix} \overline{\boldsymbol{\theta}}_1 \\ \overline{\boldsymbol{\theta}}_2 \end{bmatrix}\,, \quad \mathbf{P}_1 = \begin{bmatrix} 0 & 0 & 0 & 0 & 0 & 0 \\ 0 & 0 & N_3 & 0 & 0 & N_4 \\ 0 & -N_3 & 0 & 0 & -N_4 & 0 \end{bmatrix}\,. \tag{4.115}$$

The local rotation of the cross-section is evaluated as follows

$$\overline{\boldsymbol{\theta}} = \mathbf{P}_2 \begin{bmatrix} \overline{\boldsymbol{\theta}}_1 \\ \overline{\boldsymbol{\theta}}_2 \end{bmatrix}\,, \quad \mathbf{P}_2 = \begin{bmatrix} N_1 & 0 & 0 & N_2 & 0 & 0 \\ 0 & N_5 & 0 & 0 & N_6 & 0 \\ 0 & 0 & N_5 & 0 & 0 & N_6 \end{bmatrix}\,. \tag{4.116}$$

Both element types were implemented by neglecting the nonlinear terms in the expressions of the curvatures k_1, k_2, k_3 and bending shear strains γ_{12}, γ_{13}. Extensive numerical testing showed that this simplification had no effect whatsoever on the accuracy of the results; i.e. including these terms generates differences of less than 0.01% in the final results. On the other hand, certain tests showed that the Wagner term $\frac{1}{2}\,r^2\,\overline{\theta}^2_{1,x}$ in the expression of ε_{11} can not be neglected or even be replaced by its average value($\frac{1}{2}\,\frac{I_o}{A}\,\overline{\theta}^2_{1,x}$) over the cross-section.

The Maple codes of these local beam elements, taken from the work of Battini [5], are given as follows

Maple code of *t3d* element

```
>with(linalg):
>du:=u12/L:
>t1:=(t11+t12)/2:
>t2:=(t21+t22)/2:
>t3:=(t31+t32)/2:
>dt1:=(t12-t11)/L:
>dt2:=(t22-t21)/L:
>dt3:=(t32-t31)/L:
>g12:=-t3:
>g13:=t2:
>k1:=dt1:
>k2:=-dt3:
>k3:=dt2:
>Phi1:=A*du^2+Iyy*k2^2+Izz*k3^2+Irr/4*dt1^4+Io*du*dt1^2:
>Phi2:=A*(g12^2+g13^2)+J*k1^2:
>Phi:=1/2*L*(E*Phi1+G*Phi2):
>fl:=grad(Phi,[u,t11,t21,t31,t12,t22,t32]):
>kl:=hessian(Phi,[u,t11,t21,t31,t12,t22,t32]):
```

Maple code of *b3d* element

```
>with(linalg):
>u21:=0:
>u31:=0:
>u22:=0:
>u32:=0:
>f1:=1-3*(x/L)^2+2*(x/L)^3:
>f2:=x*(1-x/L)^2:
>f3:=1-f1:
>f4:=x^2*(x/L-1)/L:
>u2:=f1*u21+f2*t31+f3*u22+f4*t32:
>du2:=diff(u2,x):
>ddu2:=diff(du2,x):
>u3:=f1*u31-f2*t21+f3*u32-f4*t22:
>du3:=diff(u3,x):
>ddu3:=diff(du3,x):
>t1:=(1-x/L)*t11+x/L*t12:
>dt1:=diff(t1,x):
>k1:=dt1:
>k2:=-ddu2:
>k3:=-ddu3:
>eav:=u12/L+1/2/L*int(du2^2+du3^2+Io/A*dt1^2,x=0..L):
>Phi1:=A*eav^2+Iyy*k2^2+Izz*k3^2+1/4*(Irr-Io^2/A)*dt1^4:
>Phi:=1/2*int(E*Phi1+G*J*k1^2,x=0..L):
>fl:=grad(Phi,[u,t11,t21,t31,t12,t22,t32]):
>kl:=hessian(Phi,[u,t11,t21,t31,t12,t22,t32]):
```

4.5 Inertia force vector and tangent dynamic matrix

In this section, the derivation of the inertia force vector and the tangent dynamic matrix presented in [39] is briefly summarized. The novelty of the approach is that the same corotational kinematics description is adopted to formulate both inertia and internal terms, which ensures the consistency of the formulation. As already mentioned, this 3D corotational dynamic formulation is the extension of the 2D one proposed in [37].

Using the cross-section centroid as the reference point, the kinetic energy of a spatial beam element is given by

$$K = \frac{1}{2}\int_{l_o} \{\dot{\mathbf{u}}^{\mathrm{T}} A_\rho \dot{\mathbf{u}} + \dot{\mathbf{w}}^{\mathrm{T}} \mathbf{I}_\rho \dot{\mathbf{w}}\} \mathrm{d}l\,, \tag{4.117}$$

where $\dot{\mathbf{u}}$, $\dot{\mathbf{w}}$ are the translational and angular velocity of the cross-section and $\mathbf{I}_\rho$ is the spatial inertia dyadic. Please note that in order to simplify the notations, in this section, the superscripts "g" which refer to global quantities are dropped for $\mathbf{u}$, $\dot{\mathbf{w}}$ and their derivatives.

The variation of the kinetic energy can be expressed as (see [21])

$$\delta K = -\int_{l_o} \left\{ \delta\mathbf{u}^{\mathrm{T}} A_\rho \ddot{\mathbf{u}} + \delta\mathbf{w}^{\mathrm{T}} \left[\mathbf{I}_\rho \ddot{\mathbf{w}} + \widetilde{\dot{\mathbf{w}}} \mathbf{I}_\rho \dot{\mathbf{w}} \right] \right\} \mathrm{d}l\,. \tag{4.118}$$

The inertia force vector is then derived from the following relation

$$\delta K = -\mathbf{f}_k^{\mathrm{T}} \delta\mathbf{d}_g\,. \tag{4.119}$$

Translational displacement variables

The position of the cross-section centroid in the global coordinate system is given by

$$\mathrm{OG} = \mathbf{x}_1^g + \mathbf{u}_1^g + (x + \overline{u}_1)\,\mathbf{r}_1 + \overline{u}_2 \mathbf{r}_2 + \overline{u}_3 \mathbf{r}_3\,. \tag{4.120}$$

Using Eqs. (4.2), (4.6) and (4.114), the variation of the above equation is obtained

$$\delta\mathrm{OG} = \delta\mathbf{u} = \mathbf{N}\,\delta\mathbf{d}_g + \mathbf{R}_r \delta\mathbf{u}_l + \delta\mathbf{R}_r \mathbf{u}_l\,, \tag{4.121}$$

with $\mathbf{N} = \begin{bmatrix} N_1\mathbf{I} & \mathbf{0} & N_2\mathbf{I} & \mathbf{0} \end{bmatrix}$.

In the corotational approach, the local rotations at the nodes $\overline{\boldsymbol{\theta}}_i$ $(i = 1,2)$, defined in Eq. (4.8), are small and the operator $\mathbf{T}_s(\overline{\boldsymbol{\theta}}_i)$ is close to the identity matrix. Consequently, see Eq. (3.8), the following approximation is adopted

$$\delta\overline{\mathbf{w}}_i \approx \delta\overline{\boldsymbol{\theta}}_i\,. \tag{4.122}$$

It can be observed that for the internal force vector, this simplification, which implies to neglect the first change of variables in Section 4.2, cannot be performed. Using Eqs. (4.28) and (4.122), the differentiation of Eq. (4.115) is obtained as

$$\delta\mathbf{u}_l \approx \mathbf{P}_1 \begin{bmatrix} \delta\overline{\mathbf{w}}_1 \\ \delta\overline{\mathbf{w}}_2 \end{bmatrix} = \mathbf{P}_1\,\mathbf{P}\,\mathbf{E}^{\mathrm{T}}\,\delta\mathbf{d}_g\,. \tag{4.123}$$

Finally, the expression (4.121) can be rewritten in a more compact form as

$$\delta\mathbf{u} = \mathbf{R}_r\,\mathbf{H}_1\,\mathbf{E}^{\mathrm{T}}\,\delta\mathbf{d}_g\,, \tag{4.124}$$

with

$$\mathbf{H}_1 = \mathbf{N} + \mathbf{P}_1\,\mathbf{P} - \widetilde{\mathbf{u}}_l\,\mathbf{G}^{\mathrm{T}}\,. \tag{4.125}$$

Finite rotation variables

Using Eqs. (4.24) and (4.25), the spatial spin variables, associated to the global rotation of a cross-section, are evaluated using

$$\delta\mathbf{w} = \mathbf{R}_r \delta\mathbf{w}^e = \mathbf{R}_r \left(\delta\mathbf{w}_r^e + \delta\overline{\mathbf{w}}\right). \tag{4.126}$$

Combining the approximation defined in Eq. (4.122) with Eqs. (4.116), (4.28) and (4.29), the spatial spin variables are computed from the global nodal displacement vector by

$$\delta\mathbf{w} = \mathbf{R}_r \mathbf{H}_2 \mathbf{E}^{\mathrm{T}} \delta\mathbf{d}_g, \tag{4.127}$$

where

$$\mathbf{H}_2 = \mathbf{P}_2 \mathbf{P} + \mathbf{G}^{\mathrm{T}}. \tag{4.128}$$

Inertia force vector and tangent dynamic matrix

By inserting the expressions of $\delta\mathbf{u}$ and $\delta\mathbf{w}$ given in Eqs. (4.124) and (4.127) into Eq. (4.118), the inertia force vector is obtained as

$$\mathbf{f}_k = \mathbf{E}\left[\int_{l_o}\left\{\mathbf{H}_1^{\mathrm{T}}\mathbf{R}_r^{\mathrm{T}} A_\rho \ddot{\mathbf{u}} + \mathbf{H}_2^{\mathrm{T}}\mathbf{R}_r^{\mathrm{T}}\left[\mathbf{I}_\rho\dot{\mathbf{w}} + \widetilde{\mathbf{w}}\mathbf{I}_\rho\mathbf{w}\right]\right\}\mathrm{d}l\right]. \tag{4.129}$$

Linearization of this force vector is evaluated as follows

$$\Delta\mathbf{f}_k = \mathbf{M}\Delta\ddot{\mathbf{d}}_g + \mathbf{C}_k\Delta\dot{\mathbf{d}}_g + \mathbf{K}_k\Delta\mathbf{d}_g. \tag{4.130}$$

Some authors proposed to keep only the mass matrix $\mathbf{M}$, and to eliminate the gyroscopic $\mathbf{C}_k$ and centrifugal $\mathbf{K}_k$ dynamic matrices [11, 24]. However, in [38], extensive numerical studies showed that it is better to keep also the gyroscopic matrix in order to enhance the computational efficiency. The same approach was used in [39]. The centrifugal matrix, whose derivation is complicated and would give a lengthy mathematical expression, was neglected. Therefore, the iterative scheme of the present formulation was implemented with the following approximative linearization

$$\Delta\mathbf{f}_k \approx \mathbf{M}\Delta\ddot{\mathbf{d}}_g + \mathbf{C}_k\Delta\dot{\mathbf{d}}_g. \tag{4.131}$$

The expressions of the mass matrix $\mathbf{M}$ and of the gyroscopic matrix $\mathbf{C}_k$ are given by

$$\mathbf{M} = \mathbf{E}\left\{\int_{l_o}\left(\mathbf{H}_1^{\mathrm{T}} A_\rho \mathbf{H}_1 + \mathbf{H}_2^{\mathrm{T}}\mathbf{I}_\rho^e\mathbf{H}_2\right)\mathrm{d}l\right\}\mathbf{E}^{\mathrm{T}} = \mathbf{E}\,\mathbf{M}^e\,\mathbf{E}^{\mathrm{T}}, \tag{4.132}$$

$$\begin{aligned}\mathbf{C}_k = \mathbf{E}\Bigg\{&\int_{l_o}\mathbf{H}_1^{\mathrm{T}} A_\rho\left(\mathbf{C}_1+\mathbf{C}_3\right)\mathrm{d}l + \int_{l_o}\mathbf{H}_2^{\mathrm{T}}\mathbf{I}_\rho^e\left(\mathbf{C}_2+\mathbf{C}_4\right)\mathrm{d}l\\ &+\int_{l_o}\mathbf{H}_2^{\mathrm{T}}\left(\widetilde{\dot{\mathbf{w}}^e}\mathbf{I}_\rho^e - \widetilde{\mathbf{I}_\rho^e\mathbf{w}^e}\right)\mathbf{H}_2\mathrm{d}l\Bigg\}\mathbf{E}^{\mathrm{T}} = \mathbf{E}\,\mathbf{C}_k^e\,\mathbf{E}^{\mathrm{T}}.\end{aligned} \tag{4.133}$$

4.6 Numerical example - Right-angle cantilever beam

This classic example, introduced by Simo and Vu-Quoc [55], has often been used in order to validate various nonlinear dynamic formulations [24, 30, 35, 43]. A right-angle cantilever, depicted in Fig. 4.3, is subjected to an out-of-plane concentrated load applied at the elbow. Each member of the cantilever has a length $L = 10$. The material properties are $GA = EA = 10^6$, $GJ = EI = 10^3$. The mass per unit length of the beam and the inertia dyadic of the cross section in the initial configuration are $A_\rho = 1$ and $\mathbf{J}_\rho = \mathrm{diag}(20, 10, 10)$, respectively.

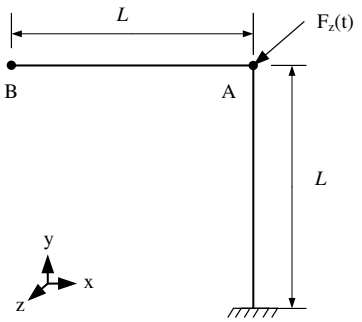

Fig. 4.3: Right-angle cantilever beam : geometrical data.

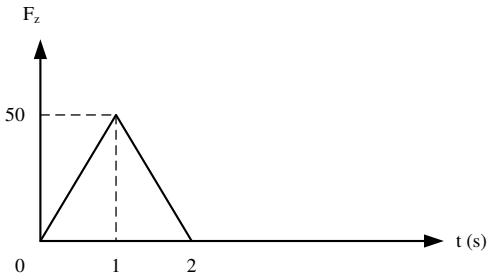

Fig. 4.4: Right-angle cantilever beam - Loading history.

The load (see Fig. 4.4) acts only during $0 \leq t(s) \leq 2$ and thereafter the cantilever undergoes large-scale free vibrations. The resulting amplitude of vibration is of the same order of magnitude as the structure's dimensions. The purpose of this dynamic example is to assess both the cubic and the linear corotational formulations. The first one employs cubic interpolation for all terms whereas the second uses cubic interpolation for the internal force vector and the corresponding stiffness matrix, the inertia terms being evaluated considering linear interpolation. It can be observed that linear local interpolations imply $\mathbf{u}_l = \mathbf{0}_{3\times 1}$, which simplifies significantly the computations.

The predictions of these formulations are compared against the total Lagrangian formulation proposed by Simo and Vu-Quoc [53–55]. In this formulation which employs spatial spin variables, the internal force vector and the tangent stiffness matrix are numerically integrated using one Gauss point whereas the inertia force vector and the dynamic tangent matrix are numerically integrated using two Gauss points. All the three formulations are implemented using Matlab. The same levels of optimisation in forming the element matrices and force vectors are carefully checked.

The solutions given by the three dynamic formulations are compared against a reference solution. The latter is obtained by increasing the number of elements until the three dynamic formulations converge towards the same results.

The HHT α method [13] with $\alpha = -0.05$ was employed. Regarding the predictor to initiate the iterative procedure, Pred. 4 (see Section 3.2) was adopted. This predictor was the most effective among the four ones compared in [38].

Damping was not considered and the following convergence criterion was used: the norm of the residual vector must be less than the prescribed tolerance $\varepsilon_f = 10^{-5}$.

The reference solution was obtained with a total of 20 beam elements (10 elements per member) whereas the predictions of the three aforementioned formulations were calculated using only 4 elements (2 elements per member). The time evolution of the out-of-plane displacement of node A was depicted in Fig. 4.5. The computations were performed with $\Delta t = 0.25$ s. It can be seen that with only 4 beam elements, the cubic corotational approach gave almost the same results as the reference solution over the whole time domain. The results obtained with the linear corotational approach were very close to the reference solution with minor differences. However, the results obtained with the formulation of Simo and Vu-Quoc deviated

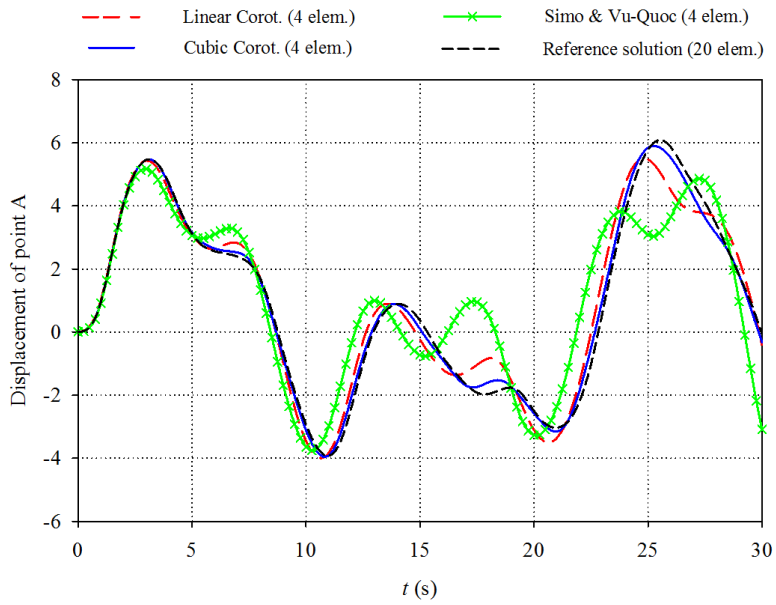

Fig. 4.5: Right-angle cantilever beam - Time evolution of the out-of-plane displacement of point A.

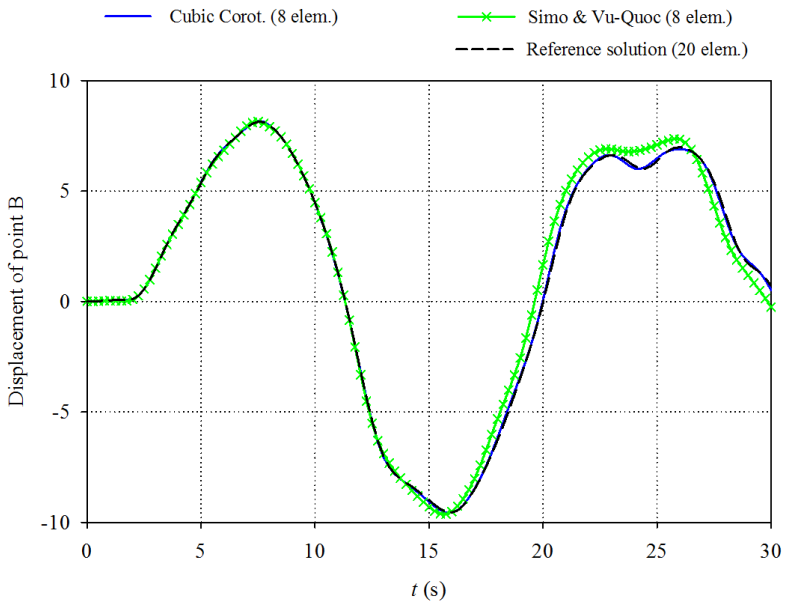

Fig. 4.6: Right-angle cantilever beam - Time evolution of the out-of-plane displacement of point B.

significantly from the reference solution which is obviously due to the linear nature of the interpolation.

The time evolution of the out-of-plane displacement of node B, calculated with a total of 8 beam elements (4 elements per member), was depicted in Fig. 4.6. It can be noted that the differences between the formulation of Simo and Vu-Quoc and the reference solution became smaller, but also that the cubic corotational formulation gave very accurate results.

In the current example, the energy blow-up could happen at approximately $t = 45$ s. This numerical instability was reported by Jelenić and Crisfield [34, 35] and by Zupan et al. [58]. Therefore, to assess the stability of the HHT α method when combined with the new cubic formulation, this example was run for a time period of 150 s using a total of 20 beam elements and a time step $\Delta t = 0.25$ s. The time evolution of the total energy was depicted in Fig. 4.7. The result indicated that the new formulation was stable during the time period under consideration. The dissipation of energy between $t = 2$ s and $t = 30$ s was about 3%.

The CPU time and the total number of iterations required for each formulation were presented in Table 4.1. With the same number of elements, the linear corotational approach was the fastest approach and the cubic corotational approach was the slowest one. This was expected since several inertia terms disappear when local linear interpolations are adopted. Moreover, in the linear corotational approach, the inertia force vector and the tangent dynamic matrix were integrated using two Gauss points, whereas the dynamic terms of the cubic corotational one were integrated using three Gauss points.

Table 4.1: Right-angle cantilever beam - CPU time (Total number of iterations).

Number of beam elements	Linear corot.	Cubic corot.	Simo & Vu-Quoc
4	3.66 (633)	5.31 (637)	4.59 (521)
20	19.84 (636)	25.61 (612)	22.90 (517)

This example shows that with coarse meshes, Simo and Vu-Quoc's two-noded formulation and the linear corotational one give less accurate results compared to the cubic corotational approach which provides very accurate results. This demonstrates the importance of an accurate description of the deformations in the dynamic terms, which is not possible with linear interpolations. With fine meshes, all formulations give the same results.

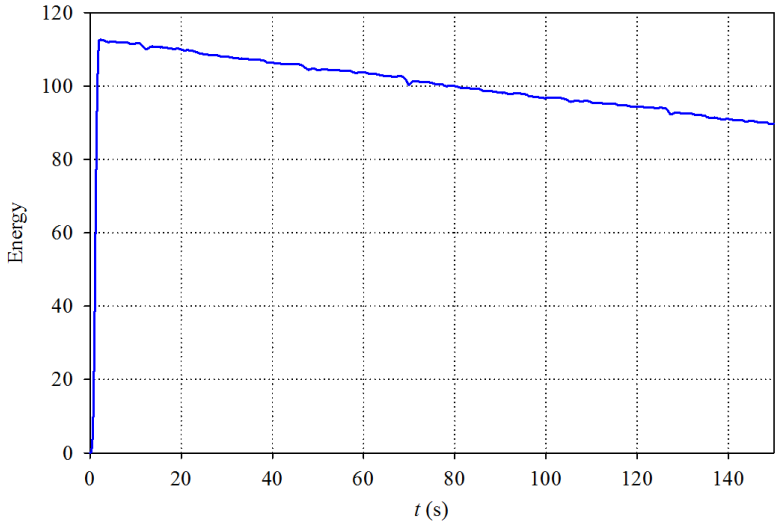

Fig. 4.7: Right-angle cantilever beam - Time evolution of the total energy.

Chapter 5

3D corotational beam elements with thin-walled cross-section

Dynamic analysis of flexible structures undergoing large displacements and finite rotations is an attractive research topic and a large number of beam finite formulations have been proposed in the literature. Many of them have been formulated in the total Lagrangian context [4, 10, 11, 20, 30, 32, 34, 35, 41, 43, 55, 57, 58], and in the corotational context [9, 14–17, 19, 24–26, 33, 37, 39, 44, 46, 56]. However, the number of formulations which deal with nonlinear dynamics of beams with arbitrary thin-walled cross-sections is very limited [25].

In [40], a new dynamic formulation for nonlinear analysis of beams with arbitrary thin-walled cross-sections was proposed. In fact, this new formulation is the extension of the one developed in [39] by taking into account the warping deformations and the eccentricity of the shear center. Hence, the corotational method was used to derive both internal and inertia terms. For local beam description, linear interpolation was adopted for the axial displacement, whereas cubic interpolations were used for the transverse displacements and for the axial rotation.

In order to introduce the warping deformations, the kinematic description proposed by Gruttmann et al. [22] was adopted to derive both internal and inertia force vectors. Consequently, the beam element had seven degrees of freedom at each node. Moreover, several additional terms were introduced in the expressions of the inertia force vectors and the tangent dynamic matrix. The contributions of these terms in the performance of the formulation were then investigated in the numerical examples. Regarding the static deformational terms, i.e. the internal force vector and tangent stiffness matrix, the corotational beam element developed by Battini and Pacoste [8], and presented in Chapter 4, was adopted. However, in order to introduce the bending shear deformations, the cubic Hermitian functions were modified as suggested in the Interdependent Interpolation Element (IIE) formulation [51]. Five numerical examples were analysed to evaluate the accuracy of the formulation against Abaqus 3D solid elements.

The relevant points of this new formulation is summarized in this chapter. In Section 5.1, the expression of the kinetic energy, incorporating the warping deformations and the eccentricity of the shear center is presented. Section 5.2 describes the corotational beam kinetics for thin-walled beam, while the local beam description is given in Section 5.3. The internal force vector and the tangent stiffness matrix, taken from [5], is introduced in Section 5.4. The inertia force vector and the tangent dynamic matrix is briefly presented in Section 5.5. Finally, one numerical example, taken from [40], is investigated. The purpose of this example is to assess the performance of the present formulation, and also to highlight the influence of the eccentricity of the shear center on the inertia terms.

5.1 Kinetic energy

The kinematic description proposed by Gruttmann et al. [22] is adopted (see Fig. 5.1). A beam with

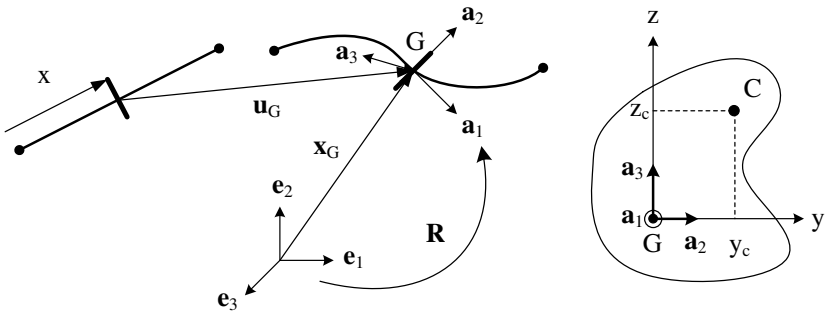

Fig. 5.1: Initial and current configuration of the beam.

an arbitrary cross-section is considered. G and C are the centroid and the shear center of the cross-section. $\mathbf{e}_i$ and $\mathbf{a}_i$ ($i = 1,2,3$) denote the global and cross-section-attached orthogonal coordinates systems, respectively. The transformation from the global coordinates system to the cross-section-attached one is defined by

$$\mathbf{a}_i = \mathbf{R}\,\mathbf{e}_i\,. \tag{5.1}$$

Let $\mathbf{x}_P(x,y,z)$ denote the position vector of an arbitrary point P in the current configuration

$$\mathbf{x}_P(x,y,z) = \mathbf{x}_G(x) + y\,\mathbf{a}_2(x) + z\,\mathbf{a}_3(x) + \alpha(x)\,\overline{\omega}(y,z)\,\mathbf{a}_1(x)\,, \tag{5.2}$$

with $\mathbf{x}_G$ denoting the position vector of G in the current configuration.
The warping function $\overline{\omega}(y,z)$ is defined within the Saint-Venant torsion theory and refers to the centroid G (see Eqs. (4.89) and (4.90)).

Using Eq. (5.1), the expression (5.2) can be put in the form

$$\mathbf{x}_P = \mathbf{x}_G + \mathbf{R}\,(\mathbf{X} + \alpha\,\mathbf{n}_{\overline{\omega}})\,, \tag{5.3}$$

with $\mathbf{X} = [0\ \ y\ \ z]^T$ and $\mathbf{n}_{\overline{\omega}} = [\overline{\omega}\ \ 0\ \ 0]^T$.
By taking the time derivative of the above expression and using Eq. (3.23), the velocity is obtained as

$$\dot{\mathbf{u}}_P = \dot{\mathbf{u}}_G + \mathbf{R}\,(-\widetilde{\mathbf{X}}\,\boldsymbol{\omega} - \alpha\,\widetilde{\mathbf{n}_{\overline{\omega}}}\,\boldsymbol{\omega} + \dot{\alpha}\,\mathbf{n}_{\overline{\omega}})\,. \tag{5.4}$$

The kinetic energy of the beam is then calculated by

$$K = \frac{1}{2}\int_V \rho\ \dot{\mathbf{u}}_P^T\,\dot{\mathbf{u}}_P\ \mathrm{d}V\,. \tag{5.5}$$

After some calculations, the spatial form is obtained as

$$K = \frac{1}{2}\int_{l_o}\left[\dot{\mathbf{u}}_G^T A_\rho\,\dot{\mathbf{u}}_G + \dot{\mathbf{w}}^T\mathbf{I}_\rho\,\dot{\mathbf{w}}\right]\mathrm{d}l + \frac{1}{2}\int_{l_o}\left[\dot{\mathbf{w}}^T\mathbf{I}_\alpha\,\dot{\mathbf{w}} - 2\,\dot{\mathbf{w}}^T\mathbf{I}_b\,\dot{\alpha} + J_{\overline{\omega}}\,\dot{\alpha}^2\right]\mathrm{d}l, \tag{5.6}$$

where

$$\mathbf{I}_\rho = \mathbf{R}\mathbf{J}_\rho\mathbf{R}^{\mathrm{T}}, \quad \mathbf{I}_{\overline{\omega}} = \mathbf{R}\mathbf{J}_{\overline{\omega}}\mathbf{R}^{\mathrm{T}}, \quad \mathbf{I}_\alpha = \mathbf{R}\mathbf{J}_\alpha\mathbf{R}^{\mathrm{T}}, \quad \mathbf{I}_b = \mathbf{R}\mathbf{J}_b, \tag{5.7}$$

$$\mathbf{J}_\rho = \int_A \rho\, \widetilde{\mathbf{X}}^{\mathrm{T}}\,\widetilde{\mathbf{X}}\ \mathrm{d}A = \rho \begin{bmatrix} I_{yy}+I_{zz} & 0 & 0 \\ 0 & I_{zz} & -I_{yz} \\ 0 & -I_{yz} & I_{yy} \end{bmatrix}, \tag{5.8}$$

$$\mathbf{J}_{\overline{\omega}} = \int_A \rho\, \widetilde{\mathbf{n}_{\overline{\omega}}}^{\mathrm{T}}\,\widetilde{\mathbf{n}_{\overline{\omega}}}\ \mathrm{d}A = \rho \begin{bmatrix} 0 & 0 & 0 \\ 0 & I_{\overline{\omega}} & 0 \\ 0 & 0 & I_{\overline{\omega}} \end{bmatrix}, \tag{5.9}$$

$$\mathbf{J}_a = \int_A \rho\, \left(\widetilde{\mathbf{X}}^{\mathrm{T}}\,\widetilde{\mathbf{n}_{\overline{\omega}}} + \widetilde{\mathbf{n}_{\overline{\omega}}}^{\mathrm{T}}\,\widetilde{\mathbf{X}}\right)\ \mathrm{d}A = \rho \begin{bmatrix} 0 & -I_{yc} & -I_{zc} \\ -I_{yc} & 0 & 0 \\ -I_{zc} & 0 & 0 \end{bmatrix}, \tag{5.10}$$

$$\mathbf{J}_b = \int_A \rho\, \widetilde{\mathbf{X}}^{\mathrm{T}}\,\mathbf{n}_{\overline{\omega}}\ \mathrm{d}A = \rho \begin{bmatrix} 0 \\ -I_{zc} \\ I_{yc} \end{bmatrix}, \tag{5.11}$$

$$\mathbf{J}_\alpha = \alpha^2\,\mathbf{J}_{\overline{\omega}} + \alpha\,\mathbf{J}_a, \quad J_{\overline{\omega}} = \rho\, I_{\overline{\omega}}, \tag{5.12}$$

$$I_{\overline{\omega}} = \int_A \overline{\omega}^2\ \mathrm{d}A = I_\omega + z_c^2 I_{yy} + y_c^2 I_{zz} - 2\,y_c\,z_c\,I_{yz}, \tag{5.13}$$

$$I_{yc} = \int_A y\,\overline{\omega}\ \mathrm{d}A = -y_c\,I_{yz} + z_c\,I_{yy}, \tag{5.14}$$

$$I_{zc} = \int_A z\,\overline{\omega}\ \mathrm{d}A = -y_c\,I_{zz} + z_c\,I_{yz}, \tag{5.15}$$

and I_{yz}, I_{yy}, I_ω are defined in (4.100).
In comparison with the kinetic energy for a solid cross-section in Eq. (4.117), the second integral in Eq. (5.6) is the additional kinetic energy due to the warping deformations and the eccentricity of shear center with respect to the centroid.

After several calculations [40], the variation of the total kinetic energy is obtained as

$$\delta K = -\int_{l_o} \left\{ \delta\mathbf{u}_{\mathrm{G}}{}^{\mathrm{T}} A_\rho \ddot{\mathbf{u}}_{\mathrm{G}} + \delta\mathbf{w}^{w\mathrm{T}} \left[\mathbf{I}_\rho^1 \ddot{\mathbf{w}}^w + \mathbf{I}_\rho^2 \dot{\mathbf{w}}^w\right] \right\} \mathrm{d}l, \tag{5.16}$$

with

$$\delta\mathbf{w}^w = \begin{bmatrix} \delta\mathbf{w} \\ \delta\alpha \end{bmatrix}, \quad \dot{\mathbf{w}}^w = \begin{bmatrix} \dot{\mathbf{w}} \\ \dot{\alpha} \end{bmatrix}, \quad \ddot{\mathbf{w}}^w = \begin{bmatrix} \ddot{\mathbf{w}} \\ \ddot{\alpha} \end{bmatrix}, \tag{5.17}$$

$$\mathbf{I}_\rho^1 = \begin{bmatrix} (\mathbf{I}_\rho + \mathbf{I}_\alpha) & -\mathbf{I}_b \\ -\mathbf{I}_b^{\mathrm{T}} & J_{\overline{\omega}} \end{bmatrix}, \quad \mathbf{I}_\rho^2 = \begin{bmatrix} \widetilde{\dot{\mathbf{w}}}\,(\mathbf{I}_\rho + \mathbf{I}_\alpha) & \mathbf{I}_c\,\dot{\mathbf{w}} \\ -\dot{\mathbf{w}}^{\mathrm{T}}\,\mathbf{I}_\alpha{}' & 0 \end{bmatrix}. \tag{5.18}$$

5.2 Beam kinematics

The corotational beam kinematics, adopted here, is similar to the one given in Section 4.1. The only difference is that in order to include warping effects, additional (warping) degrees of freedom α_i $(i = 1,2)$

are introduced at both nodes of the element. The local displacement vector thus becomes

$$\mathbf{d}_l^w = \left[\, \overline{u}\ \overline{\boldsymbol{\theta}}_1^{\mathrm{T}}\ \overline{\boldsymbol{\theta}}_2^{\mathrm{T}}\ \alpha_1\ \alpha_2 \,\right]^{\mathrm{T}}. \tag{5.19}$$

However, since the warping is in itself a deformational quantity, these additional degrees of freedom remain constant during the sequence of transformations defined in Section 4.1. Hence, referring for instance to Eq. (4.30), the variations $\delta\mathbf{d}_a$ and $\delta\mathbf{d}_g$ are rewritten as

$$\delta\mathbf{d}_a^w = \left[\, \delta\overline{u}\ \delta\overline{\mathbf{w}}_1^{\mathrm{T}}\ \delta\overline{\mathbf{w}}_2^{\mathrm{T}}\ \delta\alpha_1\ \delta\alpha_2 \,\right]^{\mathrm{T}}, \tag{5.20}$$

$$\delta\mathbf{d}_g^w = \left[\, \delta\mathbf{u}_1^{g\mathrm{T}}\ \delta\mathbf{w}_1^{g\mathrm{T}}\ \delta\mathbf{u}_2^{g\mathrm{T}}\ \delta\mathbf{w}_2^{g\mathrm{T}}\ \delta\alpha_1\ \delta\alpha_2 \,\right]^{\mathrm{T}}, \tag{5.21}$$

and the corresponding connection is defined by

$$\delta\mathbf{d}_a^w = \mathbf{B}_g^w\, \delta\mathbf{d}_g^w, \qquad \mathbf{B}_g^w = \begin{bmatrix} \mathbf{B}_g & \mathbf{0}_2 \\ \mathbf{0}_2 & \mathbf{I}_2 \end{bmatrix}, \tag{5.22}$$

with $\mathbf{B}_g$ as given in Eq. (4.30) and $\mathbf{I}_2$ denoting a 2x2 identity matrix.

5.3 Local beam kinematic description

The local motion of a beam cross-section from the initial (i.e. rotated but still undeformed) configuration to the current configuration is defined by $[\,\overline{u}_1\ \overline{u}_2\ \overline{u}_3\,]^{\mathrm{T}}$, the translation of the cross-section centroid G and $\overline{\boldsymbol{\theta}} = [\,\overline{\theta}_1\ \overline{\theta}_2\ \overline{\theta}_3\,]^{\mathrm{T}}$, the local rotation of the section and α, the warping intensity (see Eq. (5.3)).

Linear interpolation is used for the axial displacement whereas cubic interpolations are used for the transverse displacements and for the axial rotation. Then, due to the particular choice of the local degrees of freedom, one has

$$\begin{bmatrix} \overline{u}_1 \\ \overline{u}_2 \\ \overline{u}_3 \\ \overline{\theta}_1 \\ \overline{\theta}_2 \\ \overline{\theta}_3 \\ \alpha \end{bmatrix} = \begin{bmatrix} N_2 & 0 & 0 & 0 & 0 & 0 & 0 & 0 & 0 \\ 0 & 0 & 0 & N_3 & 0 & 0 & N_4 & 0 & 0 \\ 0 & 0 & -N_3 & 0 & 0 & -N_4 & 0 & 0 & 0 \\ 0 & N_7 & 0 & 0 & N_8 & 0 & 0 & N_3 & N_4 \\ 0 & 0 & N_5 & 0 & 0 & N_6 & 0 & 0 & 0 \\ 0 & 0 & 0 & N_5 & 0 & 0 & N_6 & 0 & 0 \\ 0 & N_9 & 0 & 0 & -N_9 & 0 & 0 & N_5 & N_6 \end{bmatrix} \mathbf{d}_l^w, \tag{5.23}$$

where the local nodal displacement vector $\mathbf{d}_l^w$ is defined by Eq. (5.19).
The expressions of the interpolation functions are given by

$$\begin{aligned} &N_1 = 1 - \frac{x}{l_o}, \quad N_2 = 1 - N_1, \quad N_3 = x\left(1 - \frac{x}{l_o}\right)^2, \\ &N_4 = -\left(1 - \frac{x}{l_o}\right)\frac{x^2}{l_o}, \quad N_5 = \left(1 - \frac{3x}{l_o}\right)\left(1 - \frac{x}{l_o}\right), \quad N_6 = \left(\frac{3x}{l_o} - 2\right)\frac{x}{l_o}, \\ &N_7 = 1 - \frac{3x^2}{l_o^2} + \frac{2x^3}{l_o^3}, \quad N_8 = 1 - N_7, \quad N_9 = \frac{6x^2}{l_o^3} - \frac{6x}{l_o^2}. \end{aligned}$$

Let $\mathbf{u}_l = [\,0\ \overline{u}_2\ \overline{u}_3\,]^{\mathrm{T}}$ denotes the local transverse displacement vector. From Eq. (5.23), this vector is given by

$$\mathbf{u}_l = \mathbf{P}_1 \begin{bmatrix} \overline{\boldsymbol{\theta}}_1 \\ \overline{\boldsymbol{\theta}}_2 \end{bmatrix}, \tag{5.24}$$

with

$$\mathbf{P}_1 = \begin{bmatrix} 0 & 0 & 0 & 0 & 0 & 0 \\ 0 & 0 & N_3 & 0 & 0 & N_4 \\ 0 & -N_3 & 0 & 0 & -N_4 & 0 \end{bmatrix}. \tag{5.25}$$

From Eq. (5.23), the local rotation and the warping degree of freedom are given by

$$\begin{bmatrix} \overline{\boldsymbol{\theta}} \\ \alpha \end{bmatrix} = \begin{bmatrix} \mathbf{P}_2 & \mathbf{P}_3 \\ \mathbf{P}_4 & \mathbf{P}_5 \end{bmatrix} \begin{bmatrix} \overline{\boldsymbol{\theta}}_1 \\ \overline{\boldsymbol{\theta}}_2 \\ \alpha_1 \\ \alpha_2 \end{bmatrix}, \tag{5.26}$$

with

$$\mathbf{P}_2 = \begin{bmatrix} N_7 & 0 & 0 & N_8 & 0 & 0 \\ 0 & N_5 & 0 & 0 & N_6 & 0 \\ 0 & 0 & N_5 & 0 & 0 & N_6 \end{bmatrix}, \qquad \mathbf{P}_3 = \begin{bmatrix} N_3 & N_4 \\ 0 & 0 \\ 0 & 0 \end{bmatrix}, \tag{5.27}$$

$$\mathbf{P}_4 = \begin{bmatrix} N_9 & 0 & 0 & -N_9 & 0 & 0 \end{bmatrix}, \qquad \mathbf{P}_5 = \begin{bmatrix} N_5 & N_6 \end{bmatrix}.$$

5.4 Internal force vector and tangent stiffness matrix

Including warping effects, the global internal force vector and tangent stiffness matrix are given by

$$\mathbf{f}_g^w = \mathbf{B}_g^{w\mathrm{T}}\, \mathbf{f}_a^w, \qquad \mathbf{K}_g^w = \mathbf{B}_g^{w\mathrm{T}} \mathbf{K}_a^w \mathbf{B}_g^w + \mathbf{K}_m^w, \qquad \mathbf{K}_m^w = \begin{bmatrix} \mathbf{K}_m & \mathbf{0}_2 \\ \mathbf{0}_2 & \mathbf{0}_2 \end{bmatrix}, \tag{5.28}$$

with $\mathbf{K}_m$ as defined in Eq. (4.77). The two other transformations are modified in a similar way.

The local internal force vector $\mathbf{f}_l^w$ and the local tangent stiffness matrix $\mathbf{K}_l^w$ associated with $\delta\mathbf{d}_l^w$ are derived using the shape functions introduced in Section 5.3 and the theory presented in Section 4.4. However, to incorporate the bending shear deformations, the Hermitian shape functions for the transverse displacements are slightly modified as suggested in the Interdependent Interpolation Element (IIE) [51].
Vlasov's assumption is adopted, i.e.

$$\alpha_{,x} = \overline{\theta}_{1,xx}, \tag{5.29}$$

which, since the nonlinear terms in the expression of the curvatures are neglected, is the direct consequence of Eq. (4.106). A low order of geometrical nonlinearity is introduced through a shallow arch strain description and the Wagner term.

The element was developed using Eqs. (4.95), (4.98) and (4.110). The Maple codes for $\mathbf{f}_l^w$ and $\mathbf{K}_l^w$ were given in [40].

5.5 Inertia force vector and tangent dynamic matrix

The inertia force vector is then derived from the following relation

$$\delta K = -\mathbf{f}_k^{w\mathrm{T}} \delta\mathbf{d}_g^w. \tag{5.30}$$

Translational displacement variables

The variation of the translational displacement of G is not affected by the warping deformations, therefore the translational displacement variables are calculated in the same manner as presented in Section 4.5. The expression is given as follows

$$\delta\mathbf{u} = \mathbf{R}_r \mathbf{H}_1 \mathbf{E}^{\mathrm{T}} \delta\mathbf{d}_g, \tag{5.31}$$

where

$$\mathbf{H}_1 = \mathbf{N} + \mathbf{P}_1 \mathbf{P} - \widetilde{\mathbf{u}}_l \mathbf{G}^{\mathrm{T}}. \tag{5.32}$$

Finite rotations and warping variables

Combining Eqs. (4.28) and (5.26) with the approximation defined in Eq. (4.122), the local spatial spin and warping variables are calculated as follows

$$\delta\overline{\mathbf{w}} = \begin{bmatrix}\mathbf{P}_2 & \mathbf{P}_3\end{bmatrix} \begin{bmatrix}\mathbf{P}\mathbf{E}^{\mathrm{T}} & \mathbf{0} \\ \mathbf{0} & \mathbf{I}_2\end{bmatrix} \delta\mathbf{d}_g^w = \begin{bmatrix}\mathbf{P}_2\mathbf{P} & \mathbf{P}_3\end{bmatrix} \mathbf{E}^{w\mathrm{T}} \delta\mathbf{d}_g^w, \tag{5.33}$$

$$\delta\alpha = \begin{bmatrix}\mathbf{P}_4 & \mathbf{P}_5\end{bmatrix} \begin{bmatrix}\mathbf{P}\mathbf{E}^{\mathrm{T}} & \mathbf{0} \\ \mathbf{0} & \mathbf{I}_2\end{bmatrix} \delta\mathbf{d}_g^w = \mathbf{H}_3 \mathbf{E}^{w\mathrm{T}} \delta\mathbf{d}_g^w, \tag{5.34}$$

where

$$\mathbf{E}^w = \begin{bmatrix}\mathbf{E} & \mathbf{0} \\ \mathbf{0} & \mathbf{I}_2\end{bmatrix}, \quad \mathbf{H}_3 = \begin{bmatrix}\mathbf{P}_4\mathbf{P} & \mathbf{P}_5\end{bmatrix}. \tag{5.35}$$

Combining Eq. (5.33) with Eq. (4.25), and using Eq. (4.28), the spatial spin variables, associated to the global rotation of a cross-section, are evaluated using

$$\delta\mathbf{w} = \mathbf{R}_r \mathbf{H}_2 \mathbf{E}^{w\mathrm{T}} \delta\mathbf{d}_g^w, \tag{5.36}$$

with

$$\mathbf{H}_2 = \begin{bmatrix}\mathbf{P}_2\mathbf{P} + \mathbf{G}^{\mathrm{T}} & \mathbf{P}_3\end{bmatrix}. \tag{5.37}$$

Introducing Eqs. (5.34) and (5.36) into Eq. (5.17), one obtains

$$\delta\mathbf{w}^w = \begin{bmatrix}\mathbf{R}_r & \mathbf{0} \\ \mathbf{0} & 1\end{bmatrix} \begin{bmatrix}\mathbf{H}_2 \\ \mathbf{H}_3\end{bmatrix} \mathbf{E}^{w\mathrm{T}} \delta\mathbf{d}_g^w = \mathbf{R}_r^w \mathbf{H}_2^w \mathbf{E}^{w\mathrm{T}} \delta\mathbf{d}_g^w, \tag{5.38}$$

Inertia force vector and tangent dynamic matrix

By inserting the expressions of $\delta\mathbf{u}$ and $\delta\mathbf{w}^w$ given in Eqs. (5.31) and (5.38) into Eq. (5.16), the inertia force vector is obtained as

$$\mathbf{f}_k^w = \mathbf{E}^w \left\{ \begin{bmatrix}\int_{l_o} \mathbf{H}_1^{\mathrm{T}} \mathbf{R}_r^{\mathrm{T}} A_\rho \ddot{\mathbf{u}} \mathrm{d}l \\ \mathbf{0}\end{bmatrix} + \int_{l_o} \mathbf{H}_2^{w\mathrm{T}} \mathbf{R}_r^{w\mathrm{T}} \left[\mathbf{I}_\rho^1 \ddot{\mathbf{w}}^w + \mathbf{I}_\rho^2 \dot{\mathbf{w}}^w\right] \mathrm{d}l \right\}. \tag{5.39}$$

The iterative scheme of the present formulation is implemented with the following approximative linearization

$$\Delta\mathbf{f}_k^w \approx \mathbf{M}\Delta\ddot{\mathbf{d}}_g^w + \mathbf{C}_k \Delta\dot{\mathbf{d}}_g^w. \tag{5.40}$$

The expression of the mass matrix $\mathbf{M}$ is given by

$$\begin{aligned}\mathbf{M} &= \mathbf{E}^w \left\{ \begin{bmatrix}\int_{l_o} \mathbf{H}_1^{\mathrm{T}} A_\rho \mathbf{H}_1 \, \mathrm{d}l & \mathbf{0} \\ \mathbf{0} & \mathbf{0}\end{bmatrix} + \int_{l_o} \mathbf{H}_2^{w\mathrm{T}} \mathbf{R}_r^{w\mathrm{T}} \mathbf{I}_\rho^1 \mathbf{R}_r^w \mathbf{H}_2^w \, \mathrm{d}l \right\} \mathbf{E}^{w\mathrm{T}} \\ &= \mathbf{E}^w \mathbf{M}^e \mathbf{E}^{w\mathrm{T}}. \end{aligned} \tag{5.41}$$

And the gyroscopic matrix $\mathbf{C}_k$ is calculated from

$$\mathbf{C}_k = \mathbf{E}^w \left\{ \begin{bmatrix} \int_{l_o} \mathbf{H}_1^{\mathrm{T}} A_\rho \, (\mathbf{C}_1 + \mathbf{C}_3)\, \mathrm{d}l & \mathbf{0} \\ \mathbf{0} & \mathbf{0} \end{bmatrix} + \int_{l_o} \mathbf{H}_2^{w\mathrm{T}} \mathbf{R}_r^{w\mathrm{T}} \mathbf{I}_\rho^1 \mathbf{R}_r^w \, (\mathbf{C}_2 + \mathbf{C}_4)\, \mathrm{d}l \right.$$
$$\left. + \int_{l_o} \mathbf{H}_2^{w\mathrm{T}} \mathbf{R}_r^{w\mathrm{T}} \left(\mathbf{I}_\rho^2 + \mathbf{I}_\rho^3 \right) \mathbf{R}_r^w \mathbf{H}_2^w \, \mathrm{d}l \right\} \mathbf{E}^{w\mathrm{T}} = \mathbf{E}^w \mathbf{C}_k^e \mathbf{E}^{w\mathrm{T}}, \tag{5.42}$$

where

$$\mathbf{I}_\rho^3 = \begin{bmatrix} \widetilde{(\mathbf{I}_\rho + \mathbf{I}_\alpha)} \dot{\mathbf{w}} + \mathbf{I}_c \, \dot{\alpha} & \mathbf{0} \\ -\dot{\mathbf{w}}^{\mathrm{T}} \, \mathbf{I}_\alpha{}'^{\mathrm{T}} & 0 \end{bmatrix}. \tag{5.43}$$

The warping deformations and the eccentricity of the shear center have been taken into account in deriving the inertial terms, see Eq. (5.4). Consequently, several additional terms were introduced in the expressions of the inertia force vector and the tangent (mass and gyroscopic) matrices. The importance of these terms were discussed in [40] through several numerical examples. It was found, as expected, that the warping deformations in the dynamic terms had a negligible contribution to the response and could be omitted. This is done by setting $I_\omega = 0$ in Eq. (5.13).

The eccentricity of the shear center with respect to the centroid generates extra dynamic terms whose importance was also investigated. It appeared that for slender beams, these terms did not affect the results and can be therefore neglected. But it also showed that they may have a significant contribution for short beams.

If $I_\omega = y_c = z_c = 0$ is adopted, then the expression of the inertia force vector in Eq. (5.39) can be simplified as

$$\mathbf{f}_k^w = \mathbf{E}^w \left\{ \begin{bmatrix} \int_{l_o} \mathbf{H}_1^{\mathrm{T}} \mathbf{R}_r^{\mathrm{T}} A_\rho \ddot{\mathbf{u}} \mathrm{d}l \\ \mathbf{0} \end{bmatrix} + \int_{l_o} \mathbf{H}_2^{\mathrm{T}} \mathbf{R}_r^{\mathrm{T}} \left[\mathbf{I}_\rho \ddot{\mathbf{w}} + \widetilde{\ddot{\mathbf{w}}} \mathbf{I}_\rho \dot{\mathbf{w}} \right] \mathrm{d}l \right\}, \tag{5.44}$$

and similar simplifications apply also for the expressions of the mass and gyroscopic matrices.

5.6 Numerical example - Short cantilever beam with an U cross-section

In [40], five numerical examples of beams with thin-walled cross-sections were solved using the proposed formulation. The predictions of the new formulation was compared against 3D-solid analyses performed with the commercial finite element program Abaqus. The results have demonstrated the accuracy of the formulation. In this chapter, the last example of the five is reproduced. The aim of the this example is not only to assess the performance of the present formulation, but also to highlight the influence of the eccentricity of the shear center on the inertia terms. In fact, for the first, second and fourth examples in [40], the latter did not affect the numerical results and could be neglected by replacing $y_c = z_c = 0$ in Eqs. (5.39), (5.41) and (5.42). But, this example will show a case when the contribution of the eccentricity of the shear center is important.

The cantilever beam with an U cross-section, see Fig. 5.2, was analysed. The eccentricity of the shear center is given by $z_c = -0.138$ m. The beam is subjected to two out-of-plane time-varying concentrated loads, one at the middle and one at the right end. The time-varying load applied at point A is $F_z^{\mathrm{A}} = -4F$. The time-varying load applied at point B is $F_z^{\mathrm{B}} = 2F$. The time evolution of F is given in Fig. 5.3.

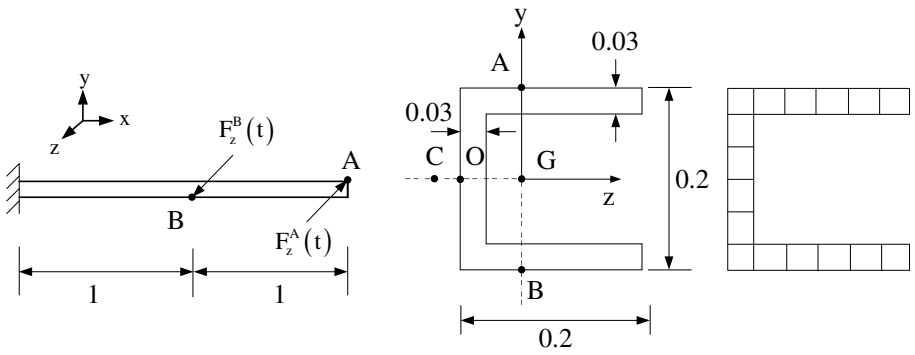

Fig. 5.2: Cantilever beam with U cross-section : geometrical data.

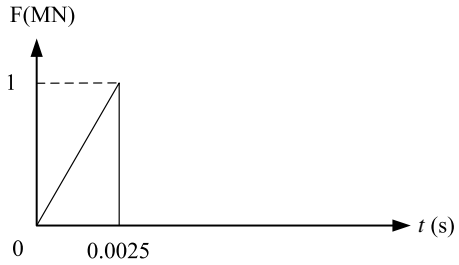

Fig. 5.3: Cantilever beam with U cross-section - Loading history.

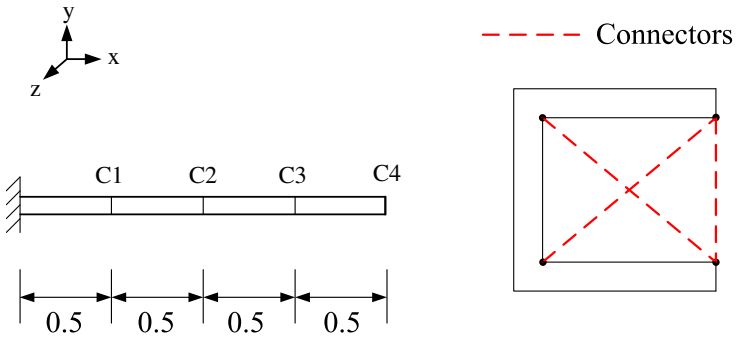

Fig. 5.4: Cantilever beam with U cross-section : Connectors in the 3D-solid model.

The following material properties were used: $E = 210$ GPa, $\nu = 0.33$ and $\rho = 7850$ kg/m^3. All the dimensions in the figures were in meter.

Two different corotational beam models with 40 elements were employed. In the first one, the warping deformations and the eccentricity of the shear center were incorporated in the inertia terms while in the second one they were neglected.

The solid mesh consisted of $16 \cdot 60 = 960$ isoparametric 20 node elements. For the 3D-solid model, four connectors were added at sections C1-C4 along the beam (see Fig. 5.4) in order to avoid in-plane

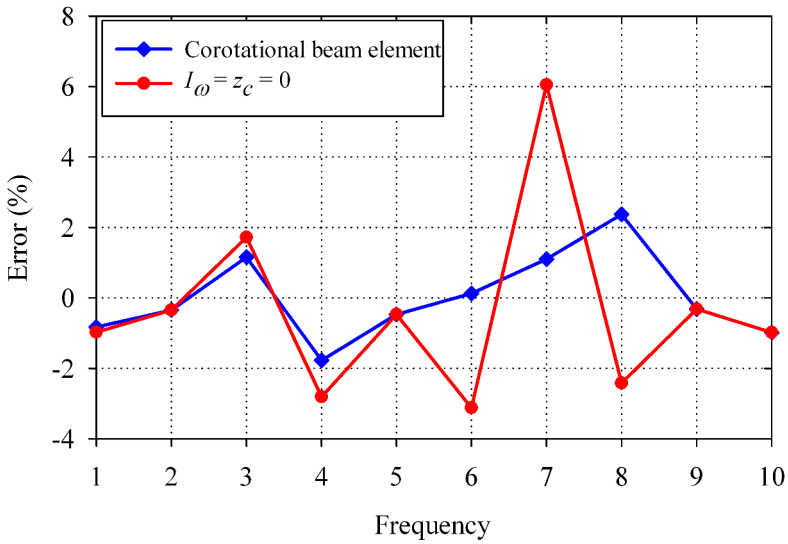

Fig. 5.5: Cantilever beam with U cross-section - Natural frequency analysis.

deformations of the flanges. The connector between 2 nodes maintained the distance of these nodes during the analysis.

The first ten linear natural frequencies of the cantilever were calculated with all the models. For the beam models, a linearized version of the corotational formulation was used. The difference between the i^{th} natural frequency given by a beam model and by the 3D-solid model was calculated as follow

$$Error^i = \left(\frac{Fre^i_{Beam}}{Fre^i_{Solid}} - 1 \right) \cdot 100\% \,. \tag{5.45}$$

The results, depicted in Fig. 5.5, showed that, for the pure bending modes $2^{\text{nd}}, 5^{\text{th}}, 10^{\text{th}}$ and the axial mode 9^{th}, the warping deformations and the eccentricity of the shear center did not effect the frequencies. However, for the torsion-bending modes, the frequencies were better estimated by the beam element which incorporated the warping deformations and the eccentricity of the shear center. The differences between this beam analysis and the 3D-solid one remained smaller than 2.5%. But, when $I_\omega = z_c = 0$, the differences could reach 6%.

The nonlinear behavior of the cantilever due to the time-varying loads were investigated. All analyzes were performed with a time step $\Delta t = 5 \cdot 10^{-5}$ s. Regarding the time integration method, the HHT α method with $\alpha = -0.05$ was used. At the beginning of each time step, the predictor Pred. 4 (see Section 3.2) was adopted. The time evolution of the displacement u_y of point O at the right end was depicted in Fig. 5.6. A very good agreement between the corotational beam and Abaqus 3D-solid analysis was obtained. However, when $I_\omega = z_c = 0$, large discrepancies between the beam and 3D-solid analysis could be noted.

This example shows that the proposed element can be used to analyse the nonlinear dynamic behavior of beams with arbitrary cross-sections and also that the additional dynamic terms due to the eccentricity of the shear center cannot be neglected. As a matter of fact, the numerical results seem to be improved if the eccentricity of the shear center is considered.

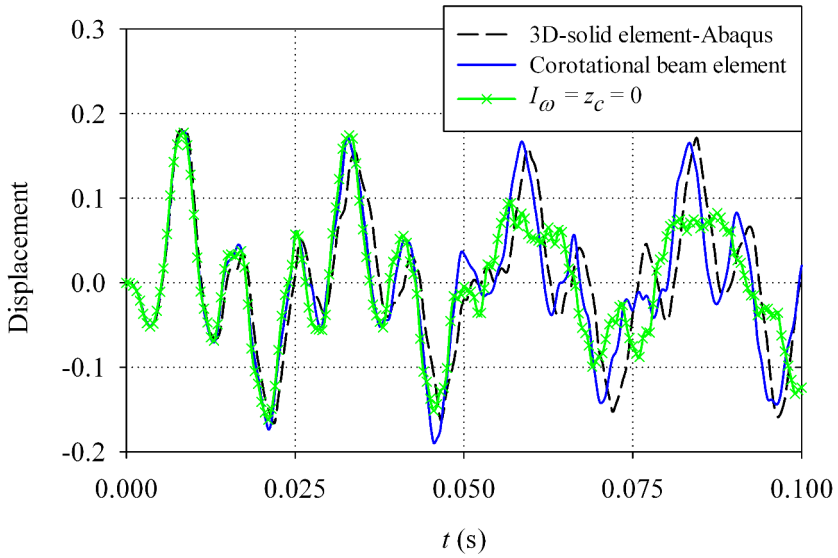

Fig. 5.6: Cantilever beam with U cross-section - Time evolution of the displacement u_y of point O.

Chapter 6

Conclusions and future research

6.1 Conclusions

The main objective of this research was to provide efficient beam formulations for nonlinear dynamics of flexible structures using the corotational method. Beam formulations in both 2D and 3D (with solid and arbitrary thin-walled cross-section) were considered.

2D beam formulation

A consistent dynamic beam formulation for the corotational approach in 2D was derived. The same corotational kinematic description was adopted for both static and dynamic parts. Moreover, in order to take into account the inertia effect due to the local transverse displacements, the local cubic interpolations were not only adopted to develop expressions of the elastic terms but also to derive the inertia terms.

This new formulation was compared with two classic formulations using constant Timoshenko and constant lumped mass matrices. Several numerical examples showed that the new formulation was more efficient than the two classic ones. Indeed, all results indicated that the new formulation required more computational time but allowed to reduce significantly the number of elements. This advantage is due to a better representation of the local displacements in the inertia terms.

Finite rotations in dynamics

The treatment of the finite rotations is one of the most important issues in the development of 3D beam elements. In the paper [38], the rotation tensor, the incremental rotational vector and the incremental Euler parameters were adopted to parameterize the finite rotations. Four dynamic formulations based on these parameterizations were compared. The first three formulations were taken from the literature [11, 30, 55]. The last one was new. In these formulations, the corotational method was used to develop expressions of the internal forces and the tangent stiffness matrices, while the dynamic terms were formulated into a total Lagrangian context. The similarities and differences between the formulations in theoretical derivations and implementations were pointed out. Many numerical examples were implemented in order to assess numerical accuracy and computational efficiency of the formulations. Beside several predictors for iterative procedure and various possibilities to simplify the tangent dynamic matrix were tested.

The numerical results showed that

- For the practical implementation, the new formulation and the one proposed by Cardona and Geradin [11] were the simplest ones: the same standard Newmark method was used for both the displace-

ments and the rotations. No quantities needed to be saved at each Gauss point.

- For all the formulations, the predictor proposed by Crisfield in [13] was the best alternative. This predictor for the general case of a non constant tangent inertia matrix was given in detail in the second paper [38].
- For each formulation, the choice of the tangent inertia matrix affects significantly the computational efficiency. For the first two formulations, the best alternative was to take the exact tangent inertia matrix. For the last two formulations, it was better to take only the mass and gyroscopic matrices.
- All the formulations gave the same numerical results but the new formulation was slightly more efficient than the other ones regarding the CPU time.

3D beam formulation with solid cross-section

A consistent 3D corotational beam element for nonlinear dynamics of flexible structures was presented. Compared with the other formulations found in the literature, the novelty of the formulation is that the corotational kinematics was used to derive both internal and inertia terms. Besides, local cubic interpolation functions were used. The inertia force vector and the tangent dynamic matrix were derived by introducing an approximation with regard to the local rotations. To enhance the efficiency of the iterative procedure, an approximative tangent dynamic matrix was adopted.

Four numerical examples were considered to compare the new formulation with two other approaches. The first approach, called as "linear corotational approach", was derived from the new formulation by replacing cubic interpolations with linear ones. The second approach was the classic total Lagrangian proposed by Simo and Vu-Quoc [53–55]. This approach can be implemented with different number of nodes. To ensure a meaningful comparison of both formulations, Simo and Vu-Quoc's approach was implemented with two nodes which correspond to a linear interpolations for all global variables.

Based on these examples, the following conclusions were drawn

- All formulations gave the same results with fine meshes.
- As expected, with coarse meshes, Simo and Vu-Quoc's two-noded formulation and the linear corotational one gave less accurate results compared to the cubic corotational approach which provided very accurate results. This demonstrated the importance of an accurate description of the deformations in the dynamic terms, which was not possible with linear interpolations.
- The linear corotational approach was faster than the cubic one. This was expected since several inertia terms disappeared when local linear interpolations were adopted. Moreover, in the linear corotational approach, the inertia force vector and the tangent dynamic matrix were integrated using two Gauss points, whereas the dynamic terms of the cubic corotational one were integrated using three Gauss points.
- As it was more involved, the cubic corotational formulation was slightly slower than linear formulations (around 12%). However, certain cases could arise where the desired accuracy could be achieved via the cubic formulation faster than the linear formulation of Simo and Vu-Quoc.

One could conclude that the new dynamic corotational formulation based on the local cubic interpolations provided sufficient accuracy with relatively low number of elements as compared to linear formulations. With the same number of elements, about the same computational time was required (this could differ a little from one example to another). However, with the present formulation, accurate results could be obtained with a smaller number of elements.

3D beam formulation with arbitrary thin-walled open cross-section

The previous 3D corotational beam element is extended for the nonlinear dynamics of structures with thin-walled cross-section by introducing the warping deformations and the eccentricity of the shear center. This led to additional terms in the expressions of the inertia force vector and the tangent (mass and gyroscopic) dynamic matrices. This element had seven degrees of freedom at each node.

Five 3D beam problems, with different thin-walled cross-sections and load pattern, were analysed. The predictions of the proposed formulation were compared against the numerical results obtained with both Abaqus beam element and 3D-solid analyses. For all the examples, a very good agreement between the results obtained with the corotational beam element and the 3D-solid element was obtained. Besides, the numerical results also showed that the warping deformations had a negligible influence in the dynamic terms and could be omitted. However, the additional dynamic terms due to the shear center eccentricity could not always be neglected. In fact, it seemed that for slender beams, the same numerical results were obtained with or without these terms. However, for short beams, the numerical results seemed to be improved if the shear center eccentricity was considered.

6.2 Future research

From the work presented in this thesis, some interesting topics for future research are suggested.

Energy conserving method

The HHT α method was used to solve the nonlinear equation of motion in this work. This method introduces a small numerical damping and limits the influence of high frequencies. However, the numerical results can be affected for long time analyses due to the dissipation of the total energy. It should be noted that the main objective of this work is to compare different beam elements, thus this disadvantage had no influence to the conclusions.

For beam structures, more robust alternatives to the HHT α method have been proposed in the literature [14, 29]. It would be interesting to implement the new beam elements with an energy conserving method.

Initially curved beam element

All the formulations in this work were developed in the context of two-noded straight beam elements. For beam structures with curved geometry, it is always possible to catch their behaviors by using a large number of straight elements. However, in order to reduce the number of elements, a curved beam element can be used. Hence, an interesting topic for a further research is to extend the elements developed in this thesis by introducing initial curvature.

Comparative study with a total Lagragian quadratic beam element

As showed in [39], to obtain accuracy results, the new dynamic corotational formulation, based on the local cubic interpolations, required a smaller number of elements than the one of Simo and Vu-Quoc, based on linear interpolations. Although, it must be emphasized that the above conclusion was based on a comparative study of two-noded elements. In the context of the total Lagrangian approach, efficient three-noded elements with quadratic shape functions can be developed, see for instance the formulation for static analysis proposed in [27, 31]. Therefore, it should be interesting for dynamic problems to compare the new corotational formulation and a total Lagrangian quadratic element.

New corotational shell finite elements for dynamics

Several corotational shell elements has been developed by Pacoste [47] and Battini [6]. All of these shell elements concern static analysis. Therefore, it would be interesting to extend the present work to the nonlinear dynamics of corotational shells.

Bibliography

[1] R. Alsafadie, J.-M. Battini, M. Hjiaj, and H. Somja. A comparative study of displacement and mixed-based corotational finite element formulations for elasto-plastic three-dimensional beam analysis. *Engerg. Computs*, 28:939–982, 2011.

[2] R. Alsafadie, M. Hjiaj, and J.-M. Battini. Corotational mixed finite element formulation for thin-walled beams with generic cross-section. *Comput. Methods Appl. Mech. Engrg.*, 199:3197–3212, 2010.

[3] J. Argyris. An excursion into large rotations. *Comput. Methods Appl. Mech. Engrg.*, 32:85–155, 1982.

[4] K.J. Bathe, E. Ramm, and E.L. Wilson. Finite element formulations for large deformation dynamic analysis. *Int. J. Num. Methods. Engrg.*, 9:353–386, 1975.

[5] J.-M. Battini. *Co-rotational beam elements in instability problems*. Phd thesis, KTH Royal Institute of Technology, Stockholm, SWEDEN, 2002.

[6] J.-M. Battini. A modified corotational framework for triangular shell elements. *Comput. Methods Appl. Mech. Engrg.*, 196:1905–1914, 2007.

[7] J.-M. Battini. Large rotations and nodal moments in corotational elements. *CMES*, 33(1):1–15, 2008.

[8] J.-M. Battini and C. Pacoste. Co-rotational beam elements with warping effects in instability problems. *Comput. Methods Appl. Mech. Engrg.*, 191:1755–1789, 2002.

[9] K. Behdinan, M.C. Stylianou, and B. Tabarrok. Co-rotational dynamic analysis of flexible beams. *Comput. Methods Appl. Mech. Engrg.*, 154:151–161, 1998.

[10] P. Betsch and P. Steinmann. Constrained dynamics of geometrically exact beams. *Comput. Mech.*, 31:49–59, 2003.

[11] A. Cardano and M. Geradin. A beam finite element non-linear theory with finite rotations. *Int. J. Num. Methods. Engrg.*, 26:2403–2438, 1988.

[12] J. Chung and Hulbert G.M. A predictor-corrector algorithm of the generalized-α method for analysis of structural dynamics. *J. Korean Soc. Noise Vibr. Eng.*, 5(2):207–213, 1995.

[13] M.A. Crisfield. *Non-Linear Finite Element Analysis of Solids and Structures: Advanced Topics*. John Wiley & Sons, Inc., New York, NY, USA, 1st edition, 1997.

[14] M.A. Crisfield, U. Galvanetto, and G. Jelenić. Dynamics of 3-d co-rotational beams. *Comput. Mech.*, 20:507–519, 1997.

[15] M.A. Crisfield and G.F. Moita. A unified co-rotational framework for solids shells and beams. *Int. J. Solids Struct.*, 33:2969–2992, 1996.

[16] M.A. Crisfield and J. Shi. An energy conserving co-rotational procedure for non-linear dynamics with finite elements. *Nonlinear Dynamics*, 9:37–52, 1996.

[17] H.A. Elkaranshawy and M.A. Dokainish. Corotational finite element analysis of planar flexible multibody systems. *Comput. Struct.*, 54(5):881–890, 1995.

[18] K. Forsell. *Instability analyses of structures under dynamic loads*. Phd dissertation, KTH, Sweden, 2000.

[19] U. Galvanetto and M.A. Crisfield. An energy conserving co-rotational procedure for dynamics of planar beam structures. *Int. J. Num. Methods. Engrg.*, 39:2265–2282, 1996.

[20] M. Geradin and A. Cardona. Kinematics and dynamics of rigid and flexible mechanisms using finite elements and quaternion algebra. *Comput. Mech.*, 4:115–135, 1989.

[21] M. Geradin and A. Cardona. *Flexible multibody dynamics: a finite element approach*. John Wiley, 2001.

[22] R. Gruttmann, R. Sauer, and R. Wagner. Theory and numerics of three-dimensional beams with elastoplastic behavior. *Int. J. Num. Meth. Engng.*, 48:1675–1702, 2000.

[23] W Guggenberger. Nonlinear analysis of space frame structures-large rotation formulations and their consistent approximations for moderate rotations. *ECCOMAS*, 11-14 September 2000.

[24] K.M. Hsiao, J.Y. Lin, and W.Y. Lin. A consistent co-rotational finite element formulation for geometrically nonlinear dynamic analysis of 3-d beams. *Comput. Methods Appl. Mech. Engrg*, 169:1–18, 1999.

[25] K.M. Hsiao, W.Y. Lin, and R.H. Chen. Geometrically non-linear dynamic analysis of thin-walled beams. *Proc. World Congress Engrg.*, II, 2009.

[26] K.M. Hsiao and R.T. Yang. A co-rotational formulation for nonlinear dynamic analysis of curved euler beam. *Comput. Struct.*, 54(6):1091–1097, 1995.

[27] A. Ibrahimbegović. On fe implementation of geometrically nonlinear reissner's beam theory: Three-dimensional curved beam elements. *Comput. Methods Appl. Mech. Engrg.*, 122:11–26, 1995.

[28] A. Ibrahimbegović. On the choice of finite rotation parameters. *Comput. Methods Appl. Mech. Engrg.*, 149:49–71, 1997.

[29] A. Ibrahimbegović and S. Mamouri. Energy conserving/decaying implicit time-stepping scheme for nonlinear dynamics of three-dimensional beams undergoing finite rotations. *Comput. Methods Appl. Mech. Engrg.*, 191:4241–4258, 2002.

[30] A. Ibrahimbegović and M.A. Mikdad. Finite rotations in dynamics of beams and implicit time-stepping schemes. *Int. J. Num. Methods. Engrg.*, 41:781–814, 1998.

[31] A. Ibrahimbegović and R.L. Taylor. On the role of frame-invariance in structural mechanics models at finite rotations. *Comput. Methods Appl. Mech. Engrg.*, 191:5159–5176, 2002.

[32] M. Iura and S.N. Atluri. Dynamic analysis of finitely stretched and rotated three-dimensional space-curved beams. *Comput. Struct.*, 29:875–889, 1988.

[33] M. Iura and S.N. Atluri. Dynamic analysis of planar flexible beams with finite rotations by using inertial and rotating frames. *Comput. Struct.*, 55(3):453–462, 1995.

[34] G. Jelenić and M.A. Crisfield. Interpolation of rotational variables in nonlinear dynamics of 3d beams. *Int. J. Num. Methods. Engrg.*, 43:1193–1222, 1998.

[35] G. Jelenić and M.A. Crisfield. Geometrically exact 3d beam theory: implementation of a strain-invariant element for stactics and dynamics. *Comput. Methods Appl. Mech. Engrg.*, 171:141–171, 1999.

[36] S. Krenk. *Non-linear modeling and analysis of solids and structures*. Cambridge University Press, 2009.

[37] T.-N. Le, J.-M. Battini, and M. Hjiaj. Efficient formulation for dynamics of corotational 2d beams. *Comput. Mech.*, 48(2):153–161, 2011.

[38] T.-N. Le, J.-M. Battini, and M. Hjiaj. Dynamics of 3d beam elements in a corotational context: A comparative study of established and new formulations. *Finite Elem. Anal. Des.*, 61:97–111, 2012.

[39] T.-N. Le, J.-M. Battini, and M. Hjiaj. A consistent 3d corotational beam element for nonlinear dynamic analysis of flexible structures. *Comput. Methods Appl. Mech. Engrg.*, accepted, 2013.

[40] T.-N. Le, J.-M. Battini, and M. Hjiaj. Corotational formulation for nonlinear dynamics of beams with arbitrary thin-walled cross-sections. *Comput. Struct.*, accepted, 2013.

[41] E.V. Lens and A. Cardona. A nonlinear beam element formulation in the framework of an energy preserving time integration scheme for constrained multibody systems dynamics. *Comput. Struct.*, 86:47–63, 2008.

[42] J. Mäkinen. Critical study of newmark-scheme on manifold of finite rotations. *Comput. Methods Appl. Mech. Engrg.*, 191:817–828, 2001.

[43] J. Mäkinen. Total lagrangian reissner's geometrically exact beam element without singularities. *Int. J. Num. Methods. Engrg.*, 70:1009–1048, 2007.

[44] N. Masuda, T. Nishiwaki, and M. Minaaawa. Nonlinear dynamic analysis of frame structures. *Comput. Struct.*, 27(1):103–110, 1987.

[45] B. Nour-Omid and C.C. Rankin. Finite rotation analysis and consistent linearization using projectors. *Comput. Methods Appl. Mech. Engrg.*, 93:353–384, 1991.

[46] C. Oran and A. Kassimali. Large deformations of framed structures under static and dynamic loads. *Comput. Struct.*, 6:539–547, 1976.

[47] C. Pacoste. Corotational flat facet triangular elements for shell instability analysis. *Comput. Methods Appl. Mech. Engrg.*, 156:75–110, 1998.

[48] C. Pacoste and A. Eriksson. Element behavior in post-critical plane frame analysis. *Comput. Methods Appl. Mech. Engrg.*, 125:319–343, 1995.

[49] C. Pacoste and A. Eriksson. Beam elements in instability problems. *Comput. Methods Appl. Mech. Engrg.*, 144:163–197, 1997.

[50] C.C. Rankin and B. Nour-Omid. The use of projectors to improve finite element performance. *Comput. Struct.*, 30:257–267, 1988.

[51] J.N. Reddy. On locking-free shear deformable beam finite elements. *Comput. Methods Appl. Mech. Engrg.*, 149:113–132, 1997.

[52] I. Sheinman. Dynamic large-displacement analysis of curved beams involving shear deformation. *Int. J. Solids Structures*, 16:1037–1049, 1980.

[53] J.C. Simo. A finite strain beam formulation. the three-dimensional dynamic problem. part i. *Comput. Methods Appl. Mech. Engrg.*, 49:55–70, 1985.

[54] J.C. Simo and L. Vu-Quoc. On the dynamics of flexible beams under large overall motions - the plane case: Part i. *J. Appl. Mech. ASME*, 53:849–863, 1986.

[55] J.C. Simo and L. Vu-Quoc. On the dynamics in space of rods undergoing large motions - a geometrically exact approach. *Comput. Methods Appl. Mech. Engrg.*, 66:125–161, 1988.

[56] Q. Xue and J.L. Meek. Dynamic response and instability of frame structures. *Comput. Methods Appl. Mech. Engrg.*, 190:5233–5242, 2001.

[57] E. Zupan, M. Saje, and D. Zupan. Quaternion-based dynamics of geometrically nonlinear spatial beams using the Runge – Kutta method. *Finite Elem. Anal. Des.*, 54:48–60, 2012.

[58] E. Zupan, M. Saje, and D. Zupan. Dynamics of spatial beams in quaternion description based on the newmark integration scheme. *Comput. Mech.*, 51:47–64, 2013.

Paper 1: Efficient formulation for dynamics of corotational 2D beams

Computational Mechanics, Volume 48, Number 2: 153-161, August 2011
DOI: 10.1007/s00466-011-0585-6

Computational Mechanics.
Comput. Mech., Volume 48, Issue 2, pp 153-161 (2011).

Efficient formulation for dynamics of corotational 2D beams

Thanh-Nam Le [1,2] , Jean-Marc Battini [2] , Mohammed Hjiaj [1]

[1] *Université Européenne de Bretagne, INSA de Rennes - LGCGM/Structural Engineering Research Group, 20 avenue des Buttes de Coësmes, CS 70839, 35708 Rennes Cedex 7, France.*

[2] *KTH, Royal Institute of Technology - Department of Civil and Architectural Engineering, SE-10044 Stockholm, Sweden.*

Abstract

The corotational method is an attractive approach to derive nonlinear beam finite elements. In a number of papers, this method was employed to investigate the nonlinear dynamic analysis of 2D beams. However, most of the approaches found in the literature adopted either a lumped mass matrix or linear local interpolations to derive the inertia terms (which gives the classical linear and constant Timoshenko mass matrix), although local cubic interpolations were used to derive the elastic force vector and the tangent stiffness matrix. In this paper, a new corotational formulation for nonlinear dynamic analysis is presented. Cubic interpolations are used to derive both the inertia and elastic terms. Numerical examples show that the proposed approach is more efficient than using lumped or Timoshenko mass matrices.

Key words: Nonlinear dynamic analysis; Corotational formulation; 2D beam element;

1 Introduction

The corotational approach is a well known method to derive efficient nonlinear finite beam elements [1–11]. The main idea is to decompose the motion of the element into rigid body and pure deformational parts. During the rigid body motion, a local coordinates system, fixed to the element, moves and rotates with it. The deformational part is measured in this local system. The main interest of the approach is that different assumptions can be made to represent the local deformations, giving different possibilities for the local element formulation.

Regarding the dynamic formulation of 2D corotational beams, several options are available. If linear interpolations are used for the local formulation, e.g. by taking the classical linear Timoshenko element, then inertia corotational terms are easily derived and the classical linear and constant Timoshenko mass matrix is obtained. However, linear interpolations assume that the transverse displacements are equal to zero along the element, which is not accurate, especially for flexible beams. If cubic interpolations are used for the local formulation, e.g. by taking the classical linear Bernoulli element, then the derivation of the inertia terms becomes very complicated. In [2], Crisfield et al. suggested that this derivation is impossible due to its complexity. Therefore, they used the constant Timoshenko mass matrix although they adopted local cubic interpolations to derive the elastic force vector and the tangent stiffness matrix. The same approach was adopted in [6]. In [7–9], the authors used a constant lumped mass matrix without any attempt to check its accuracy. In [10], Behdinan et al. proposed a corotational dynamic formulation. But the cubic shape functions were used to describe the global displacements, which is not consistent with the idea of the corotational method.

In fact, to the authors' knowledge, there is no general formulation for the dynamic of corotational 2D beam elements in the literature. The purpose of this paper is to present such a formulation by considering local cubic interpolations not only to obtain the elastic terms but also to derive the inertia terms. The cubic shape functions of the Interdependent Interpolation Element (IIE) [12] are used to derive the local elastic force vector and local tangent stiffness matrix. These shape functions are based on the hermitian ones but a modification is introduced in order to consider the bending shear deformations. For the inertia terms, numerical calculations have shown that both IIE and hermitian shape functions give the same numerical results. Therefore, inertia terms are calculated by considering hermitian shape functions for the local kinematics.

The rest of the paper is organized as follows. In Sects. 2 and 3 the corotational kinematics of a 2D beam element and the derivation of the elastic force vector and the tangent stiffness matrix are presented. More details about the derivation can be found in [13]. Sections 4 and 5 are devoted to the derivation of the inertia terms. In Sect. 6, four examples are presented in order to assess the accuracy of the present dynamic formulation. Finally, conclusions are given in Sect. 7.

2 Beam kinematics

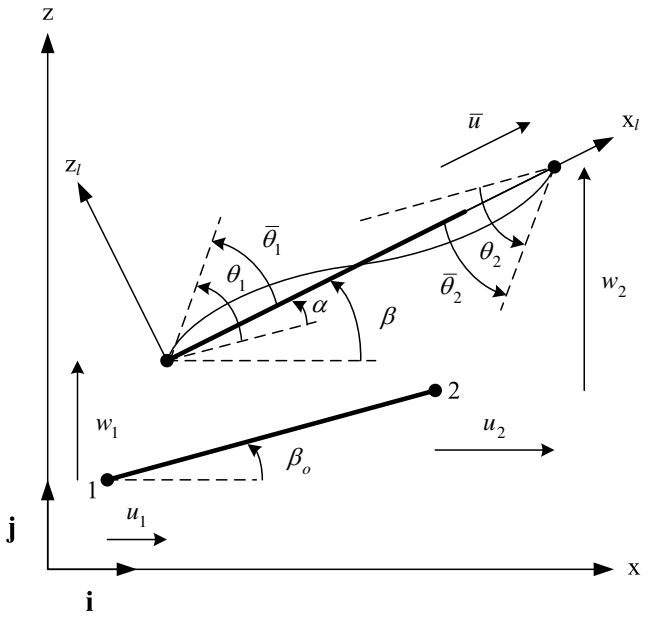

Fig. 1. Beam kinematics 1.

The notations used are defined in Fig. 1. The coordinates for the nodes 1 and 2 in the global coordinate system (x,z) are (x_1,z_1) and (x_2,z_2). The vector of global displacements is defined by

$$\mathbf{q} = \begin{bmatrix} u_1 & w_1 & \theta_1 & u_2 & w_2 & \theta_2 \end{bmatrix}^{\mathrm{T}}, \tag{1}$$

while the vector of local displacements is defined by

$$\overline{\mathbf{q}} = \begin{bmatrix} \overline{u} & \overline{\theta}_1 & \overline{\theta}_2 \end{bmatrix}^{\mathrm{T}}. \tag{2}$$

The components of $\overline{\mathbf{q}}$ can be computed according to

$$\overline{u} = l_n - l_o \,, \tag{3}$$

$$\overline{\theta}_1 = \theta_1 - \alpha = \theta_1 - \beta + \beta_o \,, \tag{4}$$

$$\overline{\theta}_2 = \theta_2 - \alpha = \theta_2 - \beta + \beta_o \,. \tag{5}$$

In Eq. (3), l_o and l_n denote the initial and current lengths of the element :

$$l_o = [\,(x_2 - x_1)^2 + (z_2 - z_1)^2\,]^{1/2} \,, \tag{6}$$

$$l_n = [\,(x_2 + u_2 - x_1 - u_1)^2 + (z_2 + w_2 - z_1 - w_1)^2\,]^{1/2} \,. \tag{7}$$

The current angle of the local system with respect to the global system is denoted as β and is given by

$$c = \cos\beta = \frac{1}{l_n}(x_2 + u_2 - x_1 - u_1) \,, \tag{8}$$

$$s = \sin\beta = \frac{1}{l_n}(z_2 + w_2 - z_1 - w_1) \,. \tag{9}$$

The differentiation of the expression for the angle β (9) gives

$$\delta\beta = \frac{1}{l_n}\begin{bmatrix} s & -c & 0 & -s & c & 0 \end{bmatrix}\delta\mathbf{q} \,. \tag{10}$$

The differentiation of the expressions (3) to (5) yield to

$$\delta\overline{\mathbf{q}} = \mathbf{B}\,\delta\mathbf{q} \,, \tag{11}$$

with

$$\mathbf{B} = \begin{bmatrix} \mathbf{b}_1 \\ \mathbf{b}_2 \\ \mathbf{b}_3 \end{bmatrix} = \begin{bmatrix} -c & -s & 0 & c & s & 0 \\ -s/l_n & c/l_n & 1 & s/l_n & -c/l_n & 0 \\ -s/l_n & c/l_n & 0 & s/l_n & -c/l_n & 1 \end{bmatrix} \,. \tag{12}$$

3 Elastic force vector and tangent stiffness matrix

By equating the virtual work in the local and global systems, the relation between the local elastic force vector $\mathbf{f}_l$ and the global one $\mathbf{f}_g$ is obtained as

$$V = \delta\mathbf{q}^{\mathrm{T}}\mathbf{f}_g = \delta\overline{\mathbf{q}}^{\mathrm{T}}\mathbf{f}_l = \delta\mathbf{q}^{\mathrm{T}}\mathbf{B}^{\mathrm{T}}\mathbf{f}_l \,. \tag{13}$$

The equation (13) must apply for any arbitrary $\delta\mathbf{q}$. Hence the global elastic force vector $\mathbf{f}_g$ is given by

$$\mathbf{f}_g = \mathbf{B}^{\mathrm{T}}\mathbf{f}_l \quad \text{with} \quad \mathbf{f}_l = \begin{bmatrix} N & M_1 & M_2 \end{bmatrix}^{\mathrm{T}} \,. \tag{14}$$

The global tangent stiffness matrix is defined by

$$\delta\mathbf{f}_g = \mathbf{K}_g\,\delta\mathbf{q} \,. \tag{15}$$

By taking the differentiation of the expression for the internal force vector (14), the global stiffness matrix is obtained

$$\mathbf{K}_g = \mathbf{B}^{\mathrm{T}}\mathbf{K}_l\,\mathbf{B} + \frac{\mathbf{z}\,\mathbf{z}^{\mathrm{T}}}{l_n}N + \frac{1}{l_n^2}(\mathbf{r}\,\mathbf{z}^{\mathrm{T}} + \mathbf{z}\,\mathbf{r}^{\mathrm{T}})(M_1 + M_2) \,, \tag{16}$$

where

$$\mathbf{r} = \begin{bmatrix} -c & -s & 0 & c & s & 0 \end{bmatrix}^{\mathrm{T}} , \tag{17}$$

$$\mathbf{z} = \begin{bmatrix} s & -c & 0 & -s & c & 0 \end{bmatrix}^{\mathrm{T}} . \tag{18}$$

The local elastic force vector $\mathbf{f}_l$ and local tangent stiffness matrix $\mathbf{K}_l$, which is defined by $\delta\mathbf{f}_l = \mathbf{K}_l\,\delta\overline{\mathbf{q}}$, depend on the definition of the local formulation. In this work, the shape functions of the IIE are used together with a shallow arch beam theory. The shallow arch longitudinal and shear strains are given by

$$\varepsilon = \frac{1}{l_o}\int_{l_o}\left[\frac{\partial u}{\partial x} + \frac{1}{2}\left(\frac{\partial w}{\partial x}\right)^2\right]\mathrm{d}x - \frac{\partial^2 w}{\partial x^2}\,z\,, \tag{19}$$

$$\gamma = \frac{\partial w}{\partial x} + \vartheta\,. \tag{20}$$

The shape functions of the IIE element [12] are based on the exact solution of the homogeneous form of the equilibrium equations for the Timoshenko beam. The axial displacement u, the transverse displacement w and the local rotation ϑ are given by

$$u = \frac{x}{l_o}\,\overline{u}\,, \tag{21}$$

$$w = \varphi_1\overline{\theta}_1 + \varphi_2\overline{\theta}_2\,, \tag{22}$$

$$\vartheta = \varphi_3\overline{\theta}_1 + \varphi_4\overline{\theta}_2\,, \tag{23}$$

where

$$\varphi_1 = \mu\,x\left[6\,\Omega\left(1-\frac{x}{l_o}\right) + \left(1-\frac{x}{l_o}\right)^2\right]\,, \tag{24}$$

$$\varphi_2 = \mu\,x\left[6\,\Omega\left(\frac{x}{l_o}-1\right) - \frac{x}{l_o} + \frac{x^2}{l_o^2}\right]\,, \tag{25}$$

$$\varphi_3 = \mu\left(1 + 12\,\Omega - \frac{12\,\Omega\,x}{l_o} - \frac{4\,x}{l_o} + \frac{3\,x^2}{l_o^2}\right)\,, \tag{26}$$

$$\varphi_4 = \mu\left(\frac{12\,\Omega\,x}{l_o} - \frac{2\,x}{l_o} + \frac{3\,x^2}{l_o^2}\right)\,, \tag{27}$$

$$\Omega = \frac{E\,I}{G\,A\,K_s\,l_o^2}\,, \tag{28}$$

$$\mu = \frac{1}{1+12\Omega}\,, \tag{29}$$

A, I : Section's area and second moment of area ,

K_s : Shear correction coefficient .

For a rectangular cross-section, $K_s = \dfrac{5}{6}$.

With $\Omega = 0$, the hermitian shape functions of the classical Bernoulli elements are recovered. The interest of IIE formulation is to keep the accuracy inherent to the cubic interpolation and with Ω to add the bending shear deformation.

The MAPLE code for obtaining the local elastic force vector and the tangent stiffness matrix is given in Appendix A.

4 Inertia force vector and mass matrix

The inertia force vector is calculated from the kinetic energy by using the Lagrange's equation of motion:

$$\mathbf{f}_K = \frac{\mathrm{d}}{\mathrm{d}t}\left[\frac{\partial K}{\partial \dot{\mathbf{q}}}\right] - \left[\frac{\partial K}{\partial \mathbf{q}}\right] . \tag{30}$$

The kinetic energy K of an element is given as

$$K = \frac{1}{2}\rho\left\{\int_{l_o} A(\dot{u}_{\mathrm{G}}^2 + \dot{w}_{\mathrm{G}}^2)\mathrm{d}l + \int_{l_o} I\,\dot{\theta}^2 \mathrm{d}l\right\} , \tag{31}$$

where

ρ : Mass per unit volume,

u_{G} , w_{G}: Global displacements of the cross-section centroid,

θ : Global rotation of the section.

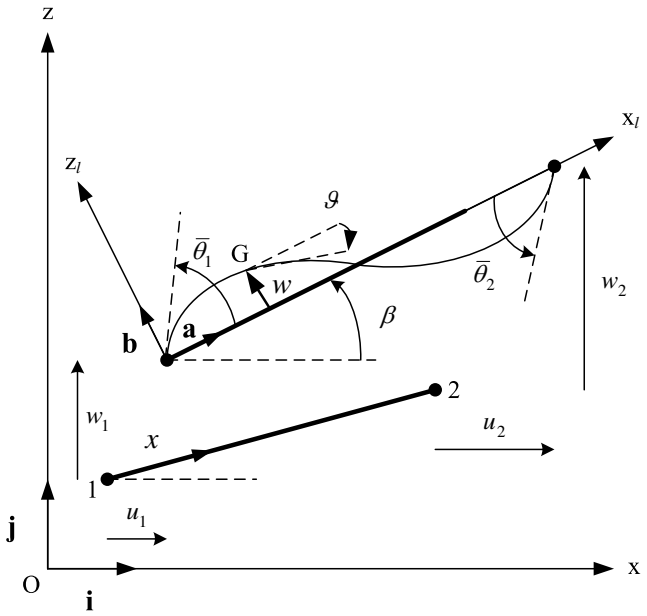

Fig. 2. Beam kinematics 2.

The global position of the cross-section centroid is given by (see Fig. 2)

$$\mathrm{OG} = (x_1 + u_1)\,\mathbf{i} + (z_1 + w_1)\,\mathbf{j} + \frac{l_n}{l_o} x\,\mathbf{a} + w\,\mathbf{b} , \tag{32}$$

with

$$\mathbf{a} = \cos\beta\,\mathbf{i} + \sin\beta\,\mathbf{j} , \tag{33}$$

$$\mathbf{b} = -\sin\beta\,\mathbf{i} + \cos\beta\,\mathbf{j} . \tag{34}$$

Equation (32) can be written as

$$\mathrm{OG} = \left[x_1 + u_1 + \frac{l_n}{l_o} x\cos\beta - w\sin\beta\right]\mathbf{i} + \left[z_1 + w_1 + \frac{l_n}{l_o} x\sin\beta + w\cos\beta\right]\mathbf{j} . \tag{35}$$

Using Eqs. (8) and (9), the above equation becomes

$$\mathrm{OG} = \left[x_1 + u_1 + \frac{x}{l_o}(x_2 + u_2 - x_1 - u_1) - w\sin\beta\right]\mathbf{i} + \left[z_1 + w_1 + \frac{x}{l_o}(z_2 + w_2 - z_1 - w_1) + w\cos\beta\right]\mathbf{j}\,. \tag{36}$$

So, the velocities components are given by

$$\dot{u}_\mathrm{G} = \dot{u}_1 + \frac{x}{l_o}(\dot{u}_2 - \dot{u}_1) - \dot{w}\sin\beta - w\dot{\beta}\cos\beta\,, \tag{37}$$

$$\dot{w}_\mathrm{G} = \dot{w}_1 + \frac{x}{l_o}(\dot{w}_2 - \dot{w}_1) + \dot{w}\cos\beta - w\dot{\beta}\sin\beta\,, \tag{38}$$

and the global rotation of the cross section is given by

$$\dot{\theta} = \dot{\vartheta} + \dot{\alpha} = \dot{\vartheta} + \dot{\beta}\,. \tag{39}$$

For the dynamic formulation, Ω is taken to 0. Extensive numerical studies performed by the authors have shown that this simplification does not modify the numerical results. Then, the local velocities are interpolated using

$$\dot{w} = x\left(1 - \frac{x}{l_o}\right)^2(\dot{\theta}_1 - \dot{\beta}) - \left(1 - \frac{x}{l_o}\right)\frac{x^2}{l_o}(\dot{\theta}_2 - \dot{\beta})\,, \tag{40}$$

$$\dot{\vartheta} = \left(1 - \frac{x}{l_o}\right)\left(1 - \frac{3x}{l_o}\right)(\dot{\theta}_1 - \dot{\beta}) + \frac{x}{l_o}\left(-2 + \frac{3x}{l_o}\right)(\dot{\theta}_2 - \dot{\beta})\,. \tag{41}$$

The exact expression of the kinetic energy K can be obtained by substituting (37),(38) and (39) into (31), and by using (10) to calculate $\dot{\beta}$. K can be written as

$$K = \frac{1}{2}\,\dot{\mathbf{q}}^\mathrm{T}\mathbf{M}\dot{\mathbf{q}}\,. \tag{42}$$

The local mass matrix $\mathbf{M}_l$ is defined by

$$\mathbf{M} = \mathbf{T}^\mathrm{T}\mathbf{M}_l\mathbf{T}\,, \tag{43}$$

where $\mathbf{T}$ is rotation matrix,

$$\mathbf{T} = \begin{bmatrix} c & s & 0 & 0 & 0 & 0 \\ -s & c & 0 & 0 & 0 & 0 \\ 0 & 0 & 1 & 0 & 0 & 0 \\ 0 & 0 & 0 & c & s & 0 \\ 0 & 0 & 0 & -s & c & 0 \\ 0 & 0 & 0 & 0 & 0 & 1 \end{bmatrix}.$$

Consequently, one obtains

$$K = \frac{1}{2}\dot{\mathbf{q}}^\mathrm{T}\mathbf{T}^\mathrm{T}\mathbf{M}_l\mathbf{T}\dot{\mathbf{q}}\,. \tag{44}$$

At this point, two simplifications are introduced in the expression of the local mass matrix. The local displacement w is assumed small and therefore the terms containing w^2 are neglected. Furthermore, the approximation $l_n = l_o$ is considered (small axial deformation assumption). With these simplifications, the local mass matrix is only function of $\overline{\theta}_1$ and $\overline{\theta}_2$ and is given by

$$\mathbf{M}_l = \mathbf{M}_{l1} + \mathbf{M}_{l2}\,, \tag{45}$$

where $\mathbf{M}_{l1}$ is the mass matrix for local axial and transverse displacements, defined as

$$\mathbf{M}_{l1} = \frac{\rho A l_o}{420} \begin{bmatrix} 140 & m_1 & 0 & 70 & -m_1 & 0 \\ m_1 & 156 & 22l_o & m_2 & 54 & -13l_o \\ 0 & 22l_o & 4l_o^2 & 0 & 13l_o & -3l_o^2 \\ 70 & m_2 & 0 & 140 & -m_2 & 0 \\ -m_1 & 54 & 13l_o & -m_2 & 156 & -22l_o \\ 0 & -13l_o & -3l_o^2 & 0 & -22l_o & 4l_o^2 \end{bmatrix},$$

with

$$m_1 = (21\overline{\theta}_1 - 14\overline{\theta}_2), \;\; m_2 = (14\overline{\theta}_1 - 21\overline{\theta}_2)\,.$$

$\mathbf{M}_{l2}$ is the mass matrix for rotation, defined as

$$\mathbf{M}_{l2} = \frac{\rho I}{30 l_o} \begin{bmatrix} 0 & 0 & 0 & 0 & 0 & 0 \\ 0 & 36 & 3l_o & 0 & -36 & 3l_o \\ 0 & 3l_o & 4l_o^2 & 0 & -3l_o & -l_o^2 \\ 0 & 0 & 0 & 0 & 0 & 0 \\ 0 & -36 & -3l_o & 0 & 36 & -3l_o \\ 0 & 3l_o & -l_o^2 & 0 & -3l_o & 4l_o^2 \end{bmatrix}.$$

The differentiations of the kinetic energy can be computed as

$$\frac{\partial K}{\partial \dot{\mathbf{q}}} = \mathbf{M}\,\dot{\mathbf{q}}\,, \tag{46}$$

$$\frac{\mathrm{d}}{\mathrm{d}t}\left[\frac{\partial K}{\partial \dot{\mathbf{q}}}\right] = \mathbf{M}\,\ddot{\mathbf{q}} + \dot{\mathbf{M}}\,\dot{\mathbf{q}}\,. \tag{47}$$

$\mathbf{M}$ is function of $\beta, \overline{\theta}_1, \overline{\theta}_2$ which vary with time:

$$\dot{\mathbf{M}} = \frac{\partial \mathbf{M}}{\partial \beta}\,\dot{\beta} + \frac{\partial \mathbf{M}}{\partial \overline{\theta}_1}\,\dot{\overline{\theta}}_1 + \frac{\partial \mathbf{M}}{\partial \overline{\theta}_2}\,\dot{\overline{\theta}}_2\,. \tag{48}$$

Using the notation $\dfrac{\partial \mathbf{M}}{\partial \beta} = \mathbf{M}_\beta; \dfrac{\partial \mathbf{M}}{\partial \overline{\theta}_1} = \mathbf{M}_{\overline{\theta}_1}; \dfrac{\partial \mathbf{M}}{\partial \overline{\theta}_2} = \mathbf{M}_{\overline{\theta}_2}$, the above equation can be rewritten in a more compact form

$$\dot{\mathbf{M}} = \mathbf{M}_\beta\left(\frac{\mathbf{z}^{\mathrm{T}}}{l_n}\dot{\mathbf{q}}\right) + \mathbf{M}_{\overline{\theta}_1}(\mathbf{b}_2^{\mathrm{T}}\dot{\mathbf{q}}) + \mathbf{M}_{\overline{\theta}_2}(\mathbf{b}_3^{\mathrm{T}}\dot{\mathbf{q}})\,. \tag{49}$$

The differentiation of K with respect to $\mathbf{q}$ is given by

$$\begin{aligned}\left[\frac{\partial K}{\partial \mathbf{q}}\right] &= \frac{\partial K}{\partial \beta}\frac{\partial \beta}{\partial \mathbf{q}} + \frac{\partial K}{\partial \overline{\theta}_1}\frac{\partial \overline{\theta}_1}{\partial \mathbf{q}} + \frac{\partial K}{\partial \overline{\theta}_2}\frac{\partial \overline{\theta}_2}{\partial \mathbf{q}} \\ &= \left(\frac{1}{2}\dot{\mathbf{q}}^{\mathrm{T}}\mathbf{M}_\beta\dot{\mathbf{q}}\right)\frac{\mathbf{z}}{l_n} + \left(\frac{1}{2}\dot{\mathbf{q}}^{\mathrm{T}}\mathbf{M}_{\overline{\theta}_1}\dot{\mathbf{q}}\right)\mathbf{b}_2 + \left(\frac{1}{2}\dot{\mathbf{q}}^{\mathrm{T}}\mathbf{M}_{\overline{\theta}_2}\dot{\mathbf{q}}\right)\mathbf{b}_3\,.\end{aligned} \tag{50}$$

Substituting (49), (50) into (30), one obtains the expression of $\mathbf{f}_K$ as

$$\begin{aligned}\mathbf{f}_K = \mathbf{M}\,\ddot{\mathbf{q}} &+ \left\{\mathbf{M}_\beta\left(\frac{\mathbf{z}^{\mathrm{T}}}{l_n}\dot{\mathbf{q}}\right) + \mathbf{M}_{\overline{\theta}_1}(\mathbf{b}_2^{\mathrm{T}}\dot{\mathbf{q}}) + \mathbf{M}_{\overline{\theta}_2}(\mathbf{b}_3^{\mathrm{T}}\dot{\mathbf{q}})\right\}\dot{\mathbf{q}} \\ &- \left(\frac{1}{2}\dot{\mathbf{q}}^{\mathrm{T}}\mathbf{M}_\beta\dot{\mathbf{q}}\right)\frac{\mathbf{z}}{l_n} - \left(\frac{1}{2}\dot{\mathbf{q}}^{\mathrm{T}}\mathbf{M}_{\overline{\theta}_1}\dot{\mathbf{q}}\right)\mathbf{b}_2 - \left(\frac{1}{2}\dot{\mathbf{q}}^{\mathrm{T}}\mathbf{M}_{\overline{\theta}_2}\dot{\mathbf{q}}\right)\mathbf{b}_3\,.\end{aligned} \tag{51}$$

The expression of $\mathbf{M}_\beta$ is given by

$$\mathbf{M}_\beta = \frac{\mathrm{d}\mathbf{T}}{\mathrm{d}\beta}^{\mathrm{T}} \mathbf{M}_l \mathbf{T} + \mathbf{T}^{\mathrm{T}} \mathbf{M}_l \frac{\mathrm{d}\mathbf{T}}{\mathrm{d}\beta} , \tag{52}$$

where

$$\frac{\mathrm{d}\mathbf{T}}{\mathrm{d}\beta} = \begin{bmatrix} 0 & 1 & 0 & 0 & 0 & 0 \\ -1 & 0 & 0 & 0 & 0 & 0 \\ 0 & 0 & 0 & 0 & 0 & 0 \\ 0 & 0 & 0 & 0 & 1 & 0 \\ 0 & 0 & 0 & -1 & 0 & 0 \\ 0 & 0 & 0 & 0 & 0 & 0 \end{bmatrix} \mathbf{T} = \mathbf{I}_1 \mathbf{T} . \tag{53}$$

Hence,

$$\mathbf{M}_\beta = \mathbf{T}^{\mathrm{T}} (\mathbf{I}_1^{\mathrm{T}} \mathbf{M}_l + \mathbf{M}_l \mathbf{I}_1) \mathbf{T} = \mathbf{T}^{\mathrm{T}} \mathbf{M}_l^\beta \mathbf{T} , \tag{54}$$

and $\mathbf{M}_{\overline{\theta}_1}, \mathbf{M}_{\overline{\theta}_2}$ are calculated by

$$\mathbf{M}_{\overline{\theta}_1} = \mathbf{T}^{\mathrm{T}} \frac{\partial \mathbf{M}_l}{\partial \overline{\theta}_1} \mathbf{T} = \mathbf{T}^{\mathrm{T}} \mathbf{M}_{l,\overline{\theta}_1} \mathbf{T} , \tag{55}$$

$$\mathbf{M}_{\overline{\theta}_2} = \mathbf{T}^{\mathrm{T}} \frac{\partial \mathbf{M}_l}{\partial \overline{\theta}_2} \mathbf{T} = \mathbf{T}^{\mathrm{T}} \mathbf{M}_{l,\overline{\theta}_2} \mathbf{T} , \tag{56}$$

where

$$\mathbf{M}_{l,\overline{\theta}_1} = \frac{\rho A l_o}{60} \begin{bmatrix} 0 & 3 & 0 & 0 & -3 & 0 \\ 3 & 0 & 0 & 2 & 0 & 0 \\ 0 & 0 & 0 & 0 & 0 & 0 \\ 0 & 2 & 0 & 0 & -2 & 0 \\ -3 & 0 & 0 & -2 & 0 & 0 \\ 0 & 0 & 0 & 0 & 0 & 0 \end{bmatrix} , \mathbf{M}_{l,\overline{\theta}_2} = \frac{\rho A l_o}{60} \begin{bmatrix} 0 & -2 & 0 & 0 & 2 & 0 \\ -2 & 0 & 0 & -3 & 0 & 0 \\ 0 & 0 & 0 & 0 & 0 & 0 \\ 0 & -3 & 0 & 0 & 3 & 0 \\ 2 & 0 & 0 & 3 & 0 & 0 \\ 0 & 0 & 0 & 0 & 0 & 0 \end{bmatrix} .$$

5 Nonlinear equation of the motion

The nonlinear equation of motion is

$$\mathbf{f}_K(\mathbf{q}, \dot{\mathbf{q}}, \ddot{\mathbf{q}}) + \mathbf{f}_g(\mathbf{q}) = \mathbf{p} , \tag{57}$$

where

$\mathbf{f}_K$: Inertia force vector,

$\mathbf{f}_g$: Elastic force vector,

$\mathbf{p}$: Applied external loads.

To solve numerically (57) using Newton's methods, the differentiation of each terms must be calculated. The following notations are used

$$\mathbf{K}_g = \frac{\partial \mathbf{f}_g}{\partial \mathbf{q}} \ , \tag{58}$$

$$\mathbf{M} = \frac{\partial \mathbf{f}_K}{\partial \ddot{\mathbf{q}}} \ , \tag{59}$$

$$\mathbf{C}_K = \frac{\partial \mathbf{f}_K}{\partial \dot{\mathbf{q}}} \ , \tag{60}$$

$$\mathbf{K}_K = \frac{\partial \mathbf{f}_K}{\partial \mathbf{q}} \ . \tag{61}$$

The stiffness matrix $\mathbf{K}_g$ and the mass matrix $\mathbf{M}$ are defined in previous sections. Using (51), $\mathbf{C}_K$ can be computed as

$$\mathbf{C}_K = \dot{\mathbf{M}} + \mathbf{C}_1 - \mathbf{C}_1^{\mathrm{T}} \ , \tag{62}$$

with

$$\mathbf{C}_1 = \mathbf{M}_\beta \left(\dot{\mathbf{q}} \frac{\mathbf{z}^{\mathrm{T}}}{l_n} \right) + \mathbf{M}_{\overline{\theta}_1} \left(\dot{\mathbf{q}} \, \mathbf{b}_2^{\mathrm{T}} \right) + \mathbf{M}_{\overline{\theta}_2} \left(\dot{\mathbf{q}} \, \mathbf{b}_3^{\mathrm{T}} \right) . \tag{63}$$

For the expression of $\mathbf{K}_K$, the derivation of each term of $\mathbf{f}_K$ with respect to $\mathbf{q}$ is calculated

$$\mathbf{K}_1 = \frac{\partial \mathbf{M}\ddot{\mathbf{q}}}{\partial \mathbf{q}} = \mathbf{M}_\beta \ddot{\mathbf{q}} \frac{\mathbf{z}^{\mathrm{T}}}{l_n} + \mathbf{M}_{\overline{\theta}_1} \ddot{\mathbf{q}} \mathbf{b}_2^{\mathrm{T}} + \mathbf{M}_{\overline{\theta}_2} \ddot{\mathbf{q}} \mathbf{b}_3^{\mathrm{T}} \ , \tag{64}$$

$$\begin{aligned} \mathbf{K}_2 = {} & \left(\frac{\mathbf{z}^{\mathrm{T}}}{l_n} \dot{\mathbf{q}} \right) \left(\frac{\partial \mathbf{M}_\beta}{\partial \beta} \dot{\mathbf{q}} \frac{\mathbf{z}^{\mathrm{T}}}{l_n} + \frac{\partial \mathbf{M}_\beta}{\partial \overline{\theta}_1} \dot{\mathbf{q}} \mathbf{b}_2^{\mathrm{T}} + \frac{\partial \mathbf{M}_\beta}{\partial \overline{\theta}_2} \dot{\mathbf{q}} \mathbf{b}_3^{\mathrm{T}} \right) + (\mathbf{b}_2^{\mathrm{T}} \dot{\mathbf{q}}) \frac{\partial \mathbf{M}_{\overline{\theta}_1}}{\partial \beta} \dot{\mathbf{q}} \frac{\mathbf{z}^{\mathrm{T}}}{l_n} \\ & + (\mathbf{b}_3^{\mathrm{T}} \dot{\mathbf{q}}) \frac{\partial \mathbf{M}_{\overline{\theta}_2}}{\partial \beta} \dot{\mathbf{q}} \frac{\mathbf{z}^{\mathrm{T}}}{l_n} - \left(\mathbf{M}_\beta - \mathbf{M}_{\overline{\theta}_1} - \mathbf{M}_{\overline{\theta}_2} \right) \dot{\mathbf{q}} \, \dot{\mathbf{q}}^{\mathrm{T}} \left(\frac{\mathbf{r}\,\mathbf{z}^{\mathrm{T}} + \mathbf{r}\,\mathbf{z}^{\mathrm{T}}}{l_n^2} \right) , \end{aligned} \tag{65}$$

$$\begin{aligned} \mathbf{K}_3 = \frac{1}{2} \Bigg[& \left(\dot{\mathbf{q}}^{\mathrm{T}} \frac{\partial \mathbf{M}_\beta}{\partial \beta} \dot{\mathbf{q}} \right) \frac{\mathbf{z}\,\mathbf{z}^{\mathrm{T}}}{l_n^2} + \left(\dot{\mathbf{q}}^{\mathrm{T}} \frac{\partial \mathbf{M}_\beta}{\partial \overline{\theta}_1} \dot{\mathbf{q}} \right) \frac{\mathbf{z}}{l_n} \mathbf{b}_2^{\mathrm{T}} \\ & + \left(\dot{\mathbf{q}}^{\mathrm{T}} \frac{\partial \mathbf{M}_\beta}{\partial \overline{\theta}_2} \dot{\mathbf{q}} \right) \frac{\mathbf{z}}{l_n} \mathbf{b}_3^{\mathrm{T}} + \left(\dot{\mathbf{q}}^{\mathrm{T}} \frac{\partial \mathbf{M}_\beta}{\partial \overline{\theta}_1} \dot{\mathbf{q}} \right) \mathbf{b}_2 \frac{\mathbf{z}^{\mathrm{T}}}{l_n} + \left(\dot{\mathbf{q}}^{\mathrm{T}} \frac{\partial \mathbf{M}_\beta}{\partial \overline{\theta}_2} \dot{\mathbf{q}} \right) \mathbf{b}_3 \frac{\mathbf{z}^{\mathrm{T}}}{l_n} \\ & - \dot{\mathbf{q}}^{\mathrm{T}} \left(\mathbf{M}_\beta - \mathbf{M}_{\overline{\theta}_1} - \mathbf{M}_{\overline{\theta}_2} \right) \dot{\mathbf{q}} \left(\frac{\mathbf{r}\,\mathbf{z}^{\mathrm{T}} + \mathbf{r}\,\mathbf{z}^{\mathrm{T}}}{l_n^2} \right) \Bigg] . \end{aligned} \tag{66}$$

So $\mathbf{K}_K$ is given by

$$\mathbf{K}_K = \mathbf{K}_1 + \mathbf{K}_2 - \mathbf{K}_3 \ . \tag{67}$$

By using the relations (53), (54), (55) and (56), the following expressions are obtained

$$\frac{\partial \mathbf{M}_\beta}{\partial \beta} = \mathbf{T}^{\mathrm{T}} (\mathbf{I}_1^{\mathrm{T}} \mathbf{M}_l^\beta + \mathbf{M}_l^\beta \mathbf{I}_1) \mathbf{T} \ , \tag{68}$$

$$\frac{\partial \mathbf{M}_\beta}{\partial \overline{\theta}_1} = \frac{\partial \mathbf{M}_{\overline{\theta}_1}}{\partial \beta} = \mathbf{T}^{\mathrm{T}} (\mathbf{I}_1^{\mathrm{T}} \mathbf{M}_{l,\overline{\theta}_1} + \mathbf{M}_{l,\overline{\theta}_1} \mathbf{I}_1) \mathbf{T} \ , \tag{69}$$

$$\frac{\partial \mathbf{M}_\beta}{\partial \overline{\theta}_2} = \frac{\partial \mathbf{M}_{\overline{\theta}_2}}{\partial \beta} = \mathbf{T}^{\mathrm{T}} (\mathbf{I}_1^{\mathrm{T}} \mathbf{M}_{l,\overline{\theta}_2} + \mathbf{M}_{l,\overline{\theta}_2} \mathbf{I}_1) \mathbf{T} \ . \tag{70}$$

6 Numerical examples

The purpose of the four numerical applications presented in this section is to assess the performance of the dynamic corotational formulation proposed in Sects. 4 and 5. In particular, the predictions of the new formulation are compared against results obtained with the two formulations usually found in the literature, i.e. the lumped mass matrix and the Timoshenko mass matrix. These two constant mass matrices are given by

$$\mathbf{M}_{\text{Lumped}} = \frac{\rho A l_o}{2} \begin{bmatrix} 1 & 0 & 0 & 0 & 0 & 0 \\ 0 & 1 & 0 & 0 & 0 & 0 \\ 0 & 0 & l_o^2/12 & 0 & 0 & 0 \\ 0 & 0 & 0 & 1 & 0 & 0 \\ 0 & 0 & 0 & 0 & 1 & 0 \\ 0 & 0 & 0 & 0 & 0 & l_o^2/12 \end{bmatrix},$$

$$\mathbf{M}_{\text{Timoshenko}} = \rho l_o \begin{bmatrix} A/3 & 0 & 0 & A/6 & 0 & 0 \\ 0 & A/3 & 0 & 0 & A/6 & 0 \\ 0 & 0 & I/3 & 0 & 0 & I/3 \\ A/6 & 0 & 0 & A/3 & 0 & 0 \\ 0 & A/6 & 0 & 0 & A/3 & 0 \\ 0 & 0 & I/3 & 0 & 0 & I/3 \end{bmatrix}.$$

For all dynamic formulations, the elastic force vector and tangent stiffness matrix have been derived using the IIE shape functions in order to account for shear deformability. For each example, the three dynamic formulations are compared with a reference solution. This solution is obtained with a large number of elements and is identical for the three considered dynamic formulations. The reference solution has also been checked with Abaqus (Total Lagrangian formulation) and the same results have been obtained.

To solve the equation of motion, the Alpha method, which is presented in [14], is employed, with $\alpha = -0.01$. This moderate value of α gives a small numerical damping, which limits the influence of higher frequencies on the response.

Damping is not considered.

For the presentation of the results, the following colors are used in all figures:

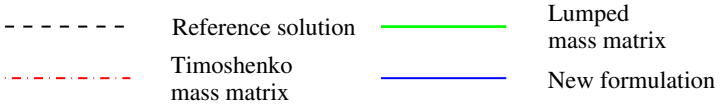

6.1 Cantilever beam

The first example, described in Fig. 3, is a cantilever beam of length $L = 10$ m with uniform cross-section, clamped at one end and subjected to a sinusoidal tip force $P = P_o \sin(wt)$ at the free end. The amplitude of

the load P_o is taken equal to 10 MN and its frequency w is 50 rad/s. The cross-section depth and width are $a = 0.25$ m and $e = 0.5$ m, respectively. The elastic modulus of the beam E is 210 GPa and the mass per unit volume is $\rho = 7850$ kg/m^3.

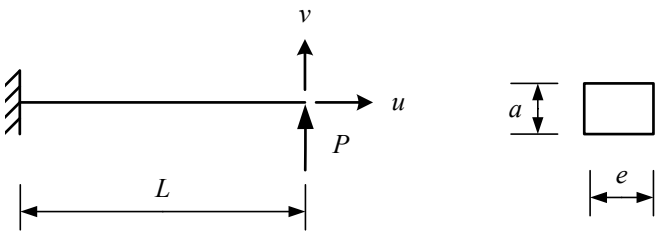

Fig. 3. Cantilever beam : geometrical data.

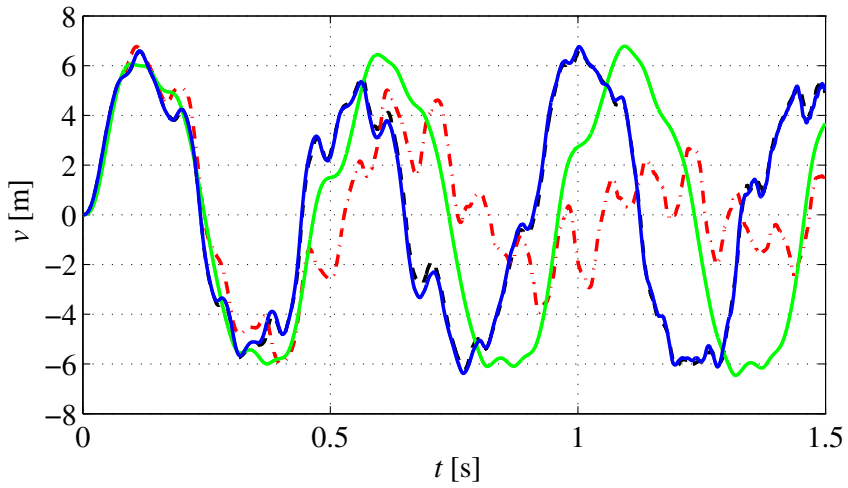

Fig. 4. Cantilever beam - Vertical displacement history.

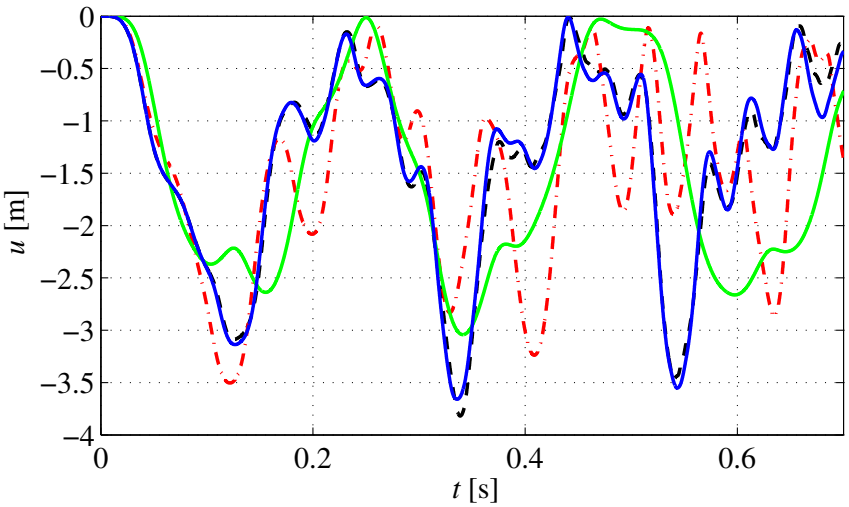

Fig. 5. Cantilever beam - Horizontal displacement history.

The reference solution, obtained with 48 elements, and the results obtained with 3 formulations considering only 3 elements, with the time step size $\Delta t = 10^{-4}$ s, are shown in Figs. 4 and 5. It can be observed that the proposed formulation gives results that are in very agreement with the reference solution with only three elements. However, the results obtained with the lumped and Timoshenko approaches do not agree well with the reference solution over the whole time domain.

6.2 Shallow arch

Consider a shallow, circular, elastic arch (see Fig. 6) of span $L = 10$ m with clamped ends. The radius R of the arch is equal to 10 m with $\phi = 30^\circ$. The shallow arch has a uniform rectangular cross-section and is subjected to a sinusoidal concentrated vertical force $P = P_o \sin(wt)$ at mid-span. The amplitude of the load P_o is taken equal to -80 MN and its frequency w is 1000 rad/s. The arch has cross-sectional area $A = 0.087$ m^2, modulus of elasticity $E = 210$ GPa, second moment of area $I = 3.562 \cdot 10^{-3}$m^4 and mass per unit volume $\rho = 7850$ kg/m^3. The time step size is chosen to be $\Delta t = 5 \cdot 10^{-5}$ s.

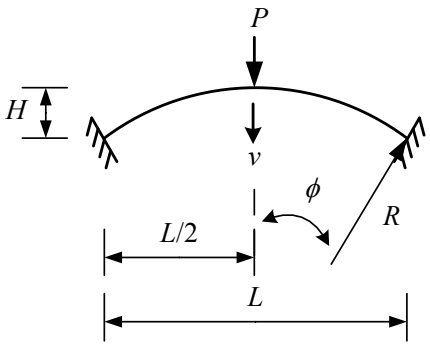

Fig. 6. Shallow arch: geometrical data.

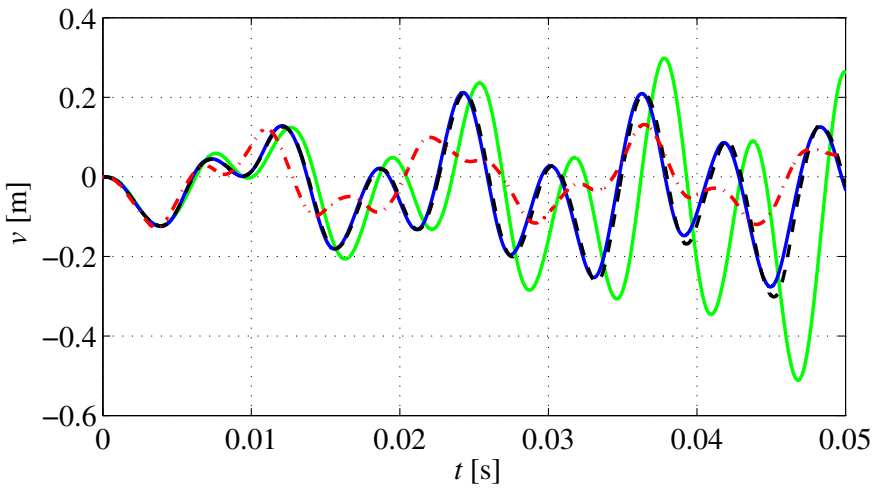

Fig. 7. Shallow arch - Vertical displacement history.

In Fig. 7, the mid-span vertical displacement $v(t)$ history is depicted for the 3 different dynamic formulations as well as the reference solution, which has been obtained with 48 elements. Only six elements have been used for the computations with the three formulations. It can be observed that the results obtained with the new approach are nearly identical to the reference solution. However, large discrepancies between

the results obtained with the lumped and Timoshenko approaches and the reference solution can be observed. This indicates that the present formulation is able to capture the nonlinear dynamical behavior of structures with minimal number of elements.

6.3 Lee's frame

A Lee's frame with uniform rectangular cross-section subjected to a suddenly applied constant load $P_o = 4.1$ MN is considered, (see Fig. 8). The frame and cross-section data (see Fig. 8) are : $L = 2.4$ m, $a = 0.2$ m and $e = 0.3$ m. The members of the frame have modulus of elasticity $E = 210$ GPa and mass per unit volume $\rho = 7850$ kg/m^3.

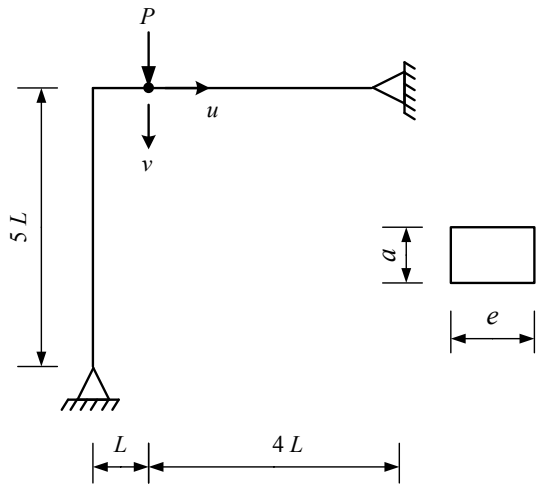

Fig. 8. Lee's frame: geometrical data.

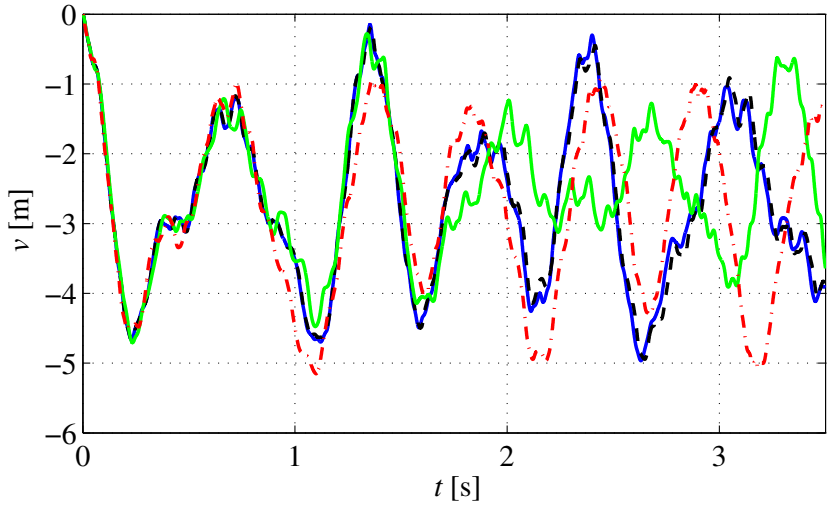

Fig. 9. Lee's frame - Vertical displacement history.

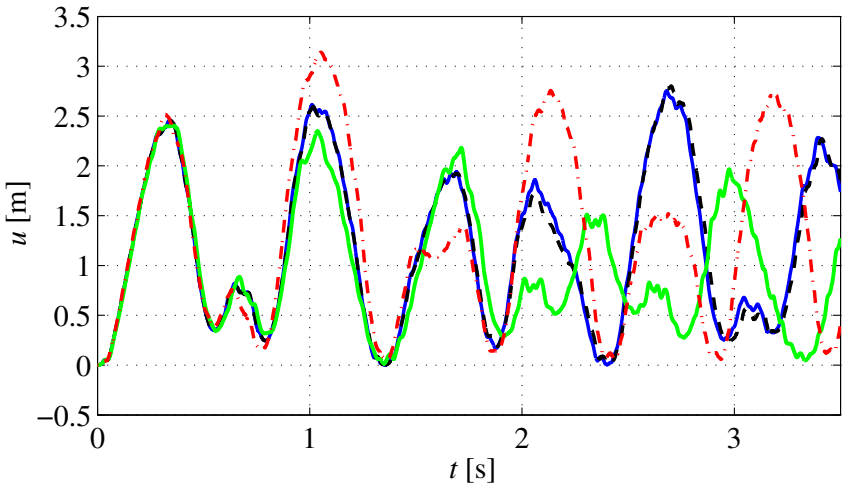

Fig. 10. Lee's frame - Horizontal displacement history.

The loading is defined as follows:

$$P = \begin{cases} 0 & \text{if } t \leq 0 \\ P_o & \text{if } t > 0 \end{cases}$$

The reference solution has been obtained with 60 elements whereas only 10 elements have been used to perform the computations with the proposed formulation as well as the lumped mass and Timoshenko formulations. The time step size is $\Delta t = 2.5 \cdot 10^{-3}$ s. The time histories of the vertical and horizontal displacement are depicted in Figs. 9 and 10, respectively. Again, it can be observed that, with only 10 elements, the results obtained with the new approach are in good agreement with the reference solution. However, the discrepancy between the reference solution and the results obtained with the lumped and Timoshenko formulations is not negligible.

6.4 Free vibration beam

In this example, the free vibration of the simple supported beam of length $L = 30$ m, shown in Fig. 11, is considered. The beam has a uniform square cross-section $a = 1$ m, modulus of elasticity $E = 210$ GPa and mass per unit volume $\rho = 7850$ kg/m^3.

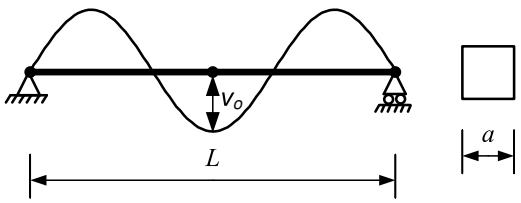

Fig. 11. Simply supported beam.

An initial displacement corresponding to the third eigenmode is applied. Then, the structure is released with an initial zero velocity. The beam undergoes free vibration with a shape corresponding to the third eigenmode. The nodal displacements are computed using the time integration method. The third natural

frequency is then determinated by considering the times at which the nodal displacements reach a maximum value. Two cases are tested. In the first case, the displacement at mid span is $V_o = 0.01$ m. In the second one, V_o is increased to 1 m .

With 64 elements, the 3 formulations give almost the same frequency. The differences are about 7‰. The average of these three values is taken as reference frequency. With $V_o = 0.01$ m, $f_{\text{ref}} = 31.127$ Hz. With $V_o = 1$ m, $f_{\text{ref}} = 47.644$ Hz.

The beam is also modeled with 8, 16 and 32 elements.

The ratios between calculated frequencies and the reference ones are given in Tables 1 and 2.

It can be shown that with only eight elements, the new formulation gives very accurate results. But with two classical formulations, a larger number of elements is required.

Table 1. With $V_o = 0.01$ m.

Number of elements	8	16	32	64
Lumped mass matrix	1.058	1.012	1.001	1.002
Timoshenko mass matrix	1.117	1.012	1.007	1.000
New formulation	1.002	1.001	1.001	0.998

Table 2. With $V_o = 1$ m.

Number of elements	8	16	32	64
Lumped mass matrix	1.049	1.040	1.006	1.003
Timoshenko mass matrix	1.114	1.042	1.015	1.001
New formulation	1.006	1.001	1.001	0.996

7 Conclusion

In this paper, a new dynamic formulation for corotational 2D beam was presented. When compared existing formulations, the distinguishing feature is the use of cubic interpolation functions to derive both the inertia and elastic terms. The inertia terms were analytically developed by introducing some approximations regarding the local kinematical quantities. Several numerical examples have demonstrated the superiority of the new formulation over the two classical approaches, in which linear Timoshenko and lumped mass matrices are used. Indeed, all results indicate that the new formulation requires more computational time but allows to reduce significantly the number of elements. This advantage is due to a better representation of the local displacements in the inertia terms.

One interesting aspect is to investigate if the present approach can be extended to 3D corotational beams. As a matter of fact, in the literature, linear interpolations are most of the time used to derive inertia terms for 3D beams. However, it has been shown [15] that, for static analyses, corotational 3D beams using local cubic interpolations are more efficient than similar elements using local linear interpolations.

Appendix A Local elastic force vector and tangent stiffness matrix

```
>with(linalg):
>mu:= 1/(1+12*Omega);
>
>phi_1:= mu*x*((1-x/L)^2+6*Omega*(1-x/L));
```

```
>phi_2:= mu*x*(-x/L+x^2/L^2+6*Omega*(x/L-1));
>phi_3:= mu*(1-4*x/L+3*x^2/L^2+12*Omega*(1-x/L));
>phi_4:= mu*(-2*x/L+3*x^2/L^2+12*Omega*x/L);
>
>w:= phi_1*tl1+phi_2*tl2:
>t:= phi_3*tl1+phi_4*tl2:
>dw:= diff(w,x):
>dt:= diff(t,x):
>
>eps:= simplify(u/L+1/2/L*int(dw^2,x=0..L)):
>GA:= EI/Omega/L^2:
>Ep:= EA*eps^2+EI*dt^2+GA*(t+dw)^2:
>Epp:= 1/2*int(Ep,x=0..L):
>
>fl:= simplify(grad(Epp,[u,tl1,tl2])):
>kl:= simplify(hessian(Epp,[u,tl1,tl2])):
```

References

[1] M.A. Crisfield, J. Shi, An energy conserving co-rotational procedure for non-linear dynamics with finite elements, Nonlinear Dyn., Vol 9, 37-52 (1994).

[2] M.A. Crisfield, U. Galvanetto, G. Jelenic, Dynamics of 3-D co-rotational beams, Comput. Mech., Vol 20, 507-519 (1997).

[3] U. Galvanetto, M.A. Crisfield, An energy conserving co-rotational procedure for dynamics of planar beam structures, Int. J. Num. Methods. Engrg., Vol 39, 2265-2282 (1996).

[4] K.M. Hsiao, R.T. Yang, A co-rotational formulation for nonlinear dynamic analysis of curved Euler beam, Comput. Struct. , Vol 54, No.6, 1091-1097 (1995).

[5] K.M. Hsiao, J.Y. Lin, W.Y. Lin, A consisten co-rotational finite element formulation for geometrically nonlinear dynamic analysis of 3-D beams, Comput. Methods Appl. Mech. Engrg., Vol 169, 1-18 (1999).

[6] M. Iura and S.N. Atluri, Dynamic analysis of planar flexible beams with finite rotations by using inertial and rotating frames, Comput. Struct., Vol 55, No.3, 453-462 (1995).

[7] C. Oran, A. Kassimali, Large deformations of framed structures under static and dynamic loads, Comput. Struct., Vol 6, 539-547 (1976).

[8] N. Masuda. T. Nishiwaki and M. Minaaawa, Nonlinear dynamic analysis of frame structures, Comput. Struct., Vol 27, No.1, 103-110 (1987).

[9] Q. Xue and J.L Meek, Dynamic response and instability of frame structures, Comput. Methods Appl. Mech. Engrg., Vol 190, 5233-5242 (2001).

[10] K. Behdinan, M.C Stylianou, B. Tabarrok, Co-rotational dynamic analysis of flexible beams, Comput. Methods Appl. Mech. Engrg., Vol 154, 151-161 (1998).

[11] H.A. Elkaranshawy and M.A. Dokainish, Corotational finite element analysis of planar flexible multibody systems, Comput. Struct., Vol 54, No.5, 881-890 (1995).

[12] J.N. Reddy, On locking-free shear deformable beam finite elements, Comput. Methods Appl. Mech. Engrg., Vol 149, 113-132 (1997).

[13] M.A. Crisfield, Non-Linear Finite Element Analysis of Solids and Structures, Volume 1: Essentials, 201-233. Wiley, Chischester (1997).

[14] M.A. Crisfield, Non-Linear Finite Element Analysis of Solids and Structures, Volume 2: Advanced Topics, 455-456. Wiley, Chischester (1997).

[15] R. Alsafadie, J.-M. Battini, M. Hjiaj, H. Somja, A comparative study of displacement and mixed-based corotational finite element formulations for elasto-plastic three-dimensional beam analysis, Engerg. Computs., Vol 28, No.7, 939-982 (2011).

Paper 2: Dynamics of 3D beam elements in a corotational context: a comparative study of established and new formulations

Finite Elements in Analysis and Design, Volume 61: 97-111, November 2012
DOI: 10.1016/j.finel.2012.06.007

Finite Elements in Analysis and Design.
Finite Elem. Anal. Des., Volume 61, pp 97-111 (2012).

Dynamics of 3D beam elements in a corotational context: A comparative study of established and new formulations

Thanh-Nam Le [1,2] , Jean-Marc Battini [2] , Mohammed Hjiaj [1]

[1] *Université Européenne de Bretagne, INSA de Rennes - LGCGM/Structural Engineering Research Group, 20 avenue des Buttes de Coësmes, CS 70839, 35708 Rennes Cedex 7, France.*

[2] *KTH, Royal Institute of Technology - Department of Civil and Architectural Engineering, SE-10044 Stockholm, Sweden.*

Abstract

This paper deals with Newmark time stepping methods and finite rotations for nonlinear finite element analysis of flexible beam structures. The corotational method is used to develop expressions of the internal forces and the corresponding tangent stiffness matrices. For the dynamic part, four formulations based on different parameterizations of rotations are compared. The first three are classic formulations taken from the literature with some modifications for two of them. The last one is new and uses three of the four Euler parameters (quaternion) as rotational variables. For all these approaches, theoretical derivations as well as practical implementations are given in detail. The similarities and differences between the formulations are pointed out. Six numerical examples are studied in order to compare these four formulations in terms of numerical accuracy and computational efficiency. Regarding efficiency, the choice of the predictor at each time step and the possibility to simplify the tangent inertia matrix are carefully investigated. The numerical results show that these four formulations have the same numerical accuracy, but that the computational efficiency depends on the choice of the tangent inertia matrix. Besides, the new formulation proposed in this paper turns out to be the fastest one.

Key words: Time stepping method; Finite rotations; Nonlinear dynamics; 3D beam elements;

Notation		$\mathbf{R}$	rotation matrix
$\mathbf{I}, \mathbf{0}_{[3x3]}$	identity and zero matrix 3x3	$\boldsymbol{\theta}, \boldsymbol{\Theta}$	spatial and material incremental rotational vectors
$\dot{\mathbf{x}}$	time derivative of a vector $\mathbf{x}$	$\dot{\mathbf{w}}, \ddot{\mathbf{w}}$	spatial angular velocity and acceleration vectors
K	kinetic energy	$\dot{\boldsymbol{\omega}}, \ddot{\boldsymbol{\omega}}$	material angular velocity and acceleration vectors
$\mathbf{f}_{\text{ext}}, \mathbf{f}_k, \mathbf{f}_g$	external, inertia and internal force vectors	A_ρ	mass per unit length of the beam
$\mathbf{u}, \dot{\mathbf{u}}, \ddot{\mathbf{u}}$	displacement, velocity and acceleration vectors	$\mathbf{J}_\rho$	inertia dyadic of the cross section in the initial configuration
$\delta\mathbf{w}, \delta\boldsymbol{\omega}$	spatial and material spin variables	h, γ, β	time step size and Newmark method's parameters

1 Introduction

Flexible beams are used in many applications, for instance large deployable space structures, aircrafts and wind turbine propellers, offshore platforms. These structures undergo large displacements and finite rotations. Their nonlinear dynamic behavior is usually simulated using spatial nonlinear beam finite elements.

One way to develop nonlinear beam elements is to use the corotational approach. The idea is to decompose the motion of the element into rigid body and pure deformational parts by introducing a local coordinates system which moves and rotates with the element. The deformational part is measured in this local system. This method has been extensively applied for nonlinear static analysis. However, its application in nonlinear dynamic analysis is rather limited, especially for 3D beams [8,14]. The reason is that the decomposition in rigid body and deformational parts leads to very complicated expressions for the dynamic terms. One solution, which is investigated in this paper, is to use the corotational method to develop expressions of the internal forces and the related tangent stiffness matrices, while the dynamic terms are formulated into a total Lagrangian context.

One important issue in the development of nonlinear dynamic beam elements is the treatment of the finite rotations. More specifically, the finite rotations are non-commutative and non-additive, thus they cannot be treated in a simple manner as the translational displacements. As a consequence, the standard Newmark time stepping method cannot be directly applied to finite rotations. Therefore, this method must be reformulated according to the parametrization of the finite rotations. Several ways to parameterize finite rotations in nonlinear dynamic analysis can be found in the literature. In one of the first key papers in the field, Simo and Vu-Quoc [28] chose spatial spin variables. This parametrization was also employed in the works of Crisfield et al. [8], Jelenić and Crisfield [19,20] and Hsiao et al. [14]. In [6] Cardona and Geradin presented three formulations. The first one used material spin variables. The second one used total rotational vectors. The main advantage is that the rotational variables become additive. However, the angles of the rotations in this case are restricted to 2π. As a remedy, Cardona and Geradin introduced the notion of incremental rotational vector in their third formulation. The idea is that additive updates still applied but only within each increment. The incremental rotational vectors were also adopted by Ibrahimbegović and Mikdad [17]. Mäkinen [23] presented a beam finite element based on the total rotational vector with a switching procedure to avoid the limitations of rotation angles. Another possibility of the parametrization based on the conformal rotational vector was adopted by Iura and Atluri [18], Geradin and Cardona [11]. Recently, Betsch and Steinmann [5] proposed to use the rotation matrix to parameterize nodal rotations. The rotation matrix was then linearly interpolated. However, this formulation required nine rotational variables at each node and the orthonormality of the interpolated rotation matrix was not ensured.

Regarding the issue of the time stepping methods for the finite rotations, two main approaches have been used. In the first one, proposed by Simo and Vu-Quoc [28], the Newmark equations were written using the material incremental rotational vector, the material angular velocity and the material acceleration. This approach was adopted in [8, 18–20]. Ibrahimbegović and Mikdad [17] reformulated this method using spatial forms. In the second approach, introduced by Cardona and Geradin [6], the standard Newmark algorithm was applied to the incremental rotational vector and its time derivatives. Hence, the update procedure of the rotational quantities takes a similar form as the displacements. In the works of Forsell [10] and Mäkinen [23], this approach was adopted using the total rotational vectors.

In this paper, four nonlinear dynamic formulations of 3D beam elements are compared. For all of them, the inertia force vector and tangent inertia matrix are derived in a total Lagrangian context and computed using two Gauss points. The first formulation has been proposed by Simo and Vu-Quoc [28] and uses spatial spin variables. A modification of the computation of the rotational quantities at the Gauss points is introduced in order to get a higher efficiency. The second formulation is based on the incremental rotational vector and has been presented by Ibrahimbegović and Mikdad [17]. The third one is also based on the incremental rotational vector and has been proposed by Cardona and Geradin [6]. Here, it is reformulated using the spatial form of the incremental rotational vector instead of the material one. The fourth formulation is new. The idea is to employ three of the four Euler parameters (quaternion) as rotational variables. This approach has been introduced by Battini [4] for static analysis and is now developed for dynamics. For all these approaches, theoretical derivations and practical implementations are given in detail. The similarities and differences between them are also pointed out.

Regarding the static deformational terms, i.e. the internal force vector and tangent stiffness matrix, the corotational beam elements developed by Battini and Pacoste [2,4] are employed. Consequently, the local

displacements and rotations are interpolated, which allows an exact integration of the internal force vector and tangent stiffness matrix.

Six numerical examples are considered using the HHT α method. The purpose is to compare the four formulations in terms of numerical accuracy and computational efficiency. Regarding efficiency, the choice of the predictor and the possibility to simplify the tangent inertia matrix are carefully investigated.

The outline of this paper is as follows: Section 2 gives a short presentation of the different parameterizations of the finite rotations. Sections 3 - 6 describe in detail the four formulations. Section 7 summaries most important findings regarding the formulations. Different predictors to be considered at the start of each time step are discussed in Section 8. Six numerical examples are presented in Section 9 and conclusions are derived in Section 10.

2 Parametrization of finite rotation

In this section, the basic relations concerning the parameterizations of finite rotations are briefly presented. For a more complete description, the reader is referred to textbooks and review papers such as [1,9,12,21, 30].

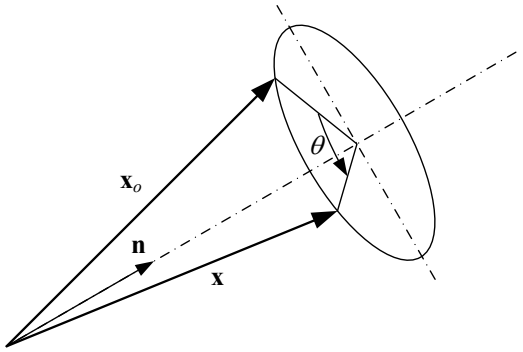

Fig. 1. Finite rotation of a vector.

The coordinate of a vector $\mathbf{x}_o$ that is rotated into the position $\mathbf{x}$ (see Fig. 1) is given by the relation

$$\mathbf{x} = \mathbf{R}\,\mathbf{x}_o\,. \tag{1}$$

Due to its orthonormality, the rotation matrix $\mathbf{R}$ can be parameterized using only three independent parameters. One possibility is to use the rotational vector defined by

$$\boldsymbol{\theta} = \theta\,\mathbf{n}\,, \tag{2}$$

where $\mathbf{n}$ is a unit vector defining the axis of the rotation and $\theta = (\boldsymbol{\theta}^{\mathrm{T}}\boldsymbol{\theta})^{1/2}$ is the angle of the rotation.

The relation between the rotation matrix and the rotational vector is given by the Rodrigues' formula

$$\mathbf{R} = \mathbf{I} + \frac{\sin\theta}{\theta}\widetilde{\boldsymbol{\theta}} + \frac{1-\cos\theta}{\theta^2}\widetilde{\boldsymbol{\theta}}\widetilde{\boldsymbol{\theta}} = \exp(\widetilde{\boldsymbol{\theta}})\,, \tag{3}$$

where $\widetilde{\boldsymbol{\theta}}$ is the skew matrix associated with the vector $\boldsymbol{\theta}$.

The variation of the rotation matrix in spatial and material form is given by

$$\delta\mathbf{R} = \widetilde{\delta\mathbf{w}}\mathbf{R} = \mathbf{R}\widetilde{\delta\boldsymbol{\omega}}\,. \tag{4}$$

Physically, $\widetilde{\delta\mathbf{w}}$ and $\widetilde{\delta\boldsymbol{\omega}}$ represent infinitesimal spatial and material rotations superposed onto the rotation $\mathbf{R}$. $\delta\mathbf{w}$, which is also denoted as spatial spin variables, is related to the variation of the rotational vector through

$$\delta\mathbf{w} = \mathbf{T}_s(\boldsymbol{\theta})\,\delta\boldsymbol{\theta}\,, \tag{5}$$

with

$$\mathbf{T}_s(\boldsymbol{\theta}) = \mathbf{I} + \frac{1-\cos\theta}{\theta^2}\widetilde{\boldsymbol{\theta}} + \frac{\theta-\sin\theta}{\theta^3}\widetilde{\boldsymbol{\theta}}\,\widetilde{\boldsymbol{\theta}}\,. \tag{6}$$

The inverse relation of Eq. (5) is

$$\delta\boldsymbol{\theta} = \mathbf{T}_s^{-1}(\boldsymbol{\theta})\,\delta\mathbf{w}\,, \tag{7}$$

with

$$\mathbf{T}_s^{-1}(\boldsymbol{\theta}) = \frac{(\theta/2)}{\tan(\theta/2)}\mathbf{I} + \left(1 - \frac{(\theta/2)}{\tan(\theta/2)}\right)\frac{\boldsymbol{\theta}\boldsymbol{\theta}^{\mathrm{T}}}{\theta^2} - \frac{1}{2}\widetilde{\boldsymbol{\theta}}\,. \tag{8}$$

One interesting property existing between the operator $\mathbf{T}_s(\boldsymbol{\theta})$ and the rotation matrix $\exp(\widetilde{\boldsymbol{\theta}})$, given in [25], is

$$\mathbf{T}_s(\boldsymbol{\theta}) = \mathbf{T}_s^{\mathrm{T}}(\boldsymbol{\theta})\exp(\widetilde{\boldsymbol{\theta}})\,. \tag{9}$$

Another possibility to parameterize the rotation matrix is to use the vectorial part of the Euler parameters (quaternion), which by introducing the scaling factor 2 gives

$$\mathbf{q} = 2\,\sin\frac{\theta}{2}\,\mathbf{n}\,. \tag{10}$$

In terms of $\mathbf{q}$, the rotational tensor $\mathbf{R}$ is given by

$$\mathbf{R}(\mathbf{q}) = (2q_o^2 - 1)\mathbf{I} + \frac{1}{2}\mathbf{q}\mathbf{q}^{\mathrm{T}} + q_o\widetilde{\mathbf{q}}\,, \tag{11}$$

with $q_o = (1 - \mathbf{q}^{\mathrm{T}}\mathbf{q}\,/4)^{1/2}$.

It can be observed that this parametrization requires only three parameters $\mathbf{q}$ (see Eq. (10)) instead of four $(\mathbf{q}, q_o)$ as usually found in the literature.

The relation between the spatial spin variables and the Euler parameters is given by

$$\delta\mathbf{w} = \mathbf{T}_q(\mathbf{q})\,\delta\mathbf{q}\,, \tag{12}$$

with

$$\mathbf{T}_q(\mathbf{q}) = q_o\mathbf{I} + \frac{\mathbf{q}\mathbf{q}^{\mathrm{T}}}{4\,q_o} + \frac{\widetilde{\mathbf{q}}}{2}\,. \tag{13}$$

The spatial angular velocity and acceleration are related to the rotational vector and to the Euler parameters by

$$\dot{\mathbf{w}} = \mathbf{T}_s(\boldsymbol{\theta})\,\dot{\boldsymbol{\theta}} = \mathbf{T}_q(\mathbf{q})\,\dot{\mathbf{q}}\,, \tag{14}$$

$$\ddot{\mathbf{w}} = \mathbf{T}_s(\boldsymbol{\theta})\,\ddot{\boldsymbol{\theta}} + \dot{\mathbf{T}}_s(\boldsymbol{\theta})\,\dot{\boldsymbol{\theta}} = \mathbf{T}_q(\mathbf{q})\,\ddot{\mathbf{q}} + \dot{\mathbf{T}}_q(\mathbf{q})\,\dot{\mathbf{q}}\,. \tag{15}$$

The expressions of $\dot{\mathbf{T}}_s(\boldsymbol{\theta})\,\dot{\boldsymbol{\theta}}$ and $\dot{\mathbf{T}}_q(\mathbf{q})\,\dot{\mathbf{q}}$ are given in Appendices A and B, respectively.

The angular velocity and acceleration can be expressed in the material configuration. The material and spatial quantities are connected by the relations

$$\dot{\mathbf{w}} = \mathbf{R}\,\dot{\boldsymbol{\omega}}\,, \tag{16}$$

$$\ddot{\mathbf{w}} = \mathbf{R}\,\ddot{\boldsymbol{\omega}}\,. \tag{17}$$

If the spatial spin variables are used to parameterize finite rotations, the update of the rotation matrix at i^{th} iteration of step $(n+1)$ is performed according to

$$\mathbf{R}^i_{n+1} = \exp(\widetilde{\Delta\mathbf{w}})\mathbf{R}^{i-1}_{n+1}\,, \tag{18}$$

where $\Delta\mathbf{w}$ is the iterative spatial spin variables.

If the rotational vector or the Euler parameters are used as parameters (see [3, 25]), then the rotations become additive and are updated at each iteration using

$$\boldsymbol{\theta}^i = \boldsymbol{\theta}^{i-1} + \Delta\boldsymbol{\theta}\,, \tag{19}$$

$$\mathbf{q}^i = \mathbf{q}^{i-1} + \Delta\mathbf{q}\,. \tag{20}$$

However, the relations in Eqs. (5) and (12) cease to be bijections respectively for $\theta = 2\pi$ and for $\theta = \pi$ (which corresponds to $q_o = 0$). Consequently, the angle of rotation is limited to 2π with the parametrization using the rotational vector and π in case of the Euler parameters. In many dynamic analysis, angles of rotations can become larger than these limitations.

In order to overcome this inconvenience, Cardona and Geradin [6], Ibrahimbegović [16] and Battini [4] proposed to apply Eqs. (5) and (12) only within an increment, and introduced the concept of incremental rotational vector and incremental Euler parameters. Then, the update procedure at step $(n+1)$ is performed in the following way: at the beginning of the step, the incremental rotational vector and the incremental Euler parameters are set equal to zero ($\boldsymbol{\theta}^0_{n+1} = \mathbf{q}^0_{n+1} = \mathbf{0}_{[3\text{x}1]}$). At i^{th} iteration, they are updated using

$$\boldsymbol{\theta}^i_{n+1} = \boldsymbol{\theta}^{i-1}_{n+1} + \Delta\boldsymbol{\theta}\,, \tag{21}$$

$$\mathbf{q}^i_{n+1} = \mathbf{q}^{i-1}_{n+1} + \Delta\mathbf{q}\,, \tag{22}$$

and the rotation matrix is updated using

$$\mathbf{R}^i_{n+1} = \exp(\widetilde{\boldsymbol{\theta}^i_{n+1}})\,\mathbf{R}_n\,, \tag{23}$$

$$\mathbf{R}^i_{n+1} = \mathbf{R}(\mathbf{q}^i_{n+1})\,\mathbf{R}_n\,, \tag{24}$$

where $\boldsymbol{\theta}^i_{n+1}, \mathbf{q}^i_{n+1}$ are the spatial incremental rotational vector and the spatial incremental Euler parameters, respectively.

Hence, additive updates still apply within each increment. The amplitude of the rotations are just limited within each increment, which is not a problem.
In the following, the spatial spin variables, the spatial incremental rotational vector and the spatial incremental Euler parameters are used to parameterize nodal rotations. However during the derivations, the material incremental rotational vector $\boldsymbol{\Theta}$ is employed. The relations connecting spatial and material incremental rotational vectors are given by

$$\exp(\widetilde{\boldsymbol{\theta}^i_{n+1}})\,\mathbf{R}_n = \mathbf{R}_n \exp(\widetilde{\boldsymbol{\Theta}^i_{n+1}})\,, \tag{25}$$

$$\boldsymbol{\theta}^i_{n+1} = \mathbf{R}_n\,\boldsymbol{\Theta}^i_{n+1}\,. \tag{26}$$

3 Formulation using the spatial spin variables

This formulation has been proposed by Simo and Vu-Quoc in [28]. However, a modification of the computation of the rotational quantities at the Gauss points is introduced in order to get a more efficient im-

plementation. In this approach, spatial spin variables are used to parameterize nodal rotations. The inertia force vector and tangent inertia matrix are expressed in terms of material velocity and acceleration.

3.1 Inertia force vector

Using the section's center of mass as the reference point, the kinetic energy of a beam element in spatial form is obtained as

$$K = \frac{1}{2}\int_{l_o} \{\dot{\mathbf{u}}^{\mathrm{T}} A_\rho \dot{\mathbf{u}} + \dot{\mathbf{w}}^{\mathrm{T}} \mathbf{I}_\rho \dot{\mathbf{w}}\} \mathrm{d}l\,, \tag{27}$$

where $\mathbf{I}_\rho$ is the spatial inertia dyadic tensor given by

$$\mathbf{I}_\rho = \mathbf{R}\,\mathbf{J}_\rho\,\mathbf{R}^{\mathrm{T}}\,, \tag{28}$$

and l_o the initial length of the beam element.

The variation of the kinetic energy can be expressed as (see [12])

$$\delta K = -\int_{l_o} \left\{ \delta\mathbf{u}^{\mathrm{T}} A_\rho \ddot{\mathbf{u}} + \delta\mathbf{w}^{\mathrm{T}} \left[\mathbf{I}_\rho \ddot{\mathbf{w}} + \widetilde{\dot{\mathbf{w}}} \mathbf{I}_\rho \dot{\mathbf{w}} \right] \right\} \mathrm{d}l\,. \tag{29}$$

The previous equation is rewritten in terms of the material velocity and acceleration using Eqs. (16), (17) and (28)

$$\delta K = -\int_{l_o} \left\{ \delta\mathbf{u}^{\mathrm{T}} A_\rho \ddot{\mathbf{u}} + \delta\mathbf{w}^{\mathrm{T}} \mathbf{R} \left[\mathbf{J}_\rho \dot{\boldsymbol{\omega}} + \widetilde{\boldsymbol{\omega}} \mathbf{J}_\rho \boldsymbol{\omega} \right] \right\} \mathrm{d}l\,. \tag{30}$$

The inertia force vector is derived from the following relation

$$\delta K = -\mathbf{f}_k^{\mathrm{T}} \delta\mathbf{d}\,, \tag{31}$$

where $\delta\mathbf{d} = \left[\begin{array}{cccc} \delta\mathbf{u}_1^{\mathrm{T}} & \delta\mathbf{w}_1^{\mathrm{T}} & \delta\mathbf{u}_2^{\mathrm{T}} & \delta\mathbf{w}_2^{\mathrm{T}} \end{array} \right]^{\mathrm{T}}$ is the vector of nodal displacements and nodal spatial spin variables.

The displacements and spin variables are linearly interpolated using

$$\delta\mathbf{u} = N_1 \delta\mathbf{u}_1 + N_2 \delta\mathbf{u}_2\,, \tag{32}$$

$$\delta\mathbf{w} = N_1 \delta\mathbf{w}_1 + N_2 \delta\mathbf{w}_2\,. \tag{33}$$

By replacing Eqs. (32) and (33) into Eq. (31), the expression of the inertia force vector is obtained as

$$\mathbf{f}_k = \left[\begin{array}{c} \int_{l_o} N_1 A_\rho \ddot{\mathbf{u}} \mathrm{d}l \\ \int_{l_o} N_1 \mathbf{R} \left[\mathbf{J}_\rho \dot{\boldsymbol{\omega}} + \widetilde{\boldsymbol{\omega}} \mathbf{J}_\rho \boldsymbol{\omega} \right] \mathrm{d}l \\ \int_{l_o} N_2 A_\rho \ddot{\mathbf{u}} \mathrm{d}l \\ \int_{l_o} N_2 \mathbf{R} \left[\mathbf{J}_\rho \dot{\boldsymbol{\omega}} + \widetilde{\boldsymbol{\omega}} \mathbf{J}_\rho \boldsymbol{\omega} \right] \mathrm{d}l \end{array} \right]. \tag{34}$$

3.2 Update procedure for Newmark time stepping method

The classic Newmark method is used for translational velocity and acceleration. However due to the non-additive property of finite rotations, the update procedure for rotational quantities needs to be carefully treated.

The standard relations for displacements are

$$\mathbf{u}_{n+1} = \mathbf{u}_n + h\dot{\mathbf{u}}_n + h^2\left[(\frac{1}{2}-\beta)\ddot{\mathbf{u}}_n + \beta\,\ddot{\mathbf{u}}_{n+1}\right], \tag{35}$$

$$\dot{\mathbf{u}}_{n+1} = \dot{\mathbf{u}}_n + h\left[(1-\gamma)\ddot{\mathbf{u}}_n + \gamma\ddot{\mathbf{u}}_{n+1}\right], \tag{36}$$

which gives for the iterative quantities

$$\dot{\mathbf{u}}^i_{n+1} = \dot{\mathbf{u}}^{i-1}_{n+1} + \frac{\gamma}{\beta h}(\mathbf{u}^i_{n+1} - \mathbf{u}^{i-1}_{n+1}) = \dot{\mathbf{u}}^{i-1}_{n+1} + \frac{\gamma}{\beta h}\Delta\mathbf{u}^i_{n+1}, \tag{37}$$

$$\ddot{\mathbf{u}}^i_{n+1} = \ddot{\mathbf{u}}^{i-1}_{n+1} + \frac{1}{\beta h^2}(\mathbf{u}^i_{n+1} - \mathbf{u}^{i-1}_{n+1}) = \ddot{\mathbf{u}}^{i-1}_{n+1} + \frac{1}{\beta h^2}\Delta\mathbf{u}^i_{n+1}. \tag{38}$$

According to Simo and Wong [29], only direct addition of angular velocity in a material form makes physical sense. Therefore, the classic Newmark updates are only directly applied to material angular velocity, material acceleration and material incremental rotational vector. The updating algorithm is given by

$$\boldsymbol{\Theta}_{n+1} = h\dot{\boldsymbol{\omega}}_n + h^2\left[(\frac{1}{2}-\beta)\ddot{\boldsymbol{\omega}}_n + \beta\,\ddot{\boldsymbol{\omega}}_{n+1}\right], \tag{39}$$

$$\dot{\boldsymbol{\omega}}_{n+1} = \dot{\boldsymbol{\omega}}_n + h\left[(1-\gamma)\ddot{\boldsymbol{\omega}}_n + \gamma\ddot{\boldsymbol{\omega}}_{n+1}\right], \tag{40}$$

which gives results for the iterative quantities in

$$\dot{\boldsymbol{\omega}}^i_{n+1} = \dot{\boldsymbol{\omega}}^{i-1}_{n+1} + \frac{\gamma}{\beta h}[\boldsymbol{\Theta}^i_{n+1} - \boldsymbol{\Theta}^{i-1}_{n+1}], \tag{41}$$

$$\ddot{\boldsymbol{\omega}}^i_{n+1} = \ddot{\boldsymbol{\omega}}^{i-1}_{n+1} + \frac{1}{\beta h^2}[\boldsymbol{\Theta}^i_{n+1} - \boldsymbol{\Theta}^{i-1}_{n+1}]. \tag{42}$$

Using Eq. (26), the material velocity and acceleration are updated using

$$\dot{\boldsymbol{\omega}}^i_{n+1} = \dot{\boldsymbol{\omega}}^{i-1}_{n+1} + \frac{\gamma}{\beta h}\mathbf{R}^{\mathrm{T}}_n[\boldsymbol{\theta}^i_{n+1} - \boldsymbol{\theta}^{i-1}_{n+1}], \tag{43}$$

$$\ddot{\boldsymbol{\omega}}^i_{n+1} = \ddot{\boldsymbol{\omega}}^{i-1}_{n+1} + \frac{1}{\beta h^2}\mathbf{R}^{\mathrm{T}}_n[\boldsymbol{\theta}^i_{n+1} - \boldsymbol{\theta}^{i-1}_{n+1}]. \tag{44}$$

Since this formulation adopts the spatial spin variables as nodal parameters, linearizations of the material velocity and acceleration in terms of spatial spin variables must be performed. By combining the previous equations with Eq. (7), these linearizations are obtained as

$$\Delta\dot{\boldsymbol{\omega}}^i_{n+1} = \frac{\gamma}{\beta h}\mathbf{R}^{\mathrm{T}}_n\Delta\boldsymbol{\theta}^i_{n+1} = \frac{\gamma}{\beta h}\mathbf{R}^{\mathrm{T}}_n\mathbf{T}_s^{-1}(\boldsymbol{\theta}^i_{n+1})\Delta\mathbf{w}^i_{n+1}, \tag{45}$$

$$\Delta\ddot{\boldsymbol{\omega}}^i_{n+1} = \frac{1}{\beta h^2}\mathbf{R}^{\mathrm{T}}_n\Delta\boldsymbol{\theta}^i_{n+1} = \frac{1}{\beta h^2}\mathbf{R}^{\mathrm{T}}_n\mathbf{T}_s^{-1}(\boldsymbol{\theta}^i_{n+1})\Delta\mathbf{w}^i_{n+1}. \tag{46}$$

3.3 Tangent inertia matrix

To solve the nonlinear equilibrium equation, a linearization of the inertia force vector is required. This linearization is straightforward for translational terms and only the derivation for rotational terms is presented here.

At the i^{th} iteration of the time instant t_{n+1}, the variation of the rotation kinetic energy is taken from Eq. (30)

$$\begin{aligned}\Pi^i_{n+1} = -\delta K^i_{\mathrm{Rot},n+1} &= \int_{l_o}\delta\mathbf{w}^{\mathrm{T}}\mathbf{R}^i_{n+1}\left[\mathbf{J}_\rho\ddot{\boldsymbol{\omega}}^i_{n+1} + \widetilde{\dot{\boldsymbol{\omega}}^i_{n+1}}\mathbf{J}_\rho\dot{\boldsymbol{\omega}}^i_{n+1}\right]\mathrm{d}l \\ &= \int_{l_o}\delta\mathbf{w}^{\mathrm{T}}\mathbf{R}^i_{n+1}\mathbf{a}^i_{n+1}\mathrm{d}l\,.\end{aligned} \tag{47}$$

Linearization of the previous equation gives

$$\Delta\Pi^i_{n+1} = \int_{l_o} \delta\mathbf{w}^{\mathrm{T}}(\Delta\mathbf{R}^i_{n+1})\,\mathbf{a}^i_{n+1}\mathrm{d}l + \int_{l_o} \delta\mathbf{w}^{\mathrm{T}}\mathbf{R}^i_{n+1}(\Delta\mathbf{a}^i_{n+1})\mathrm{d}l\,. \tag{48}$$

The expression in the first integral of Eq. (48) can be straightforwardly reformulated as

$$(\Delta\mathbf{R}^i_{n+1})\,\mathbf{a}^i_{n+1} = \widetilde{\Delta\mathbf{w}^i_{n+1}}\mathbf{R}^i_{n+1}\mathbf{a}^i_{n+1} = -\widetilde{\mathbf{R}^i_{n+1}\mathbf{a}^i_{n+1}}\,\Delta\mathbf{w}^i_{n+1}\,. \tag{49}$$

The second integral of Eq. (48) contains linearlizations of the material angular velocity and the material angular acceleration. This expression can be developed as follows:

$$\mathbf{R}^i_{n+1}(\Delta\mathbf{a}^i_{n+1}) = \mathbf{R}^i_{n+1}\left[\mathbf{J}_\rho\Delta\dot{\boldsymbol{\omega}}^i_{n+1} + (\widetilde{\dot{\boldsymbol{\omega}}^i_{n+1}}\mathbf{J}_\rho - \widetilde{\mathbf{J}_\rho\dot{\boldsymbol{\omega}}^i_{n+1}})\Delta\boldsymbol{\omega}^i_{n+1}\right]. \tag{50}$$

Using relations (45) and (46), the previous equation can be rewritten as

$$\begin{aligned}\mathbf{R}^i_{n+1}(\Delta\mathbf{a}^i_{n+1}) = {}& \frac{1}{\beta h^2}\mathbf{R}^i_{n+1}\mathbf{J}_\rho\mathbf{R}^{\mathrm{T}}_n\mathbf{T}_s^{-1}(\boldsymbol{\theta}^i_{n+1})\,\Delta\mathbf{w}^i_{n+1}\\ &+ \frac{\gamma}{\beta h}\mathbf{R}^i_{n+1}(\widetilde{\dot{\boldsymbol{\omega}}^i_{n+1}}\mathbf{J}_\rho - \widetilde{\mathbf{J}_\rho\dot{\boldsymbol{\omega}}^i_{n+1}})\mathbf{R}^{\mathrm{T}}_n\mathbf{T}_s^{-1}(\boldsymbol{\theta}^i_{n+1})\,\Delta\mathbf{w}^i_{n+1}\,.\end{aligned} \tag{51}$$

Inserting Eqs. (49) and (51) into Eq. (48), one obtains

$$\begin{aligned}\Delta\Pi^i_{n+1} = {}& \frac{1}{\beta h^2}\int_{l_o}\delta\mathbf{w}^{\mathrm{T}}\mathbf{R}^i_{n+1}\mathbf{J}_\rho\mathbf{R}^{\mathrm{T}}_n\mathbf{T}_s^{-1}(\boldsymbol{\theta}^i_{n+1})\,\Delta\mathbf{w}^i_{n+1}\mathrm{d}l\\ &+\frac{\gamma}{\beta h}\int_{l_o}\delta\mathbf{w}^{\mathrm{T}}\mathbf{R}^i_{n+1}(\widetilde{\dot{\boldsymbol{\omega}}^i_{n+1}}\mathbf{J}_\rho - \widetilde{\mathbf{J}_\rho\dot{\boldsymbol{\omega}}^i_{n+1}})\mathbf{R}^{\mathrm{T}}_n\mathbf{T}_s^{-1}(\boldsymbol{\theta}^i_{n+1})\,\Delta\mathbf{w}^i_{n+1}\mathrm{d}l\\ &-\int_{l_o}\delta\mathbf{w}^{\mathrm{T}}\,\widetilde{\mathbf{R}^i_{n+1}\mathbf{a}^i_{n+1}}\,\Delta\mathbf{w}^i_{n+1}\mathrm{d}l\,.\end{aligned} \tag{52}$$

Consequently, the 6x6 blocks of the tangent inertia matrix, including the translational terms, are given by

$$\begin{aligned}\mathbf{K}^i_{\mathrm{Dyn},n+1} = {}& \frac{1}{\beta h^2}\begin{bmatrix}\int N_aN_bA_\rho\mathrm{d}l\,\mathbf{I} & \mathbf{0}_{[3\mathrm{x}3]}\\ \mathbf{0}_{[3\mathrm{x}3]} & \int N_aN_b\mathbf{R}^i_{n+1}\mathbf{J}_\rho\mathbf{R}^{\mathrm{T}}_n\mathbf{T}_s^{-1}(\boldsymbol{\theta}^i_{n+1})\mathrm{d}l\end{bmatrix}\\ &+\frac{\gamma}{\beta h}\begin{bmatrix}\mathbf{0}_{[3\mathrm{x}3]} & \mathbf{0}_{[3\mathrm{x}3]}\\ \mathbf{0}_{[3\mathrm{x}3]} & \int N_aN_b\mathbf{R}^i_{n+1}(\widetilde{\dot{\boldsymbol{\omega}}^i_{n+1}}\mathbf{J}_\rho - \widetilde{\mathbf{J}_\rho\dot{\boldsymbol{\omega}}^i_{n+1}})\mathbf{R}^{\mathrm{T}}_n\mathbf{T}_s^{-1}(\boldsymbol{\theta}^i_{n+1})\mathrm{d}l\end{bmatrix}\\ &-\begin{bmatrix}\mathbf{0}_{[3\mathrm{x}3]} & \mathbf{0}_{[3\mathrm{x}3]}\\ \mathbf{0}_{[3\mathrm{x}3]} & \int N_aN_b\,\widetilde{\mathbf{R}^i_{n+1}\mathbf{a}^i_{n+1}}\,\mathrm{d}l\end{bmatrix},\end{aligned} \tag{53}$$

where $a,b = [1,2]$.

As written above, the tangent inertia matrix can be considered as a sum of mass, gyroscopic and centrifugal matrices:

$$\mathbf{K}_{\mathrm{Dyn}} = \frac{1}{\beta h^2}\mathbf{M} + \frac{\gamma}{\beta h}\mathbf{C}_k + \mathbf{K}_k\,, \tag{54}$$

where $\mathbf{K}_k$, $\mathbf{C}_k$ and $\mathbf{M}$ respectively denote centrifugal matrix, gyroscopic matrix and mass matrix.

3.4 Implementation

The configuration at the $(i-1)^{\text{th}}$ iteration of step $(n+1)$ is known. The nodal displacement and rotational quantities are

$$\mathbf{u}_{n+1}^{i-1}, \quad \dot{\mathbf{u}}_{n+1}^{i-1}, \quad \ddot{\mathbf{u}}_{n+1}^{i-1}, \quad \mathbf{R}_n, \quad \boldsymbol{\theta}_{n+1}^{i-1}.$$

The nodal iterative quantities are

$$\Delta\mathbf{u}_{n+1}^{i}, \quad \Delta\mathbf{w}_{n+1}^{i}.$$

The nodal displacement quantities are updated using

$$\begin{aligned}
\mathbf{u}_{n+1}^{i} &= \mathbf{u}_{n+1}^{i-1} + \Delta\mathbf{u}_{n+1}^{i}, \\
\dot{\mathbf{u}}_{n+1}^{i} &= \dot{\mathbf{u}}_{n+1}^{i-1} + \frac{\gamma}{\beta h}\Delta\mathbf{u}_{n+1}^{i}, \\
\ddot{\mathbf{u}}_{n+1}^{i} &= \ddot{\mathbf{u}}_{n+1}^{i-1} + \frac{1}{\beta h^2}\Delta\mathbf{u}_{n+1}^{i}.
\end{aligned}$$

This update procedure of the displacements is used for all the following formulations.

The nodal incremental rotational vector is updated using

$$\exp(\widetilde{\boldsymbol{\theta}_{n+1}^{i}}) = \exp(\widetilde{\Delta\mathbf{w}_{n+1}^{i}})\exp(\widetilde{\boldsymbol{\theta}_{n+1}^{i-1}}).$$

The inertia force vector (Eq. (34)) and the tangent inertia matrix (Eq. (53)) are computed using two Gauss points. The displacements quantities at each Gauss point are linearly interpolated from the nodal values. The spatial spin variables at the Gauss point $\Delta\mathbf{w}_{n+1}^{G,i}$ are computed as linear interpolation of the nodal values. The spatial incremental rotational vector, the material angular velocity and acceleration at each Gauss point are computed using Eqs. (43) and (44)

$$\exp(\widetilde{\boldsymbol{\theta}_{n+1}^{G,i}}) = \exp(\widetilde{\Delta\mathbf{w}_{n+1}^{G,i}})\exp(\widetilde{\boldsymbol{\theta}_{n+1}^{G,i-1}}), \tag{55}$$

$$\dot{\boldsymbol{\omega}}_{n+1}^{G,i} = \dot{\boldsymbol{\omega}}_{n+1}^{G,i-1} + \frac{\gamma}{\beta h}\mathbf{R}_n^{G\mathrm{T}}[\boldsymbol{\theta}_{n+1}^{G,i} - \boldsymbol{\theta}_{n+1}^{G,i-1}], \tag{56}$$

$$\ddot{\boldsymbol{\omega}}_{n+1}^{G,i} = \ddot{\boldsymbol{\omega}}_{n+1}^{G,i-1} + \frac{1}{\beta h^2}\mathbf{R}_n^{G\mathrm{T}}[\boldsymbol{\theta}_{n+1}^{G,i} - \boldsymbol{\theta}_{n+1}^{G,i-1}], \tag{57}$$

where $\mathbf{R}_n^G$ is the rotation matrix at the Gauss point at the end of the step n and $\boldsymbol{\theta}_{n+1}^{G,i}$ the spatial incremental rotational vector at the Gauss point.

The approach presented in Eqs. (55) - (57) is different from the one of Simo et al. [28], who proposed to calculate $\boldsymbol{\theta}_{n+1}^{G,i}$, $\dot{\boldsymbol{\omega}}_{n+1}^{G,i}$, $\ddot{\boldsymbol{\omega}}_{n+1}^{G,i}$ by taking linear interpolations of the nodal values $\boldsymbol{\theta}_{n+1}^{i}$, $\dot{\boldsymbol{\omega}}_{n+1}^{i}$, $\ddot{\boldsymbol{\omega}}_{n+1}^{i}$. Extensive numerical tests performed by the authors showed that these two approaches give the same numerical results, but the approach presented here requires less iterations.

At the end of step $(n+1)$, the nodal material angular velocity $\dot{\boldsymbol{\omega}}_{n+1}$ and acceleration $\ddot{\boldsymbol{\omega}}_{n+1}$, which are required for the predictor of the step $(n+2)$ are calculated by (see Eqs. (23), (26), (39) and (40))

$$\begin{aligned}
\boldsymbol{\Theta}_{n+1} &= \mathbf{R}_n^{\mathrm{T}}\boldsymbol{\theta}_{n+1}, \\
\dot{\boldsymbol{\omega}}_{n+1} &= \frac{\gamma}{\beta h}\boldsymbol{\Theta}_{n+1} + \frac{\beta-\gamma}{\beta}\dot{\boldsymbol{\omega}}_n + \frac{(\beta-0.5\gamma)h}{\beta}\ddot{\boldsymbol{\omega}}_n, \qquad (58) \\
\ddot{\boldsymbol{\omega}}_{n+1} &= \frac{1}{\beta h^2}\boldsymbol{\Theta}_{n+1} - \frac{1}{\beta h}\dot{\boldsymbol{\omega}}_n - \frac{0.5-\beta}{\beta}\ddot{\boldsymbol{\omega}}_n, \qquad (59) \\
\mathbf{R}_{n+1} &= \exp(\widetilde{\boldsymbol{\theta}_{n+1}})\,\mathbf{R}_n.
\end{aligned}$$

4 Formulation using the incremental rotational vector Type 1

The formulation proposed by Ibrahimbegović and Mikdad in [17] is now presented. The same Newmark update procedure for the rotational part as in the previous formulation is adopted. However, the spatial incremental rotational vector is chosen to parameterize the nodal rotations. Besides, the material angular velocity and material angular acceleration are replaced by the spatial quantities in the expressions of the inertia force vector and the tangent inertia matrix.

4.1 Inertia force vector

The nodal variables are

$$\delta\mathbf{d} = \begin{bmatrix} \delta\mathbf{u}_1^{\mathrm{T}} & \delta\boldsymbol{\theta}_1^{\mathrm{T}} & \delta\mathbf{u}_2^{\mathrm{T}} & \delta\boldsymbol{\theta}_2^{\mathrm{T}} \end{bmatrix}^{\mathrm{T}}.$$

The spatial incremental rotational vectors are linearly interpolated using

$$\delta\boldsymbol{\theta} = N_1\delta\boldsymbol{\theta}_1 + N_2\delta\boldsymbol{\theta}_2\,. \tag{60}$$

The change of variables given by Eq. (5) is applied to Eq. (29). Hence, the variation of kinetic energy in terms of the spatial incremental rotational vector is

$$\delta K = -\int_{l_o} \left\{ \delta\mathbf{u}^{\mathrm{T}} A_\rho \ddot{\mathbf{u}} + \delta\boldsymbol{\theta}^{\mathrm{T}}\, \mathbf{T}_s^{\mathrm{T}}(\boldsymbol{\theta}) \left[\mathbf{I}_\rho \dot{\mathbf{w}} + \widetilde{\dot{\mathbf{w}}}\mathbf{I}_\rho \dot{\mathbf{w}} \right] \right\} \mathrm{d}l\,. \tag{61}$$

Inserting Eqs. (32) and (60) into Eq. (61), the inertia force is obtained as

$$\mathbf{f}_k = \begin{bmatrix} \int N_1 A_\rho \ddot{\mathbf{u}} \mathrm{d}l \\ \int N_1 \mathbf{T}_s^{\mathrm{T}}(\boldsymbol{\theta}) \left[\mathbf{I}_\rho \dot{\mathbf{w}} + \widetilde{\dot{\mathbf{w}}}\mathbf{I}_\rho \dot{\mathbf{w}} \right] \mathrm{d}l \\ \int N_2 A_\rho \ddot{\mathbf{u}} \mathrm{d}l \\ \int N_2 \mathbf{T}_s^{\mathrm{T}}(\boldsymbol{\theta}) \left[\mathbf{I}_\rho \dot{\mathbf{w}} + \widetilde{\dot{\mathbf{w}}}\mathbf{I}_\rho \dot{\mathbf{w}} \right] \mathrm{d}l \end{bmatrix}. \tag{62}$$

4.2 Update procedure for Newmark time stepping method

The same Newmark procedures as in Eqs. (39), (40) and (45), (46) are employed, but the spatial angular velocity and acceleration are used instead of material ones. By multiplying Eq. (39) with $\mathbf{R}_n$, Eq. (40) with $\mathbf{R}_{n+1}$ and using Eqs. (16), (17), (26), the Newmark algorithm takes the following form

$$\boldsymbol{\theta}_{n+1} = h\dot{\mathbf{w}}_n + h^2 \left[(\frac{1}{2} - \beta)\ddot{\mathbf{w}}_n + \beta\, \boldsymbol{\Lambda}_{n+1}^{\mathrm{T}} \ddot{\mathbf{w}}_{n+1} \right], \tag{63}$$

$$\dot{\mathbf{w}}_{n+1} = \boldsymbol{\Lambda}_{n+1} \left[\dot{\mathbf{w}}_n + h(1-\gamma)\ddot{\mathbf{w}}_n \right] + h\gamma\ddot{\mathbf{w}}_{n+1}\,, \tag{64}$$

which gives results for the iterative quantities in the following

$$\dot{\mathbf{w}}_{n+1}^i = \boldsymbol{\Lambda}_{n+1}^i \left[\frac{\gamma}{\beta h}\boldsymbol{\theta}_{n+1}^i + \frac{\beta-\gamma}{\beta}\dot{\mathbf{w}}_n + \frac{(\beta - 0.5\gamma)h}{\beta}\ddot{\mathbf{w}}_n \right], \tag{65}$$

$$\ddot{\mathbf{w}}_{n+1}^i = \boldsymbol{\Lambda}_{n+1}^i \left[\frac{1}{\beta h^2}\boldsymbol{\theta}_{n+1}^i - \frac{1}{\beta h}\dot{\mathbf{w}}_n - \frac{0.5-\beta}{\beta}\ddot{\mathbf{w}}_n \right], \tag{66}$$

where $\boldsymbol{\Lambda}_{n+1}^i = \exp(\widetilde{\boldsymbol{\theta}_{n+1}^i})$.

4.3 Tangent inertia matrix

The tangent inertia matrix needs to be computed by taking the differentiation of Eq. (61). However, since $\mathbf{I}_\rho$ is not constant, this differentiation is complicated. Therefore, Eq. (47) is used instead to derive the tangent inertia matrix.

The change of variable defined in Eq. (5) is applied to Eq. (47). Accordingly, the variation of the rotation kinetic energy is expressed as

$$\begin{aligned}\Pi^i_{n+1} &= \int_{l_o} \delta\boldsymbol{\theta}^{\mathrm{T}}\, \mathbf{T}_s^{\mathrm{T}}(\boldsymbol{\theta}^i_{n+1})\mathbf{R}^i_{n+1}\left[\mathbf{J}_\rho\dot{\boldsymbol{\omega}}^i_{n+1} + \widetilde{\boldsymbol{\omega}^i_{n+1}}\mathbf{J}_\rho\boldsymbol{\omega}^i_{n+1}\right]\mathrm{d}l \\ &= \int_{l_o} \delta\boldsymbol{\theta}^{\mathrm{T}}\, \mathbf{T}_s^{\mathrm{T}}(\boldsymbol{\theta}^i_{n+1})\mathbf{R}^i_{n+1}\mathbf{a}^i_{n+1}\mathrm{d}l\,. \end{aligned} \tag{67}$$

Linearization of the previous equation gives

$$\begin{aligned}\Delta\Pi^i_{n+1} &= \int_{l_o} \delta\boldsymbol{\theta}^{\mathrm{T}}\, (\Delta\mathbf{T}_s^{\mathrm{T}}(\boldsymbol{\theta}^i_{n+1}))\mathbf{R}^i_{n+1}\mathbf{a}^i_{n+1}\mathrm{d}l \\ &+ \int_{l_o} \delta\boldsymbol{\theta}^{\mathrm{T}}\, \mathbf{T}_s^{\mathrm{T}}(\boldsymbol{\theta}^i_{n+1})(\Delta\mathbf{R}^i_{n+1})\mathbf{a}^i_{n+1}\mathrm{d}l \\ &+ \int_{l_o} \delta\boldsymbol{\theta}^{\mathrm{T}}\, \mathbf{T}_s^{\mathrm{T}}(\boldsymbol{\theta}^i_{n+1})\mathbf{R}^i_{n+1}(\Delta\mathbf{a}^i_{n+1})\mathrm{d}l\,. \end{aligned} \tag{68}$$

The first term is a well known derivative (more details can be found in [15])

$$(\Delta\mathbf{T}_s^{\mathrm{T}}(\boldsymbol{\theta}^i_{n+1}))\mathbf{R}^i_{n+1}\mathbf{a}^i_{n+1} = \boldsymbol{\Xi}(\mathbf{R}^i_{n+1}\mathbf{a}^i_{n+1})\Delta\boldsymbol{\theta}^i_{n+1}\,, \tag{69}$$

where

$$\boldsymbol{\Xi}(\mathbf{x}) = c_1\,\mathbf{x}\boldsymbol{\theta}^{\mathrm{T}} - c_2\,\widetilde{\boldsymbol{\theta}}\,\mathbf{x}\boldsymbol{\theta}^{\mathrm{T}} + c_3\,(\boldsymbol{\theta}^{\mathrm{T}}\mathbf{x})\,\boldsymbol{\theta}\boldsymbol{\theta}^{\mathrm{T}} + c_4\,\widetilde{\mathbf{x}} + c_5\,\left[\boldsymbol{\theta}\mathbf{x}^{\mathrm{T}} + (\boldsymbol{\theta}^{\mathrm{T}}\mathbf{x})\mathbf{I}\right], \tag{70}$$

$$\begin{aligned} c_1 &= \frac{\theta\,\cos\theta - \sin\theta}{\theta^3}, \qquad c_2 = \frac{\theta\sin\theta + 2\cos\theta - 2}{\theta^4}, \\ c_3 &= \frac{3\sin\theta - 2\theta - \theta\,\cos\theta}{\theta^5}, \quad c_4 = \frac{1-\cos\theta}{\theta^2}, \quad c_5 = \frac{\theta - \sin\theta}{\theta^3}. \end{aligned}$$

Here, $\mathbf{x}$ denotes a vector [3x1].

The second and the third terms of Eq. (68) have been calculated in Eqs. (49) and (51). They can be reformulated in terms of the incremental rotational variables using Eq. (5)

$$(\Delta\mathbf{R}^i_{n+1})\,\mathbf{a}^i_{n+1} = -\widetilde{\mathbf{R}^i_{n+1}\mathbf{a}^i_{n+1}}\,\mathbf{T}_s(\boldsymbol{\theta}^i_{n+1})\,\Delta\boldsymbol{\theta}^i_{n+1}\,, \tag{71}$$

$$\begin{aligned}\mathbf{R}^i_{n+1}(\Delta\mathbf{a}^i_{n+1}) &= \frac{1}{\beta h^2}\mathbf{R}^i_{n+1}\mathbf{J}_\rho\mathbf{R}^{\mathrm{T}}_n\,\Delta\boldsymbol{\theta}^i_{n+1} \\ &+ \frac{\gamma}{\beta h}\mathbf{R}^i_{n+1}(\widetilde{\boldsymbol{\omega}^i_{n+1}}\mathbf{J}_\rho - \widetilde{\mathbf{J}_\rho\boldsymbol{\omega}^i_{n+1}})\mathbf{R}^{\mathrm{T}}_n\,\Delta\boldsymbol{\theta}^i_{n+1}\,. \end{aligned} \tag{72}$$

Since only the spatial quantities are used in this formulation, the material quantities in previous equations need to be transformed into spatial form. With the Eqs. (16), (17), (26) and (28), the following relations are readily derived

$$\mathbf{R}^i_{n+1}\mathbf{J}_\rho\mathbf{R}^{\mathrm{T}}_n = \mathbf{I}^i_{\rho,n+1}\boldsymbol{\Lambda}^i_{n+1}\,, \tag{73}$$

$$\begin{aligned}\mathbf{R}^i_{n+1}\mathbf{a}^i_{n+1} &= \mathbf{R}^i_{n+1}\left[\mathbf{J}_\rho\dot{\boldsymbol{\omega}}^i_{n+1} + \widetilde{\boldsymbol{\omega}^i_{n+1}}\mathbf{J}_\rho\boldsymbol{\omega}^i_{n+1}\right] \\ &= \mathbf{I}^i_{\rho,n+1}\dot{\mathbf{w}}^i_{n+1} + \widetilde{\mathbf{w}^i_{n+1}}\mathbf{I}^i_{\rho,n+1}\dot{\mathbf{w}}^i_{n+1} = \mathbf{A}^i_{n+1}\,, \end{aligned} \tag{74}$$

$$\begin{aligned}\mathbf{R}^i_{n+1}(\widetilde{\boldsymbol{\omega}^i_{n+1}}\mathbf{J}_\rho - \widetilde{\mathbf{J}_\rho\boldsymbol{\omega}^i_{n+1}})\mathbf{R}^{\mathrm{T}}_n &= (\widetilde{\mathbf{w}^i_{n+1}}\mathbf{I}^i_{\rho,n+1} - \widetilde{\mathbf{I}^i_{\rho,n+1}\dot{\mathbf{w}}^i_{n+1}})\boldsymbol{\Lambda}^i_{n+1} \\ &= \mathbf{b}^i_{n+1}\,\boldsymbol{\Lambda}^i_{n+1}\,. \end{aligned} \tag{75}$$

With these results, Eqs. (69), (71) and (72) are rewritten as

$$(\Delta \mathbf{T}_s^{\mathrm{T}}(\boldsymbol{\theta}_{n+1}^i))\mathbf{R}_{n+1}^i \mathbf{a}_{n+1}^i = \boldsymbol{\Xi}(\mathbf{A}_{n+1}^i)\Delta\boldsymbol{\theta}_{n+1}^i\,, \tag{76}$$

$$(\Delta \mathbf{R}_{n+1}^i)\,\mathbf{a}_{n+1}^i = -\widetilde{\mathbf{A}_{n+1}^i}\,\mathbf{T}_s(\boldsymbol{\theta}_{n+1}^i)\,\Delta\boldsymbol{\theta}_{n+1}^i\,, \tag{77}$$

$$\mathbf{R}_{n+1}^i(\Delta \mathbf{a}_{n+1}^i) = \frac{1}{\beta h^2}\mathbf{I}_{\rho,n+1}^i \boldsymbol{\Lambda}_{n+1}^i\,\Delta\boldsymbol{\theta}_{n+1}^i + \frac{\gamma}{\beta h}\mathbf{b}_{n+1}^i\,\boldsymbol{\Lambda}_{n+1}^i\,\Delta\boldsymbol{\theta}_{n+1}^i\,. \tag{78}$$

The explicit form of Eq. (68) is then obtained as

$$\begin{aligned}\Delta\Pi_{n+1}^i =& \frac{1}{\beta h^2}\int_{l_o} \delta\boldsymbol{\theta}^{\mathrm{T}}\,\mathbf{T}_s^{\mathrm{T}}(\boldsymbol{\theta}_{n+1}^i)\mathbf{I}_{\rho,n+1}^i\,\boldsymbol{\Lambda}_{n+1}^i\Delta\boldsymbol{\theta}_{n+1}^i \mathrm{d}l \\ &+ \frac{\gamma}{\beta h}\int_{l_o} \delta\boldsymbol{\theta}^{\mathrm{T}}\,\mathbf{T}_s^{\mathrm{T}}(\boldsymbol{\theta}_{n+1}^i)\mathbf{b}_{n+1}^i\,\boldsymbol{\Lambda}_{n+1}^i\Delta\boldsymbol{\theta}_{n+1}^i \mathrm{d}l \\ &- \int_{l_o} \delta\boldsymbol{\theta}^{\mathrm{T}}\left[\mathbf{T}_s^{\mathrm{T}}(\boldsymbol{\theta}_{n+1}^i)\,\widetilde{\mathbf{A}_{n+1}^i}\,\mathbf{T}_s(\boldsymbol{\theta}_{n+1}^i) - \boldsymbol{\Xi}(\mathbf{A}_{n+1}^i)\right]\Delta\boldsymbol{\theta}_{n+1}^i \mathrm{d}l\,.\end{aligned} \tag{79}$$

Consequently, the 6x6 blocks of the tangent inertia matrix, including the translational terms, are given by

$$\begin{aligned}\mathbf{K}_{\mathrm{Dyn},n+1}^i =& \frac{1}{\beta h^2}\begin{bmatrix}\int N_a N_b A_\rho \mathrm{d}l\,\mathbf{I} & \mathbf{0}_{[3\mathrm{x}3]} \\ \mathbf{0}_{[3\mathrm{x}3]} & \int N_a N_b \mathbf{T}_s^{\mathrm{T}}(\boldsymbol{\theta}_{n+1}^i)\mathbf{I}_{\rho,n+1}^i\,\boldsymbol{\Lambda}_{n+1}^i \mathrm{d}l\end{bmatrix} \\ &+ \frac{\gamma}{\beta h}\begin{bmatrix}\mathbf{0}_{[3\mathrm{x}3]} & \mathbf{0}_{[3\mathrm{x}3]} \\ \mathbf{0}_{[3\mathrm{x}3]} & \int N_a N_b \mathbf{T}_s^{\mathrm{T}}(\boldsymbol{\theta}_{n+1}^i)\mathbf{b}_{n+1}^i\,\boldsymbol{\Lambda}_{n+1}^i \mathrm{d}l\end{bmatrix} \\ &- \begin{bmatrix}\mathbf{0}_{[3\mathrm{x}3]} & \mathbf{0}_{[3\mathrm{x}3]} \\ \mathbf{0}_{[3\mathrm{x}3]} & \int N_a N_b \left[\mathbf{T}_s^{\mathrm{T}}(\boldsymbol{\theta}_{n+1}^i)\,\widetilde{\mathbf{A}_{n+1}^i}\,\mathbf{T}_s(\boldsymbol{\theta}_{n+1}^i) - \boldsymbol{\Xi}(\mathbf{A}_{n+1}^i)\right]\mathrm{d}l\end{bmatrix},\end{aligned} \tag{80}$$

where $a,b = [1,2]$.

4.4 Implementation of the rotational variables

The configuration at the $(i-1)^{\text{th}}$ iteration of step $(n+1)$ is known. The nodal spatial incremental rotational vector is

$$\boldsymbol{\theta}_{n+1}^i\,.$$

The iterative incremental rotational vector is

$$\Delta\boldsymbol{\theta}_{n+1}^i\,.$$

The nodal spatial incremental rotational vector is updated with

$$\boldsymbol{\theta}_{n+1}^i = \boldsymbol{\theta}_{n+1}^{i-1} + \Delta\boldsymbol{\theta}_{n+1}^i\,.$$

The inertia force vector (Eq. (62)) and the tangent inertia matrix (Eq. (80)) are computed using two Gauss points. At each Gauss point, the spatial angular velocity and acceleration are updated with (see Eqs. (65) and (66))

$$\dot{\mathbf{w}}_{n+1}^{G,i} = \exp(\widetilde{\boldsymbol{\theta}_{n+1}^{G,i}})\left[\frac{\gamma}{\beta h}\boldsymbol{\theta}_{n+1}^{G,i} + \frac{\beta-\gamma}{\beta}\dot{\mathbf{w}}_n^G + \frac{(\beta-0.5\gamma)h}{\beta}\ddot{\mathbf{w}}_n^G\right], \tag{81}$$

$$\ddot{\mathbf{w}}_{n+1}^{G,i} = \exp(\widetilde{\boldsymbol{\theta}_{n+1}^{G,i}})\left[\frac{1}{\beta h^2}\boldsymbol{\theta}_{n+1}^{G,i} - \frac{1}{\beta h}\dot{\mathbf{w}}_n^G - \frac{0.5-\beta}{\beta}\ddot{\mathbf{w}}_n^G\right], \tag{82}$$

where $\dot{\mathbf{w}}_n^G, \ddot{\mathbf{w}}_n^G$ are the spatial angular velocity and acceleration at the Gauss point at the end of the step n, respectively.

$\boldsymbol{\theta}_{n+1}^{G,i}$ is the spatial incremental rotational vector at the Gauss point and computed from linear interpolations of the nodal values $\boldsymbol{\theta}_{n+1}^{i}$.

At the end of the step $(n+1)$, the nodal spatial angular velocity and acceleration $\dot{\mathbf{w}}_{n+1}, \ddot{\mathbf{w}}_{n+1}$ which are required for the predictor of the step $(n+2)$ are calculated according to

$$\dot{\mathbf{w}}_{n+1} = \exp(\widetilde{\boldsymbol{\theta}_{n+1}}) \left[\frac{\gamma}{\beta h}\boldsymbol{\theta}_{n+1} + \frac{\beta-\gamma}{\beta}\dot{\mathbf{w}}_n + \frac{(\beta-0.5\gamma)h}{\beta}\ddot{\mathbf{w}}_n \right], \tag{83}$$

$$\ddot{\mathbf{w}}_{n+1} = \exp(\widetilde{\boldsymbol{\theta}_{n+1}}) \left[\frac{1}{\beta h^2}\boldsymbol{\theta}_{n+1} - \frac{1}{\beta h}\dot{\mathbf{w}}_n - \frac{0.5-\beta}{\beta}\ddot{\mathbf{w}}_n \right]. \tag{84}$$

5 Formulation using the incremental rotational vector Type 2

This formulation, based on the incremental rotational vector in material form, has been proposed by Cardona and Geradin in [6]. This approach is reformulated here using the spatial form of the incremental rotational vector. The same parametrization of finite rotations as in Section 4 is adopted. However, the additive property of the spatial incremental rotational vector is used and the classic Newmark update procedure for translations is also applied to the rotational variables.

The iterative quantities are given by

$$\dot{\boldsymbol{\theta}}_{n+1}^{i} = \dot{\boldsymbol{\theta}}_{n+1}^{i-1} + \frac{\gamma}{\beta h}\Delta\boldsymbol{\theta}_{n+1}^{i}, \tag{85}$$

$$\ddot{\boldsymbol{\theta}}_{n+1}^{i} = \ddot{\boldsymbol{\theta}}_{n+1}^{i-1} + \frac{1}{\beta h^2}\Delta\boldsymbol{\theta}_{n+1}^{i}. \tag{86}$$

5.1 Internal force

This formulation uses the same variables as in the formulation presented in Section 4. Hence, the inertial force vector takes the same expression as in Eq. (62):

$$\mathbf{f}_k = \begin{bmatrix} \int N_1 A_\rho \ddot{\mathbf{u}} \mathrm{d}l \\ \int N_1 \mathbf{T}_s^{\mathrm{T}}(\boldsymbol{\theta}) \left[\mathbf{I}_\rho \dot{\mathbf{w}} + \widetilde{\dot{\mathbf{w}}} \mathbf{I}_\rho \dot{\mathbf{w}} \right] \mathrm{d}l \\ \int N_2 A_\rho \ddot{\mathbf{u}} \mathrm{d}l \\ \int N_2 \mathbf{T}_s^{\mathrm{T}}(\boldsymbol{\theta}) \left[\mathbf{I}_\rho \dot{\mathbf{w}} + \widetilde{\dot{\mathbf{w}}} \mathbf{I}_\rho \dot{\mathbf{w}} \right] \mathrm{d}l \end{bmatrix}. \tag{87}$$

The spatial angular velocity and acceleration $\dot{\mathbf{w}}, \ddot{\mathbf{w}}$ are calculated from $\dot{\boldsymbol{\theta}}, \ddot{\boldsymbol{\theta}}$ using the relations (14) and (15).

5.2 Tangent inertia matrix

The tangent operator of this formulation is calculated using the same expression as in Eq. (68). The first and the second terms of Eq. (68) are given in Eqs. (76) and (77).

However, the third term of Eq. (68) can not be computed using Eq. (78), since the update procedures in Eqs. (45) and (46) are no longer available.

To derive this term, the expression of the material angular velocity is rewritten using Eqs. (9), (14) and (16)

$$\dot{\boldsymbol{\omega}}_{n+1} = \mathbf{R}_{n+1}^{\mathrm{T}} \dot{\mathbf{w}}_{n+1} = \mathbf{R}_n^{\mathrm{T}} \mathbf{T}_s^{\mathrm{T}}(\boldsymbol{\theta}_{n+1})\, \dot{\boldsymbol{\theta}}_{n+1}\,. \tag{88}$$

The time differentiation of the previous equation gives the expression of the material angular acceleration as

$$\ddot{\boldsymbol{\omega}}_{n+1} = \mathbf{R}_n^{\mathrm{T}} \left[\mathbf{T}_s^{\mathrm{T}}(\boldsymbol{\theta}_{n+1})\, \ddot{\boldsymbol{\theta}}_{n+1} + \dot{\mathbf{T}}_s^{\mathrm{T}}(\boldsymbol{\theta}_{n+1})\, \dot{\boldsymbol{\theta}}_{n+1} \right]. \tag{89}$$

Linearization of the previous equations gives

$$\Delta\dot{\boldsymbol{\omega}}_{n+1} = \mathbf{R}_n^{\mathrm{T}} \left[\mathbf{T}_s^{\mathrm{T}}(\boldsymbol{\theta}_{n+1})\, \Delta\dot{\boldsymbol{\theta}}_{n+1} + \boldsymbol{\Xi}(\dot{\boldsymbol{\theta}}_{n+1}) \Delta\boldsymbol{\theta}_{n+1} \right], \tag{90}$$

$$\Delta\ddot{\boldsymbol{\omega}}_{n+1} = \mathbf{R}_n^{\mathrm{T}} \left[\mathbf{T}_s^{\mathrm{T}}(\boldsymbol{\theta}_{n+1})\, \Delta\ddot{\boldsymbol{\theta}}_{n+1} + \boldsymbol{\Xi}(\ddot{\boldsymbol{\theta}}_{n+1}) \Delta\boldsymbol{\theta}_{n+1} + \boldsymbol{\Omega}_1 \Delta\dot{\boldsymbol{\theta}}_{n+1} + \boldsymbol{\Omega}_2 \Delta\boldsymbol{\theta}_{n+1} \right], \tag{91}$$

where

$$\Delta(\dot{\mathbf{T}}_s^{\mathrm{T}}(\boldsymbol{\theta})\, \dot{\boldsymbol{\theta}}) = \boldsymbol{\Omega}_1\, \Delta\dot{\boldsymbol{\theta}} + \boldsymbol{\Omega}_2\, \Delta\boldsymbol{\theta}\,. \tag{92}$$

The expressions of $\boldsymbol{\Omega}_1, \boldsymbol{\Omega}_2$ are given in Appendix A.

Inserting Eqs. (90) and (91) into Eq. (50), the third term of Eq. (68) reads

$$\begin{aligned} \mathbf{R}_{n+1}^i(\Delta\mathbf{a}_{n+1}^i) = {} & \mathbf{I}_{\rho,n+1}^i \mathbf{T}_s(\boldsymbol{\theta}_{n+1}^i)\, \Delta\ddot{\boldsymbol{\theta}}_{n+1}^i + \left[\mathbf{b}_{n+1}^i \mathbf{T}_s(\boldsymbol{\theta}_{n+1}^i) + \mathbf{I}_{\rho,n+1}^i \boldsymbol{\Lambda}_{n+1}^i \boldsymbol{\Omega}_1 \right] \Delta\dot{\boldsymbol{\theta}}_{n+1}^i \\ & + \left[\mathbf{I}_{\rho,n+1}^i \boldsymbol{\Lambda}_{n+1}^i (\boldsymbol{\Xi}(\ddot{\boldsymbol{\theta}}_{n+1}^i) + \boldsymbol{\Omega}_2) + \mathbf{b}_{n+1}^i \boldsymbol{\Lambda}_{n+1}^i \boldsymbol{\Xi}(\dot{\boldsymbol{\theta}}_{n+1}^i) \right] \Delta\boldsymbol{\theta}_{n+1}^i\,. \end{aligned} \tag{93}$$

The explicit form of Eq. (68) is finally obtained using Eqs. (76), (77) and (93)

$$\begin{aligned} \Delta\Pi_{n+1}^i = {} & \frac{1}{\beta h^2} \int_{l_o} \delta\boldsymbol{\theta}^{\mathrm{T}}\, \mathbf{T}_s^{\mathrm{T}}(\boldsymbol{\theta}_{n+1}^i) \mathbf{I}_{\rho,n+1}^i\, \mathbf{T}_s(\boldsymbol{\theta}_{n+1}^i) \Delta\boldsymbol{\theta}_{n+1}^i \mathrm{d}l \\ & + \frac{\gamma}{\beta h} \int_{l_o} \delta\boldsymbol{\theta}^{\mathrm{T}}\, \mathbf{T}_s^{\mathrm{T}}(\boldsymbol{\theta}_{n+1}^i) \left[\mathbf{b}_{n+1}^i \mathbf{T}_s(\boldsymbol{\theta}_{n+1}^i) + \mathbf{I}_{\rho,n+1}^i \boldsymbol{\Lambda}_{n+1}^i \boldsymbol{\Omega}_1 \right] \Delta\boldsymbol{\theta}_{n+1}^i \mathrm{d}l \\ & - \int_{l_o} \delta\boldsymbol{\theta}^{\mathrm{T}} \left[\mathbf{T}_s^{\mathrm{T}}(\boldsymbol{\theta}_{n+1}^i) \widetilde{\mathbf{A}_{n+1}^i}\, \mathbf{T}_s(\boldsymbol{\theta}_{n+1}^i) - \boldsymbol{\Xi}(\mathbf{A}_{n+1}^i) \right] \Delta\boldsymbol{\theta}_{n+1}^i \mathrm{d}l \\ & + \int_{l_o} \delta\boldsymbol{\theta}^{\mathrm{T}}\, \mathbf{T}_s^{\mathrm{T}}(\boldsymbol{\theta}_{n+1}^i) \left[\mathbf{I}_{\rho,n+1}^i \boldsymbol{\Lambda}_{n+1}^i (\boldsymbol{\Xi}(\ddot{\boldsymbol{\theta}}_{n+1}^i) + \boldsymbol{\Omega}_2) \right. \\ & \left. + \mathbf{b}_{n+1}^i \boldsymbol{\Lambda}_{n+1}^i \boldsymbol{\Xi}(\dot{\boldsymbol{\theta}}_{n+1}^i) \right] \Delta\boldsymbol{\theta}_{n+1}^i \mathrm{d}l\,. \end{aligned} \tag{94}$$

Consequently, the 6x6 blocks of the tangent inertia matrix, including the translational terms, are expressed as

$$\begin{aligned} \mathbf{K}_{\mathrm{Dyn},n+1}^i = {} & \frac{1}{\beta h^2} \begin{bmatrix} \int N_a N_b A_\rho \mathrm{d}l\, \mathbf{I} & \mathbf{0}_{[3\mathrm{x}3]} \\ \mathbf{0}_{[3\mathrm{x}3]} & \int N_a N_b \mathbf{T}_s^{\mathrm{T}}(\boldsymbol{\theta}_{n+1}^i) \mathbf{I}_{\rho,n+1}^i\, \mathbf{T}_s(\boldsymbol{\theta}_{n+1}^i) \mathrm{d}l \end{bmatrix} \\ & + \frac{\gamma}{\beta h} \begin{bmatrix} \mathbf{0}_{[3\mathrm{x}3]} & \mathbf{0}_{[3\mathrm{x}3]} \\ \mathbf{0}_{[3\mathrm{x}3]} & \int N_a N_b \mathbf{T}_s^{\mathrm{T}}(\boldsymbol{\theta}_{n+1}^i) \left[\mathbf{b}_{n+1}^i \mathbf{T}_s(\boldsymbol{\theta}_{n+1}^i) + \mathbf{I}_{\rho,n+1}^i \boldsymbol{\Lambda}_{n+1}^i \boldsymbol{\Omega}_1 \right] \mathrm{d}l \end{bmatrix} \\ & - \begin{bmatrix} \mathbf{0}_{[3\mathrm{x}3]} & \mathbf{0}_{[3\mathrm{x}3]} \\ \mathbf{0}_{[3\mathrm{x}3]} & \int N_a N_b \left[\mathbf{T}_s^{\mathrm{T}}(\boldsymbol{\theta}_{n+1}^i) \widetilde{\mathbf{A}_{n+1}^i}\, \mathbf{T}_s(\boldsymbol{\theta}_{n+1}^i) - \boldsymbol{\Xi}(\mathbf{A}_{n+1}^i) \right] \mathrm{d}l \end{bmatrix} \\ & + \begin{bmatrix} \mathbf{0}_{[3\mathrm{x}3]} & \mathbf{0}_{[3\mathrm{x}3]} \\ \mathbf{0}_{[3\mathrm{x}3]} & \int N_a N_b \left[\mathbf{I}_{\rho,n+1}^i \boldsymbol{\Lambda}_{n+1}^i (\boldsymbol{\Xi}(\ddot{\boldsymbol{\theta}}_{n+1}^i) + \boldsymbol{\Omega}_2) + \mathbf{b}_{n+1}^i \boldsymbol{\Lambda}_{n+1}^i \boldsymbol{\Xi}(\dot{\boldsymbol{\theta}}_{n+1}^i) \right] \mathrm{d}l \end{bmatrix}, \end{aligned} \tag{95}$$

where $a, b = [1,2]$.

5.3 Implementation of the rotational variables

The configuration at the $(i-1)^{\text{th}}$ iteration of step $(n+1)$ is known. The nodal rotational quantities are

$$\boldsymbol{\theta}_{n+1}^{i-1}, \quad \dot{\boldsymbol{\theta}}_{n+1}^{i-1}, \quad \ddot{\boldsymbol{\theta}}_{n+1}^{i-1},$$

and the iterative quantity is

$$\Delta\boldsymbol{\theta}_{n+1}^{i}.$$

The nodal rotational quantities are updated according to

$$\begin{aligned}
\boldsymbol{\theta}_{n+1}^{i} &= \boldsymbol{\theta}_{n+1}^{i-1} + \Delta\boldsymbol{\theta}_{n+1}^{i}, \\
\dot{\boldsymbol{\theta}}_{n+1}^{i} &= \dot{\boldsymbol{\theta}}_{n+1}^{i-1} + \frac{\gamma}{\beta h}\Delta\boldsymbol{\theta}_{n+1}^{i}, \\
\ddot{\boldsymbol{\theta}}_{n+1}^{i} &= \ddot{\boldsymbol{\theta}}_{n+1}^{i-1} + \frac{1}{\beta h^2}\Delta\boldsymbol{\theta}_{n+1}^{i}.
\end{aligned}$$

The inertia force vector (Eq. (87)) and the tangent inertia matrix (Eq. (95)) are computed using two Gauss points. The rotational quantities at each Gauss point $\boldsymbol{\theta}_{n+1}^{G,i}, \dot{\boldsymbol{\theta}}_{n+1}^{G,i}, \ddot{\boldsymbol{\theta}}_{n+1}^{G,i}$ are linearly interpolated from the nodal values. Then, the spatial angular velocity and acceleration at the Gauss point are computed using Eqs. (14) and (15)

$$\dot{\mathbf{w}}_{n+1}^{G,i} = \mathbf{T}_s(\boldsymbol{\theta}_{n+1}^{G,i})\,\dot{\boldsymbol{\theta}}_{n+1}^{G,i}, \tag{96}$$

$$\ddot{\mathbf{w}}_{n+1}^{G,i} = \mathbf{T}_s(\boldsymbol{\theta}_{n+1}^{G,i})\,\ddot{\boldsymbol{\theta}}_{n+1}^{G,i} + \dot{\mathbf{T}}_s(\boldsymbol{\theta}_{n+1}^{G,i})\,\dot{\boldsymbol{\theta}}_{n+1}^{G,i}. \tag{97}$$

6 Formulation using the incremental Euler parameters

A new dynamic formulation using the incremental Euler parameters is presented. Here, this approach has been introduced by Battini [4] for static analysis and is now developed for dynamics (see also [31]). The same Newmark update procedure as the one presented in Section 5 is adopted, but the rotational vector is replaced with the vectorial part of the Euler parameters (see Eq. (10)), and $\boldsymbol{\theta}, \dot{\boldsymbol{\theta}}, \ddot{\boldsymbol{\theta}}$ are replaced with $\mathbf{q}, \dot{\mathbf{q}}, \ddot{\mathbf{q}}$. In a comparison to the previous one, the interest of this approach is the simple, and computationally efficient expressions for the inertia force vector and the dynamic tangent matrix.

The iterative quantities are given by

$$\dot{\mathbf{q}}_{n+1}^{i} = \dot{\mathbf{q}}_{n+1}^{i-1} + \frac{\gamma}{\beta h}\Delta\mathbf{q}_{n+1}^{i}, \tag{98}$$

$$\ddot{\mathbf{q}}_{n+1}^{i} = \ddot{\mathbf{q}}_{n+1}^{i-1} + \frac{1}{\beta h^2}\Delta\mathbf{q}_{n+1}^{i}. \tag{99}$$

6.1 Internal force

The nodal displacements and nodal spatial incremental Euler parameters are

$$\delta\mathbf{d} = \begin{bmatrix} \delta\mathbf{u}_1^{\mathrm{T}} & \delta\mathbf{q}_1^{\mathrm{T}} & \delta\mathbf{u}_2^{\mathrm{T}} & \delta\mathbf{q}_2^{\mathrm{T}} \end{bmatrix}^{\mathrm{T}}.$$

In order to compute the inertia terms, the incremental Euler parameters (quaternion) need to be interpolated. However, since the Euler parameters are related to the rotational vector by a sinus function (see Eq. (10)), its interpolation is not trivial. In the literature, quaternion is usually interpolated using SLERP (SphericaL linear intERPolation), which is commonly used in computer graphics [27]. The interpolated quaternion using SLERP can be written as (see [13, 26])

$$\mathbf{q} = N_1 \mathbf{q}_1 + N_2 \mathbf{q}_2 \,, \tag{100}$$

with

$$N_1 = \frac{\sin\left(\frac{1}{2}(1-\xi)\phi\right)}{\sin\phi} \,, \qquad N_2 = \frac{\sin\left(\frac{1}{2}(1+\xi)\phi\right)}{\sin\phi} \,, \tag{101}$$

ϕ is the angle between two quaternions. However, in case of incremental Euler parameters, this angle is small. Hence, the previous interpolations can be approximated by linear ones

$$N_1 = \frac{1}{2}(1-\xi) \,, \qquad N_2 = \frac{1}{2}(1+\xi) \,. \tag{102}$$

With these interpolations and considering the changes of variables defined in Eqs. (5) and (12), it can be recognized that the inertia force vector in case of Euler parameters has a similar expression as in Eq. (87) and is obtained by replacing $\mathbf{T}_s^{\mathrm{T}}(\boldsymbol{\theta})$ with $\mathbf{T}_q^{\mathrm{T}}(\mathbf{q})$

$$\mathbf{f}_k = \begin{bmatrix} \int N_1 A_\rho \ddot{\mathbf{u}} \mathrm{d}l \\ \int N_1 \mathbf{T}_q^{\mathrm{T}}(\mathbf{q}) \left[\mathbf{I}_\rho \dot{\mathbf{w}} + \widetilde{\mathbf{w}} \mathbf{I}_\rho \mathbf{w} \right] \mathrm{d}l \\ \int N_2 A_\rho \ddot{\mathbf{u}} \mathrm{d}l \\ \int N_2 \mathbf{T}_q^{\mathrm{T}}(\mathbf{q}) \left[\mathbf{I}_\rho \dot{\mathbf{w}} + \widetilde{\mathbf{w}} \mathbf{I}_\rho \mathbf{w} \right] \mathrm{d}l \end{bmatrix} . \tag{103}$$

6.2 Tangent inertia matrix

The expression of the tangent inertia matrix in this case is similar to (95). It is obtained by replacing $\mathbf{T}_s^{\mathrm{T}}(\boldsymbol{\theta})$ and its derivatives in Eq. (95) with $\mathbf{T}_q^{\mathrm{T}}(\mathbf{q})$ and its derivatives.

The derivatives of $\mathbf{T}_q^{\mathrm{T}}(\mathbf{q})$ are given by

$$\Delta(\mathbf{T}_q^{\mathrm{T}}(\mathbf{q}))\mathbf{x} = \mathbf{Q}(\mathbf{x})\Delta\mathbf{q} \,, \tag{104}$$

$$\Delta(\dot{\mathbf{T}}_q^{\mathrm{T}}(\mathbf{q})\,\dot{\mathbf{q}}) = \mathbf{Q}_1\,\Delta\dot{\mathbf{q}} + \mathbf{Q}_2\,\Delta\mathbf{q} \,, \tag{105}$$

where

$$\mathbf{Q}(\mathbf{x}) = \frac{-\mathbf{x}\mathbf{q}^{\mathrm{T}} + \mathbf{q}\mathbf{x}^{\mathrm{T}} + (\mathbf{q}^{\mathrm{T}}\mathbf{x})\,\mathbf{I}}{4\,q_o} + \frac{\mathbf{q}\mathbf{q}^{\mathrm{T}}\mathbf{x}\mathbf{q}^{\mathrm{T}}}{16\,q_o^3} + \frac{\widetilde{\mathbf{x}}}{2} \,. \tag{106}$$

Here, $\mathbf{x}$ denotes a vector [3x1].

The expressions for $\mathbf{Q}_1, \mathbf{Q}_2$ are given in Appendix B, respectively. It is worth pointing out that the expressions for $\mathbf{Q}_1$ and $\mathbf{Q}_2$ are simpler than the ones for $\boldsymbol{\Omega}_1$ and $\boldsymbol{\Omega}_2$.

Consequently, the 6x6 blocks of the tangent inertia matrix, including the translational terms, are expressed as

$$
\begin{aligned}
\mathbf{K}^{i}_{\mathrm{Dyn},n+1} = \frac{1}{\beta h^2}
&\begin{bmatrix} \int N_a N_b A_\rho \mathrm{d}l\, \mathbf{I} & \mathbf{0}_{[3\mathrm{x}3]} \\ \mathbf{0}_{[3\mathrm{x}3]} & \int N_a N_b \mathbf{T}_q^{\mathrm{T}}(\mathbf{q}^i_{n+1}) \mathbf{I}^i_{\rho,n+1}\, \mathbf{T}_q(\mathbf{q}^i_{n+1}) \mathrm{d}l \end{bmatrix} \\
+ \frac{\gamma}{\beta h}
&\begin{bmatrix} \mathbf{0}_{[3\mathrm{x}3]} & \mathbf{0}_{[3\mathrm{x}3]} \\ \mathbf{0}_{[3\mathrm{x}3]} & \int N_a N_b \mathbf{T}_q^{\mathrm{T}}(\mathbf{q}^i_{n+1}) \left[\mathbf{b}^i_{n+1} \mathbf{T}_q(\mathbf{q}^i_{n+1}) + \mathbf{I}^i_{\rho,n+1} \mathbf{R}(\mathbf{q}^i_{n+1}) \mathbf{Q}_1 \right] \mathrm{d}l \end{bmatrix} \\
-
&\begin{bmatrix} \mathbf{0}_{[3\mathrm{x}3]} & \mathbf{0}_{[3\mathrm{x}3]} \\ \mathbf{0}_{[3\mathrm{x}3]} & \int N_a N_b \left[\mathbf{T}_q^{\mathrm{T}}(\mathbf{q}^i_{n+1}) \widetilde{\mathbf{A}^i_{n+1}}\, \mathbf{T}_q(\mathbf{q}^i_{n+1}) - \mathbf{Q}(\mathbf{A}^i_{n+1}) \right] \mathrm{d}l \end{bmatrix} \\
+
&\begin{bmatrix} \mathbf{0}_{[3\mathrm{x}3]} & \mathbf{0}_{[3\mathrm{x}3]} \\ \mathbf{0}_{[3\mathrm{x}3]} & \int N_a N_b \left[\mathbf{I}^i_{\rho,n+1} \mathbf{R}(\mathbf{q}^i_{n+1}) (\mathbf{Q}(\ddot{\mathbf{q}}^i_{n+1}) + \mathbf{Q}_2) + \mathbf{b}^i_{n+1} \mathbf{R}(\mathbf{q}^i_{n+1}) \mathbf{Q}(\dot{\mathbf{q}}^i_{n+1}) \right] \mathrm{d}l \end{bmatrix},
\end{aligned}
\tag{107}
$$

where $a, b = [1, 2]$.

7 Some general remarks on the discussed formulations

Regarding the presented formulations, some relevant remarks are summarized as follows:

- In all formulations, the rotational variables are linearly interpolated from the nodal quantities (see Eqs. (33), (60) and (100)). However, it can be observed that the rotational variables at two nodes of an element belong to two different tangent spaces. Consequently, these linear interpolations are not formally correct. It can also be noted that this problem concerns only the inertial terms. For the deformational static terms, the corotational approach is used, and local quantities related to the moving local frame are interpolated.

- As pointed out by Mäkinen [22], the Newmark update procedures used for the first two formulations (see Eqs. (39) and (40)) involve vectors that do not belong to the same tangent space. Indeed, the vectors $\dot{\boldsymbol{\omega}}_{n+1}$ and $\ddot{\boldsymbol{\omega}}_{n+1}$ lie in a tangent space different from the one containing vectors $\boldsymbol{\Theta}_{n+1}$, $\dot{\boldsymbol{\omega}}_n$ and $\ddot{\boldsymbol{\omega}}_n$. Hence, these update procedures are not formally correct. It should be emphasized that this problem does not occur in the last two formulations. For the third formulation, the Newmark update procedures are performed using

$$
\boldsymbol{\theta}_{n+1} = h\dot{\boldsymbol{\theta}}_n + h^2 \left[(\frac{1}{2} - \beta)\ddot{\boldsymbol{\theta}}_n + \beta\, \ddot{\boldsymbol{\theta}}_{n+1} \right], \tag{108}
$$

$$
\dot{\boldsymbol{\theta}}_{n+1} = \dot{\boldsymbol{\theta}}_n + h \left[(1-\gamma)\ddot{\boldsymbol{\theta}}_n + \gamma \ddot{\boldsymbol{\theta}}_{n+1} \right]. \tag{109}
$$

  For the fourth formulation, $\boldsymbol{\theta}, \dot{\boldsymbol{\theta}}, \ddot{\boldsymbol{\theta}}$ are replaced with $\mathbf{q}, \dot{\mathbf{q}}, \ddot{\mathbf{q}}$.
  The quantities at the beginning of the step $\dot{\boldsymbol{\theta}}_n$ and $\ddot{\boldsymbol{\theta}}_n$ ($\dot{\mathbf{q}}_n$ and $\ddot{\mathbf{q}}_n$ for the fourth formulation) belong to the tangent space associated to $\mathbf{R}_n$. Therefore they are different from the same quantities at the end of the previous step, which are associated to $\mathbf{R}_{n-1}$. By noting that at the beginning of the step: $\boldsymbol{\theta}_n = \mathbf{q}_n = \mathbf{0}_{[3\mathrm{x}1]}$, $\mathbf{T}_s(\mathbf{0}_{[3\mathrm{x}1]}) = \mathbf{T}_q(\mathbf{0}_{[3\mathrm{x}1]}) = \mathbf{I}$ and $\dot{\mathbf{T}}_s(\boldsymbol{\theta})\dot{\boldsymbol{\theta}} = \dot{\mathbf{T}}_q(\mathbf{q})\dot{\mathbf{q}} = \mathbf{0}_{[3\mathrm{x}1]}$, the initial quantities are obtained using Eqs. (14) and (15) as

$$
\dot{\boldsymbol{\theta}}_n = \dot{\mathbf{q}}_n = \dot{\mathbf{w}}_n, \tag{110}
$$

$$
\ddot{\boldsymbol{\theta}}_n = \ddot{\mathbf{q}}_n = \ddot{\mathbf{w}}_n. \tag{111}
$$

Consequently, all vector quantities in these Newmark time stepping formulations belong to the same tangent space.

- In the last two formulations, all the current quantities required at each Gauss point are directly linearly interpolated from the current nodal ones (see Eqs. (96) and (97)). However, in the first two formulations, at each Gauss point, the current quantities are calculated using the previous quantities (see Eqs. (56), (57) and (81), (82)). Consequently, the quantities at the Gauss point need to be saved, which requires more memory space, especially for large scale problems.

8 Predictors for Newmark scheme

In the nonlinear dynamic analysis of structures, displacements (rotations), velocities and accelerations need to be computed at each time step. For these three unknowns, Newmark time stepping method gives only two relations. Thus one unknown must be predicted as the initial value for the solution at the time t_{n+1}. A poor predictor can increase the number of iterations and in some cases makes the procedure fail to converge.

In this work, four predictors, found in the literature, have been implemented and tested:

- The first predictor, called as "Unchanged displacements", is used by Simo and Vu-Quoc [28]. The displacements and the rotations at t_n are taken as predictor for the solution at t_{n+1}.
- The second one, referred to "Null accelerations", is used by Cardona and Geradin [6], Mäkinen [22], Chung and Hulbert [7]. Zero translational and rotational accelerations are taken as predictor for the solution at t_{n+1}.
- The third one, called as "Unchanged accelerations", used by Forsell [10], proposes to take the translational and rotational accelerations at t_n as predictor for the solution at t_{n+1}.
  In case of rotational variables, the three possible predictors in conjunction with the four presented formulations are summarized in Table 1.

Table 1. Predictors for the rotational variables.

Approach	Unchanged displacements (Pred. 1)	Null accelerations (Pred. 2)	Unchanged accelerations (Pred. 3)
Spat. Spin. Var.	$\boldsymbol{\Theta}^0_{n+1} = \mathbf{0}_{[3x1]}$	$\ddot{\boldsymbol{\omega}}^0_{n+1} = \mathbf{0}_{[3x1]}$	$\ddot{\boldsymbol{\omega}}^0_{n+1} = \ddot{\boldsymbol{\omega}}_n$
Inc. Rot. V. 1	$\boldsymbol{\theta}^0_{n+1} = \mathbf{0}_{[3x1]}$	$\ddot{\mathbf{w}}^0_{n+1} = \mathbf{0}_{[3x1]}$	$\ddot{\mathbf{w}}^0_{n+1} = \exp(\widetilde{\boldsymbol{\theta}^0_{n+1}})\ddot{\mathbf{w}}_n$
Inc. Rot. V. 2	$\boldsymbol{\theta}^0_{n+1} = \mathbf{0}_{[3x1]}$	$\ddot{\boldsymbol{\theta}}^0_{n+1} = \mathbf{0}_{[3x1]}$	$\ddot{\boldsymbol{\theta}}^0_{n+1} = \ddot{\boldsymbol{\theta}}_n$
Inc. Euler	$\mathbf{q}^0_{n+1} = \mathbf{0}_{[3x1]}$	$\ddot{\mathbf{q}}^0_{n+1} = \mathbf{0}_{[3x1]}$	$\ddot{\mathbf{q}}^0_{n+1} = \ddot{\mathbf{q}}_n$

With the predicted unknown, the others are calculated using Eqs. (39) and (40) for the first formulation, Eqs. (63) and (64) for the second one, and Eqs. (108) and (109) for the last two formulations.

- The last predictor (Pred. 4), proposed by Crisfield [9], suggests to use the tangent operator at t_n to predict initial values at t_{n+1}. In [9], this predictor is only presented in the case of a linear inertia force vector. This predictor is extended here for an arbitrarily nonlinear inertia force vector.

The Newmark time-integration formulas are recalled below

$$\mathbf{d}_{n+1} = \mathbf{d}_n + h\dot{\mathbf{d}}_n + h^2\left[(\frac{1}{2}-\beta)\ddot{\mathbf{d}}_n + \beta\,\ddot{\mathbf{d}}_{n+1}\right], \tag{112}$$

$$\dot{\mathbf{d}}_{n+1} = \dot{\mathbf{d}}_n + h\left[(1-\gamma)\ddot{\mathbf{d}}_n + \gamma\ddot{\mathbf{d}}_{n+1}\right]. \tag{113}$$

With some manipulations, Eqs. (112) and (113) are transformed into

$$\Delta\ddot{\mathbf{d}} = \frac{1}{\beta h^2}\left(\Delta\mathbf{d} - h\dot{\mathbf{d}}_n - \frac{h^2}{2}\ddot{\mathbf{d}}_n\right), \tag{114}$$

$$\Delta\dot{\mathbf{d}} = \frac{\gamma}{\beta h}\Delta\mathbf{d} - \frac{\gamma}{\beta}\dot{\mathbf{d}}_n + \frac{h(2\beta-\gamma)}{2\beta}\ddot{\mathbf{d}}_n. \tag{115}$$

In this work, the nonlinear problems are solved using the HHT α method, which can be considered as a variant of the Newmark algorithm. In the HHT α method, the dynamic equilibrium equation is rewritten as

$$(1+\alpha)\mathbf{f}_{\text{ext},n+1} - (1+\alpha)\mathbf{f}_{g,n+1} - \mathbf{f}_{k,n+1} + \alpha(\mathbf{f}_{g,n} - \mathbf{f}_{\text{ext},n}) = \mathbf{0}. \tag{116}$$

Using a truncated Taylor series, one obtains

$$\mathbf{f}_{g,n+1} = \mathbf{f}_{g,n} + \frac{\partial \mathbf{f}_g}{\partial \mathbf{d}}\Delta\mathbf{d} = \mathbf{f}_{g,n} + \mathbf{K}_{\text{Static},n}\Delta\mathbf{d}, \tag{117}$$

$$\begin{aligned}\mathbf{f}_{k,n+1} &= \mathbf{f}_{k,n} + \frac{\partial \mathbf{f}_k}{\partial \mathbf{d}}\Delta\mathbf{d} + \frac{\partial \mathbf{f}_k}{\partial \dot{\mathbf{d}}}\Delta\dot{\mathbf{d}} + \frac{\partial \mathbf{f}_k}{\partial \ddot{\mathbf{d}}}\Delta\ddot{\mathbf{d}} \\ &= \mathbf{f}_{k,n} + \mathbf{K}_{k,n}\Delta\mathbf{d} + \mathbf{C}_{k,n}\Delta\dot{\mathbf{d}} + \mathbf{M}_n\Delta\ddot{\mathbf{d}}.\end{aligned} \tag{118}$$

To obtain the predictor's expression, Eqs. (114), (115), (117) and (118) are inserted into Eq. (116), which leads to

$$\begin{aligned}\mathbf{K}_{\text{Total},n}\Delta\mathbf{d} =& (1+\alpha)\mathbf{f}_{\text{ext},n+1} - \mathbf{f}_{g,n} - \mathbf{f}_{k,n} - \alpha\mathbf{f}_{\text{ext},n} \\ &+ \mathbf{C}_{k,n}\left(\frac{\gamma}{\beta}\dot{\mathbf{d}}_n - \frac{h(2\beta-\gamma)}{2\beta}\ddot{\mathbf{d}}_n\right) + \frac{\mathbf{M}_n}{\beta h^2}\left(h\dot{\mathbf{d}}_n + \frac{h^2}{2}\ddot{\mathbf{d}}_n\right),\end{aligned} \tag{119}$$

where

$$\mathbf{K}_{\text{Total},n} = (1+\alpha)\mathbf{K}_{\text{Static},n} + \mathbf{K}_{\text{Dyn},n}.$$

At t_{n+1}, by noting that $\mathbf{d}_n = [\mathbf{u}_n^{\mathrm{T}}, \mathbf{0}_{[1\text{x}3]}]^{\mathrm{T}}$, $\mathbf{d}$ is initialized as follows:

$$\mathbf{d}_{n+1}^0 = \mathbf{d}_n + \Delta\mathbf{d}. \tag{120}$$

This procedure applies the classic Newmark formulations to the rotational variables, so it is only formally correct for the last two dynamic formulations. Despite this fact, this procedure is also implemented for the first two formulations with $\dot{\mathbf{d}}_n = [\dot{\mathbf{u}}_n^{\mathrm{T}}, \dot{\mathbf{w}}_n^{\mathrm{T}}]^{\mathrm{T}}$ and $\ddot{\mathbf{d}}_n = [\ddot{\mathbf{u}}_n^{\mathrm{T}}, \ddot{\mathbf{w}}_n^{\mathrm{T}}]^{\mathrm{T}}$. At the beginning of the step $\mathbf{d}_n = [\mathbf{u}_n^{\mathrm{T}}, \mathbf{0}_{[1\text{x}3]}]^{\mathrm{T}}$. Consequently, for the predictor, $\Delta\mathbf{w} = \Delta\boldsymbol{\theta}$ (see Eq. (5)) and $\Delta\mathbf{d} = [\Delta\mathbf{u}^{\mathrm{T}}, \Delta\boldsymbol{\theta}^{\mathrm{T}}]^{\mathrm{T}}$.

9 Numerical examples

In this section, six numerical examples are analyzed using the four dynamic formulations. The first three problems are taken from the literature whereas the last three ones are new. In all examples involving curved geometry, the latter has been approximated via linear straight elements. These six examples are solved using the HHT α method with $\alpha = -0.01$. For the deformational static part, the corotational formulation with the local element *t3d* proposed in [2] is adopted. The following convergence criterion is adopted: the norm of the residual vector must be less than the prescribed tolerance $\varepsilon_f = 10^{-5}$.

The first objective is to assess the accuracy of the four formulations. For that, the displacements of the structures are computed and presented in Section 9.1. It has been observed that for all the examples, the

four formulations give exactly the same results. Besides, for the first three examples, all formulations give the same results as reported in the literature.

The second objective is to study and assess the computational efficiency of each formulation. The following aspects are investigated:

- The choice of predictor: the four predictors described in Section 8 are implemented for each formulation. The performance of the predictors is analyzed in Section 9.2.
- The choice of the tangent inertia matrix: in order to reduce the CPU time, Geradin and Cardona [6, 12] recommended to keep only the mass matrix and to neglect the gyroscopic and centrifugal matrices. In this work, another simplification is proposed and the following three alternatives are tested: the exact tangent inertia matrix (i.e. mass, gyroscopic and centrifugal terms), only the mass matrix (as proposed in [6, 12]) and the mass and gyroscopic terms (the new proposal). The results are discussed in Section 9.3.
- The computational efficiency in terms of CPU time: the purpose is to compare the four formulations and for each formulation to determine the best predictor and the best tangent inertia matrix. To ensure a fair comparison in terms of CPU time, all the four formulations are implemented using Matlab.

9.1 Test examples

For all numerical examples, the mass per unit length of the beam and the inertia dyadic of the cross section in initial configuration are

$$A_\rho = 1\,, \quad \mathbf{J}_\rho = \mathrm{diag}(20, 10, 10)\,. \tag{121}$$

The other material properties are given in Table 2.

Table 2. Material properties.

Examples	$EA = GA$	$EI = GJ$
1, 5	10^6	10^3
2, 3, 4, 6	10^4	500

Again, since all formulations provide the same numerical results, the curves presented in this section can be obtained with any of the formulations discussed.

9.1.1 Example 1: Right-angle cantilever beam

This classic example, introduced by Simo and Vu-Quoc [28], has often been used in order to check the ability of various nonlinear dynamic formulations [14, 17, 20, 23]. A right-angle cantilever, depicted in Fig. 2, is subjected to an out-of-plane concentrated load applied at the elbow. The load acts only during $0 \leq t(\mathrm{s}) \leq 2$ and thereafter the cantilever undergoes large-scale free vibrations. The amplitude of vibration is of the same order of magnitude as the structure's dimensions. The frame is modeled with a total of 20 beam elements (10 elements per member) and the computations are performed with $\Delta t = 0.25$ s. The elbow and the tip out-of-plane displacements histories are given in Fig. 3.

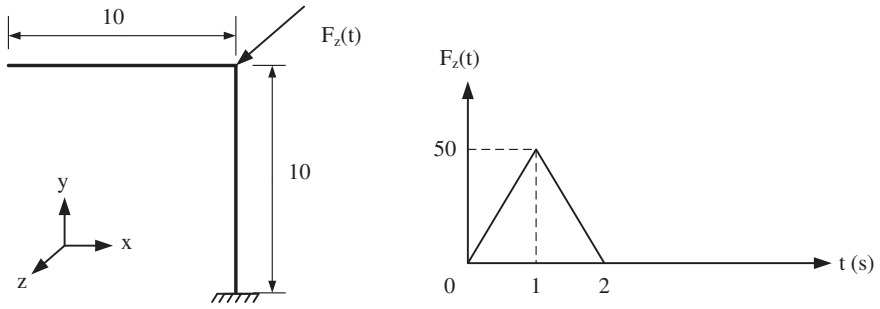

Fig. 2. Right-angle cantilever beam and loading.

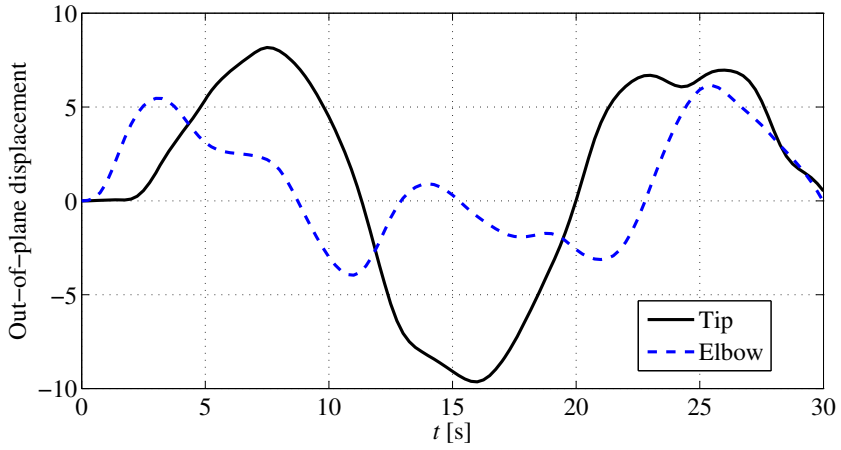

Fig. 3. Right-angle cantilever beam. Out-of-plane displacement time history.

9.1.2 Example 2: Free-free flexible beam with disks

The second example, proposed by Ibrahimbegović and Mikdad [17], analyzes the flight of a flexible beam with rigid disks attached to it. The initial configuration is given in Fig. 4. The disks have a point mass $M = 10.0$ and an inertia matrix $\mathbf{J}_\rho = \text{diag}(200.0, 100.0, 100.0)$. The system is set into motion by applying a couple of out-of-plane force $F_z(t)$ and an in-plane force $F_x(t)$ with $F_x(t) = 2F_z(t)$. The beam is discretized using 10 beam elements and the disks are modeled with one-node element. The time-step size $\Delta t = 0.10$ s is chosen and time histories for the displacements of the beam's lower right end are presented in Fig. 5.

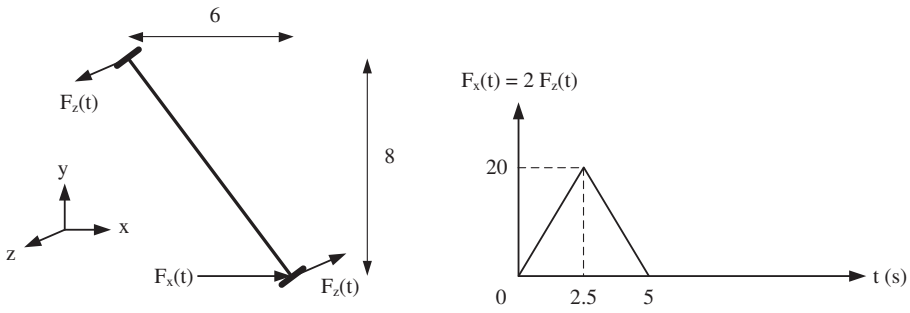

Fig. 4. Free-free flexible beam with disks and loading.

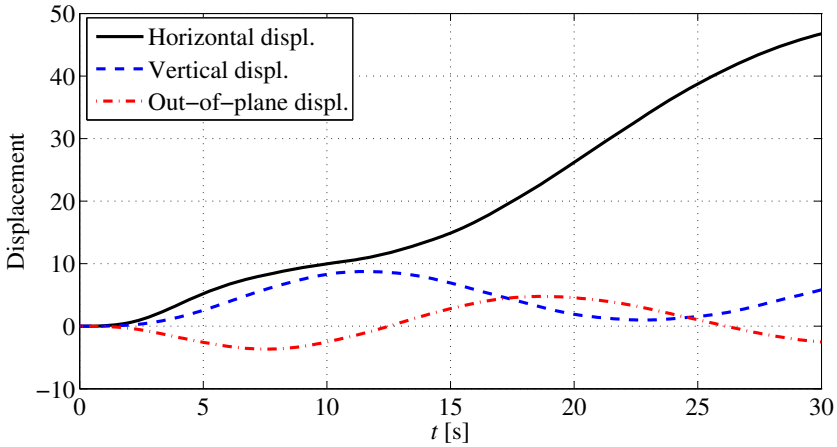

Fig. 5. Free-free flexible beam with disks. End responses time-history.

9.1.3 Example 3: Ring with finite rotations

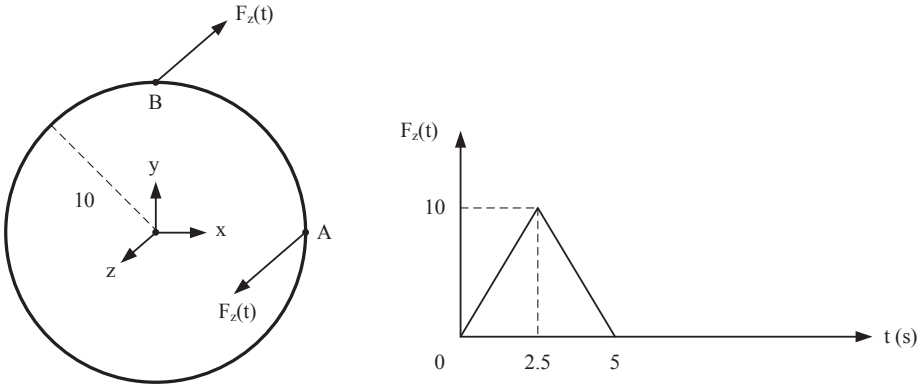

Fig. 6. Ring with finite rotations and loading.

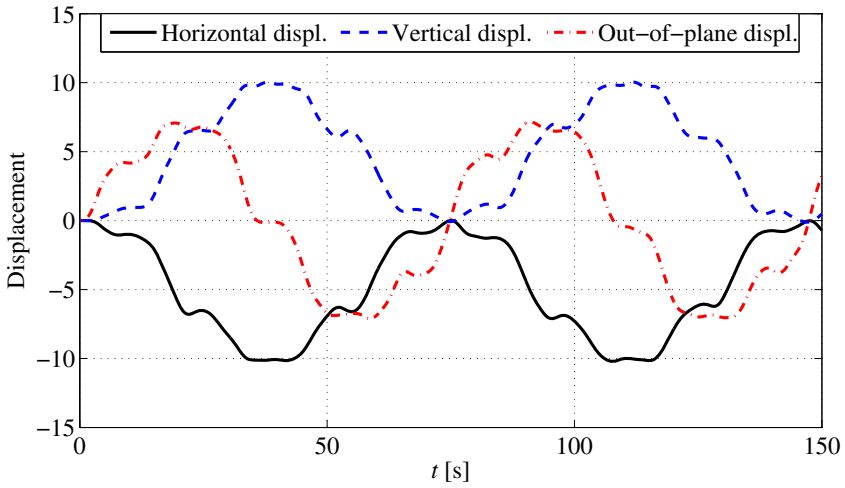

Fig. 7. Ring. Point A responses time-history.

The third example, proposed by Mikdad [24], presents the nonlinear dynamic response of a ring. The initial configuration and the loading history are given in Fig. 6. No static or kinematic boundary conditions are present for this problem, which means that the ring is free to move in the 3D space according to the laws of dynamics. Two out-of-plane dynamic loads are applied at points A and B of the ring. The dynamic analysis is performed using 16 straight beam elements with a time-step size $\Delta t = 0.10$ s. The displacements of the point A are presented in Fig. 7.

9.1.4 Example 4: Rotating beam

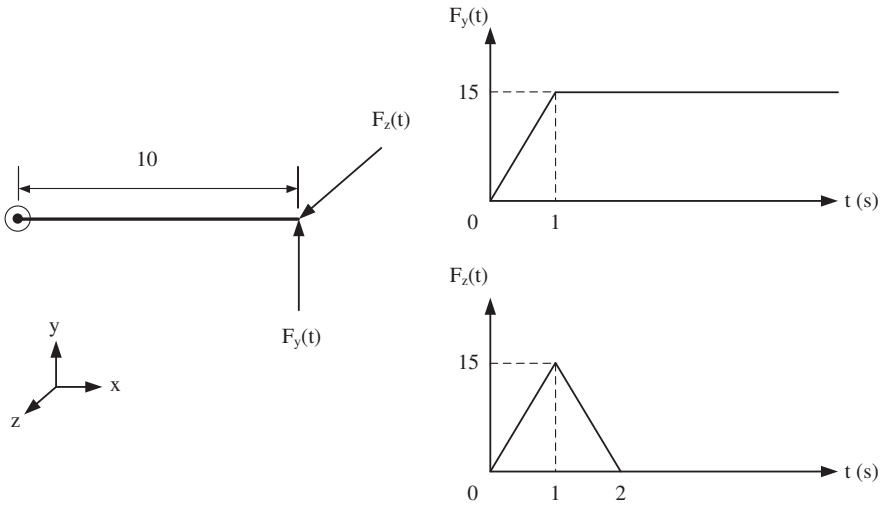

Fig. 8. Rotating beam and loading.

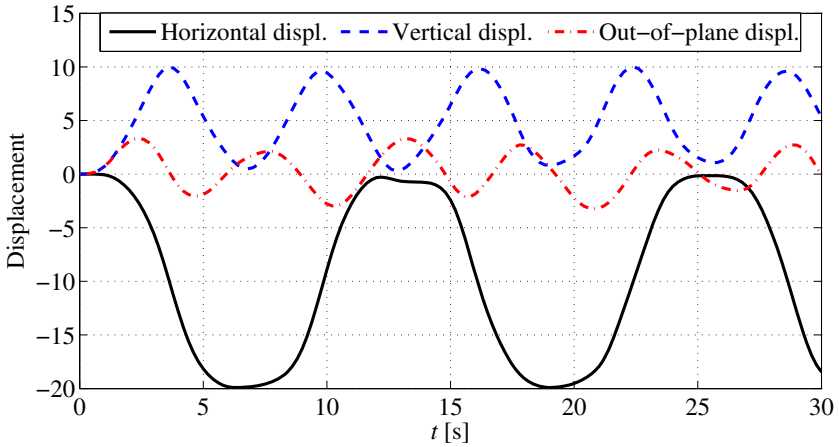

Fig. 9. Rotating beam. End responses time-history.

This example deals with a beam which can rotate freely about the z-axis at its left-end. The beam is set into motion by two dynamic loads applied at the free-end of the beam in the y and z directions. The initial configuration and the loading history are described in Fig. 8. The structure is analyzed using 10 beam elements with a time-step size $\Delta t = 0.20$ s. The displacements of the free-end are plotted in Fig. 9.

9.1.5 *Example 5: Cantilever 45^o bend*

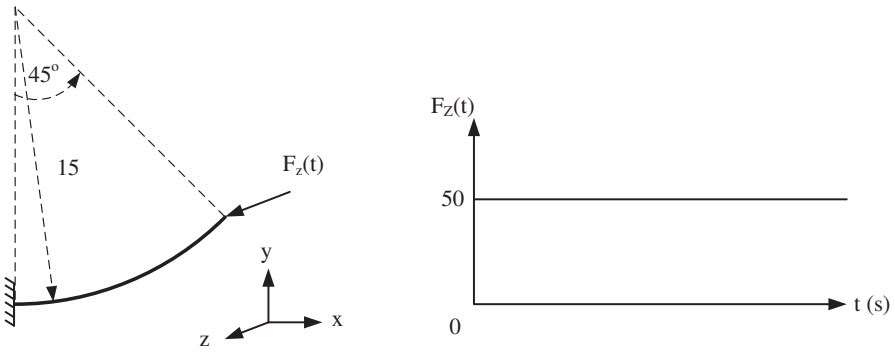

Fig. 10. Cantilever 45^o bend and loading.

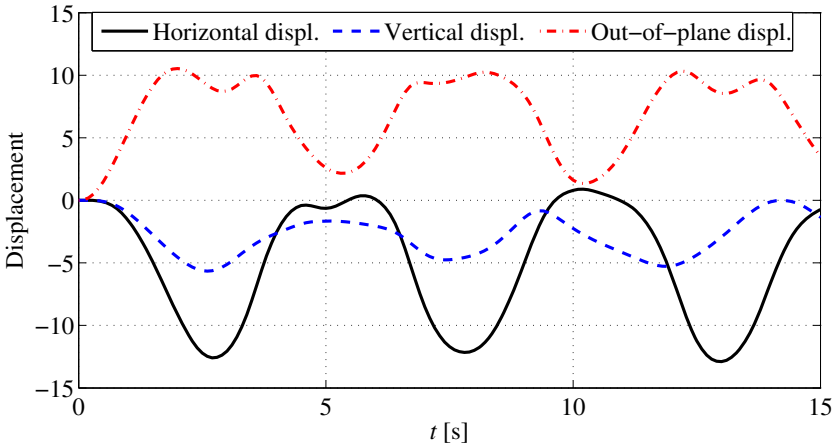

Fig. 11. Cantilever 45^o bend. End responses time-history.

The 3D structure considered here is a cantilever 45^o bend located in the x-y plane. The beam is clamped at the left end and set in to motion by a suddenly applied load in the z direction at the right end. The initial configuration and the loading history are given in Fig. 10. Ten straight beam elements are used to model the beam and a time-step size $\Delta t = 0.10$ s is chosen. The displacements of the free-end are shown in Fig. 11.

9.1.6 *Example 6: Deep circular arch*

In the last example, the nonlinear dynamic behavior of a deep circular arch is analyzed. The arch is located in the x-y plane and fully clamped at both ends (see Fig. 12). Two dynamic forces are applied at the middle of the arch, one in the y-direction and another in the z-direction. The shape and duration of the loading are given in Fig. 12. The computation is performed using 12 straight beam elements with a time-step size $\Delta t = 0.10$ s. The displacements of the point A, at one third of the beam, are depicted in Fig. 13.

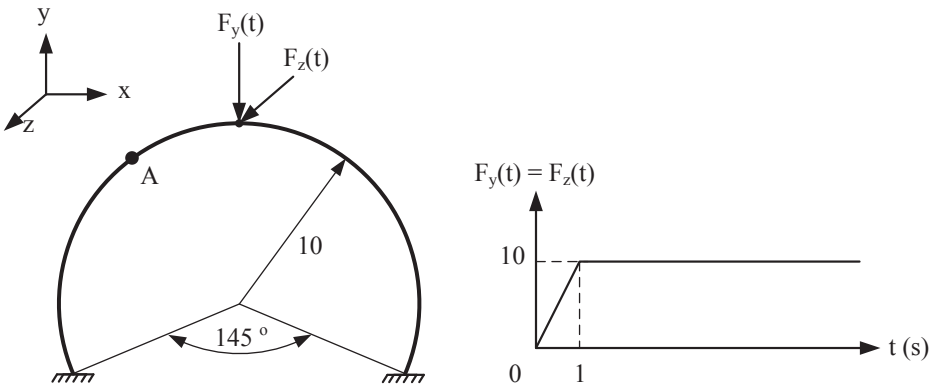

Fig. 12. Deep circular arch and loading.

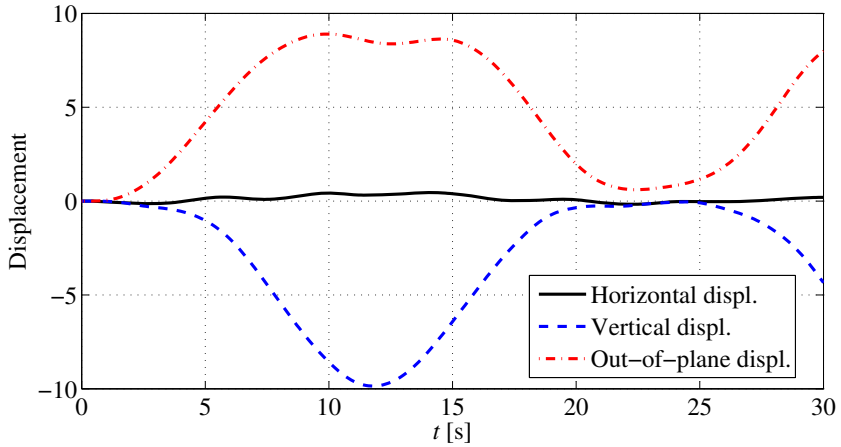

Fig. 13. Deep circular arch. Point A displacements time-history.

9.2 Choice of the predictor

The four predictors described in Section 8 are compared considering examples 1, 2 and 4 with several time-step sizes. The exact tangent inertia matrices are used. The total numbers of iterations for the whole time history and for each formulation are given in Tables 3-6.

The results show that Pred. 2 and Pred. 3 require a smaller time-step size to converge compared to the two other predictors. One can notice that in these two predictors, the initial value of the acceleration at t_{n+1} is equal to zero or to the acceleration at t_n. However, in dynamic analysis, the accelerations are rarely null or unchanged, and with these two predictors, a small time-step is required to ensure convergence. Consequently, these two predictors are not very efficient.

Pred. 1 converges in all the cases except one, but requires the largest number of iterations. In fact, this predictor assumes that the configuration of the structure does not change during a time step which does not happen in almost all cases.

For all the formulations, the best alternative is to use Pred. 4. The number of iterations is significantly smaller than for Pred. 1 and the convergence is obtained in all cases. This can be explained by the fact that Pred. 4 assumes linearity of the system during the time step. This is often a good approximation, especially with small time steps. From now, only Pred. 4 is used in the numerical calculations.

Table 3. Spatial spin variables - number of iterations.

Example	Pred. 1	Pred. 2	Pred. 3	Pred. 4
Ex. 1 - $\Delta t = 0.25$ s	753			573
Ex. 1 - $\Delta t = 0.20$ s	863	736	778	638
Ex. 1 - $\Delta t = 0.15$ s	1063	836		806
Ex. 2 - $\Delta t = 0.25$ s	479	363	363	357
Ex. 2 - $\Delta t = 0.10$ s	1181	902	901	878
Ex. 4 - $\Delta t = 0.20$ s	906	755		681
Ex. 4 - $\Delta t = 0.15$ s	1093	917	867	823

Table 4. Incremental Rotational Vector 1 - number of iterations.

Example	Pred. 1	Pred. 2	Pred. 3	Pred. 4
Ex. 1 - $\Delta t = 0.25$ s	749			573
Ex. 1 - $\Delta t = 0.20$ s		747		656
Ex. 1 - $\Delta t = 0.15$ s	1028	838		806
Ex. 2 - $\Delta t = 0.25$ s	479	363	363	357
Ex. 2 - $\Delta t = 0.10$ s	1181	902	901	877
Ex. 4 - $\Delta t = 0.20$ s	894	754		688
Ex. 4 - $\Delta t = 0.15$ s	1073	908	859	831

Table 5. Incremental Rotational Vector 2 - number of iterations.

Example	Pred. 1	Pred. 2	Pred. 3	Pred. 4
Ex. 1 - $\Delta t = 0.25$ s	753			588
Ex. 1 - $\Delta t = 0.20$ s	846	746		638
Ex. 1 - $\Delta t = 0.15$ s	1027	836	809	807
Ex. 2 - $\Delta t = 0.25$ s	479	363	363	357
Ex. 2 - $\Delta t = 0.10$ s	1181	902	897	877
Ex. 4 - $\Delta t = 0.20$ s	892	753		687
Ex. 4 - $\Delta t = 0.15$ s	1072	908	860	831

Table 6. Incremental Quaternion - number of iterations.

Example	Pred. 1	Pred. 2	Pred. 3	Pred. 4
Ex. 1 - $\Delta t = 0.25$ s	741			580
Ex. 1 - $\Delta t = 0.20$ s	845	745		657
Ex. 1 - $\Delta t = 0.15$ s	1028	837	810	807
Ex. 2 - $\Delta t = 0.25$ s	479	363	363	357
Ex. 2 - $\Delta t = 0.10$ s	1181	902	897	877
Ex. 4 - $\Delta t = 0.20$ s	895	755	790	689
Ex. 4 - $\Delta t = 0.15$ s	1072	908	860	829

9.3 Exact versus simplified dynamic tangent matrix and comparison of the four formulations

Six numerical examples are analyzed using the four formulations. For each formulation, the exact tangent inertia matrix, the simplified matrix proposed by the authors (Simpl. 1) and the one proposed by Geradin and Cardona (Simpl. 2) are tested. Table 7 shows the CPU time and the total number of iterations (in parentheses) for each formulation.

Table 7. Numerical performances.

Example	Spat. Spin. Var.	Inc. Rot. V. 1	Inc. Rot. V. 2	Inc. Euler
Ex. 1 - Exact	23.4 (573)	25.0 (579)	29.2 (578)	26.1 (580)
Ex. 1 - Simpl. 1	23.5 (629)		22.6 (587)	21.6 (594)
Ex. 1 - Simpl. 2	26.7 (755)	27.9 (764)	26.1 (771)	25.3 (769)
Ex. 2 - Exact	19.5 (878)	21.9 (877)	25.1 (877)	22.5 (877)
Ex. 2 - Simpl. 1	19.2 (885)	20.2 (882)	20.0 (881)	18.6 (881)
Ex. 2 - Simpl. 2	22.8 (1150)	23.8 (1140)	21.8 (1144)	21.1 (1154)
Ex. 3 - Exact	147.1 (4464)	155.4 (4448)	183.8 (4449)	165.4 (4450)
Ex. 3 - Simpl. 1	137.0 (4488)	147.1 (4487)	143.6 (4486)	135.3 (4486)
Ex. 3 - Simpl. 2	161.8 (5706)	172.5 (5708)	159.3 (5706)	153.4 (5706)
Ex. 4 - Exact	14.7 (681)	15.7 (688)	17.9 (687)	16.4 (689)
Ex. 4 - Simpl. 1	15.1 (752)	15.0 (725)	14.4 (706)	13.8 (706)
Ex. 4 - Simpl. 2	16.3 (862)	16.9 (856)	15.8 (862)	15.6 (873)
Ex. 5 - Exact	12.5 (604)	13.5 (605)	15.8 (605)	14.0 (605)
Ex. 5 - Simpl. 1	14.0 (727)	13.9 (690)	12.9 (654)	12.5 (666)
Ex. 5 - Simpl. 2	15.0 (832)	15.6 (821)	14.8 (827)	14.1 (831)
Ex. 6 - Exact	22.2 (873)	23.9 (874)	28.9 (874)	25.3 (874)
Ex. 6 - Simpl. 1	21.5 (895)	22.6 (894)	22.1 (892)	20.7 (892)
Ex. 6 - Simpl. 2	25.4 (1120)	26.4 (1121)	24.8 (1121)	24.3 (1121)

From the numerical results, it can be concluded that:

- For the first two formulations, Simpl. 2 is the slowest alternative. It increases the total number of iterations by about 25% to 38% compared with the exact matrix. In fact, for these formulations, the tangent matrices do not require a lot of CPU time, so the CPU time gained by the simplification cannot compensate for the CPU time needed for the extra iterations. From the results, it is quite difficult to make a choice between the exact dynamic tangent matrix and the first simplification. Depending on the problem, the exact matrix can be the best or the contrary. However, the difference in terms of CPU time cost between these two matrices are small and in one case, Inc. Rot. V. 1 with Simpl. 1 cannot converge. The authors recommend to use the exact tangent matrix with these two formulations.

- For the last two formulations, the best alternative is to use Simpl. 1 which reduces the CPU time by about 25% when compared to the exact matrix and by about 15% when compared to Simpl. 2.

- Between the fastest procedures for each formulation, the difference in CPU time is small. But the formulation using the spatial Euler parameters with Simpl. 1 seems to be the best alternative.

9.4 Influence of the time-step size

The previous results have shown that the formulation using the spatial Euler parameters with Simpl. 1 is the fastest. However, the examples are solved with only one time-step size. To have a more complete view, the examples 2, 4, 5 are repeated with different time steps. The formulations Spat. Spin. Var. and Inc. Rot. V. 1 are implemented with the exact tangent inertia matrix. The other two formulations are implemented using Simpl. 1.

Table 8. Numerical performances with various time-step size.

Example	Spat. Spin. Var.	Inc. Rot. V. 1	Inc. Rot. V. 2	Inc. Euler
Ex. 2 - $\Delta t = 0.1$ s	19.5 (878)	21.9 (877)	20.0 (881)	18.6 (881)
Ex. 2 - $\Delta t = 0.5$ s	5.7 (239)	5.9 (237)	5.3 (239)	4.9 (239)
Ex. 4 - $\Delta t = 0.1$ s	24.9 (1185)	26.6 (1185)	24.4 (1192)	23.1 (1192)
Ex. 4 - $\Delta t = 0.2$ s	14.7 (681)	15.7 (688)	14.4 (706)	13.8 (706)
Ex. 5 - $\Delta t = 0.05$ s	23.1 (1140)	25.1 (1140)	23.5 (1184)	22.0 (1185)
Ex. 5 - $\Delta t = 0.1$ s	12.5 (604)	13.5 (605)	12.9 (654)	12.5 (666)

The results are presented in Table 8. They show that the choice of time-step size does not affect the hierarchy between the formulations.

10 Conclusion

In this paper, four dynamic formulations for spatial beam elements have been compared. For all these formulations the inertia vector and the tangent inertia matrix are derived in a total Lagrangian context, but differ in the way the spatial rotations are handled. The first three formulations are taken from the literature with some modifications whereas the last one is new. The new idea was to parameterize the rotations using the first three Euler parameters. All formulations have been described in detail. Similarities and differences between them have been pointed out. The corotational approach has been used to derive the internal force vectors and the tangent stiffness matrices. Six numerical applications have been used to test the accuracy and efficiency of each dynamic formulation. In particular, the choice of the predictor and the possibility of taking a simplified tangent inertia matrix have been carefully studied. The following conclusions can be drawn:

- The new formulation and the one proposed by Cardona and Geradin [6] are the easiest ones to implement: they use the same standard Newmark method for the displacements and the rotations. They do not require storage of various quantities at each Gauss points.
- For all the formulations, the predictor proposed by Crisfield in [9] seems to be the best alternative. The expression of this predictor for the general case of a nonconstant tangent inertia matrix is given in the paper.
- For each formulation, the choice of the tangent inertia matrix affects significantly the computational efficiency. For the first two formulations, the best alternative is to take the exact tangent inertia matrix. For the last two formulations, it is better to consider only the mass and gyroscopic matrices.
- All the formulations give the same numerical results but the new formulation proposed in the paper is slightly more efficient than the other ones regarding the CPU time.

Appendix A Expressions of $\boldsymbol{\Omega}_1$ and $\boldsymbol{\Omega}_2$

From Eqs. (69) and (70), it is obtained

$$\dot{\mathbf{T}}_s^{\mathrm{T}}(\boldsymbol{\theta})\,\dot{\boldsymbol{\theta}} = \boldsymbol{\Xi}(\dot{\boldsymbol{\theta}})\dot{\boldsymbol{\theta}} = \left\{ c_1\,\dot{\boldsymbol{\theta}}\,\boldsymbol{\theta}^{\mathrm{T}} - c_2\,\widetilde{\boldsymbol{\theta}}\,\dot{\boldsymbol{\theta}}\,\boldsymbol{\theta}^{\mathrm{T}} + c_3\,(\boldsymbol{\theta}^{\mathrm{T}}\dot{\boldsymbol{\theta}})\,\boldsymbol{\theta}\,\boldsymbol{\theta}^{\mathrm{T}} + c_5\,\left[\boldsymbol{\theta}\,\dot{\boldsymbol{\theta}}^{\mathrm{T}} + (\boldsymbol{\theta}^{\mathrm{T}}\dot{\boldsymbol{\theta}})\mathbf{I}\right] \right\}\dot{\boldsymbol{\theta}}. \tag{122}$$

Linearization of this equation takes form

$$\Delta(\dot{\mathbf{T}}_s^{\mathrm{T}}(\boldsymbol{\theta})\,\dot{\boldsymbol{\theta}}) = \boldsymbol{\Omega}_1\,\Delta\dot{\boldsymbol{\theta}} + \boldsymbol{\Omega}_2\,\Delta\boldsymbol{\theta}\,, \tag{123}$$

where

$$\begin{aligned}
\boldsymbol{\Omega}_1 &= (c_1+c_5)\left[(\boldsymbol{\theta}^{\mathrm{T}}\dot{\boldsymbol{\theta}})\mathbf{I} + \dot{\boldsymbol{\theta}}\boldsymbol{\theta}^{\mathrm{T}}\right] - c_2(\boldsymbol{\theta}^{\mathrm{T}}\dot{\boldsymbol{\theta}}\widetilde{\boldsymbol{\theta}} + \widetilde{\boldsymbol{\theta}}\dot{\boldsymbol{\theta}}\boldsymbol{\theta}^{\mathrm{T}}) \\
&\quad + 2c_3\boldsymbol{\theta}^{\mathrm{T}}\dot{\boldsymbol{\theta}}\boldsymbol{\theta}\boldsymbol{\theta}^{\mathrm{T}} + 2c_5\boldsymbol{\theta}\dot{\boldsymbol{\theta}}^{\mathrm{T}}, \qquad (124)\\
\boldsymbol{\Omega}_2 &= c_1\dot{\boldsymbol{\theta}}\dot{\boldsymbol{\theta}}^{\mathrm{T}} - c_2(\widetilde{\dot{\boldsymbol{\theta}}}\dot{\boldsymbol{\theta}}\dot{\boldsymbol{\theta}}^{\mathrm{T}} - \dot{\boldsymbol{\theta}}^{\mathrm{T}}\boldsymbol{\theta}\widetilde{\dot{\boldsymbol{\theta}}}) + c_3\left[2\boldsymbol{\theta}^{\mathrm{T}}\dot{\boldsymbol{\theta}}\boldsymbol{\theta}\dot{\boldsymbol{\theta}}^{\mathrm{T}} + (\boldsymbol{\theta}^{\mathrm{T}}\dot{\boldsymbol{\theta}})^2\mathbf{I}\right] + c_5(\dot{\boldsymbol{\theta}}\dot{\boldsymbol{\theta}}^{\mathrm{T}} + \dot{\boldsymbol{\theta}}^{\mathrm{T}}\dot{\boldsymbol{\theta}}\mathbf{I}) \\
&\quad + c_6(\dot{\boldsymbol{\theta}}\boldsymbol{\theta}^{\mathrm{T}})^2 - c_7\widetilde{\boldsymbol{\theta}}(\dot{\boldsymbol{\theta}}\boldsymbol{\theta}^{\mathrm{T}})^2 + c_8(\boldsymbol{\theta}^{\mathrm{T}}\dot{\boldsymbol{\theta}})^2\boldsymbol{\theta}\boldsymbol{\theta}^{\mathrm{T}} + c_9(\boldsymbol{\theta}^{\mathrm{T}}\dot{\boldsymbol{\theta}}\boldsymbol{\theta} + \boldsymbol{\theta}\dot{\boldsymbol{\theta}}^{\mathrm{T}}\dot{\boldsymbol{\theta}})\boldsymbol{\theta}^{\mathrm{T}}, \qquad (125)
\end{aligned}$$

$$c_6 = -\frac{\theta^2\sin\theta + 3\theta\cos\theta - 3\sin\theta}{\theta^5}, \quad c_7 = -\frac{\theta^2\cos\theta + 5\theta\sin\theta + 8\cos\theta - 8}{\theta^6},$$
$$c_8 = \frac{\theta^2\sin\theta + 7\theta\cos\theta + 8\theta - 15\sin\theta}{\theta^7}, \quad c_9 = \frac{-2\theta - \theta\cos\theta + 3\sin\theta}{\theta^5}.$$

Appendix B Expressions of $\mathbf{Q}_1$ and $\mathbf{Q}_2$

From Eqs. (104) and (106), it is obtained

$$\dot{\mathbf{T}}_q^{\mathrm{T}}(\mathbf{q})\dot{\mathbf{q}} = \left(\dot{\mathbf{q}}^{\mathrm{T}}\dot{\mathbf{q}} + \frac{(\mathbf{q}^{\mathrm{T}}\dot{\mathbf{q}})^2}{4\,q_o^2}\right)\frac{\mathbf{q}}{4\,q_o}\,. \tag{126}$$

Linearization of this equation takes form

$$\Delta(\dot{\mathbf{T}}_q^{\mathrm{T}}(\mathbf{q})\,\dot{\mathbf{q}}) = \mathbf{Q}_1\,\Delta\dot{\mathbf{q}} + \mathbf{Q}_2\,\Delta\mathbf{q}\,, \tag{127}$$

$$\mathbf{Q}_1 = \frac{\mathbf{q}\dot{\mathbf{q}}^{\mathrm{T}}}{2\,q_o} + \frac{\mathbf{q}^{\mathrm{T}}\dot{\mathbf{q}}\,\mathbf{q}\,\mathbf{q}^{\mathrm{T}}}{8\,q_o^3}\,, \tag{128}$$

$$\mathbf{Q}_2 = \frac{\mathbf{q}^{\mathrm{T}}\dot{\mathbf{q}}\,\mathbf{q}\,\dot{\mathbf{q}}^{\mathrm{T}}}{8\,q_o^3} + \frac{(\mathbf{q}^{\mathrm{T}}\dot{\mathbf{q}})^2\,\mathbf{q}\,\mathbf{q}^{\mathrm{T}}}{32\,q_o^5} + \left(\frac{\dot{\mathbf{q}}^{\mathrm{T}}\dot{\mathbf{q}}}{4\,q_o} + \frac{(\mathbf{q}^{\mathrm{T}}\dot{\mathbf{q}})^2}{16\,q_o^3}\right)\left(\mathbf{I} + \frac{\mathbf{q}\mathbf{q}^{\mathrm{T}}}{4\,q_o^2}\right). \tag{129}$$

References

[1] J. Argyris, An excursion into large rotations, Comput. Methods Appl. Mech. Engrg., Vol. 32, 85-155 (1982).

[2] J.-M. Battini, C. Pacoste, Co-rotational beam elements with warping effects in instability problems, Comput. Methods Appl. Mech. Engrg., Vol. 191, 1755-1789 (2002).

[3] J.-M. Battini, A modified corotational framework for triangular shell elements, Comput. Methods Appl. Mech. Engrg., Vol. 196, 1905-1914 (2007).

[4] J.-M. Battini, Large rotations and nodal moments in corotational elements, CMES, Vol. 33, N. 1, 1-15 (2008).

[5] P. Betsch, P. Steinmann, Constrained dynamics of geometrically exact beams, Comput. Mech., Vol. 31, 49-59 (2003).

[6] A. Cardona, M. Geradin, A beam finite element non-linear theory with finite rotations, Int. J. Num. Methods. Engrg., Vol. 26, 2403-2438 (1988).

[7] J. Chung, G.M. Hulbert, A predictor-corrector algorithm of the generalized-α Method for analysis of structural dynamics, J. KSNVE, Vol. 5, N. 2 , 207-213 (1995).

[8] M.A. Crisfield, U. Galvanetto, G. Jelenić, Dynamics of 3-D co-rotational beams, Comput. Mech., Vol. 20, 507-519 (1997).

[9] M.A. Crisfield, Non-Linear Finite Element Analysis of Solids and Structures, Volume 2: Advanced Topics, Wiley, Chischester (1997).

[10] K. Forsell, Instability analyses of structures under dynamic loads, PhD dissertation, KTH, Sweden (2000).

[11] M. Geradin, A. Cardona, Kinematics and dynamics of rigid and flexible mechanisms using finite elements and quaternion algebra, Comput. Mech., Vol. 4, 115-135 (1989).

[12] M. Geradin, A. Cardona, Flexible multibody dynamics : A finite element approach, 120-127. Wiley, Chischester (2001).

[13] S. Ghosh, D. Roy, Consistent quaternion interpolation for objective finite element approximation of geometrically exact beam, Comput. Methods Appl. Mech. Engrg., Vol. 198, 555-571 (2008).

[14] K.M. Hsiao, J.Y. Lin, W.Y. Lin, A consistent co-rotational finite element formulation for geometrically nonlinear dynamics analysis of 3-D beams, Comput. Methods Appl. Mech. Engrg., Vol. 169, 1-18 (1999).

[15] A. Ibrahimbegović, F. Frey, I. Kožar, Computational aspects of vector-like parameterization of three-dimensional finite rotations, Int. J. Num. Methods. Engrg., Vol. 38, 3653-3673 (1995).

[16] A. Ibrahimbegović, On the choice of finite rotation parameters, Comput. Methods Appl. Mech. Engrg., Vol. 149, 49-71 (1997).

[17] A. Ibrahimbegović, M.A. Mikdad, Finite rotations in dynamics of beams and implicit time-stepping schemes, Int. J. Num. Methods. Engrg., Vol. 41, 781-814 (1998).

[18] M. Iura, S.N. Atluri, Dynamic analysis of finitely stretched and rotated three-dimensional space-curved beams, Comput. & Struc., Vol. 29, 875-889 (1988).

[19] G. Jelenić, M.A. Crisfield, Interpolation of rotational variables in nonlinear dynamics of 3D beams, Int. J. Num. Methods. Engrg., Vol. 43, 1193-1222 (1998).

[20] G. Jelenić, M.A. Crisfield, Geometrically exact 3D beam theory: implementation of a strain-invariant element for stactics and dynamics, Comput. Methods Appl. Mech. Engrg., Vol. 171, 141-171 (1999).

[21] S. Krenk, Non-Linear Modeling And Analysis Of Solids And Structures, 47-75, Cambridge University Press, New York (2009).

[22] J. Mäkinen, Critical study of Newmark-scheme on manifold of finite rotations, Comput. Methods Appl. Mech. Engrg., Vol. 191, 817-828 (2001).

[23] J. Mäkinen, Total Lagrangian Reissner's geometrically exact beam element without singularities, Int. J. Num. Methods. Engrg., Vol. 70, 1009-1048 (2007).

[24] M.A. Mikdad, Statique et dynamique des poutres en grande rotation et resolution des problemes d'instabilite non lineaire, PhD dissertation, Uni.Tec.Compi., France (1998).

[25] C. Pacoste, Corotational flat facet triangular elements for shell instability analysis, Comput. Methods Appl. Mech. Engrg., Vol. 156, 75-110 (1998).

[26] I. Romero, The interpolation of rotations and its application to finite element models of geometrically exact rods, Comp. Mech., Vol. 34, 121-133 (2004).

[27] K. Shoemake, Animating rotation with quaternion curves, SIGGRAPH' 85: Proceedings of the 12th annual conference on Computer graphics and interactive techniques, 245-254 (1985).

[28] J.C. Simo, L. Vu-Quoc, On the dynamics in space of rods undergoing large motions - A geometrically exact approach, Comput. Methods Appl. Mech. Engrg., Vol. 66, 125-161 (1988).

[29] J.C. Simo, K.K. Wong, Unconditionally stable algorithms for rigid body dynamics that exactly preserve energy and momentum, Int. J. Num. Methods. Engrg., Vol. 31, 19-52 (1991).

[30] K.W. Spring, Euler parameters and the use of quaternion algebra in the manipulation of finite rotations: a review, Mech. Mach. Theo., Vol. 21, N. 5, 365-373 (1986).

[31] O.A. Bauchau, Flexible Multibody Dynamics, 537-538. Springer, Dordrecht (2011).

Paper 3: A consistent 3D corotational beam element for nonlinear dynamic analysis of flexible structures

Accepted for publication in Computer Methods in Applied Mechanics and Engineering, 2013
DOI: 10.1016/j.cma.2013.11.007

Computer Methods in Applied Mechanics and Engineering.
Comput. Methods Appl. Mech. Engrg. (2013).

A consistent 3D corotational beam element for nonlinear dynamic analysis of flexible structures

Thanh-Nam Le [1,2] , Jean-Marc Battini [2] , Mohammed Hjiaj [1]

[1] *Université Européenne de Bretagne, INSA de Rennes - LGCGM/Structural Engineering Research Group, 20 avenue des Buttes de Coësmes, CS 70839, 35708 Rennes Cedex 7, France.*

[2] *KTH, Royal Institute of Technology - Department of Civil and Architectural Engineering, SE-10044 Stockholm, Sweden.*

Abstract

The purpose of the paper is to present a corotational beam element for the nonlinear dynamic analysis of 3D flexible frames. The novelty of the formulation lies in the use of the corotational framework (i.e. the decomposition into rigid body motion and pure deformation) to derive not only the internal force vector and the tangent stiffness matrix but also the inertia force vector and the tangent dynamic matrix. As a consequence, cubic interpolations are adopted to formulate both inertia and internal local terms. In the derivation of the dynamic terms, an approximation for the local rotations is introduced and a concise expression for the global inertia force vector is obtained. To enhance the efficiency of the iterative procedure, an approximate expression of the tangent dynamic matrix is adopted. Four numerical examples are considered to assess the performance of the new formulation against the one suggested by Simo and Vu-Quoc [48]. It was observed that the proposed formulation proves to combine accuracy with efficiency. In particular, the present approach achieves the same level of accuracy as the formulation of Simo and Vu-Quoc but with a significantly smaller number of elements.

Key words: Corotational method; Nonlinear dynamics; 3D beam elements; Finite rotations;

1 Introduction

Flexible beams are used in many applications, for instance large deployable space structures, aircrafts and wind turbines propellers, offshore platforms. These structures undergo large displacements and finite rotations, but the strains remain small. Their nonlinear dynamic behavior is often simulated using geometrically nonlinear spatial beam elements. In the literature, several approaches have been used to develop such elements. A large number of them have been formulated in the total Lagrangian context [4, 9, 10, 19, 26, 29, 31, 32, 36, 38, 48, 52, 53]. An other attractive way to develop effective nonlinear dynamic beam elements, which is adopted in the present work, is to use the corotational approach. Indeed, this framework has been adopted by several authors to develop efficient beam and shell elements for the nonlinear static and dynamic analysis of flexible structures [1, 6, 8, 11, 13–18, 21, 22, 30, 39, 41, 43, 50]. Several versions of the corotational method have been proposed in the literature. The one employed in this work has been proposed by Rankin and Nour-Omid [40, 44], and then further developed by Battini and Pacoste [5]. The main idea of the method is to decompose the motion of the element into rigid body and pure deformational parts. During the rigid body motion, a local coordinates system, attached to the element, moves and rotates with it. The deformational part is measured in this local system. The main interest of the approach is that different assumptions can be made to represent the local deformations, giving rise to different possibilities for the local element formulation.

For the geometrically and materially static nonlinear analysis of beam structures with corotational approach, several local formulations have been proposed by Battini and Pacoste [5], and Alsafadie et al. [2]. The results of a comparative study of 3D beam formulations, which can be found in [2], have shown that local beam elements based on cubic interpolations are more efficient and accurate than the ones which employ linear interpolations. However, in dynamics, one has to deal with the inertia terms which by nature are complicate to formulate. This is particularly true in the corotational formulation of Bernoulli-type beam elements. This difficulty has hampered the development of the corotational approach in nonlinear dynamics. To avoid the consistent derivation of the inertia terms, several routes have been considered.

For 2D dynamic analysis, quite a few authors [39, 41, 50] have adopted the constant lumped mass matrix without any attempt to check its accuracy. Iura and Atluri [30] suggested to simply switch to a Timoshenko beam model where the mass matrix is constant and therefore the inertia terms are simple to evaluate. Behdinan et al. [8] proposed a 2D corotational dynamic formulation where cubic interpolations have been used to describe the global displacements, which is not consistent with the idea of the corotational method as originally introduced by Nour-Omid and Rankin [40]. More recently, Le et al. [34] developed a consistent 2D corotational beam element for nonlinear dynamics. Cubic interpolations were used to describe the local displacements and to derive both inertia and internal terms. Numerical results demonstrated that the formulation is more efficient than the classic formulations (i.e. with the constant Timoshenko and the constant lumped mass matrices). For 3D dynamic analysis, Crisfield et al. [16] suggested to use a constant Timoshenko mass matrix along with local cubic interpolations to derive the internal force vector and the corresponding tangent stiffness matrix. As pointed out by Crisfield et al. [16], this combination is not consistent but it provides reasonable results when the number of elements is large enough. Hsiao et al. [22] presented a corotational formulation for the nonlinear analysis of 3D beams. However the corotational framework adopted in [22] is different from the classic one as proposed by Nour-Omid and Rankin [40] and adopted in this paper.

The objective of this paper is to extend the consistent 2D corotational dynamic formulation presented in [34] to 3D beam structures. Hence, the corotational framework (i.e. the decomposition into rigid body motion and pure deformation) is used to derive not only the internal force vector and the tangent stiffness matrix but also the inertia force vector and the tangent dynamic matrix. The element has two nodes and is initially straight. The same cubic interpolations are adopted to formulate both inertia and internal local terms. In doing so, the complex expressions of the inertia terms are significantly simplified by adopting a proper approximation for the local rotations. To enhance the efficiency of the iterative procedure, the less significant term in the tangent dynamic matrix is ignored (see [35]).

Regarding the time-stepping scheme, the classic HHT α method (with $\alpha = -0.05$) is adopted in this work. This energy-dissipative method, which is implemented in several commercial FEM programs (Abaqus, Lusas) and was employed by many authors [10, 16, 32], limits the influence of high frequencies by introducing a numerical damping. The latter often avoids numerical instability, but also results in dissipation of the total energy. It can be noted that for beam structures, more robust alternatives to the HHT α method have been proposed in the literature [27].

Four numerical examples are presented with the objective to compare the performances of the new formulation against two other approaches. The first approach is similar to the one presented above, but linear local interpolations, instead of cubic ones, are used to derive only the dynamic terms. The purpose is to evaluate the influence of the choice of the local interpolations on the dynamic terms. The second approach is the classic total Lagrangian formulation proposed by Simo and Vu-Quoc [46–48].

The paper is organized as follows. Section 2 presents some aspects of the parametrization of finite rotations that are essentials for the subsequent developments. Section 3 is devoted to the corotational beam kinematics, whilst the local beam element formulation is introduced in Section 4. The internal force vector and the tangent stiffness matrix are briefly presented in Section 5. More details about the derivation can be found in [5]. Sections 6 and 7 focus on the derivation of the inertia terms and the time stepping method. In Section 8, four examples are presented in order to assess the accuracy of the present dynamic formulation.

Finally, conclusions are given in Section 9.

2 Parametrization of finite rotations

Due to the complex nature of 3D finite rotations, the parametrization of the finite rotations is a central issue in the development of 3D beam elements. In the literature, many ways to parameterize the finite rotations have been proposed, e.g.: spin variables, rotational vector, Euler parameters, Rodrigues parameters. In the current work, spatial spin variables and spatial rotational vector are used.

In this section, the relations required for the development of the present formulation are introduced. For a more complete description of the finite rotations, the reader is referred to textbooks and papers such as [3, 7, 12, 20, 23, 25, 33].

The coordinate of a vector $\mathbf{x}_o$ that is rotated into the position $\mathbf{x}$ (see Fig. 1) is given by the relation

$$\mathbf{x} = \mathbf{R}\,\mathbf{x}_o\,. \tag{1}$$

Due to its orthonormality, the rotation matrix $\mathbf{R}$ can be parameterized using only three independent pa-

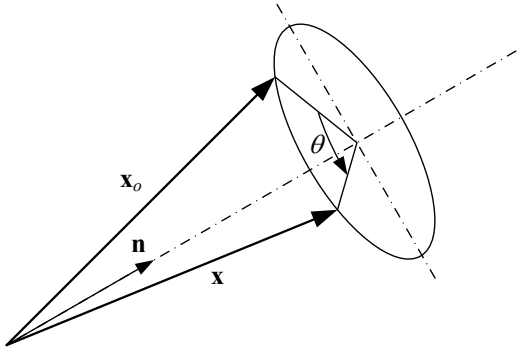

Fig. 1. Finite rotation of a vector.

rameters. One possibility is to use the rotational vector defined by

$$\boldsymbol{\theta} = \theta\,\mathbf{n}\,, \tag{2}$$

where $\mathbf{n}$ is a unit vector defining the axis of the rotation and $\theta = (\boldsymbol{\theta}^{\mathrm{T}}\boldsymbol{\theta})^{1/2}$ is the angle of the rotation.

The relation between the rotation matrix and the rotational vector is given by the Rodrigues' formula

$$\mathbf{R} = \mathbf{I} + \frac{\sin\theta}{\theta}\widetilde{\boldsymbol{\theta}} + \frac{1-\cos\theta}{\theta^2}\widetilde{\boldsymbol{\theta}}\widetilde{\boldsymbol{\theta}} = \exp(\widetilde{\boldsymbol{\theta}})\,, \tag{3}$$

where $\widetilde{\boldsymbol{\theta}}$ is the skew matrix associated with the vector $\boldsymbol{\theta}$, $\mathbf{I}$ is the 3×3 identity matrix.

The variation $\delta\mathbf{R}$ of the rotation matrix $\mathbf{R}$ is calculated according to

$$\delta\mathbf{R} = \widetilde{\delta\mathbf{w}}\mathbf{R}\,. \tag{4}$$

Physically, $\widetilde{\delta\mathbf{w}}$ represents infinitesimal spatial rotation superimposed to the rotation $\mathbf{R}$. $\delta\mathbf{w}$, which is the spatial spin variable vector, is related to the variation of the rotational vector through

$$\delta\mathbf{w} = \mathbf{T}_s(\boldsymbol{\theta})\,\delta\boldsymbol{\theta}\,, \tag{5}$$

with

$$\mathbf{T}_s(\boldsymbol{\theta}) = \mathbf{I} + \frac{1-\cos\theta}{\theta^2}\widetilde{\boldsymbol{\theta}} + \frac{\theta-\sin\theta}{\theta^3}\widetilde{\boldsymbol{\theta}}\widetilde{\boldsymbol{\theta}}\,. \tag{6}$$

The inverse relation of Eq. (5) is

$$\delta\boldsymbol{\theta} = \mathbf{T}_s^{-1}(\boldsymbol{\theta})\,\delta\mathbf{w}\,, \tag{7}$$

with

$$\mathbf{T}_s^{-1}(\boldsymbol{\theta}) = \frac{(\theta/2)}{\tan(\theta/2)}\mathbf{I} + \left(1 - \frac{(\theta/2)}{\tan(\theta/2)}\right)\frac{\boldsymbol{\theta}\boldsymbol{\theta}^{\mathrm{T}}}{\theta^2} - \frac{1}{2}\widetilde{\boldsymbol{\theta}}\,. \tag{8}$$

In order to simulate dynamic behavior of beam structures, angular velocities and accelerations must be calculated. Considering Eq. (4), the angular velocity can be expressed in spatial form as

$$\widetilde{\dot{\mathbf{w}}} = \dot{\mathbf{R}}\mathbf{R}^{\mathrm{T}}\,. \tag{9}$$

By taking the time derivatives of Eq. (9), the angular acceleration in spatial form is given by

$$\widetilde{\ddot{\mathbf{w}}} = \ddot{\mathbf{R}}\mathbf{R}^{\mathrm{T}} + \dot{\mathbf{R}}\dot{\mathbf{R}}^{\mathrm{T}}\,. \tag{10}$$

Using Eq. (5), the spatial angular velocity can directly be calculated from the rotational vector

$$\dot{\mathbf{w}} = \mathbf{T}_s(\boldsymbol{\theta})\dot{\boldsymbol{\theta}}\,. \tag{11}$$

3 Beam kinematics

In this paper, the corotational framework introduced by Nour-Omid and Rankin [40], and further developed by Pacoste and Eriksson [42] and Battini and Pacoste [5] is fully adopted.

The definition of the corotational two node beam element described in this section involves several coordinate systems, see Fig. 2. First a global reference system is defined by the triad of unit orthogonal vectors $\mathbf{e}_j$ $(j = 1,2,3)$. Next, a local system which continuously rotates and translates with the element is selected. The orthonormal basis vectors of the local system are denoted by $\mathbf{r}_j$ $(j = 1,2,3)$. In the initial (undeformed) configuration, the local system is defined by the orthonormal triad $\mathbf{e}_j^o$. In addition, $\mathbf{t}_j^1$ and $\mathbf{t}_j^2$ $(j = 1,2,3)$, denote two unit triads rigidly attached to nodes 1 and 2.

According to the main idea of the corotational formulation, the motion of the element from the initial to the final deformed configuration is split into a rigid body component and a deformational part. The rigid body motion consists of a rigid translation and rotation of the local element frame. The origin of the local system is taken at node 1 and thus the rigid translation is defined by $\mathbf{u}_1^g$, the translation at node 1. Here and in the sequel, superscript g indicates quantities expressed in the global reference system. The rigid rotation is such that the new orientation of the local reference system is defined by an orthogonal matrix $\mathbf{R}_r$, given by

$$\mathbf{R}_r = [\,\mathbf{r}_1\ \mathbf{r}_2\ \mathbf{r}_3\,]\,. \tag{12}$$

The first coordinate axis of the local system is defined by the line connecting nodes 1 and 2 of the element. Consequently, $\mathbf{r}_1$ is given by

$$\mathbf{r}_1 = \frac{\mathbf{x}_2^g + \mathbf{u}_2^g - \mathbf{x}_1^g - \mathbf{u}_1^g}{l_n}\,, \tag{13}$$

with $\mathbf{x}_i^g$ $(i = 1,2)$ denoting the nodal coordinates in the initial undeformed configuration and l_n denoting the current length of the beam, i.e.

$$l_n = \|\mathbf{x}_2^g + \mathbf{u}_2^g - \mathbf{x}_1^g - \mathbf{u}_1^g\|\,. \tag{14}$$

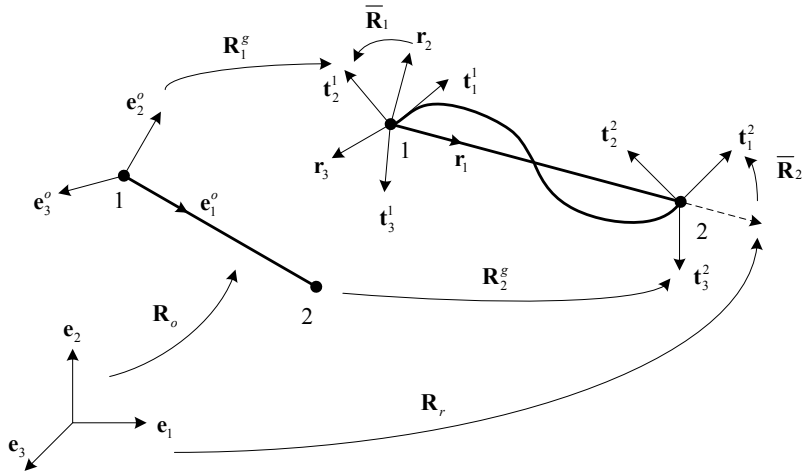

Fig. 2. Beam kinematics and the coordinate systems.

The remaining two axes are determined with the help of an auxiliary vector $\mathbf{p}$. In the initial configuration $\mathbf{p}$ is directed along the local $\mathbf{e}_2^o$ direction, whereas in the deformed configuration its orientation is obtained from

$$\mathbf{p} = \frac{1}{2}(\mathbf{p}_1 + \mathbf{p}_2), \qquad \mathbf{p}_i = \mathbf{R}_i^g \mathbf{R}_o [0\ 1\ 0]^{\mathrm{T}} \qquad (i = 1,2), \tag{15}$$

where $\mathbf{R}_1^g$ and $\mathbf{R}_2^g$ are the orthogonal matrices used to specify the orientation of the nodal triads $\mathbf{t}_j^1$ and $\mathbf{t}_j^2$ respectively, and $\mathbf{R}_o$ specifies the orientation of the local frame in the initial configuration, i.e. $\mathbf{R}_o = [\mathbf{e}_1^o\ \mathbf{e}_2^o\ \mathbf{e}_3^o]$. The unit vectors $\mathbf{r}_2$ and $\mathbf{r}_3$ are then computed by the following vector products

$$\mathbf{r}_3 = \frac{\mathbf{r}_1 \times \mathbf{p}}{\|\mathbf{r}_1 \times \mathbf{p}\|}, \qquad \mathbf{r}_2 = \mathbf{r}_3 \times \mathbf{r}_1, \tag{16}$$

resulting in the orthogonal matrix $\mathbf{R}_r$ (Eq. (12)) being completely determined.

The rigid motion previously described, is accompanied by local deformational displacements and rotations with respect to the local element axes. In this context, due to the particular choice of the local system, the local translations at node 1 are zero. Moreover, at node 2, the only non zero component is the translation along $\mathbf{r}_1$. This can easily be evaluated according to

$$\overline{u} = l_n - l_o, \tag{17}$$

with l_o denoting the length of the beam in the original undeformed configuration. Here and in the sequel, an overbar denotes a deformational kinematic quantity.

The global rotations at node i can be expressed in terms of the rigid rotation of the local axes, defined by $\mathbf{R}_r$, followed by a local rotation relative to these axes. The latter is defined by the orthogonal matrix $\overline{\mathbf{R}}_i$. Consequently, the orientation of the nodal triad $\mathbf{t}_j^i$ can be obtained by means of the product $\mathbf{R}_r \overline{\mathbf{R}}_i$. On the other hand, (see Fig. 2) this orientation can also be obtained through the product $\mathbf{R}_i^g \mathbf{R}_o$, which gives

$$\overline{\mathbf{R}}_i = \mathbf{R}_r^{\mathrm{T}} \mathbf{R}_i^g \mathbf{R}_o \qquad (i = 1,2). \tag{18}$$

The local rotations are then evaluated from

$$\overline{\boldsymbol{\theta}}_i = \log\left(\overline{\mathbf{R}}_i\right) \qquad (i = 1,2). \tag{19}$$

Due to the choice of the local coordinate system, the local nodal displacement vector $\mathbf{d}_l$ has only seven components and is given by

$$\mathbf{d}_l = \left[\overline{u}\ \ \overline{\boldsymbol{\theta}}_1^{\mathrm{T}}\ \ \overline{\boldsymbol{\theta}}_2^{\mathrm{T}}\right]^{\mathrm{T}}. \tag{20}$$

The variation of the local nodal displacement vector is

$$\delta \mathbf{d}_l = \left[\delta \overline{u} \;\; \delta \overline{\boldsymbol{\theta}}_1^{\mathrm{T}} \;\; \delta \overline{\boldsymbol{\theta}}_2^{\mathrm{T}} \right]^{\mathrm{T}}, \tag{21}$$

and the global counterpart is given by

$$\delta \mathbf{d}_g = \left[\delta \mathbf{u}_1^{g\mathrm{T}} \;\; \delta \mathbf{w}_1^{g\mathrm{T}} \;\; \delta \mathbf{u}_2^{g\mathrm{T}} \;\; \delta \mathbf{w}_2^{g\mathrm{T}} \right]^{\mathrm{T}}, \tag{22}$$

with $\delta \mathbf{w}_i^g \; (i = 1,2)$ denoting spatial spin variables defined by

$$\delta \mathbf{R}_i^g = \widetilde{\delta \mathbf{w}_i^g}\, \mathbf{R}_i^g \,. \tag{23}$$

For the rotational terms, the variation of Eq. (18) is needed

$$\delta \overline{\mathbf{R}}_i = \delta \mathbf{R}_r^{\mathrm{T}}\, \mathbf{R}_i^g\, \mathbf{R}_o + \mathbf{R}_r^{\mathrm{T}}\, \delta \mathbf{R}_i^g\, \mathbf{R}_o \,, \tag{24}$$

where $\delta \overline{\mathbf{R}}_i$ and $\delta \mathbf{R}_r$ are computed using Eq. (4), i.e.

$$\delta \overline{\mathbf{R}}_i = \widetilde{\delta \overline{\mathbf{w}}_i}\, \overline{\mathbf{R}}_i, \qquad \delta \mathbf{R}_r = \widetilde{\delta \mathbf{w}_r^g}\, \mathbf{R}_r \,. \tag{25}$$

$\delta \mathbf{R}_r^{\mathrm{T}}$ is calculated via the orthogonality condition $\mathbf{R}_r \mathbf{R}_r^{\mathrm{T}} = \mathbf{I}$. Taking the variation of this relation and combining the outcome with Eq. (25) results in

$$\delta \mathbf{R}_r^{\mathrm{T}} = -\mathbf{R}_r^{\mathrm{T}}\, \widetilde{\delta \mathbf{w}_r^g} \,. \tag{26}$$

Using Eqs. (23), (25) and (26), Eq. (24) can be rewritten as

$$\begin{aligned} \widetilde{\delta \overline{\mathbf{w}}_i}\, \overline{\mathbf{R}}_i &= -\mathbf{R}_r^{\mathrm{T}}\, \widetilde{\delta \mathbf{w}_r^g}\, \mathbf{R}_i^g\, \mathbf{R}_o + \mathbf{R}_r^{\mathrm{T}}\, \widetilde{\delta \mathbf{w}_i^g}\, \mathbf{R}_i^g\, \mathbf{R}_o \\ &= -\mathbf{R}_r^{\mathrm{T}}\, \widetilde{\delta \mathbf{w}_r^g}\, \mathbf{R}_r \mathbf{R}_r^{\mathrm{T}}\, \mathbf{R}_i^g\, \mathbf{R}_o + \mathbf{R}_r^{\mathrm{T}}\, \widetilde{\delta \mathbf{w}_i^g}\, \mathbf{R}_r \mathbf{R}_r^{\mathrm{T}}\, \mathbf{R}_i^g\, \mathbf{R}_o \\ &= (\widetilde{\delta \mathbf{w}_i^e} - \widetilde{\delta \mathbf{w}_r^e})\, \overline{\mathbf{R}}_i \,, \end{aligned} \tag{27}$$

where use of Eq. (18) has been made along the fact that $\mathbf{R}_r$ transforms a vector and a tensor from global to local coordinates according to

$$\mathbf{x}^e = \mathbf{R}_r^{\mathrm{T}}\, \mathbf{x}^g, \qquad \widetilde{\mathbf{x}^e} = \mathbf{R}_r^{\mathrm{T}}\, \widetilde{\mathbf{x}^g}\, \mathbf{R}_r \,. \tag{28}$$

Thus, Eq. (27) gives

$$\delta \overline{\mathbf{w}}_i = \delta \mathbf{w}_i^e - \delta \mathbf{w}_r^e \qquad (i = 1,2) \,. \tag{29}$$

Further, let

$$\delta \mathbf{d}_g^e = \mathbf{E}^{\mathrm{T}}\, \delta \mathbf{d}_g, \qquad \mathbf{E} = \begin{bmatrix} \mathbf{R}_r & \mathbf{0} & \mathbf{0} & \mathbf{0} \\ \mathbf{0} & \mathbf{R}_r & \mathbf{0} & \mathbf{0} \\ \mathbf{0} & \mathbf{0} & \mathbf{R}_r & \mathbf{0} \\ \mathbf{0} & \mathbf{0} & \mathbf{0} & \mathbf{R}_r \end{bmatrix}, \tag{30}$$

with $\mathbf{0}$ denoting the 3×3 zero matrix.

Using the chain rule, $\delta \overline{\mathbf{w}}_i$ is evaluated as

$$\delta \overline{\mathbf{w}}_i = \frac{\partial \overline{\mathbf{w}}_i}{\partial \mathbf{d}_g^e}\, \frac{\partial \mathbf{d}_g^e}{\partial \mathbf{d}_g}\, \delta \mathbf{d}_g = \frac{\partial \overline{\mathbf{w}}_i}{\partial \mathbf{d}_g^e}\, \mathbf{E}^{\mathrm{T}}\, \delta \mathbf{d}_g \qquad (i = 1,2) \,. \tag{31}$$

Then Eq. (29) can be rewritten as

$$\begin{bmatrix} \delta\overline{\mathbf{w}}_1 \\ \delta\overline{\mathbf{w}}_2 \end{bmatrix} = \left(\begin{bmatrix} \mathbf{0} & \mathbf{I} & \mathbf{0} & \mathbf{0} \\ \mathbf{0} & \mathbf{0} & \mathbf{0} & \mathbf{I} \end{bmatrix} - \begin{bmatrix} \mathbf{G}^{\mathrm{T}} \\ \mathbf{G}^{\mathrm{T}} \end{bmatrix} \right) \mathbf{E}^{\mathrm{T}} \delta\mathbf{d}_g = \mathbf{P}\mathbf{E}^{\mathrm{T}} \delta\mathbf{d}_g \,, \tag{32}$$

where the matrix $\mathbf{G}$ is defined by

$$\mathbf{G}^{\mathrm{T}} = \frac{\partial \mathbf{w}_r^e}{\partial \mathbf{d}_g^e} \,. \tag{33}$$

The expression of $\mathbf{G}$ is obtained from Eq. (25) which, using Eq. (28), can be rewritten as

$$\widetilde{\delta\mathbf{w}_r^e} = \mathbf{R}_r^{\mathrm{T}} \delta\mathbf{R}_r, \qquad \delta\mathbf{w}_r^e = \begin{bmatrix} -\mathbf{r}_2^{\mathrm{T}} \delta\mathbf{r}_3 \\ -\mathbf{r}_3^{\mathrm{T}} \delta\mathbf{r}_1 \\ \mathbf{r}_2^{\mathrm{T}} \delta\mathbf{r}_1 \end{bmatrix} . \tag{34}$$

For the local coordinate system defined in Eqs. (13) - (16), the above equation yield to

$$\mathbf{G}^{\mathrm{T}} = \begin{bmatrix} 0 & 0 & \frac{\eta}{l_n} & \frac{\eta_{12}}{2} & -\frac{\eta_{11}}{2} & 0 & 0 & 0 & -\frac{\eta}{l_n} & \frac{\eta_{22}}{2} & -\frac{\eta_{21}}{2} & 0 \\ 0 & 0 & \frac{1}{l_n} & 0 & 0 & 0 & 0 & 0 & -\frac{1}{l_n} & 0 & 0 & 0 \\ 0 & -\frac{1}{l_n} & 0 & 0 & 0 & 0 & 0 & \frac{1}{l_n} & 0 & 0 & 0 & 0 \end{bmatrix} , \tag{35}$$

$$\eta = \frac{p_1}{p_2} \,, \qquad \eta_{11} = \frac{p_{11}}{p_2} \,, \qquad \eta_{12} = \frac{p_{12}}{p_2} \,, \qquad \eta_{21} = \frac{p_{21}}{p_2} \,, \qquad \eta_{22} = \frac{p_{22}}{p_2} \,, \tag{36}$$

where (see Eq. (15)) p_j and p_{ij} are the components of the vectors $\mathbf{R}_r^{\mathrm{T}}\,\mathbf{p}$ and $\mathbf{R}_r^{\mathrm{T}}\,\mathbf{p}_i$, respectively.

4 Local beam kinematic description

The main interest of the corotational method is the separation of the local deformation and the rigid body motion. Consequently, different assumptions can be made to represent the local displacements, giving rise to different choices for the interpolation functions. In this section, the local beam kinematics, adopted to derive both inertia and internal terms, is presented.

The local motion of a beam cross-section from the initial (i.e. rotated but still undeformed) configuration to the current configuration is defined by the translation of the cross-section centroid G and the cross-section rotation (see Figs. 3 and 4).

Let $[\,\overline{u}_1 \;\; \overline{u}_2 \;\; \overline{u}_3\,]^{\mathrm{T}}$ and $\overline{\boldsymbol{\theta}} = [\,\overline{\theta}_1 \;\; \overline{\theta}_2 \;\; \overline{\theta}_3\,]^{\mathrm{T}}$ denote the local displacement vector of G and the local cross-section rotation, respectively. These quantities are interpolated from the local nodal values based on the Bernoulli hypothesis, i.e. linear interpolations for the axial displacement and axial rotation, cubic interpolations for

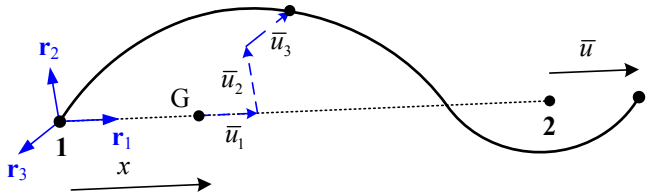

Fig. 3. Local beam configuration - Translation.

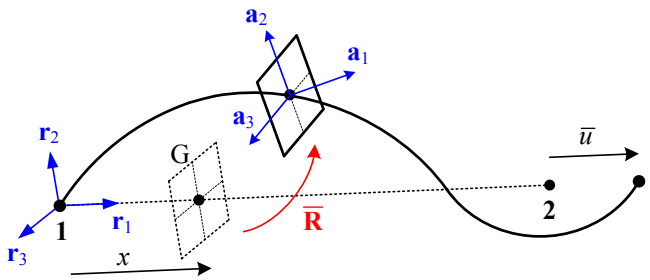

Fig. 4. Local beam configuration - Rotation.

the transverse displacements. Then, due to the particular choice of the local degrees of freedom, one has

$$\begin{bmatrix} \overline{u}_1 \\ \overline{u}_2 \\ \overline{u}_3 \\ \overline{\theta}_1 \\ \overline{\theta}_2 \\ \overline{\theta}_3 \end{bmatrix} = \begin{bmatrix} N_2 & 0 & 0 & 0 & 0 & 0 & 0 \\ 0 & 0 & 0 & N_3 & 0 & 0 & N_4 \\ 0 & 0 & -N_3 & 0 & 0 & -N_4 & 0 \\ 0 & N_1 & 0 & 0 & N_2 & 0 & 0 \\ 0 & 0 & N_5 & 0 & 0 & N_6 & 0 \\ 0 & 0 & 0 & N_5 & 0 & 0 & N_6 \end{bmatrix} \mathbf{d}_l \,, \tag{37}$$

where the local nodal displacement vector $\mathbf{d}_l$ is defined by Eq. (20).

The expressions of the interpolation functions are given by

$$\begin{aligned} N_1 &= 1 - \frac{x}{l_o} \,, \qquad N_2 = 1 - N_1 \,, \\ N_3 &= x\left(1 - \frac{x}{l_o}\right)^2 \,, \quad N_4 = -\left(1 - \frac{x}{l_o}\right)\frac{x^2}{l_o} \,, \\ N_5 &= \left(1 - \frac{3x}{l_o}\right)\left(1 - \frac{x}{l_o}\right) \,, \quad N_6 = \left(\frac{3x}{l_o} - 2\right)\frac{x}{l_o} \,. \end{aligned}$$

Let $\mathbf{u}_l = [\,0 \;\; \overline{u}_2 \;\; \overline{u}_3\,]^{\mathrm{T}}$ denotes the local transverse displacement vector. This vector is evaluated by

$$\mathbf{u}_l = \mathbf{P}_1 \begin{bmatrix} \overline{\boldsymbol{\theta}}_1 \\ \overline{\boldsymbol{\theta}}_2 \end{bmatrix} \,, \tag{38}$$

with $\mathbf{P}_1 = \begin{bmatrix} 0 & 0 & 0 & 0 & 0 & 0 \\ 0 & 0 & N_3 & 0 & 0 & N_4 \\ 0 & -N_3 & 0 & 0 & -N_4 & 0 \end{bmatrix}$.

The local cross-section rotation is evaluated as follows

$$\overline{\boldsymbol{\theta}} = \mathbf{P}_2 \begin{bmatrix} \overline{\boldsymbol{\theta}}_1 \\ \overline{\boldsymbol{\theta}}_2 \end{bmatrix}, \tag{39}$$

with $\mathbf{P}_2 = \begin{bmatrix} N_1 & 0 & 0 & N_2 & 0 & 0 \\ 0 & N_5 & 0 & 0 & N_6 & 0 \\ 0 & 0 & N_5 & 0 & 0 & N_6 \end{bmatrix}$.

In the present formulation, bending shear deformations are not considered. Such deformations can easily be introduced by modifying the Hermitian shape functions as suggested in the Interdependent Interpolation Element (IIE) formulation [45].

5 Internal force vector and tangent stiffness matrix

The purpose of this section is to present briefly the derivation of the inertial force vector and the tangent stiffness matrix. A complete description can be found in [5].

The local nodal displacements and rotations defined in Eq. (20) are extracted from the global degrees of freedom using Eqs. (17), (18) and (19).

Using the local beam kinematics presented in Section 4 together with a shallow arch strain description, the local internal force vector $\mathbf{f}_l$ and the local tangent stiffness matrix $\mathbf{K}_l$ associated with $\delta\mathbf{d}_l$ (see Eq. (21)) are computed. The Maple codes for $\mathbf{f}_l$ and $\mathbf{K}_l$ are given in [5].

The global internal force vector $\mathbf{f}_g$ and the global tangent stiffness matrix $\mathbf{K}_g$ associated with $\delta\mathbf{d}_g$ (see Eq. (22)) are obtained through a change of variables based on the transformation matrix $\mathbf{B}$ defined by

$$\delta\mathbf{d}_l = \mathbf{B}\,\delta\mathbf{d}_g\,. \tag{40}$$

By equating the internal virtual work in both the global and local systems, the expression of the global internal force vector $\mathbf{f}_g$ is obtained as

$$\mathbf{f}_g = \mathbf{B}^{\mathrm{T}}\mathbf{f}_l\,. \tag{41}$$

By taking the variation of Eq. (41), the expression of the global tangent stiffness matrix $\mathbf{K}_g$ is obtained

$$\mathbf{K}_g = \mathbf{B}^{\mathrm{T}}\mathbf{K}_l\mathbf{B} + \left.\frac{\partial(\mathbf{B}^{\mathrm{T}}\mathbf{f}_l)}{\partial\mathbf{d}_g}\right|_{\mathbf{f}_l}. \tag{42}$$

In fact, the change of variables defined by Eqs. (41) and (42) must be performed in two steps. The reason is that $\delta\overline{\boldsymbol{\theta}}_i$ $(i=1,2)$ in Eq. (21) is the variation of the rotational vector associated with $\overline{\mathbf{R}}_i$ (see Eq. (19)) whereas $\delta\overline{\mathbf{w}}_i$ in Eq. (29) represents the spatial spin rotations associated with $\overline{\mathbf{R}}_i$ (see Eq. (25)).

Consequently, the additional local quantities $\delta\mathbf{d}_a$ defined by

$$\delta\mathbf{d}_a = \left[\,\delta\overline{u}\;\;\delta\overline{\mathbf{w}}_1^{\mathrm{T}}\;\;\delta\overline{\mathbf{w}}_2^{\mathrm{T}}\,\right]^{\mathrm{T}}, \tag{43}$$

are introduced.

Using Eq. (7), a first change of variables, from $\delta\mathbf{d}_l$ to $\delta\mathbf{d}_a$, is performed. Using the variation of Eq. (17) and Eq. (32), a second change of variables, from $\delta\mathbf{d}_a$ to $\delta\mathbf{d}_g$, is performed. This gives the expressions of $\mathbf{f}_g$ and $\mathbf{K}_g$. The details regarding these two changes of variables and the final expressions of $\mathbf{f}_g$ and $\mathbf{K}_g$ are given in [5].

6 Inertia force vector and tangent dynamic matrix

This section is devoted to the derivation of the inertia force vector and the tangent dynamic matrix. The novelty of the approach presented here is that the same corotational kinematics description is adopted to formulate both inertia and internal terms, which ensures the consistency of the formulation. As already mentioned, the current 3D formulation is the extension of the 2D one proposed by the authors [34].

Using the cross-section centroid as the reference point, the kinetic energy of a spatial beam element is given by

$$K = \frac{1}{2}\int_{l_o} \{\dot{\mathbf{u}}^{\mathrm{T}} A_\rho \dot{\mathbf{u}} + \dot{\mathbf{w}}^{\mathrm{T}} \mathbf{I}_\rho \dot{\mathbf{w}}\} \mathrm{d}l\,, \tag{44}$$

where $\dot{\mathbf{u}}$, $\dot{\mathbf{w}}$ are the translational and angular velocity of the cross-section. Please note that in order to simplify the notations, in this section, the superscripts "g" which refer to global quantities are dropped for $\mathbf{u}$, $\dot{\mathbf{w}}$ and their derivatives.

$\mathbf{I}_\rho$ is the spatial inertia dyadic tensor given by

$$\mathbf{I}_\rho = \mathbf{R}^g \mathbf{R}_o \mathbf{J}_\rho \left(\mathbf{R}^g \mathbf{R}_o\right)^{\mathrm{T}}, \tag{45}$$

in which $\mathbf{J}_\rho$ is the inertia dyadic of the cross-section in the initial configuration.

The variation of the kinetic energy can be expressed as (see [20])

$$\delta K = -\int_{l_o} \left\{ \delta \mathbf{u}^{\mathrm{T}} A_\rho \ddot{\mathbf{u}} + \delta \mathbf{w}^{\mathrm{T}} \left[\mathbf{I}_\rho \ddot{\mathbf{w}} + \widetilde{\dot{\mathbf{w}}} \mathbf{I}_\rho \dot{\mathbf{w}} \right] \right\} \mathrm{d}l\,. \tag{46}$$

The inertia force vector is then derived from the following relation

$$\delta K = -\mathbf{f}_k^{\mathrm{T}} \delta \mathbf{d}_g\,. \tag{47}$$

6.1 Translational displacement variables

The position of the cross-section centroid in the global coordinate system is given by (see Fig. 3)

$$\mathrm{OG} = \mathbf{x}_1^g + \mathbf{u}_1^g + (x + \overline{u}_1)\,\mathbf{r}_1 + \overline{u}_2 \mathbf{r}_2 + \overline{u}_3 \mathbf{r}_3\,. \tag{48}$$

By introducing Eqs. (17) and (37) into Eq. (48), one obtains

$$\mathrm{OG} = \mathbf{x}_1^g + \mathbf{u}_1^g + \frac{l_n}{l_o} x \mathbf{r}_1 + \overline{u}_2 \mathbf{r}_2 + \overline{u}_3 \mathbf{r}_3\,. \tag{49}$$

By inserting the expression (13) for $\mathbf{r}_1$ in the above relation, one obtains

$$\begin{aligned} \mathrm{OG} &= \mathbf{x}_1^g + \mathbf{u}_1^g + \frac{\mathbf{x}_2^g + \mathbf{u}_2^g - \mathbf{x}_1^g - \mathbf{u}_1^g}{l_o} x + \overline{u}_2 \mathbf{r}_2 + \overline{u}_3 \mathbf{r}_3 \\ &= N_1 \mathbf{x}_1^g + N_2 \mathbf{x}_2^g + N_1 \mathbf{u}_1^g + N_2 \mathbf{u}_2^g + \mathbf{R}_r \mathbf{u}_l\,, \end{aligned} \tag{50}$$

with $\mathbf{u}_l$ as defined in Eq. (38).

Then by taking the variation of the above equation, the following expression is obtained

$$\delta \mathrm{OG} = \delta \mathbf{u} = \mathbf{N}\,\delta \mathbf{d}_g + \mathbf{R}_r \delta \mathbf{u}_l + \delta \mathbf{R}_r \mathbf{u}_l\,, \tag{51}$$

with $\mathbf{N} = \begin{bmatrix} N_1\mathbf{I} & \mathbf{0} & N_2\mathbf{I} & \mathbf{0} \end{bmatrix}$.
One interesting property of $\mathbf{N}$ is that

$$\mathbf{N} = \mathbf{R}_r \mathbf{N} \mathbf{E}^{\mathrm{T}}. \tag{52}$$

The variation $\delta\mathbf{R}_r$ is calculated using Eqs. (25) and (28) as

$$\delta\mathbf{R}_r = \mathbf{R}_r\,\widetilde{\delta\mathbf{w}_r^e}\,. \tag{53}$$

From Eqs. (30) and (33), $\delta\mathbf{w}_r^e$ is obtained as

$$\delta\mathbf{w}_r^e = \mathbf{G}^{\mathrm{T}}\,\mathbf{E}^{\mathrm{T}}\,\delta\mathbf{d}_g\,. \tag{54}$$

By taking the differentiation of Eq. (38), one obtains

$$\delta\mathbf{u}_l = \mathbf{P}_1 \begin{bmatrix} \delta\overline{\boldsymbol{\theta}}_1 \\ \delta\overline{\boldsymbol{\theta}}_2 \end{bmatrix}. \tag{55}$$

In the corotational approach, the local rotations at the nodes $\overline{\boldsymbol{\theta}}_i$ $(i=1,2)$, defined in Eq. (19), are small and the operator $\mathbf{T}_s(\overline{\boldsymbol{\theta}}_i)$ is close to the identity matrix. Consequently, see Eq. (5), the following approximation is adopted

$$\delta\overline{\mathbf{w}}_i \approx \delta\overline{\boldsymbol{\theta}}_i\,. \tag{56}$$

It can be observed that for the internal force vector, this simplification, which implies to neglect the first change of variables in Section 5, cannot be performed.

Then, using Eqs. (32) and (56), the expression in (55) becomes

$$\delta\mathbf{u}_l \approx \mathbf{P}_1 \begin{bmatrix} \delta\overline{\mathbf{w}}_1 \\ \delta\overline{\mathbf{w}}_2 \end{bmatrix} = \mathbf{P}_1\,\mathbf{P}\,\mathbf{E}^{\mathrm{T}}\,\delta\mathbf{d}_g\,. \tag{57}$$

Inserting Eqs. (52) - (54) and (57) into Eq. (51), one obtains

$$\delta\mathbf{u} = \mathbf{N}\,\delta\mathbf{d}_g + \mathbf{R}_r\delta\mathbf{u}_l - \mathbf{R}_r\widetilde{\mathbf{u}}_l\delta\mathbf{w}_r^e = \mathbf{R}_r\left(\mathbf{N} + \mathbf{P}_1\,\mathbf{P} - \widetilde{\mathbf{u}}_l\,\mathbf{G}^{\mathrm{T}}\right)\mathbf{E}^{\mathrm{T}}\,\delta\mathbf{d}_g\,. \tag{58}$$

By introducing the notation

$$\mathbf{H}_1 = \mathbf{N} + \mathbf{P}_1\,\mathbf{P} - \widetilde{\mathbf{u}}_l\,\mathbf{G}^{\mathrm{T}}\,, \tag{59}$$

the expression (58) can be rewritten in a more compact form as

$$\delta\mathbf{u} = \mathbf{R}_r\,\mathbf{H}_1\,\mathbf{E}^{\mathrm{T}}\,\delta\mathbf{d}_g\,. \tag{60}$$

Obviously, the translational velocity of the cross-section centroid is evaluated from

$$\dot{\mathbf{u}} = \mathbf{R}_r\,\mathbf{H}_1\,\mathbf{E}^{\mathrm{T}}\,\dot{\mathbf{d}}_g\,. \tag{61}$$

By taking the time derivative of the above equation, the expression of the translational acceleration reads as follows

$$\ddot{\mathbf{u}} = \mathbf{R}_r\,\mathbf{H}_1\,\mathbf{E}^{\mathrm{T}}\,\ddot{\mathbf{d}}_g + \left(\dot{\mathbf{R}}_r\mathbf{H}_1\,\mathbf{E}^{\mathrm{T}} + \mathbf{R}_r\,\dot{\mathbf{H}}_1\,\mathbf{E}^{\mathrm{T}} + \mathbf{R}_r\,\mathbf{H}_1\,\dot{\mathbf{E}}^{\mathrm{T}}\right)\dot{\mathbf{d}}_g\,, \tag{62}$$

with $\dot{\mathbf{H}}_1$ given in Appendix A.

By noting that $\dot{\mathbf{R}}_r = \mathbf{R}_r\,\widetilde{\dot{\mathbf{w}}_r^e}$ (see Eq. (53)), it is straightforward to obtain

$$\dot{\mathbf{E}} = \begin{bmatrix} \dot{\mathbf{R}}_r & \mathbf{0} & \mathbf{0} & \mathbf{0} \\ \mathbf{0} & \dot{\mathbf{R}}_r & \mathbf{0} & \mathbf{0} \\ \mathbf{0} & \mathbf{0} & \dot{\mathbf{R}}_r & \mathbf{0} \\ \mathbf{0} & \mathbf{0} & \mathbf{0} & \dot{\mathbf{R}}_r \end{bmatrix} = \mathbf{E}\,\mathbf{E}_t\,, \tag{63}$$

with

$$\mathbf{E}_t = \begin{bmatrix} \widetilde{\dot{\mathbf{w}}_r^e} & \mathbf{0} & \mathbf{0} & \mathbf{0} \\ \mathbf{0} & \widetilde{\dot{\mathbf{w}}_r^e} & \mathbf{0} & \mathbf{0} \\ \mathbf{0} & \mathbf{0} & \widetilde{\dot{\mathbf{w}}_r^e} & \mathbf{0} \\ \mathbf{0} & \mathbf{0} & \mathbf{0} & \widetilde{\dot{\mathbf{w}}_r^e} \end{bmatrix} . \tag{64}$$

$\dot{\mathbf{w}}_r^e$ (see Eq. (54)) is calculated as

$$\dot{\mathbf{w}}_r^e = \mathbf{G}^{\mathrm{T}} \mathbf{E}^{\mathrm{T}} \dot{\mathbf{d}}_g \, . \tag{65}$$

By introducing the notation

$$\mathbf{C}_1 = \widetilde{\dot{\mathbf{w}}_r^e} \mathbf{H}_1 + \dot{\mathbf{H}}_1 - \mathbf{H}_1 \mathbf{E}_t \, , \tag{66}$$

then Eq. (62) can be rewritten in a more compact form as

$$\ddot{\mathbf{u}} = \mathbf{R}_r \mathbf{H}_1 \mathbf{E}^{\mathrm{T}} \ddot{\mathbf{d}}_g + \mathbf{R}_r \mathbf{C}_1 \mathbf{E}^{\mathrm{T}} \dot{\mathbf{d}}_g = \mathbf{R}_r \ddot{\mathbf{u}}^e \, . \tag{67}$$

6.2 Finite rotation variables

Using Eqs. (28) and (29), the spatial spin variables, associated to the global rotation of a cross-section, are evaluated using

$$\delta \mathbf{w} = \mathbf{R}_r \delta \mathbf{w}^e = \mathbf{R}_r \left(\delta \mathbf{w}_r^e + \delta \overline{\mathbf{w}} \right) . \tag{68}$$

Combining Eq. (39) with the approximation defined in Eq. (56), the local spatial spin variables are interpolated as follows

$$\delta \overline{\mathbf{w}} = \mathbf{P}_2 \begin{bmatrix} \delta \overline{\mathbf{w}}_1 \\ \delta \overline{\mathbf{w}}_2 \end{bmatrix} . \tag{69}$$

Using Eq. (32), the above equation leads to

$$\delta \overline{\mathbf{w}} = \mathbf{P}_2 \mathbf{P} \mathbf{E}^{\mathrm{T}} \delta \mathbf{d}_g \, . \tag{70}$$

Finally, by introducing Eqs. (54) and (70) into (68), the spatial spin variables are computed from the global nodal displacement vector with

$$\delta \mathbf{w} = \mathbf{R}_r \left(\mathbf{P}_2 \mathbf{P} + \mathbf{G}^{\mathrm{T}} \right) \mathbf{E}^{\mathrm{T}} \delta \mathbf{d}_g \, . \tag{71}$$

Using the notation

$$\mathbf{H}_2 = \mathbf{P}_2 \mathbf{P} + \mathbf{G}^{\mathrm{T}} \, , \tag{72}$$

the above expression can be rewritten in a more compact form as

$$\delta \mathbf{w} = \mathbf{R}_r \mathbf{H}_2 \mathbf{E}^{\mathrm{T}} \delta \mathbf{d}_g \, . \tag{73}$$

The angular velocity is calculated with the following similar expression

$$\dot{\mathbf{w}} = \mathbf{R}_r \mathbf{H}_2 \mathbf{E}^{\mathrm{T}} \dot{\mathbf{d}}_g = \mathbf{R}_r \dot{\mathbf{w}}^e \, . \tag{74}$$

The angular acceleration is obtained by taking the time derivative of the angular velocity

$$\dot{\mathbf{w}} = \mathbf{R}_r \mathbf{H}_2 \mathbf{E}^{\mathrm{T}} \ddot{\mathbf{d}}_g + \left(\dot{\mathbf{R}}_r \mathbf{H}_2 \mathbf{E}^{\mathrm{T}} + \mathbf{R}_r \dot{\mathbf{H}}_2 \mathbf{E}^{\mathrm{T}} + \mathbf{R}_r \mathbf{H}_2 \dot{\mathbf{E}}^{\mathrm{T}} \right) \dot{\mathbf{d}}_g \, , \tag{75}$$

with $\dot{\mathbf{H}}_2$ given in Appendix A.

By introducing the notation

$$\mathbf{C}_2 = \widetilde{\dot{\mathbf{w}}_r^e}\mathbf{H}_2 + \dot{\mathbf{H}}_2 - \mathbf{H}_2\,\mathbf{E}_t\,, \tag{76}$$

the expression (75) becomes

$$\ddot{\mathbf{w}} = \mathbf{R}_r\,\mathbf{H}_2\,\mathbf{E}^{\mathrm{T}}\,\ddot{\mathbf{d}}_g + \mathbf{R}_r\,\mathbf{C}_2\,\mathbf{E}^{\mathrm{T}}\,\dot{\mathbf{d}}_g = \mathbf{R}_r\,\dot{\mathbf{w}}^e\,. \tag{77}$$

6.3 Inertia force vector and tangent dynamic matrix

By inserting the expressions of $\delta\mathbf{u}$ and $\delta\mathbf{w}$ given in Eqs. (60) and (73) into Eq. (46), the inertia force vector is obtained as

$$\mathbf{f}_k = \mathbf{E}\left[\int_{l_o}\left\{\mathbf{H}_1^{\mathrm{T}}\,\mathbf{R}_r^{\mathrm{T}}\,A_\rho\,\ddot{\mathbf{u}} + \mathbf{H}_2^{\mathrm{T}}\,\mathbf{R}_r^{\mathrm{T}}\left[\mathbf{I}_\rho\,\ddot{\mathbf{w}} + \widetilde{\dot{\mathbf{w}}}\mathbf{I}_\rho\,\dot{\mathbf{w}}\right]\right\}\mathrm{d}l\right]\,. \tag{78}$$

Using the local forms $\ddot{\mathbf{u}}^e$, $\dot{\mathbf{w}}^e$ and $\ddot{\mathbf{w}}^e$ (see Eqs. (67), (74) and (77)), the expression of the inertia force vector reduces to

$$\mathbf{f}_k = \mathbf{E}\left[\int_{l_o}\left\{\mathbf{H}_1^{\mathrm{T}}\,A_\rho\,\ddot{\mathbf{u}}^e + \mathbf{H}_2^{\mathrm{T}}\left[\mathbf{I}_\rho^e\,\ddot{\mathbf{w}}^e + \widetilde{\dot{\mathbf{w}}^e}\mathbf{I}_\rho^e\,\dot{\mathbf{w}}^e\right]\right\}\mathrm{d}l\right]\,, \tag{79}$$

with (see Eq. (45))

$$\mathbf{I}_\rho^e = {\mathbf{R}_r}^{\mathrm{T}}\,\mathbf{I}_\rho\,\mathbf{R}_r = \overline{\mathbf{R}}\,\mathbf{J}_\rho\,\overline{\mathbf{R}}^{\mathrm{T}}\,. \tag{80}$$

$\overline{\mathbf{R}}$ is the rotation matrix associated with the local cross-section rotation (see Fig. 4). Since the local rotation is small, $\overline{\mathbf{R}}$ is calculated using

$$\overline{\mathbf{R}} = \mathbf{I} + \widetilde{\overline{\boldsymbol{\theta}}}\,, \tag{81}$$

where $\overline{\boldsymbol{\theta}}$ is given by Eq. (39).

As shown in the above equation, the inertia force vector depends on $\mathbf{d}_g, \dot{\mathbf{d}}_g$ and $\ddot{\mathbf{d}}_g$. Hence, linearization of this force vector is evaluated as follows

$$\Delta\mathbf{f}_k = \mathbf{M}\Delta\ddot{\mathbf{d}}_g + \mathbf{C}_k\Delta\dot{\mathbf{d}}_g + \mathbf{K}_k\Delta\mathbf{d}_g\,. \tag{82}$$

Some authors proposed to keep only the mass matrix $\mathbf{M}$, and to eliminate the gyroscopic $\mathbf{C}_k$ and centrifugal $\mathbf{K}_k$ dynamic matrices [10, 22]. However, in [35], extensive numerical studies have shown that it is better to keep also the gyroscopic matrix in order to enhance the computational efficiency. The same approach is used here. The centrifugal matrix, whose derivation is complicated and would give a lengthy mathematical expression, is neglected. Therefore, the iterative scheme of the present formulation is implemented with the following approximative linearization

$$\Delta\mathbf{f}_k \approx \mathbf{M}\Delta\ddot{\mathbf{d}}_g + \mathbf{C}_k\Delta\dot{\mathbf{d}}_g\,. \tag{83}$$

From the expressions (67), (74) and (77), the following linearizations are derived for the translational acceleration

$$\begin{aligned}\Delta\ddot{\mathbf{u}}^e &= \mathbf{H}_1\,\mathbf{E}^{\mathrm{T}}\,\Delta\ddot{\mathbf{d}}_g + \mathbf{C}_1\,\mathbf{E}^{\mathrm{T}}\,\Delta\dot{\mathbf{d}}_g + \left(\frac{\partial\mathbf{C}_1}{\partial\dot{\mathbf{d}}_g}\Delta\dot{\mathbf{d}}_g\right)\mathbf{E}^{\mathrm{T}}\,\dot{\mathbf{d}}_g + f(\Delta\mathbf{d}_g)\\ &= \mathbf{H}_1\,\mathbf{E}^{\mathrm{T}}\,\Delta\ddot{\mathbf{d}}_g + (\mathbf{C}_1 + \mathbf{C}_3)\,\mathbf{E}^{\mathrm{T}}\,\Delta\dot{\mathbf{d}}_g + f(\Delta\mathbf{d}_g)\,,\end{aligned} \tag{84}$$

for the angular velocity

$$\Delta\dot{\mathbf{w}}^e = \mathbf{H}_2\,\mathbf{E}^{\mathrm{T}}\,\Delta\dot{\mathbf{d}}_g + f(\Delta\mathbf{d}_g)\,, \tag{85}$$

and for the angular acceleration

$$\begin{aligned}\Delta\dot{\mathbf{w}}^e &= \mathbf{H}_2\,\mathbf{E}^{\mathrm{T}}\,\Delta\ddot{\mathbf{d}}_g + \mathbf{C}_2\,\mathbf{E}^{\mathrm{T}}\,\Delta\dot{\mathbf{d}}_g + (\frac{\partial \mathbf{C}_2}{\partial \dot{\mathbf{d}}_g}\Delta\dot{\mathbf{d}}_g)\,\mathbf{E}^{\mathrm{T}}\,\dot{\mathbf{d}}_g + f(\Delta\mathbf{d}_g)\\ &= \mathbf{H}_2\,\mathbf{E}^{\mathrm{T}}\,\Delta\ddot{\mathbf{d}}_g + (\mathbf{C}_2+\mathbf{C}_4)\,\mathbf{E}^{\mathrm{T}}\,\Delta\dot{\mathbf{d}}_g + f(\Delta\mathbf{d}_g)\,,\end{aligned} \tag{86}$$

with $\mathbf{C}_3$ and $\mathbf{C}_4$ given in Appendix B.

Finally, the explicit expressions of the mass matrix $\mathbf{M}$ and of the gyroscopic matrix $\mathbf{C}_k$ are derived using the above linearizations and their expressions are given by

$$\mathbf{M} = \mathbf{E}\left\{\int_{l_o}\left(\mathbf{H}_1^{\mathrm{T}} A_\rho\,\mathbf{H}_1 + \mathbf{H}_2^{\mathrm{T}}\,\mathbf{I}_\rho^e\,\mathbf{H}_2\right)\mathrm{d}l\right\}\mathbf{E}^{\mathrm{T}} = \mathbf{E}\,\mathbf{M}^e\,\mathbf{E}^{\mathrm{T}}\,, \tag{87}$$

$$\begin{aligned}\mathbf{C}_k =& \mathbf{E}\left\{\int_{l_o}\mathbf{H}_1^{\mathrm{T}} A_\rho\,(\mathbf{C}_1+\mathbf{C}_3)\,\mathrm{d}l + \int_{l_o}\mathbf{H}_2^{\mathrm{T}}\,\mathbf{I}_\rho^e\,(\mathbf{C}_2+\mathbf{C}_4)\,\mathrm{d}l\right.\\ &\left.+\int_{l_o}\mathbf{H}_2^{\mathrm{T}}\left(\widetilde{\dot{\mathbf{w}}^e}\mathbf{I}_\rho^e - \widetilde{\mathbf{I}_\rho^e\dot{\mathbf{w}}^e}\right)\mathbf{H}_2\mathrm{d}l\right\}\mathbf{E}^{\mathrm{T}} = \mathbf{E}\,\mathbf{C}_k^e\,\mathbf{E}^{\mathrm{T}}\,.\end{aligned} \tag{88}$$

6.4 Numerical integration

The internal force vector $\mathbf{f}_g$ and the tangent stiffness matrix $\mathbf{K}_g$ are exactly evaluated without numerical integrations.

Concerning the dynamic terms, i.e. the inertia force vector $\mathbf{f}_k$, the mass matrix $\mathbf{M}$ and the gyroscopic matrix $\mathbf{C}_k$, two approaches have been implemented. The first one, referred to "cubic corotational approach", is the one presented in this section. Three Gauss points are used to integrate Eqs. (79), (87) and (88). The second approach, referred to "linear corotational approach", is obtained by assuming linear interpolations for all local quantities. This mean that the cubic interpolations N_5 and N_6 are replaced with N_1 and N_2 in Eq. (37), and that the local transverse displacements $\overline{u}_2$ and $\overline{u}_3$ are zero (see Eq. (37)). For this linear approach, two Gauss points are used to calculate the inertia force vector and the tangent dynamic matrix. It can be observed that linear local interpolations imply $\mathbf{u}_l = \mathbf{0}_{3\times 1}$, which simplifies significantly the computations.

It should be noted that, in these two corotational approaches, all the quantities at the Gauss point are directly calculated from the nodal ones. Therefore, no extra storage is needed.

7 Nonlinear equation of motion and time stepping method

The nonlinear equation of motion is

$$\mathbf{f}_{\mathrm{ext}} - \mathbf{f}_g(\mathbf{d}_g) - \mathbf{f}_k(\mathbf{d}_g,\dot{\mathbf{d}}_g,\ddot{\mathbf{d}}_g) = \mathbf{0}\,. \tag{89}$$

This equation is time-discretized using the Newmark scheme. The resulting nonlinear discrete system of equations is solved at each time step using Newton-Raphson iterations. One important issue here is that the finite rotations are non-additive and non-commutative. Consequently, they cannot be updated in the same simple way as the translational displacements. In this work, the standard Newmark method is adopted for the translational displacements and the method proposed by Simo and Vu-Quoc [48] is used for the finite rotations.

The standard relations of the Newmark method for the translational displacements are

$$\mathbf{u}_{n+1} = \mathbf{u}_n + h\dot{\mathbf{u}}_n + h^2\left[(\frac{1}{2}-\beta)\ddot{\mathbf{u}}_n + \beta\,\ddot{\mathbf{u}}_{n+1}\right], \tag{90}$$

$$\dot{\mathbf{u}}_{n+1} = \dot{\mathbf{u}}_n + h\left[(1-\gamma)\ddot{\mathbf{u}}_n + \gamma\ddot{\mathbf{u}}_{n+1}\right], \tag{91}$$

which gives for the linearizations of the translational velocity and acceleration

$$\Delta\dot{\mathbf{u}}_{n+1} = \frac{\gamma}{\beta h}\Delta\mathbf{u}_{n+1}\,, \tag{92}$$

$$\Delta\ddot{\mathbf{u}}_{n+1} = \frac{1}{\beta h^2}\Delta\mathbf{u}_{n+1}\,, \tag{93}$$

with h, γ, β denoting the time step and the parameters of Newmark method, respectively.

According to Simo and Wong [49], the above described classic Newmark scheme can directly be applied only in the material representation. This method has been adopted in many works. However, it was recently pointed out by Mäkinen [37] that this method is not consistent. Nevertheless, the inconsistency does not affect the numerical results. Therefore, this method is adopted in the present formulation. Due to the fact that the spatial spin variables are chosen to represent the finite rotations, the update procedure is reformulated in the spatial representation as (see [26, 35] for more details)

$$\boldsymbol{\theta}^{g}_{n+1} = h\dot{\mathbf{w}}_n + h^2\left[(\frac{1}{2}-\beta)\ddot{\mathbf{w}}_n + \beta\,(\boldsymbol{\Lambda}^{g}_{n+1})^{\mathrm{T}}\ddot{\mathbf{w}}_{n+1}\right], \tag{94}$$

$$\dot{\mathbf{w}}_{n+1} = \boldsymbol{\Lambda}^{g}_{n+1}\left[\dot{\mathbf{w}}_n + h(1-\gamma)\ddot{\mathbf{w}}_n\right] + h\gamma\ddot{\mathbf{w}}_{n+1}\,, \tag{95}$$

with $\boldsymbol{\theta}^{g}_{n+1}$ denoting the global incremental rotational vector, defined by

$$\boldsymbol{\Lambda}^{g}_{n+1} = \exp(\widetilde{\boldsymbol{\theta}^{g}_{n+1}}) = \mathbf{R}^{g}_{n+1}\,(\mathbf{R}^{g}_{n})^{\mathrm{T}}, \tag{96}$$

where $\mathbf{R}^{g}_{n+1}$ is the global rotation matrix at the time instant t_{n+1}.

The linearizations of the angular velocity and acceleration are given by

$$\Delta\dot{\mathbf{w}}_{n+1} = \frac{\gamma}{\beta h}\mathbf{T}_s^{-\mathrm{T}}(\boldsymbol{\theta}^{g}_{n+1})\Delta\mathbf{w}_{n+1}\,, \tag{97}$$

$$\Delta\ddot{\mathbf{w}}_{n+1} = \frac{1}{\beta h^2}\mathbf{T}_s^{-\mathrm{T}}(\boldsymbol{\theta}^{g}_{n+1})\Delta\mathbf{w}_{n+1}\,. \tag{98}$$

From the relations (94) and (95), the update procedures of the global incremental rotational vector, the angular velocities, and accelerations at the i^{th} iteration of step $(n+1)$ are performed as follows

$$\exp(\widetilde{\boldsymbol{\theta}^{g,i}_{n+1}}) = \exp(\widetilde{\Delta\mathbf{w}^{i}_{n+1}})\exp(\widetilde{\boldsymbol{\theta}^{g,i-1}_{n+1}})\,, \tag{99}$$

$$\dot{\mathbf{w}}^{i}_{n+1} = \boldsymbol{\Lambda}^{g,i}_{n+1}\left[\frac{\gamma}{\beta h}\boldsymbol{\theta}^{i}_{n+1} + \frac{\beta-\gamma}{\beta}\dot{\mathbf{w}}_n + \frac{(\beta-0.5\gamma)h}{\beta}\ddot{\mathbf{w}}_n\right], \tag{100}$$

$$\ddot{\mathbf{w}}^{i}_{n+1} = \boldsymbol{\Lambda}^{g,i}_{n+1}\left[\frac{1}{\beta h^2}\boldsymbol{\theta}^{i}_{n+1} - \frac{1}{\beta h}\dot{\mathbf{w}}_n - \frac{0.5-\beta}{\beta}\ddot{\mathbf{w}}_n\right]. \tag{101}$$

From the linearizations given by Eqs. (92), (93), (97) and (98), the following relations are obtained

$$\Delta\dot{\mathbf{d}}_{g,n+1} = \frac{\gamma}{\beta h}\,\mathbf{B}_t\,\Delta\mathbf{d}_{g,n+1}\,, \tag{102}$$

$$\Delta\ddot{\mathbf{d}}_{g,n+1} = \frac{1}{\beta h^2}\,\mathbf{B}_t\,\Delta\mathbf{d}_{g,n+1}\,, \tag{103}$$

with $\mathbf{B}_t = \begin{bmatrix} \mathbf{I} & \mathbf{0} & \mathbf{0} & \mathbf{0} \\ \mathbf{0} & \mathbf{T}_s^{-\mathrm{T}}(\boldsymbol{\theta}^{g}_{1,n+1}) & \mathbf{0} & \mathbf{0} \\ \mathbf{0} & \mathbf{0} & \mathbf{I} & \mathbf{0} \\ \mathbf{0} & \mathbf{0} & \mathbf{0} & \mathbf{T}_s^{-\mathrm{T}}(\boldsymbol{\theta}^{g}_{2,n+1}) \end{bmatrix}$.

Finally, the iterative tangent matrix required to solve the nonlinear equation of motion reads as follows

$$\mathbf{K}_{\text{Total}} = \mathbf{K}_g + \frac{1}{\beta h^2}\mathbf{M}\mathbf{B}_t + \frac{\gamma}{\beta h}\mathbf{C}_k\mathbf{B}_t\,. \tag{104}$$

8 Numerical examples

The purpose of this section is to assess the performance of the new two-noded higher order (cubic) beam element. The predictions of this new element are compared against those of two linear beam elements: the "linear" corotational beam element and the total Lagrangian formulation proposed by Simo and Vu-Quoc [46–48]. The new formulation employs cubic interpolation for all terms. The "linear" formulation uses cubic interpolation for the internal force vector and the corresponding stiffness matrix whereas the inertia terms are evaluated considering linear interpolation. In the geometrically exact beam formulation which employs spatial spin variables, the internal force vector and the tangent stiffness matrix are numerically integrated using one Gauss point whereas the inertia force vector and the dynamic tangent matrix are numerically integrated using two Gauss points. All the three formulations are implemented using Matlab. The same levels of optimisation in forming the element matrices and force vectors are carefully checked.

Four numerical examples, consisting of slender beams for which bending shear effects are negligible, are considered. For each example, the solutions given by the three dynamic formulations are compared against a reference solution. The latter is obtained by increasing the number of elements until the three dynamic formulations converge towards the same results.

Among the four examples, the first one has been proposed by Simo and Vu-Quoc [48]. This problem is very popular and has been considered by many authors as a test for nonlinear dynamic formulations involving large rotations. In this example, the reference solution is in a good agreement with the results found in the literature. For the three other examples, additional analyses with Abaqus are performed in order to assess the quality of the reference solutions. Two different beam elements are used. The first one is B31, which is based on the classical Timoshenko beam theory. The second one is B33, which is based on the classical Euler-Bernoulli beam theory. With refined meshes and refined time step sizes, these two elements converged towards the selected reference solutions. It can also be concluded that in these three examples, the shear effects are very small and can be neglected.

In their work, Simo and Vu-Quoc [48] employed the Newmark trapezoidal rule. When applied to nonlinear dynamics, this scheme can be unstable [14, 32, 51]. To avoid this problem, the HHT α method [12] with $\alpha = -0.05$ is employed in this work. This value of α, which is typically adopted in nonlinear dynamic analyses [10, 16, 32] and also used as default in Abaqus, gives a small numerical damping and limits the influence of high frequencies. However, a numerical damping gives also a dissipation of the total energy, which can affect the results for large time intervals.

During the time period under consideration, the time step size remains constant. Except for the first example, for which the time step size is taken as in the literature [26,31,32,48,53], the time step size is carefully selected. For that, the same example is run using $0.5\,\Delta t$. The time step is accepted if both runs provide the same results.

At the beginning of each time step, a predictor is used to initiate the iterative procedure. Several predictors are available in the literature and a comparative study of the performances of these predictors can be found in [35]. As shown in [35], the quality of the predictor has a significant influence on the convergence of the iterative procedure. In the present work, the predictor proposed by Crisfield [12] for the particular case of linear inertia force vector and further developed in the general case by the authors [35], is adopted. The idea of this predictor is to use the tangent operator at the time instant t_n to predict the values at the time instant t_{n+1}. This predictor is the most effective among the four ones compared in [35].

Damping is not considered and the following convergence criterion is adopted: the norm of the residual

vector must be less than the prescribed tolerance $\varepsilon_f = 10^{-5}$.

8.1 Example 1: Right-angle cantilever beam

This classic example, introduced by Simo and Vu-Quoc [48], has often been used in order to validate various nonlinear dynamic formulations [22, 26, 32, 38]. A right-angle cantilever, depicted in Fig. 5, is subjected to an out-of-plane concentrated load applied at the elbow. Each member of the cantilever has a length $L = 10$. The material properties are $GA = EA = 10^6$, $GJ = EI = 10^3$. The mass per unit length of the beam and the inertia dyadic of the cross section in the initial configuration are $A_\rho = 1$ and $\mathbf{J}_\rho = \text{diag}(20, 10, 10)$, respectively.

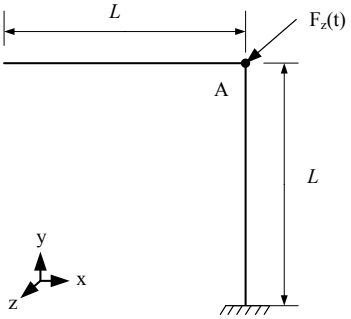

Fig. 5. Right-angle cantilever beam : geometrical data.

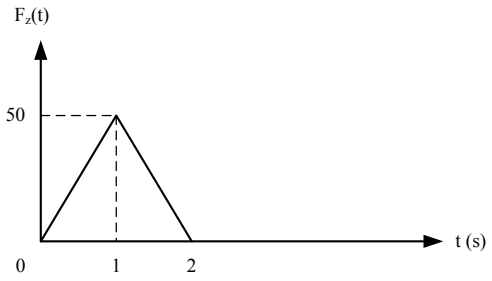

Fig. 6. Right-angle cantilever beam - Loading history.

The load (see Fig. 6) acts only during $0 \leq t(s) \leq 2$ and thereafter the cantilever undergoes large-scale free vibrations. The applied force increases linearly until the value of 50 is reached at one second and decreases from there to zero within one further second. The resulting amplitude of vibration is of the same order of magnitude as the structure's dimensions. The reference solution has been obtained with a total of 20 beam elements (10 elements per member) whereas the predictions of the three aforementioned formulations were obtained using only 4 elements (2 elements per member).

The time evolution of the displacements of node A are depicted in Figs. 7, 8 and 9. The computations are performed with $\Delta t = 0.25$ s. It can be seen that with only 4 beam elements, the cubic corotational approach gives almost the same results as the reference solution over the whole time domain. The results obtained with the linear corotational approach are very close to the reference solution with minor differences. However, the results obtained with the formulation of Simo and Vu-Quoc deviate significantly from the reference solution which is obviously due to the linear nature of the interpolation.

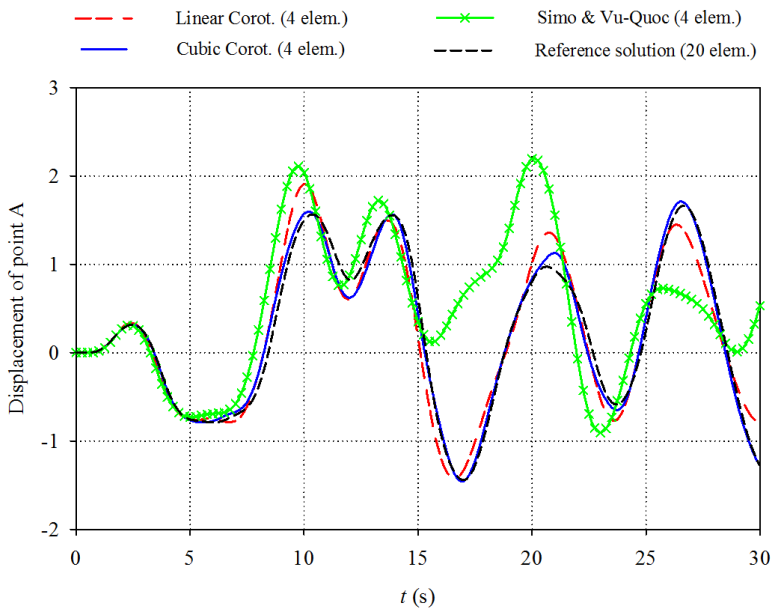

Fig. 7. Right-angle cantilever beam - Time evolution of the displacement u_y of point A.

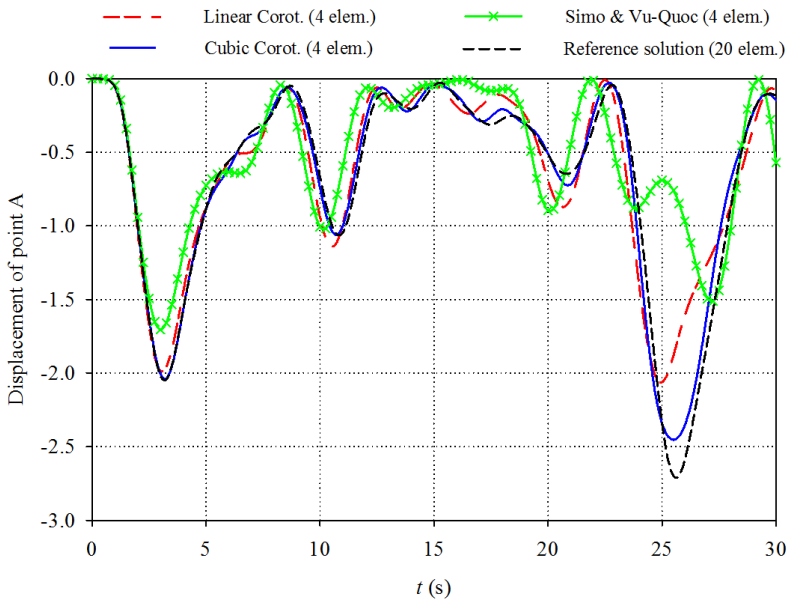

Fig. 8. Right-angle cantilever beam - Time evolution of the displacement u_x of point A.

The time evolution of the displacement u_y of node A and of the displacement u_z of node B, calculated with a total of 8 beam elements (4 elements per member), are depicted in Figs. 10 and 11. It can be noted that the differences between the formulation of Simo and Vu-Quoc and the reference solution become smaller, but also that the cubic corotational formulation gives very accurate results.

In the current example, the energy blow-up could happen at approximately $t = 45$ s. This numerical instability has been reported by Jelenić and Crisfield [31, 32] and by Zupan et al. [53]. Therefore, to assess the stability of the HHT α method when combined with the new cubic formulation, this example is run for a

time period of 150 s using a total of 20 beam elements and a time step $\Delta t = 0.25$ s. The time evolution of the total energy is depicted in Fig. 12. The result indicates that the new formulation is stable during the time period under consideration. The dissipation of energy between $t = 2$ s and $t = 30$ s is about 3%.

The CPU time and the total number of iterations required for each formulation are presented in Table 1. With the same number of elements, the linear corotational approach is the fastest approach and the cubic corotational approach is the slowest one.

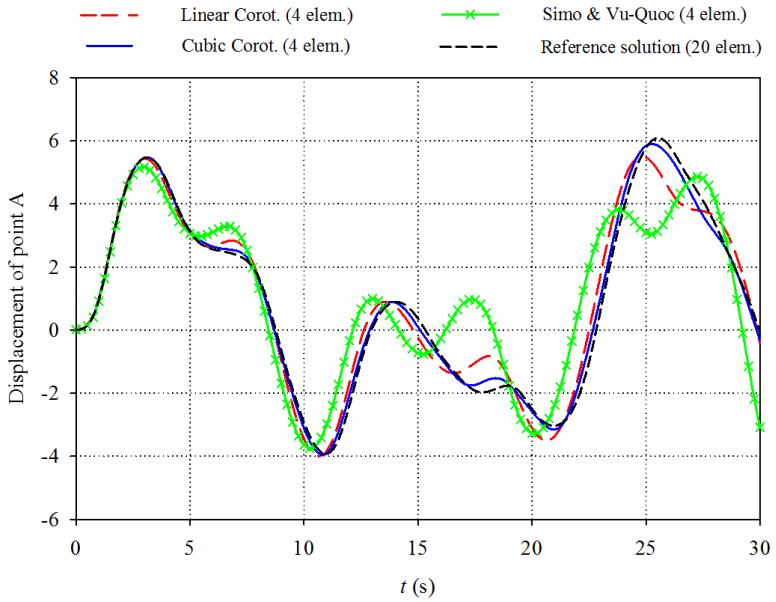

Fig. 9. Right-angle cantilever beam - Time evolution of the displacement u_z of point A.

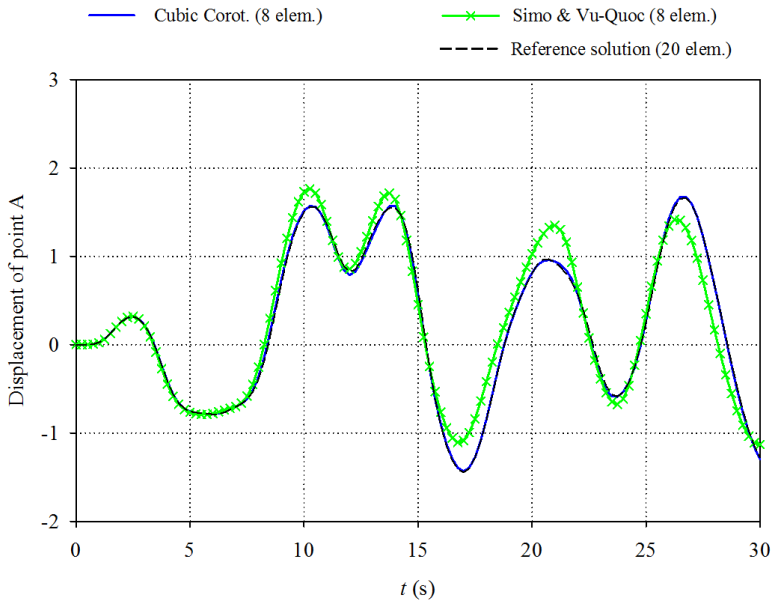

Fig. 10. Right-angle cantilever beam - Time evolution of the displacement u_y of point A.

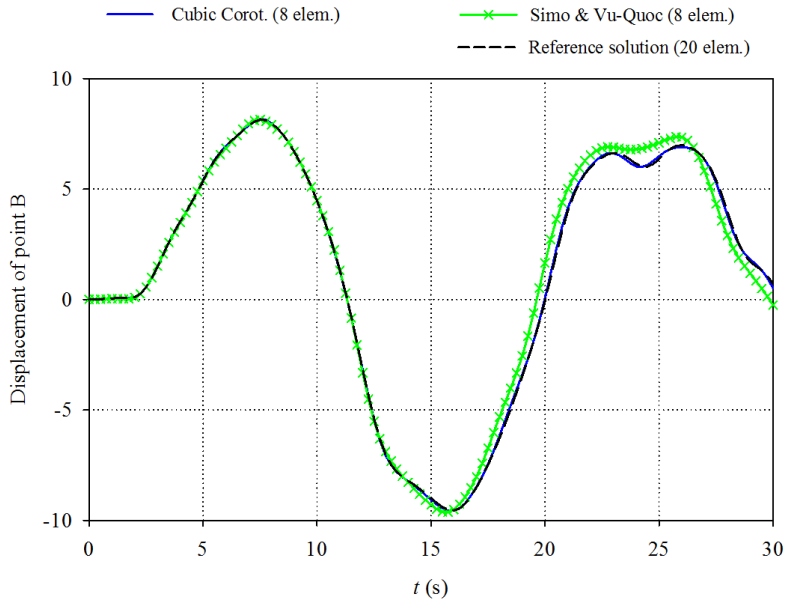

Fig. 11. Right-angle cantilever beam - Time evolution of the displacement u_z of point B.

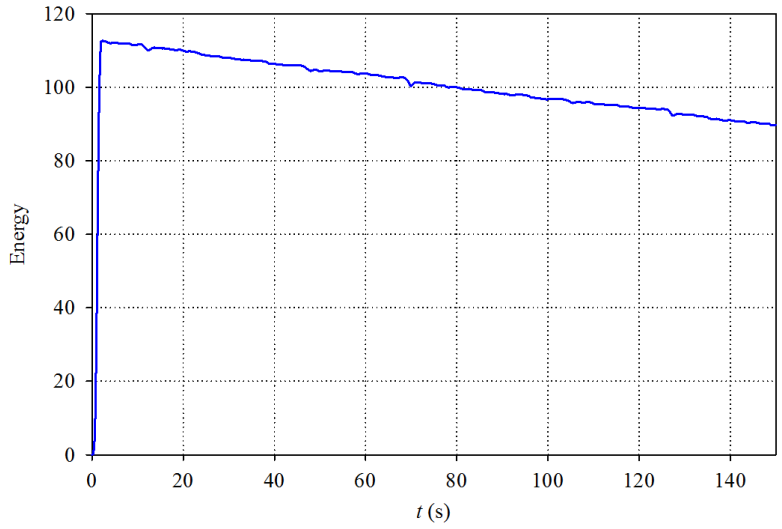

Fig. 12. Right-angle cantilever beam - Time evolution of the total energy.

Table 1. Right-angle cantilever beam - CPU time (Total number of iterations).

Number of beam elements	Linear corot.	Cubic corot.	Simo & Vu-Quoc
4	3.66 (633)	5.31 (637)	4.59 (521)
20	19.84 (636)	25.61 (612)	22.90 (517)

8.2 Example 2: Cantilever beam

The second example is a cantilever beam of length $L = 10$ m with uniform cross-section (see Fig. 13). The beam is clamped at one end and subjected to a sinusoidal out-of-plane force $F_z(t)$ and a bending moment $M_z(t)$ at the free end (see Fig. 14). The circular frequency of the force w is 50 rad/s. The bending moment

increases linearly until the value of 3 is reached at 0.3 second and decreases from there to zero within a further 0.3 second. The cross-section width and depth are $e = 0.25$ m and $a = 0.3$ m, respectively. The elastic modulus of the beam E is 210 GPa and the Poisson's ratio ν is 0.3. The mass per unit volume is $\rho = 7850$ kg/m^3.

The time step size is chosen as $\Delta t = 5 \cdot 10^{-4}$ s.

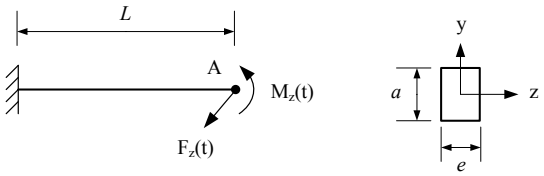

Fig. 13. Cantilever beam : geometrical data.

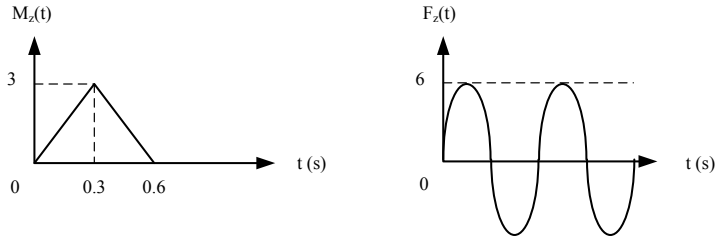

Fig. 14. Cantilever beam - Loading history.

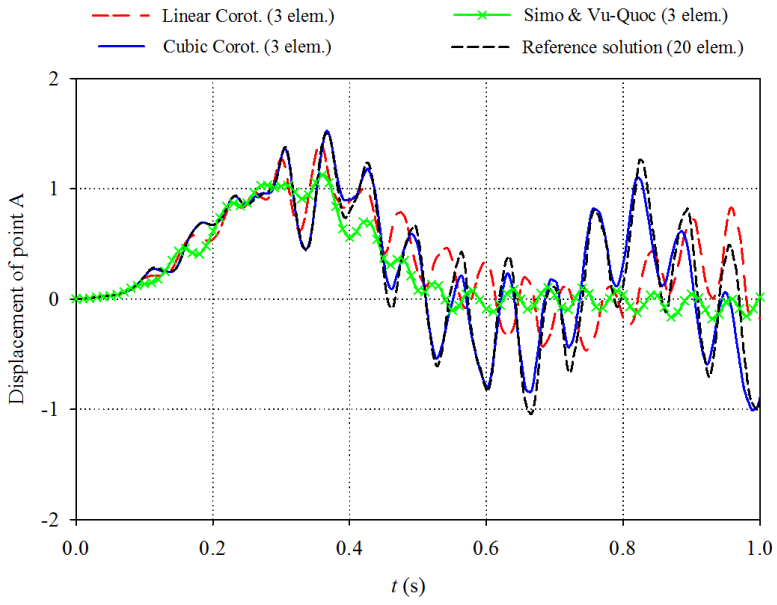

Fig. 15. Cantilever beam - Time evolution of the displacement u_y of point A.

The reference solution has been obtained with a total of 20 beam elements whereas only 3 beam elements are used for the computations with the three formulations. The displacements of the free end A are depicted

in Figs. 15, 16 and 17.

It can be noted that the results obtained with the cubic corotational approach are very close to the reference solution. However, large discrepancies between the results obtained with the two other formulations and the reference solution can be observed. As for the first example, with the same number of elements, the linear corotational approach is the fastest formulation and the cubic corotational approach is the slowest one (see Table 2).

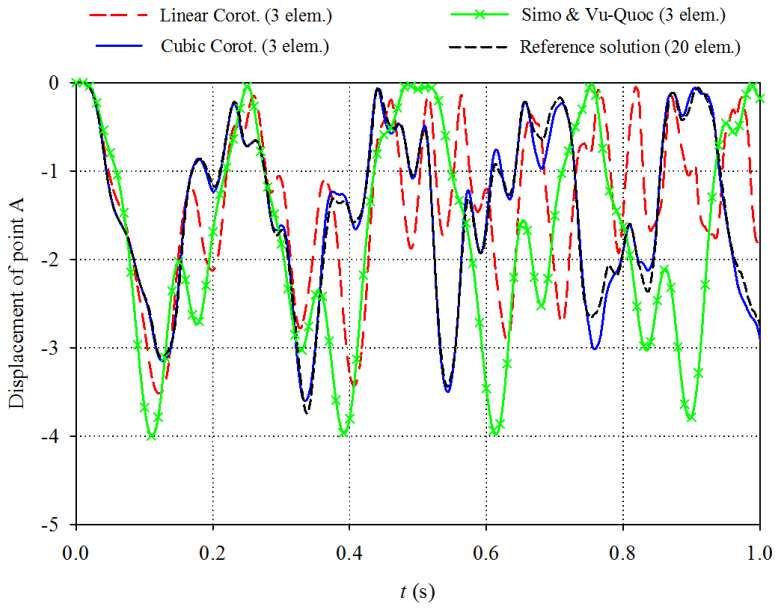

Fig. 16. Cantilever beam - Time evolution of the displacement u_x of point A.

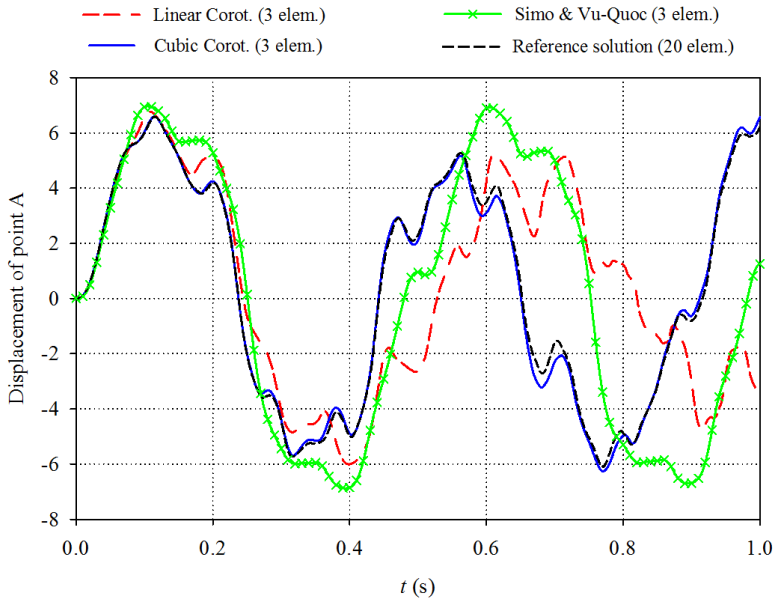

Fig. 17. Cantilever beam - Time evolution of the displacement u_z of point A.

Table 2. Cantilever beam - CPU time (Total number of iterations).

Number of beam elements	Linear corot.	Cubic corot.	Simo & Vu-Quoc
3	24.97 (5844)	34.22 (5829)	27.45 (4339)
20	164.86 (5346)	227.01 (5486)	220.94 (5394)

8.3 Example 3: Shallow arch

A circular shallow arch (see Fig. 18) of span $L = 20$ m and clamped at both ends is considered. The radius R of the arch is equal to 20 m with $\phi = 30^\circ$. The shallow arch has a uniform square cross-section with $a = 0.25$ m. The arch is subjected to a vertical force $F_y(t)$ and to an out-of-plane sinusoidal force $F_z(t)$ (see Fig. 19). The circular frequency of $F_z(t)$ is $w = 10$ rad/s and the load $F_y(t)$ is applied during a short time (0.1 second). The arch has a modulus of elasticity $E = 210$ GPa, and a Poisson's ratio $\nu = 0.3$. The mass per unit volume ρ is 7850 kg/m^3.

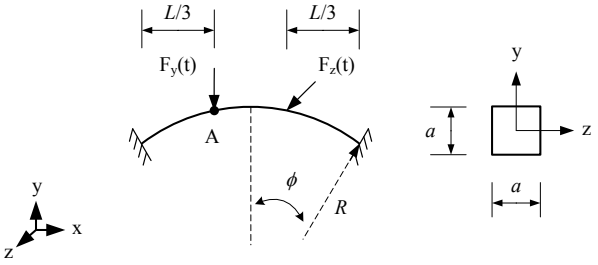

Fig. 18. Shallow arch : geometrical data.

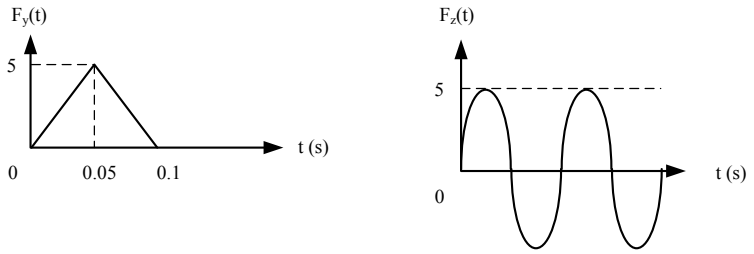

Fig. 19. Shallow arch - Loading history.

The time step size Δt is chosen to be equal to 10^{-3} s. The reference solution has been obtained with 21 elements whereas only 6 elements have been used to perform the analysis with the three formulations. The time histories of the displacements of point A are depicted in Figs. 20, 21 and 22. Again, it can be observed that, with only 6 elements, the results obtained with the cubic corotational approach are in very good agreement with the reference solution. However, the discrepancy between the reference solution and the results obtained with the two other formulations is, as expected, significant.

The CPU time and the total number of iterations required for each formulation are presented in Table 3. The results show that again the fastest formulation is the linear corotational approach. With the coarse

mesh, the cubic corotational formulation is just slightly slower than Simo and Vu-Quoc's one, and the contrary applies with the fine mesh.

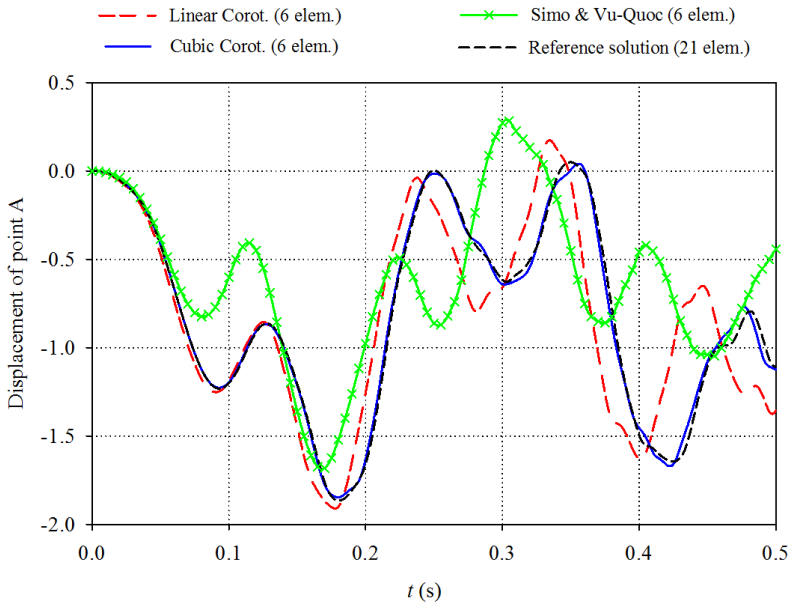

Fig. 20. Shallow arch - Time evolution of the displacement u_y of point A.

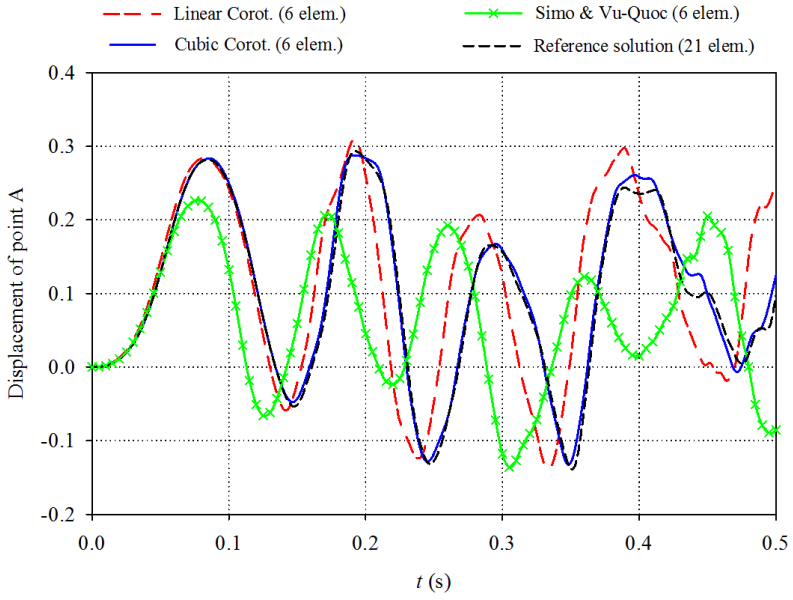

Fig. 21. Shallow arch - Time evolution of the displacement u_x of point A.

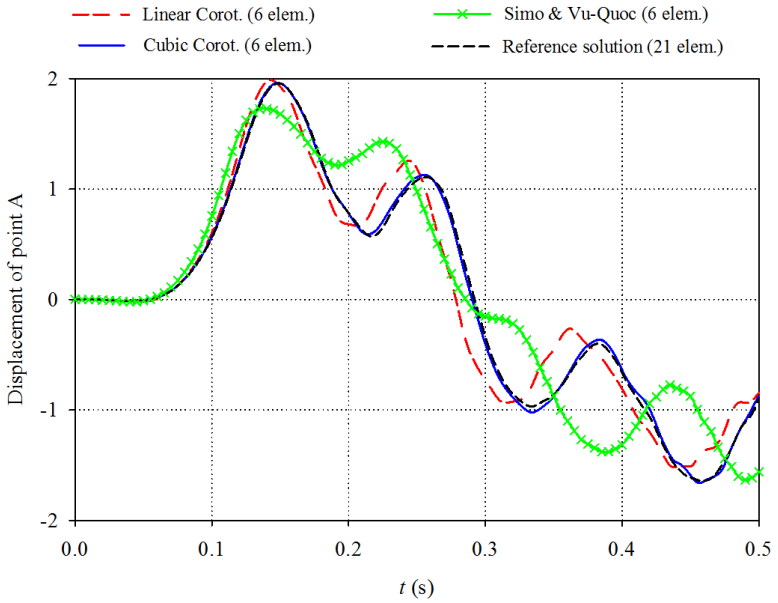

Fig. 22. Shallow arch - Time evolution of the displacement u_z of point A.

Table 3. Shallow arch - CPU time (Total number of iterations).

Number of beam elements	Linear corot.	Cubic corot.	Simo & Vu-Quoc
6	11.04 (1420)	16.32 (1412)	15.05 (1208)
21	40.63 (1292)	54.74 (1286)	58.39 (1270)

8.4 Example 4: Lee's frame

The Lee's frame with uniform rectangular cross-section and subjected to two out-of-plane forces is considered (see Figs. 23 and 24). Both forces increase linearly until the value of 3 is reached at 0.1 second and decreases from there to zero within a further 0.1 second. The frame and cross-section data are: $L = 12$ m, $a = 0.2$ m and $e = 0.3$ m. The members of the frame have a modulus of elasticity $E = 210$ GPa and a Poisson's ratio $\nu = 0.3$. The mass per unit volume ρ is 7850 kg/m^3.

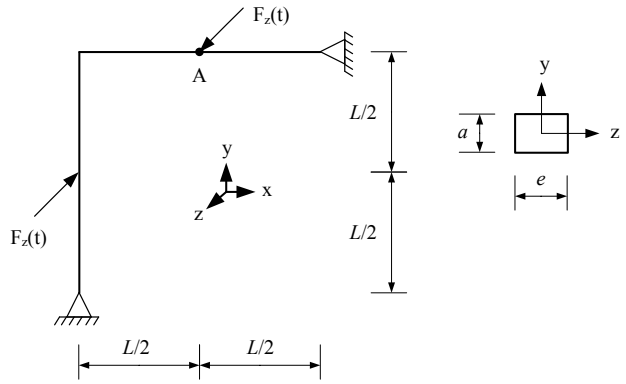

Fig. 23. Lee's frame : geometrical data.

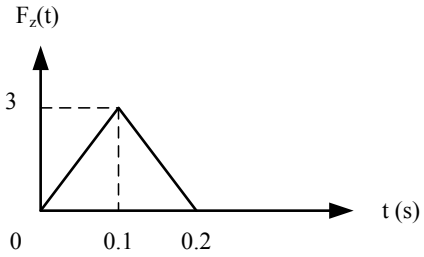

Fig. 24. Lee's frame - Loading history.

The displacements of point A are investigated. The reference solution, obtained with 40 elements (20 elements per member), and the results obtained with the three formulations considering only 8 elements (4 elements per member) are shown in Figs. 25, 26 and 27. The time step size is $\Delta t = 10^{-3}$ s.

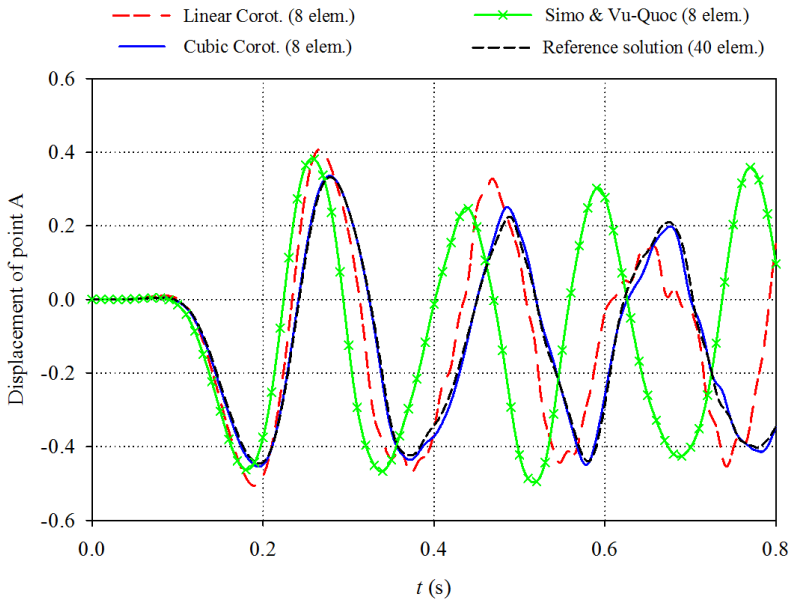

Fig. 25. Lee's frame - Time evolution of the displacement u_y of point A.

It can be observed that with only 8 elements, the cubic corotational approach gives results that are in very good agreement with the reference solution. However, the results obtained with the two other approaches are significantly different from the reference solution over the whole time domain.

The time evolution of the displacement u_z of node A, calculated with a total of 16 beam elements (8 elements per member), is depicted in Fig. 28. It can be noted that the differences between the formulation of Simo and Vu-Quoc and the reference solution become smaller, but also that the cubic corotational formulation gives very accurate results.

As shown in Figs. 27 and 28, the solutions obtained with the formulation of Simo and Vu-Quoc and with the linear corotational formulation present a "period contraction". This is due to the fact that with coarse meshes and linear interpolations, the lowest natural frequencies of the structure are not modelled accurately.

In order to assess the stability of the HHT α method when combined with the new formulation, the current example is run for a time period $t = 4$ s. The time evolution of the total energy is depicted in Fig. 29. The result indicates that the new formulation is stable within the time period under consideration. The dissipation of energy between $t = 0.2$ s and $t = 0.8$ s is 0.8%.

The CPU time and the total number of iterations required for each formulation are presented in Table 4. Again, it can be noted that the linear corotational approach is the fastest. With the coarse mesh, the cubic corotational formulation is just slightly slower than Simo and Vu-Quoc's one, and the contrary applies with the fine mesh.

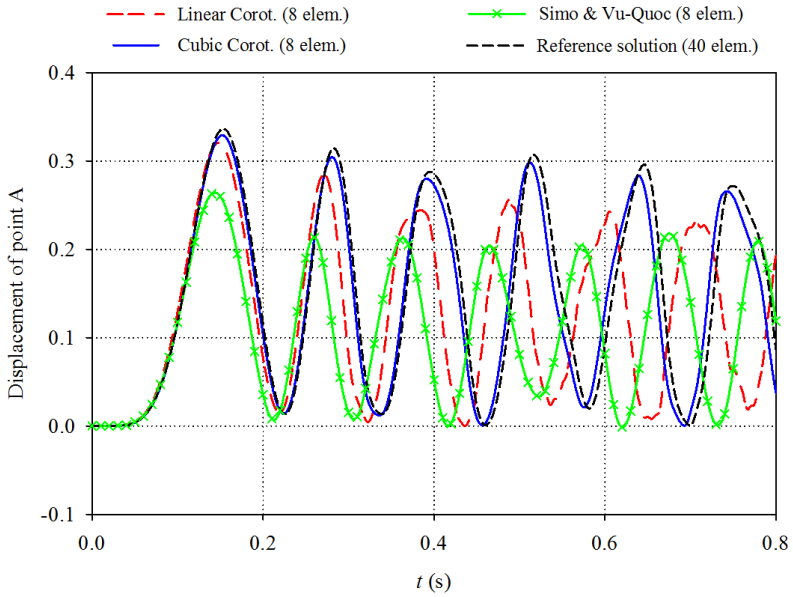

Fig. 26. Lee's frame - Time evolution of the displacement u_x of point A.

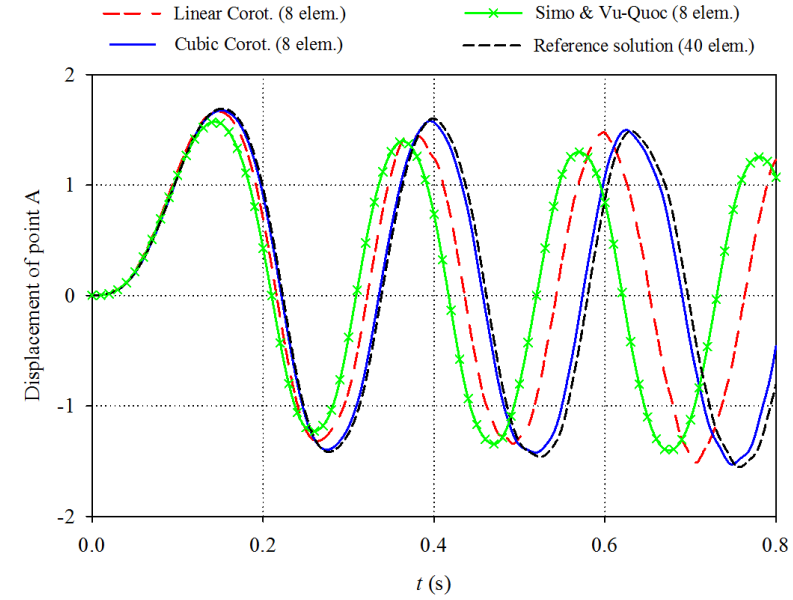

Fig. 27. Lee's frame - Time evolution of the displacement u_z of point A.

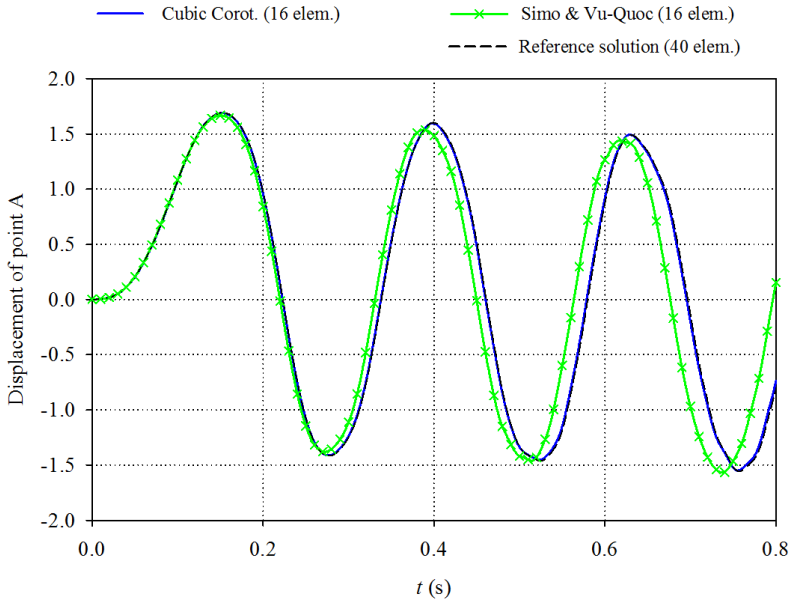

Fig. 28. Lee's frame - Time evolution of the displacement u_z of point A.

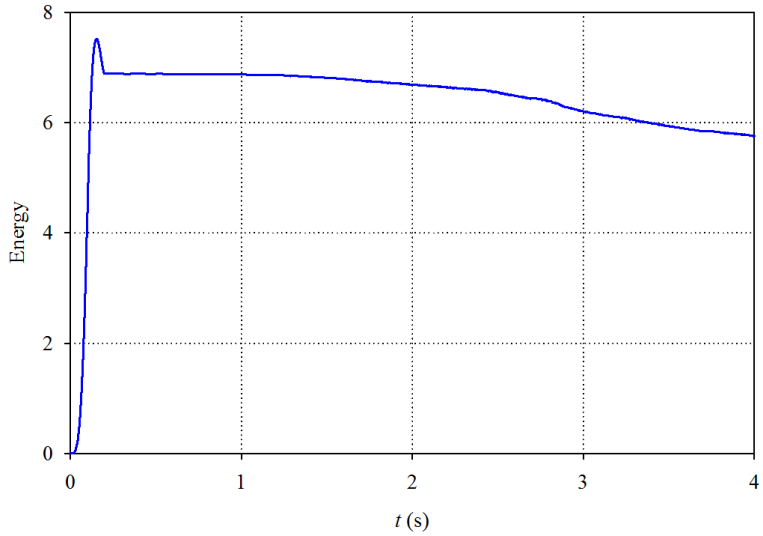

Fig. 29. Lee's frame - Time evolution of the total energy.

Table 4. Lee's frame - CPU time (Total number of iterations).

Number of beam elements	Linear corot.	Cubic corot.	Simo & Vu-Quoc
8	33.78 (2176)	42.02 (2093)	40.59 (1974)
40	122.27 (2056)	163.72 (2044)	181.97 (2072)

9 Conclusion

A new consistent 3D corotational beam element for nonlinear dynamics of flexible structures was presented. The novelty of the formulation is that the corotational framework (i.e. the decomposition into rigid body motion and pure deformation) was adopted to formulate not only the internal force vector and the tangent stiffness matrix, but also the inertia force vector and the tangent dynamic matrix. As consequence, the cubic interpolation functions were used to derive both the inertia and internal local terms. The inertia force vector and the tangent dynamic matrix were analytically formulated by introducing an approximation with regard to the local rotations. To enhance the efficiency of the iterative procedure, an approximative tangent dynamic matrix was adopted.

Four numerical examples were considered to compare the new formulation with two other approaches. The first approach, called as "linear corotational approach", is derived from the new formulation by replacing cubic interpolations with linear ones. The second approach is the classic total Lagrangian proposed by Simo and Vu-Quoc [46–48]. This approach can be implemented with different number of nodes. In order to compare formulations with the same number of degrees of freedom, Simo and Vu-Quoc's approach has been implemented with two nodes which correspond to a linear interpolations for all global variables. Based on these examples, the following conclusions can be drawn:

- All formulations give the same results with fine meshes.
- As expected, with coarse meshes, Simo and Vu-Quoc's two noded formulation and the linear corotational one give less accurate results compared to the cubic corotational approach which provides very accurate results. This demonstrates the importance of an accurate description of the deformations in the dynamic terms, which is not possible with linear interpolations.
- The linear corotational approach is faster than the cubic one. This was expected since several inertia terms disappear when local linear interpolations are adopted. Moreover, in the linear corotational approach, the inertia force vector and the tangent dynamic matrix are integrated using two Gauss points, whereas the dynamic terms of the cubic corotational one are integrated using three Gauss points.
- As it is more involved, the cubic corotational formulation is slightly slower than linear formuations (around 12%). However, certain cases can arise where the desired accuracy can be achieved via the cubic formulation faster than the linear formulation of Simo and Vu-Quoc.

One can conclude that the new dynamic corotational formulation based on the local cubic interpolations provides sufficient accuracy with relatively low number of elements as compared to linear formulations. With the same number of elements, about the same computational time is required (this can differ a little from one example to another). However, with the present formulation, accurate results can be obtained with a smaller number of elements.

It must be emphasized that the above conclusions are based on a comparative study of two-noded elements available in the literature. However, in the context of the total Lagrangian approach, efficient three-noded elements with quadratic shape functions can be developed, see for instance the formulation for static analysis proposed in [24, 28].

Appendix A Expressions of $\dot{\mathbf{H}}_1$ and $\dot{\mathbf{H}}_2$

By the definition (see Eq. (59)), one has

$$\mathbf{H}_1 = \mathbf{N} + \mathbf{P}_1 \mathbf{P} - \widetilde{\mathbf{u}}_l \mathbf{G}^{\mathrm{T}}. \tag{105}$$

The variation of the above relation reads

$$\delta \mathbf{H}_1 = \mathbf{P}_1 \, \delta \mathbf{P} - \widetilde{\delta \mathbf{u}_l} \, \mathbf{G}^{\mathrm{T}} - \widetilde{\mathbf{u}}_l \, \delta \mathbf{G}^{\mathrm{T}} , \tag{106}$$

where $\mathbf{u}_l$ are the local transverse displacements assumed to be small. Therefore, the last term in Eq. (106) is neglected. In fact, all the four examples presented in the paper have been tested with and without this term. Only negligible differences in the results have been observed.

By using the expressions of the matrices $\mathbf{P}_1$ and $\mathbf{P}$, one obtains

$$\mathbf{P}_1 \, \mathbf{P} = \begin{bmatrix} 0 & 0 & 0 & 0 & 0 & 0 & 0 & 0 & 0 & 0 & 0 & 0 \\ 0 & \dfrac{N_7}{l_n} & 0 & 0 & 0 & N_3 & 0 & \dfrac{-N_7}{l_n} & 0 & 0 & 0 & N_4 \\ 0 & 0 & \dfrac{N_7}{l_n} & 0 & -N_3 & 0 & 0 & 0 & \dfrac{-N_7}{l_n} & 0 & -N_4 & 0 \end{bmatrix} , \tag{107}$$

with $N_7 = N_3 + N_4$.

It is straightforward to take the variation

$$\begin{aligned} \delta(\mathbf{P}_1 \, \mathbf{P}) = \mathbf{P}_1 \, \delta \mathbf{P} &= \frac{N_7}{l_n^2} \, \delta l_n \begin{bmatrix} 0 & 0 & 0 & 0 & 0 & 0 & 0 & 0 & 0 & 0 & 0 & 0 \\ 0 & -1 & 0 & 0 & 0 & 0 & 0 & 1 & 0 & 0 & 0 & 0 \\ 0 & 0 & -1 & 0 & 0 & 0 & 0 & 0 & 1 & 0 & 0 & 0 \end{bmatrix} \\ &= \frac{N_7}{l_n^2} \, \delta l_n \, \mathbf{A}_1 . \end{aligned} \tag{108}$$

Referring first to the current length of the beam element l_n, the variation of Eq. (14) gives

$$\delta l_n = \mathbf{r} \, \delta \mathbf{d}_g , \qquad \mathbf{r} = \begin{bmatrix} -\mathbf{r}_1^{\mathrm{T}} & \mathbf{0}_{[1\times 3]} & \mathbf{r}_1^{\mathrm{T}} & \mathbf{0}_{[1\times 3]} \end{bmatrix} , \tag{109}$$

when $\mathbf{r}_1$ is defined in Eq. (13).

Finally, one obtains

$$\mathbf{P}_1 \, \delta \mathbf{P} = \frac{N_7}{l_n^2} \, \mathbf{A}_1 \, \mathbf{r} \, \delta \mathbf{d}_g . \tag{110}$$

By inserting Eq. (110) into Eq. (106), the variation of $\mathbf{H}_1$ is written as

$$\delta \mathbf{H}_1 = \frac{N_7}{l_n^2} \, \mathbf{A}_1 \, \mathbf{r} \, \delta \mathbf{d}_g - \widetilde{\delta \mathbf{u}_l} \, \mathbf{G}^{\mathrm{T}} . \tag{111}$$

Finally, one has

$$\dot{\mathbf{H}}_1 = \frac{N_7}{l_n^2} \, \mathbf{A}_1 \, \mathbf{r} \, \dot{\mathbf{d}}_g - \widetilde{\mathbf{u}}_l \, \mathbf{G}^{\mathrm{T}} , \tag{112}$$

with (see Eq. (57))

$$\dot{\mathbf{u}}_l = \mathbf{P}_1 \, \mathbf{P} \, \mathbf{E}^{\mathrm{T}} \, \dot{\mathbf{d}}_g . \tag{113}$$

By the definition (see Eq. (72)), one has

$$\mathbf{H}_2 = \mathbf{P}_2 \, \mathbf{P} + \mathbf{G}^{\mathrm{T}} . \tag{114}$$

By inserting the expressions of $\mathbf{P}_2$, $\mathbf{P}$ and $\mathbf{G}$ in the above relation, one obtains

$$\mathbf{H}_2 = \begin{bmatrix} 0 & 0 & 0 & N_1 & 0 & 0 & 0 & 0 & 0 & N_2 & 0 & 0 \\ 0 & 0 & \dfrac{-N_8}{l_n} & 0 & N_5 & 0 & 0 & 0 & \dfrac{N_8}{l_n} & 0 & N_6 & 0 \\ 0 & \dfrac{N_8}{l_n} & 0 & 0 & 0 & N_5 & 0 & \dfrac{-N_8}{l_n} & 0 & 0 & 0 & N_6 \end{bmatrix}, \tag{115}$$

with $N_8 = N_5 + N_6 - 1$.

The variation of Eq. (115) reads

$$\delta\mathbf{H}_2 = \frac{N_8}{l_n^2}\,\delta l_n \begin{bmatrix} 0 & 0 & 0 & 0 & 0 & 0 & 0 & 0 & 0 & 0 & 0 & 0 \\ 0 & 0 & 1 & 0 & 0 & 0 & 0 & -1 & 0 & 0 & 0 & 0 \\ 0 & -1 & 0 & 0 & 0 & 0 & 0 & 1 & 0 & 0 & 0 & 0 \end{bmatrix} = \frac{N_8}{l_n^2}\,\delta l_n\,\mathbf{A}_2\,. \tag{116}$$

With the expression of δl_n given by Eq. (109), one obtains

$$\delta\mathbf{H}_2 = \frac{N_8}{l_n^2}\,\mathbf{A}_2\,\mathbf{r}\,\delta\mathbf{d}_g\,. \tag{117}$$

Therefore, $\dot{\mathbf{H}}_2$ is computed as

$$\dot{\mathbf{H}}_2 = \frac{N_8}{l_n^2}\,\mathbf{A}_2\,\mathbf{r}\,\dot{\mathbf{d}}_g\,. \tag{118}$$

Appendix B Expressions of $\mathbf{C}_3$ and $\mathbf{C}_4$

By the definitions (see Eqs. (84) and (86)), one has

$$\mathbf{C}_3\,\mathbf{E}^{\mathrm{T}}\,\Delta\dot{\mathbf{d}}_g = (\frac{\partial\mathbf{C}_1}{\partial\dot{\mathbf{d}}_g}\Delta\dot{\mathbf{d}}_g)\,\mathbf{E}^{\mathrm{T}}\,\dot{\mathbf{d}}_g\,, \tag{119}$$

$$\mathbf{C}_4\,\mathbf{E}^{\mathrm{T}}\,\Delta\dot{\mathbf{d}}_g = (\frac{\partial\mathbf{C}_2}{\partial\dot{\mathbf{d}}_g}\Delta\dot{\mathbf{d}}_g)\,\mathbf{E}^{\mathrm{T}}\,\dot{\mathbf{d}}_g\,, \tag{120}$$

where $\mathbf{C}_1$ and $\mathbf{C}_2$ are given by Eqs. (66) and (76), respectively.

Eqs. (119) and (120) can be rewritten as

$$\mathbf{C}_3\,\mathbf{E}^{\mathrm{T}}\,\Delta\dot{\mathbf{d}}_g = \left(\widetilde{\Delta\dot{\mathbf{w}}_r^e}\,\mathbf{H}_1 + \Delta\dot{\mathbf{H}}_1 - \mathbf{H}_1\,\Delta\mathbf{E}_t\right)\mathbf{E}^{\mathrm{T}}\,\dot{\mathbf{d}}_g\,, \tag{121}$$

$$\mathbf{C}_4\,\mathbf{E}^{\mathrm{T}}\,\Delta\dot{\mathbf{d}}_g = \left(\widetilde{\Delta\dot{\mathbf{w}}_r^e}\,\mathbf{H}_2 + \Delta\dot{\mathbf{H}}_2 - \mathbf{H}_2\,\Delta\mathbf{E}_t\right)\mathbf{E}^{\mathrm{T}}\,\dot{\mathbf{d}}_g\,. \tag{122}$$

It should be noted that only the variations with respect to $\dot{\mathbf{d}}_g$ are considered.

Using Eq. (54), the first terms in Eqs. (121) and (122) can be obtained as

$$\widetilde{\Delta\dot{\mathbf{w}}_r^e}\,\mathbf{H}_i\,\mathbf{E}^{\mathrm{T}}\,\dot{\mathbf{d}}_g = \widetilde{\Delta\dot{\mathbf{w}}_r^e}\,\mathbf{H}_i\,\dot{\mathbf{d}}_g^e = -\widetilde{\mathbf{h}}_i\,\Delta\dot{\mathbf{w}}_r^e = -\widetilde{\mathbf{h}}_i\,\mathbf{G}^{\mathrm{T}}\,\mathbf{E}^{\mathrm{T}}\,\Delta\dot{\mathbf{d}}_g \quad (i=1,2)\,, \tag{123}$$

with

$$\mathbf{h}_i = \mathbf{H}_i\,\dot{\mathbf{d}}_g^e\,. \tag{124}$$

By noting that (see Eqs. (30), (54) and (57))

$$\dot{\mathbf{w}}_r^e = \mathbf{G}^{\mathrm{T}}\,\dot{\mathbf{d}}_g^e, \qquad \Delta\dot{\mathbf{u}}_l = \mathbf{P}_1\,\mathbf{P}\,\mathbf{E}^{\mathrm{T}}\,\Delta\dot{\mathbf{d}}_g\,, \tag{125}$$

and using Eqs. (112) and (118), the second terms of Eqs. (121) and (122) are given by

$$\begin{aligned}\Delta\dot{\mathbf{H}}_1\,\mathbf{E}^{\mathrm{T}}\,\dot{\mathbf{d}}_g &= \Delta\dot{\mathbf{H}}_1\,\dot{\mathbf{d}}_g^e = \left(\frac{N_7}{l_n^2}\,\mathbf{A}_1\,\mathbf{r}\,\Delta\dot{\mathbf{d}}_g - \widetilde{\Delta\dot{\mathbf{u}}_l}\,\mathbf{G}^{\mathrm{T}}\right)\dot{\mathbf{d}}_g^e \\ &= \frac{N_7}{l_n^2}\,\mathbf{A}_1\,\dot{\mathbf{d}}_g^e\,\mathbf{r}\,\Delta\dot{\mathbf{d}}_g + \widetilde{\dot{\mathbf{w}}_r^e}\,\Delta\dot{\mathbf{u}}_l = \left(\frac{N_7}{l_n^2}\,\mathbf{A}_1\,\dot{\mathbf{d}}_g^e\,\mathbf{r}^e + \widetilde{\dot{\mathbf{w}}_r^e}\mathbf{P}_1\,\mathbf{P}\right)\mathbf{E}^{\mathrm{T}}\,\Delta\dot{\mathbf{d}}_g\,, \end{aligned}\tag{126}$$

$$\Delta\dot{\mathbf{H}}_2\,\mathbf{E}^{\mathrm{T}}\,\dot{\mathbf{d}}_g = \Delta\dot{\mathbf{H}}_2\,\dot{\mathbf{d}}_g^e = \frac{N_8}{l_n^2}\,\mathbf{A}_2\,\mathbf{r}\,\Delta\dot{\mathbf{d}}_g\,\dot{\mathbf{d}}_g^e = \frac{N_8}{l_n^2}\,\mathbf{A}_2\,\dot{\mathbf{d}}_g^e\,\mathbf{r}^e\,\mathbf{E}^{\mathrm{T}}\,\Delta\dot{\mathbf{d}}_g\,, \tag{127}$$

in which

$$\mathbf{r}^e = \mathbf{r}\,\mathbf{E} = \left[\,[-1\;0\;0]\;\;\mathbf{0}_{[1\times3]}\;\;[1\;0\;0]\;\;\mathbf{0}_{[1\times3]}\,\right]. \tag{128}$$

Using Eq. (64), the last terms of Eqs. (121) and (122) are given by

$$\Delta\mathbf{E}_t\,\mathbf{E}^{\mathrm{T}}\,\dot{\mathbf{d}}_g = \Delta\mathbf{E}_t\,\dot{\mathbf{d}}_g^e = -\mathbf{F}_1\,\Delta\dot{\mathbf{w}}_r^e = -\mathbf{F}_1\,\mathbf{G}^{\mathrm{T}}\,\mathbf{E}^{\mathrm{T}}\,\Delta\dot{\mathbf{d}}_g\,, \tag{129}$$

with

$$\mathbf{F}_1 = [\,\widetilde{\dot{\mathbf{u}}_1^e}^{\mathrm{T}}\,\widetilde{\dot{\mathbf{w}}_1^e}^{\mathrm{T}}\,\widetilde{\dot{\mathbf{u}}_2^e}^{\mathrm{T}}\,\widetilde{\dot{\mathbf{w}}_2^e}^{\mathrm{T}}\,]^{\mathrm{T}}. \tag{130}$$

Finally, the expressions of $\mathbf{C}_3$ and $\mathbf{C}_4$ are evaluated by

$$\mathbf{C}_3 = -\widetilde{\mathbf{h}_1}\,\mathbf{G}^{\mathrm{T}} + \left(\frac{N_7}{l_n^2}\,\mathbf{A}_1\,\dot{\mathbf{d}}_g^e\,\mathbf{r}^e + \widetilde{\dot{\mathbf{w}}_r^e}\mathbf{P}_1\,\mathbf{P}\right) + \mathbf{H}_1\,\mathbf{F}_1\,\mathbf{G}^{\mathrm{T}}\,, \tag{131}$$

$$\mathbf{C}_4 = -\widetilde{\mathbf{h}_2}\,\mathbf{G}^{\mathrm{T}} + \frac{N_8}{l_n^2}\,\mathbf{A}_2\,\dot{\mathbf{d}}_g^e\,\mathbf{r}^e + \mathbf{H}_2\,\mathbf{F}_1\,\mathbf{G}^{\mathrm{T}}. \tag{132}$$

References

[1] R. Alsafadie, M. Hjiaj, J.-M. Battini, Corotational mixed finite element formulation for thin-walled beams with generic cross-section, Comput. Methods Appl. Mech. Engrg., Vol. 199, 3197-3212 (2010).

[2] R. Alsafadie, J.-M. Battini, M. Hjiaj, H. Somja, A comparative study of displacement and mixed-based corotational finite element formulations for elasto-plastic three-dimensional beam analysis, Engerg. Computs., Vol. 28, 7, 939-982 (2011).

[3] J. Argyris, An excursion into large rotations, Comput. Methods Appl. Mech. Engrg., Vol. 32, 85-155 (1982).

[4] K.J. Bathe, E. Ramm, Wilson E.L., Finite element formulations for large deformation dynamic analysis, Int. J. Num. Methods. Engrg., Vol. 9, 353-386 (1975).

[5] J.-M. Battini, C. Pacoste, Co-rotational beam elements with warping effects in instability problems, Comput. Methods Appl. Mech. Engrg., Vol. 191, 1755-1789 (2002).

[6] J.-M. Battini, A modified corotational framework for triangular shell elements, Comput. Methods Appl. Mech. Engrg., Vol. 196, 1905-1914 (2007).

[7] J.-M. Battini, Large rotations and nodal moments in corotational elements, CMES, Vol. 33, 1, 1-15 (2008).

[8] K. Behdinan, M.C Stylianou, B. Tabarrok, Co-rotational dynamic analysis of flexible beams, Comput. Methods Appl. Mech. Engrg., Vol. 154, 151-161 (1998).

[9] P. Betsch, P. Steinmann, Constrained dynamics of geometrically exact beams, Comput. Mech., Vol. 31, 49-59 (2003).

[10] A. Cardona, M. Geradin, A beam finite element non-linear theory with finite rotations, Int. J. Num. Methods. Engrg., Vol. 26, 2403-2438 (1988).

[11] M.A. Crisfield, Non-Linear Finite Element Analysis of Solids and Structures, Volume 1: Essentials, Wiley, Chischester (1991).

[12] M.A. Crisfield, Non-Linear Finite Element Analysis of Solids and Structures, Volume 2: Advanced Topics, Wiley, Chischester (1997).

[13] M.A. Crisfield, A consistent corotational formulation for nonlinear three-dimensional beam element, Comput. Methods Appl. Mech. Engrg., Vol. 81, 131-150 (1990).

[14] M.A. Crisfield, J. Shi, An energy conserving co-rotational procedure for non-linear dynamics with finite elements, Nonlinear Dynamics, Vol. 9, 37-52 (1996).

[15] M.A. Crisfield, G.F. Moita, A unified co-rotational framework for solids shells and beams, Int. J. Solids Struct., Vol. 33, 2969-2992 (1996).

[16] M.A. Crisfield, U. Galvanetto, G. Jelenić, Dynamics of 3-D co-rotational beams, Comput. Mech., Vol. 20, 507-519 (1997).

[17] H.A. Elkaranshawy and M.A. Dokainish, Corotational finite element analysis of planar flexible multibody systems, Comput. Struct., Vol. 54, No.5, 881-890 (1995).

[18] U. Galvanetto, M.A. Crisfield, An energy conserving co-rotational procedure for dynamics of planar beam structures, Int. J. Num. Methods. Engrg., Vol. 39, 2265-2282 (1996).

[19] M. Geradin, A. Cardona, Kinematics and dynamics of rigid and flexible mechanisms using finite elements and quaternion algebra, Comput. Mech., Vol. 4, 115-135 (1989).

[20] M. Geradin, A. Cardona, Flexible multibody dynamics : A finite element approach, 120-127. Wiley, Chischester (2001).

[21] K.M. Hsiao, R.T. Yang, A co-rotational formulation for nonlinear dynamic analysis of curved Euler beam, Comput. Struct. , Vol. 54, No.6, 1091-1097 (1995).

[22] K.M. Hsiao, J.Y. Lin, W.Y. Lin, A consistent co-rotational finite element formulation for geometrically nonlinear dynamics analysis of 3-D beams, Comput. Methods Appl. Mech. Engrg., Vol. 169, 1-18 (1999).

[23] A. Ibrahimbegović, F. Frey, I. Kožar, Computational aspects of vector-like parameterization of three-dimensional finite rotations, Int. J. Num. Methods. Engrg., Vol. 38, 3653-3673 (1995).

[24] A. Ibrahimbegović, On FE implementation of geometrically nonlinear Reissner's beam theory: Three-dimensional curved beam elements, Comput. Methods Appl. Mech. Engrg., Vol. 122, 11-26 (1995).

[25] A. Ibrahimbegović, On the choice of finite rotation parameters, Comput. Methods Appl. Mech. Engrg., Vol. 149, 49-71 (1997).

[26] A. Ibrahimbegović, M.A. Mikdad, Finite rotations in dynamics of beams and implicit time-stepping schemes, Int. J. Num. Methods. Engrg., Vol. 41, 781-814 (1998).

[27] A. Ibrahimbegović, S. Mamouri, Energy conserving/decaying implicit time-stepping scheme for nonlinear dynamics of three-dimensional beams undergoing finite rotations, Comput. Methods Appl. Mech. Engrg., Vol. 191, 4241-4258 (2002).

[28] A. Ibrahimbegović, Taylor R.L., On the role of frame-invariance in structural mechanics models at finite rotations, Comput. Methods Appl. Mech. Engrg., Vol. 191, Iss. 45, 5159-5176 (2002).

[29] M. Iura, S.N. Atluri, Dynamic analysis of finitely stretched and rotated three-dimensional space-curved beams, Comput. & Struc., Vol. 29, 875-889 (1988).

[30] M. Iura, S.N. Atluri, Dynamic analysis of planar flexible beams with finite rotations by using inertial and rotating frames, Comput. Struct., Vol. 55, No.3, 453-462 (1995).

[31] G. Jelenić, M.A. Crisfield, Interpolation of rotational variables in nonlinear dynamics of 3D beams, Int. J. Num. Methods. Engrg., Vol. 43, 1193-1222 (1998).

[32] G. Jelenić, M.A. Crisfield, Geometrically exact 3D beam theory: implementation of a strain-invariant element for stactics and dynamics, Comput. Methods Appl. Mech. Engrg., Vol. 171, 141-171 (1999).

[33] S. Krenk, Non-Linear Modeling And Analysis Of Solids And Structures, 47-75, Cambridge University Press, New York (2009).

[34] T.-N. Le, J.-M. Battini, M. Hjiaj, Efficient formulation for dynamics of corotational 2D beams, Comput. Mech., Vol. 48, No. 2, 153-161 (2011).

[35] T.-N. Le, J.-M. Battini, M. Hjiaj, Dynamics of 3D beam elements in a corotational context: A comparative study of established and new formulations, Finite Elem. Anal. Des., Vol. 61, 97-111 (2012).

[36] E.V. Lens, A. Cardona, A nonlinear beam element formulation in the framework of an energy preserving time integration scheme for constrained multibody systems dynamics, Comput. Struct. , Vol. 86, 47-63 (2008).

[37] J. Mäkinen, Critical study of Newmark-scheme on manifold of finite rotations, Comput. Methods Appl. Mech. Engrg., Vol. 191, 817-828 (2001).

[38] J. Mäkinen, Total Lagrangian Reissner's geometrically exact beam element without singularities, Int. J. Num. Methods. Engrg., Vol. 70, 1009-1048 (2007).

[39] N. Masuda, T. Nishiwaki, M. Minaaawa, Nonlinear dynamic analysis of frame structures, Comput. Struct., Vol. 27, No.1, 103-110 (1987).

[40] B. Nour-Omid, C.C. Rankin, Finite rotation analysis and consistent linearization using projectors, Comput. Methods Appl. Mech. Engrg., Vol. 93, 353-384 (1991).

[41] C. Oran, A. Kassimali, Large deformations of framed structures under static and dynamic loads, Comput. Struct., Vol. 6, 539-547 (1976).

[42] C. Pacoste, A. Eriksson, Beam elements in instability problems, Comput. Methods Appl. Mech. Engrg., Vol. 144, 163-197 (1997).

[43] C. Pacoste, Co-rotational flat facet triangular elements for shell instability analysis, Comput. Methods Appl. Mech. Engrg., Vol. 156, 75-110 (1998).

[44] C.C. Rankin, B. Nour-Omid, The use of projectors to improve finite element performance, Comput. Struct., Vol. 30, 257-267 (1988).

[45] J.N. Reddy, On locking-free shear deformable beam finite elements, Comput. Methods Appl. Mech. Engrg., Vol. 149, 113-132 (1997).

[46] J.C. Simo, A finite strain beam formulation. The three-dimensional dynamic problem. Part I, Comput. Methods Appl. Mech. Engrg., Vol. 49, 55-70 (1985).

[47] J.C. Simo, L. Vu-Quoc, A three-dimensional finite-strain rod model. Part II: computational aspects, Comput. Methods Appl. Mech. Engrg., Vol. 58, 79-116 (1986).

[48] J.C. Simo, L. Vu-Quoc, On the dynamics in space of rods undergoing large motions - A geometrically exact approach, Comput. Methods Appl. Mech. Engrg., Vol. 66, 125-161 (1988).

[49] J.C. Simo, K.K. Wong, Unconditionally stable algorithms for rigid body dynamics that exactly preserve energy and momentum, Int. J. Num. Methods. Engrg., Vol. 31, 19-52 (1991).

[50] Q. Xue, J.L Meek, Dynamic response and instability of frame structures, Comput. Methods Appl. Mech. Engrg., Vol. 190, 5233-5242 (2001).

[51] H. Weiss , Dynamics of geometrically nonlinear rods: II. Numerical methods and computational examples, Nonlinear Dynamics, Vol. 30, 383-415 (2002).

[52] E. Zupan, M. Saje, D. Zupan, Quaternion-based dynamics of geometrically nonlinear spatial beams using the RungeKutta method, Finite Elem. Anal. Des., Vol. 54, 48-60 (2012).

[53] E. Zupan, M. Saje, D. Zupan, Dynamics of spatial beams in quaternion description based on the Newmark integration scheme, Comput. Mech., Vol. 51, 47-64 (2013).

Paper 4: Corotational formulation for nonlinear dynamics of beams with arbitrary thin-walled cross-sections

Accepted for publication in Computers & Structures, 2013
DOI: 10.1016/j.compstruc.2013.11.005

Computers & Structures.
Comput. Struct. (2013).

Corotational formulation for nonlinear dynamics of beams with arbitrary thin-walled open cross-sections

Thanh-Nam Le [1,2] , Jean-Marc Battini [2] , Mohammed Hjiaj [1]

[1] *Université Européenne de Bretagne, INSA de Rennes - LGCGM/Structural Engineering Research Group, 20 avenue des Buttes de Coësmes, CS 70839, 35708 Rennes Cedex 7, France.*

[2] *KTH, Royal Institute of Technology - Department of Civil and Architectural Engineering, SE-10044 Stockholm, Sweden.*

Abstract

A new consistent corotational formulation for nonlinear dynamics of beams with arbitrary thin-walled cross-section is presented. The novelty is that the warping deformations and the eccentricity of the shear center are fully taken into account. Therefore, additional terms are introduced in the expressions of the inertia force vector and the tangent dynamic matrix. Their contribution is then investigated in several numerical examples. Besides, the element has seven degrees of freedom at each node and cubic shape functions are used to interpolate local transverse displacements and axial rotations. The formulation's accuracy is assessed considering five examples with comparisons against 3D-solid solutions.

Key words: Thin-walled; Corotational method; Nonlinear dynamics; 3D beam elements; Finite rotations;

1 Introduction

Dynamic analysis of flexible structures undergoing large displacements and finite rotations is an attractive research topic and a large number of finite beam formulations have been proposed in the literature. Many of them have been formulated in the total Lagrangian context [3,6,7,14,21,23,25,26,31,32,38,40,41], and in the corotational context [5,8–10,12,13,16–18,24,28,30,33,35,39]. However, the number of formulations which deal with nonlinear dynamics of beams with arbitrary thin-walled cross-sections is very limited [18].

The aim of this paper is to propose a new dynamic formulation for nonlinear analysis of beams with arbitrary thin-walled open cross-sections. The formulation is based on the corotational method. This method is a well-known approach to develop efficient beam elements for the nonlinear analysis of flexible structures. In fact, several versions of the corotational method have been proposed in the literature. The one used in this work is based on the work of Rankin and Nour-Omid [34, 36], further developed by Battini and Pacoste [4] for the static analysis of beams with arbitrary cross-section. The main idea of the method is to decompose the motion of the element into rigid body and pure deformational parts. During the rigid body motion, a local coordinates system, attached to the element, moves and rotates with it. The deformational part is measured in this local system. The main interest of the approach is that different assumptions can be made to represent the local deformations.

Using this corotational framework, a dynamic formulation has been proposed by the authors for the case of 2D beams [28] and the case of 3D beams with solid and double symmetric cross-sections (Saint-Venant torsion) [30]. In these works, the same kinematic assumptions have been adopted to develop the static and

the dynamic terms. In particular it has been shown that the possibility offered by the corotational method to use cubic shape functions for the local transverse displacements leads to a more efficient two-noded beam element.

The purpose of the present paper is to further develop the dynamic formulation proposed in [30] so that beams with arbitrary thin-walled open cross-sections can be studied. For that, two main ideas are used. Firstly, a seventh degree of freedom is added at each node to describe the warping of the cross-section. Consequently, the linear interpolation for the local axial rotation used in [30] is replaced by a cubic interpolation. Secondly, the main difficulty in the nonlinear analysis of beams with arbitrary cross-sections is that, due to the eccentricity of the shear center, the cross-section rotations are usually not defined at the same point. To avoid this difficulty, the kinematic description proposed by Gruttmann et al. [1] is adopted. In this approach, the warping function is modified and all the cross-section rotations are defined at the centroid.

Consequently, the inertia terms are consistent with the static ones developed by Battini and Pacoste in [4] since the same corotational kinematic description is used to derive all the terms. Regarding the dynamic terms, i.e. the inertia force vector and tangent dynamic matrix, the formulation proposed in [30] is extended and several additional terms are introduced. The contribution of these terms in the performance of the formulation is then investigated in the numerical examples. Regarding the static deformational terms, i.e. the internal force vector and tangent stiffness matrix, the corotational beam element developed by Battini and Pacoste [4] is adopted. However, in order to introduce the bending shear deformations, the cubic Hermitian functions are modified as suggested in the Interdependent Interpolation Element (IIE) formulation [37].

The outline of the paper is as follows. Section 2 presents some aspects of the parametrization of finite rotations. In Section 3, the expression of the kinetic energy is derived. Section 4 is devoted to the corotational beam kinematics. Section 5 presents the derivation of the inertia force vector and the dynamic tangent matrix. The internal force vector and the tangent stiffness matrix are shortly presented in Section 6. In Section 7, five numerical examples are analysed in order to assess the performance of the present dynamic formulation. Finally, conclusions are given in Section 8.

2 Parametrization of finite rotation

In this section, the basic relations concerning the parameterizations of finite rotations are briefly presented. For a more complete description, the reader is referred to textbooks and review papers such as [2, 11, 15, 19, 20, 27].

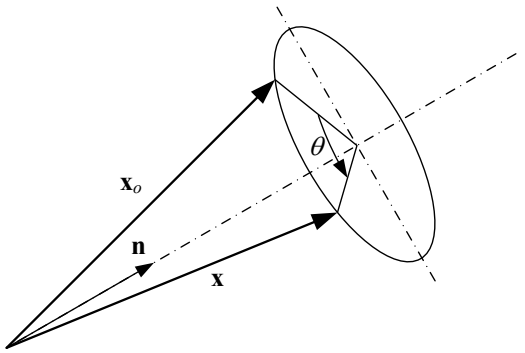

Fig. 1. Finite rotation of a vector

The coordinate of a vector $\mathbf{x}_o$ that is rotated into the position $\mathbf{x}$ (see Fig. 1) is given by the relation

$$\mathbf{x} = \mathbf{R}\,\mathbf{x}_o\,. \tag{1}$$

Due to its orthonormality, the rotation matrix $\mathbf{R}$ can be parameterized using only three independent parameters. One possibility is to use the rotational vector defined by

$$\boldsymbol{\theta} = \theta\,\mathbf{n}\,, \tag{2}$$

where $\mathbf{n}$ is a unit vector defining the axis of the rotation and $\theta = (\boldsymbol{\theta}^{\mathrm{T}}\boldsymbol{\theta})^{1/2}$ is the angle of the rotation.

The relation between the rotation matrix and the rotational vector is given by the Rodrigues' formula

$$\mathbf{R} = \mathbf{I} + \frac{\sin\theta}{\theta}\widetilde{\boldsymbol{\theta}} + \frac{1-\cos\theta}{\theta^2}\widetilde{\boldsymbol{\theta}}\widetilde{\boldsymbol{\theta}} = \exp(\widetilde{\boldsymbol{\theta}})\,, \tag{3}$$

where $\widetilde{\boldsymbol{\theta}}$ is the skew matrix associated with the vector $\boldsymbol{\theta}$.

The variation of the rotation matrix in spatial and material form is given by

$$\delta\mathbf{R} = \widetilde{\delta\mathbf{w}}\mathbf{R} = \mathbf{R}\widetilde{\delta\boldsymbol{\omega}}\,. \tag{4}$$

Physically, $\widetilde{\delta\mathbf{w}}$ represents infinitesimal spatial rotation superposed onto the rotation $\mathbf{R}$. $\delta\mathbf{w}$, which is also denoted as spatial spin variables, is related to the variation of the rotational vector through

$$\delta\mathbf{w} = \mathbf{T}_s(\boldsymbol{\theta})\,\delta\boldsymbol{\theta}\,, \tag{5}$$

with

$$\mathbf{T}_s(\boldsymbol{\theta}) = \mathbf{I} + \frac{1-\cos\theta}{\theta^2}\widetilde{\boldsymbol{\theta}} + \frac{\theta-\sin\theta}{\theta^3}\widetilde{\boldsymbol{\theta}}\widetilde{\boldsymbol{\theta}}\,. \tag{6}$$

The time derivative of the rotation matrix in spatial and material form is given by

$$\dot{\mathbf{R}} = \widetilde{\dot{\mathbf{w}}}\mathbf{R} = \mathbf{R}\widetilde{\dot{\boldsymbol{\omega}}}\,, \tag{7}$$

where the axis vectors $\dot{\mathbf{w}}$ and $\dot{\boldsymbol{\omega}}$ are spatial and material angular velocities, respectively.

The spatial and material quantities are connected by the relations

$$\delta\mathbf{w} = \mathbf{R}\,\delta\boldsymbol{\omega}\,, \tag{8}$$

$$\dot{\mathbf{w}} = \mathbf{R}\,\dot{\boldsymbol{\omega}}\,, \tag{9}$$

$$\ddot{\mathbf{w}} = \mathbf{R}\,\ddot{\boldsymbol{\omega}}\,. \tag{10}$$

The variation of the material angular velocity is given by (see [7])

$$\delta\dot{\boldsymbol{\omega}} = \dot{\delta\boldsymbol{\omega}} + \widetilde{\dot{\boldsymbol{\omega}}}\,\delta\boldsymbol{\omega}\,, \tag{11}$$

with $\dot{\delta\boldsymbol{\omega}}$ denoting the time derivative of the material spin variables.

3 Kinetic energy

In the present paper, the kinematic description proposed by Gruttmann et al. [1] is adopted (see Fig. 2). A beam with an arbitrary cross-section is considered. G and C are the centroid and the shear center of the cross-section. $\mathbf{e}_i$ and $\mathbf{a}_i$ $(i = 1,2,3)$ denote the global and cross-section-attached orthogonal coordinates

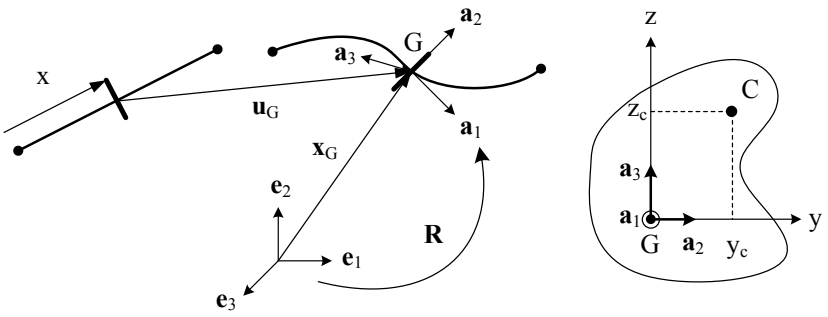

Fig. 2. Initial and current configuration of the beam

systems, respectively. The transformation from the global coordinates system to the cross-section-attached one is defined by

$$\mathbf{a}_i = \mathbf{R}\,\mathbf{e}_i\,. \tag{12}$$

Let $\mathbf{x}_{\mathrm{P}}(x,y,z)$ denote the position vector of an arbitrary point P in the current configuration

$$\mathbf{x}_{\mathrm{P}}(x,y,z) = \mathbf{x}_{\mathrm{G}}(x) + y\,\mathbf{a}_2(x) + z\,\mathbf{a}_3(x) + \alpha(x)\,\overline{\omega}(y,z)\,\mathbf{a}_1(x)\,, \tag{13}$$

with $\mathbf{x}_{\mathrm{G}}$ denoting the position vector of G in the current configuration.

The warping function $\overline{\omega}(y,z)$ is defined within the Saint-Venant torsion theory and refers to the centroid G, i.e.

$$\overline{\omega} = \omega - y_c\,z + z_c\,y\,, \tag{14}$$

where ω refers to the shear center C with coordinates $y_c\,, z_c$. Note that in connection with ω, the following normality conditions hold

$$\int_A \omega\,\mathrm{d}A = 0\,, \quad \int_A \omega\,y\,\mathrm{d}A = 0\,, \quad \int_A \omega\,z\,\mathrm{d}A = 0\,. \tag{15}$$

Using Eq. (12), the expression (13) can be put in the form

$$\mathbf{x}_{\mathrm{P}} = \mathbf{x}_{\mathrm{G}} + \mathbf{R}\,(\mathbf{X} + \alpha\,\mathbf{n}_{\overline{\omega}})\,, \tag{16}$$

with $\mathbf{X} = [0\ \ y\ \ z]^{\mathrm{T}}$ and $\mathbf{n}_{\overline{\omega}} = [\,\overline{\omega}\ \ 0\ \ 0]^{\mathrm{T}}$.

By taking the time derivative of the above expression and using Eq. (7), the velocity is obtained as

$$\begin{aligned} \dot{\mathbf{u}}_{\mathrm{P}} = \dot{\mathbf{x}}_{\mathrm{P}} &= \dot{\mathbf{x}}_{\mathrm{G}} + \mathbf{R}\,\widetilde{\boldsymbol{\omega}}(\mathbf{X} + \alpha\,\mathbf{n}_{\overline{\omega}}) + \mathbf{R}\,\dot{\alpha}\,\mathbf{n}_{\overline{\omega}} \\ &= \dot{\mathbf{u}}_{\mathrm{G}} + \mathbf{R}\,(-\widetilde{\mathbf{X}}\,\dot{\boldsymbol{\omega}} - \alpha\,\widetilde{\mathbf{n}_{\overline{\omega}}}\,\dot{\boldsymbol{\omega}} + \dot{\alpha}\,\mathbf{n}_{\overline{\omega}})\,. \end{aligned} \tag{17}$$

The kinetic energy of the beam is then calculated by

$$\begin{aligned} K = \frac{1}{2}\int_V \rho\ \dot{\mathbf{u}}_{\mathrm{P}}^{\mathrm{T}}\,\dot{\mathbf{u}}_{\mathrm{P}}\ \mathrm{d}V = \frac{1}{2}\Bigg[&\int_{l_o} \dot{\mathbf{u}}_{\mathrm{G}}^{\mathrm{T}}\,A_\rho\,\dot{\mathbf{u}}_{\mathrm{G}}\ \mathrm{d}l \\ &+ \int_V \rho\ (-\widetilde{\mathbf{X}}\,\dot{\boldsymbol{\omega}} - \alpha\,\widetilde{\mathbf{n}_{\overline{\omega}}}\,\dot{\boldsymbol{\omega}} + \dot{\alpha}\,\mathbf{n}_{\overline{\omega}})^{\mathrm{T}}\ (-\widetilde{\mathbf{X}}\,\dot{\boldsymbol{\omega}} - \alpha\,\widetilde{\mathbf{n}_{\overline{\omega}}}\,\dot{\boldsymbol{\omega}} + \dot{\alpha}\,\mathbf{n}_{\overline{\omega}})\ \mathrm{d}V\Bigg]\,. \end{aligned} \tag{18}$$

The following notations are introduced

$$I_{yz} = \int_A y\, z \, \mathrm{d}A\,, \quad I_{yy} = \int_A y^2 \, \mathrm{d}A\,, \quad I_{zz} = \int_A z^2 \, \mathrm{d}A\,, \quad I_{\omega} = \int_A \omega^2 \, \mathrm{d}A\,, \tag{19}$$

$$I_{\overline{\omega}} = \int_A \overline{\omega}^2 \, \mathrm{d}A = I_{\omega} + z_c^2 I_{yy} + y_c^2 I_{zz} - 2\, y_c\, z_c\, I_{yz}\,, \tag{20}$$

$$I_{yc} = \int_A y\, \overline{\omega} \, \mathrm{d}A = -y_c\, I_{yz} + z_c\, I_{yy}\,, \tag{21}$$

$$I_{zc} = \int_A z\, \overline{\omega} \, \mathrm{d}A = -y_c\, I_{zz} + z_c\, I_{yz}\,, \tag{22}$$

$$\mathbf{J}_{\rho} = \int_A \rho\, \widetilde{\mathbf{X}}^{\mathrm{T}}\, \widetilde{\mathbf{X}} \; \mathrm{d}A = \rho \begin{bmatrix} I_{yy} + I_{zz} & 0 & 0 \\ 0 & I_{zz} & -I_{yz} \\ 0 & -I_{yz} & I_{yy} \end{bmatrix}, \tag{23}$$

$$\mathbf{J}_{\overline{\omega}} = \int_A \rho\, \widetilde{\mathbf{n}_{\overline{\omega}}}^{\mathrm{T}}\, \widetilde{\mathbf{n}_{\overline{\omega}}} \; \mathrm{d}A = \rho \begin{bmatrix} 0 & 0 & 0 \\ 0 & I_{\overline{\omega}} & 0 \\ 0 & 0 & I_{\overline{\omega}} \end{bmatrix}, \tag{24}$$

$$\mathbf{J}_{a} = \int_A \rho \, \left(\widetilde{\mathbf{X}}^{\mathrm{T}}\, \widetilde{\mathbf{n}_{\overline{\omega}}} + \widetilde{\mathbf{n}_{\overline{\omega}}}^{\mathrm{T}}\, \widetilde{\mathbf{X}} \right) \; \mathrm{d}A = \rho \begin{bmatrix} 0 & -I_{yc} & -I_{zc} \\ -I_{yc} & 0 & 0 \\ -I_{zc} & 0 & 0 \end{bmatrix}, \tag{25}$$

$$\mathbf{J}_{b} = \int_A \rho\, \widetilde{\mathbf{X}}^{\mathrm{T}}\, \mathbf{n}_{\overline{\omega}} \; \mathrm{d}A = \rho \begin{bmatrix} 0 \\ -I_{zc} \\ I_{yc} \end{bmatrix}, \tag{26}$$

$$\mathbf{J}_{\alpha} = \alpha^2\, \mathbf{J}_{\overline{\omega}} + \alpha\, \mathbf{J}_{a}\,, \quad J_{\overline{\omega}} = \rho\, I_{\overline{\omega}}\,. \tag{27}$$

The expression of the kinetic energy can then be rewritten in the material form as

$$K = \frac{1}{2} \int_{l_o} \left[\dot{\mathbf{u}}_{\mathrm{G}}^{\mathrm{T}}\, A_{\rho}\, \dot{\mathbf{u}}_{\mathrm{G}} + \dot{\boldsymbol{\omega}}^{\mathrm{T}}\, \mathbf{J}_{\rho}\, \dot{\boldsymbol{\omega}} \right] \; \mathrm{d}l + \frac{1}{2} \int_{l_o} \left[\dot{\boldsymbol{\omega}}^{\mathrm{T}}\, \mathbf{J}_{\alpha}\, \dot{\boldsymbol{\omega}} - 2\, \dot{\boldsymbol{\omega}}^{\mathrm{T}}\, \mathbf{J}_{b}\, \dot{\alpha} + J_{\overline{\omega}}\, \dot{\alpha}^2 \right] \; \mathrm{d}l\,, \tag{28}$$

and, using Eq. (9), the spatial form is obtained

$$K = \frac{1}{2} \int_{l_o} \left[\dot{\mathbf{u}}_{\mathrm{G}}^{\mathrm{T}}\, A_{\rho}\, \dot{\mathbf{u}}_{\mathrm{G}} + \dot{\mathbf{w}}^{\mathrm{T}}\, \mathbf{I}_{\rho}\, \dot{\mathbf{w}} \right] \; \mathrm{d}l + \frac{1}{2} \int_{l_o} \left[\dot{\mathbf{w}}^{\mathrm{T}}\, \mathbf{I}_{\alpha}\, \dot{\mathbf{w}} - 2\, \dot{\mathbf{w}}^{\mathrm{T}}\, \mathbf{I}_{b}\, \dot{\alpha} + J_{\overline{\omega}}\, \dot{\alpha}^2 \right] \; \mathrm{d}l\,, \tag{29}$$

with

$$\mathbf{I}_{\rho} = \mathbf{R}\, \mathbf{J}_{\rho}\, \mathbf{R}^{\mathrm{T}}\,, \quad \mathbf{I}_{\overline{\omega}} = \mathbf{R}\, \mathbf{J}_{\overline{\omega}}\, \mathbf{R}^{\mathrm{T}}\,, \quad \mathbf{I}_{\alpha} = \mathbf{R}\, \mathbf{J}_{\alpha}\, \mathbf{R}^{\mathrm{T}}\,, \quad \mathbf{I}_{b} = \mathbf{R}\, \mathbf{J}_{b}\,. \tag{30}$$

The first integrals in Eqs. (28) and (29) are the kinetic energy due to the translation and rotation of the beam cross-section. The variation, in the spatial form, is obtained as

$$\delta K_{Trans+Rot} = -\int_{l_o} \left\{ \delta \mathbf{u}_{\mathrm{G}}{}^{\mathrm{T}} A_{\rho}\, \ddot{\mathbf{u}}_{\mathrm{G}} + \delta \mathbf{w}^{\mathrm{T}} \left[\mathbf{I}_{\rho}\, \dot{\mathbf{w}} + \widetilde{\dot{\mathbf{w}}}\, \mathbf{I}_{\rho}\, \dot{\mathbf{w}} \right] \right\} \mathrm{d}l\,. \tag{31}$$

The second integrals in Eqs. (28) and (29), named as $K_{Warping}$, are the additional kinetic energy due to the warping deformations and the eccentricity of shear center with respect to the centroid

$$K_{Warping} = \int_{l_o} k_W \ \mathrm{d}l = \frac{1}{2}\int_{l_o} \left[\dot{\boldsymbol{\omega}}^{\mathrm{T}}\,\mathbf{J}_\alpha\,\dot{\boldsymbol{\omega}} - 2\,\dot{\boldsymbol{\omega}}^{\mathrm{T}}\,\mathbf{J}_b\,\dot{\alpha} + J_{\overline{\omega}}\,\dot{\alpha}^2\right]\ \mathrm{d}l\,. \tag{32}$$

The variation of k_W is given by

$$\delta k_W = \delta\dot{\boldsymbol{\omega}}^{\mathrm{T}}\ (\mathbf{J}_\alpha\,\dot{\boldsymbol{\omega}} - \mathbf{J}_b\,\dot{\alpha}) + \delta\alpha\,\dot{\boldsymbol{\omega}}^{\mathrm{T}}\,\mathbf{J}_\alpha^{'}\,\dot{\boldsymbol{\omega}} + \delta\dot{\alpha}\ (J_{\overline{\omega}}\,\dot{\alpha} - \dot{\boldsymbol{\omega}}^{\mathrm{T}}\,\mathbf{J}_b)\,, \tag{33}$$

where

$$\mathbf{J}_\alpha^{'} = \frac{1}{2}\frac{\mathrm{d}\mathbf{J}_\alpha}{\mathrm{d}\alpha} = \alpha\,\mathbf{J}_{\overline{\omega}} + \frac{1}{2}\,\mathbf{J}_a\,. \tag{34}$$

In order to derive an expression which only depends on infinitesimal rotations, an integration in time is performed using Eqs. (11) and (33)

$$\begin{aligned}\int_{t_1}^{t_2} \delta k_W \mathrm{d}t = &\int_{t_1}^{t_2} \delta\dot{\boldsymbol{\omega}}^{\mathrm{T}}\ (\mathbf{J}_\alpha\,\dot{\boldsymbol{\omega}} - \mathbf{J}_b\,\dot{\alpha})\ \mathrm{d}t + \int_{t_1}^{t_2} \delta\boldsymbol{\omega}^{\mathrm{T}}\,\widetilde{\boldsymbol{\omega}}^{\mathrm{T}}\ (\mathbf{J}_\alpha\,\dot{\boldsymbol{\omega}} - \mathbf{J}_b\,\dot{\alpha})\ \mathrm{d}t \\ &+ \int_{t_1}^{t_2} \delta\alpha\,\dot{\boldsymbol{\omega}}^{\mathrm{T}}\,\mathbf{J}_\alpha^{'}\,\dot{\boldsymbol{\omega}}\ \mathrm{d}t + \int_{t_1}^{t_2} \delta\dot{\alpha}\ (J_{\overline{\omega}}\,\dot{\alpha} - \dot{\boldsymbol{\omega}}^{\mathrm{T}}\,\mathbf{J}_b)\ \mathrm{d}t\,.\end{aligned} \tag{35}$$

The first and fourth terms in the above expression are integrated by parts

$$\begin{aligned}\int_{t_1}^{t_2} \delta\dot{\boldsymbol{\omega}}^{\mathrm{T}}\ (\mathbf{J}_\alpha\,\dot{\boldsymbol{\omega}} - \mathbf{J}_b\,\dot{\alpha})\ \mathrm{d}t = \delta\boldsymbol{\omega}^{\mathrm{T}}\ (\mathbf{J}_\alpha\,\dot{\boldsymbol{\omega}} - \mathbf{J}_b\,\dot{\alpha})\Big|_{t_1}^{t_2} \\ - \int_{t_1}^{t_2} \delta\boldsymbol{\omega}^{\mathrm{T}}\ (\mathbf{J}_\alpha\,\ddot{\boldsymbol{\omega}} - \mathbf{J}_b\,\ddot{\alpha})\ \mathrm{d}t - \int_{t_1}^{t_2} \delta\boldsymbol{\omega}^{\mathrm{T}}\,2\,\mathbf{J}_\alpha^{'}\,\dot{\alpha}\,\dot{\boldsymbol{\omega}}\ \mathrm{d}t\,,\end{aligned} \tag{36}$$

$$\int_{t_1}^{t_2} \delta\dot{\alpha}\ (J_{\overline{\omega}}\,\dot{\alpha} - \dot{\boldsymbol{\omega}}^{\mathrm{T}}\,\mathbf{J}_b)\ \mathrm{d}t = \delta\alpha(J_{\overline{\omega}}\,\dot{\alpha} - \dot{\boldsymbol{\omega}}^{\mathrm{T}}\,\mathbf{J}_b)\Big|_{t_1}^{t_2} - \int_{t_1}^{t_2} \delta\alpha\ (J_{\overline{\omega}}\,\ddot{\alpha} - \ddot{\boldsymbol{\omega}}^{\mathrm{T}}\,\mathbf{J}_b)\ \mathrm{d}t\,. \tag{37}$$

Due to the arbitrariness of the variations $\delta\boldsymbol{\omega}$ and $\delta\alpha$

$$\delta\boldsymbol{\omega}^{\mathrm{T}}\ (\mathbf{J}_\alpha\,\dot{\boldsymbol{\omega}} - \mathbf{J}_b\,\dot{\alpha})\Big|_{t_1}^{t_2} = 0\,, \tag{38}$$

$$\delta\alpha(J_{\overline{\omega}}\,\dot{\alpha} - \dot{\boldsymbol{\omega}}^{\mathrm{T}}\,\mathbf{J}_b)\Big|_{t_1}^{t_2} = 0\,, \tag{39}$$

hence, using Eqs. (36) and (37), Eq. (33) can be rewritten as

$$\delta k_W = -\begin{bmatrix}\delta\boldsymbol{\omega}\\ \delta\alpha\end{bmatrix}^{\mathrm{T}}\begin{bmatrix}\mathbf{J}_\alpha & -\mathbf{J}_b\\ -\mathbf{J}_b^{\mathrm{T}} & J_{\overline{\omega}}\end{bmatrix}\begin{bmatrix}\ddot{\boldsymbol{\omega}}\\ \ddot{\alpha}\end{bmatrix} - \begin{bmatrix}\delta\boldsymbol{\omega}\\ \delta\alpha\end{bmatrix}^{\mathrm{T}}\begin{bmatrix}\widetilde{\boldsymbol{\omega}}\,\mathbf{J}_\alpha & \mathbf{J}_c\,\dot{\boldsymbol{\omega}}\\ -\dot{\boldsymbol{\omega}}^{\mathrm{T}}\,\mathbf{J}_\alpha^{'} & 0\end{bmatrix}\begin{bmatrix}\dot{\boldsymbol{\omega}}\\ \dot{\alpha}\end{bmatrix}, \tag{40}$$

where $\mathbf{J}_c = 2\,\mathbf{J}_\alpha^{'} + \widetilde{\mathbf{J}}_b$.

Finally, the variation of the total kinetic energy, in the spatial form, is expressed as

$$\begin{aligned}\delta K = &-\int_{l_o}\left\{\delta\mathbf{u}_{\mathrm{G}}{}^{\mathrm{T}} A_\rho\,\ddot{\mathbf{u}}_{\mathrm{G}} + \delta\mathbf{w}^{\mathrm{T}}\left[\mathbf{I}_\rho\,\dot{\mathbf{w}} + \widetilde{\mathbf{w}}\mathbf{I}_\rho\,\dot{\mathbf{w}}\right]\right\}\mathrm{d}l - \\ &\int_{l_o}\begin{bmatrix}\delta\mathbf{w}\\ \delta\alpha\end{bmatrix}^{\mathrm{T}}\begin{bmatrix}\mathbf{I}_\alpha & -\mathbf{I}_b\\ -\mathbf{I}_b^{\mathrm{T}} & J_{\overline{\omega}}\end{bmatrix}\begin{bmatrix}\ddot{\mathbf{w}}\\ \ddot{\alpha}\end{bmatrix}\mathrm{d}l - \int_{l_o}\begin{bmatrix}\delta\mathbf{w}\\ \delta\alpha\end{bmatrix}^{\mathrm{T}}\begin{bmatrix}\widetilde{\dot{\mathbf{w}}}\,\mathbf{I}_\alpha & \mathbf{I}_c\,\dot{\mathbf{w}}\\ -\dot{\mathbf{w}}^{\mathrm{T}}\,\mathbf{I}_\alpha^{'} & 0\end{bmatrix}\begin{bmatrix}\dot{\mathbf{w}}\\ \dot{\alpha}\end{bmatrix}\mathrm{d}l\,,\end{aligned} \tag{41}$$

where $\mathbf{I}_\alpha^{'} = \mathbf{R}\,\mathbf{J}_\alpha^{'}\,\mathbf{R}^{\mathrm{T}}$ and $\mathbf{I}_c = \mathbf{R}\,\mathbf{J}_c\,\mathbf{R}^{\mathrm{T}}$.

By introducing the following notations

$$\delta\mathbf{w}^w = \begin{bmatrix} \delta\mathbf{w} \\ \delta\alpha \end{bmatrix}, \quad \dot{\mathbf{w}}^w = \begin{bmatrix} \dot{\mathbf{w}} \\ \dot{\alpha} \end{bmatrix}, \quad \ddot{\mathbf{w}}^w = \begin{bmatrix} \ddot{\mathbf{w}} \\ \ddot{\alpha} \end{bmatrix}, \tag{42}$$

$$\mathbf{I}_\rho^1 = \begin{bmatrix} (\mathbf{I}_\rho + \mathbf{I}_\alpha) & -\mathbf{I}_b \\ -\mathbf{I}_b^{\mathrm{T}} & J_{\overline{\omega}} \end{bmatrix}, \quad \mathbf{I}_\rho^2 = \begin{bmatrix} \widetilde{\dot{\mathbf{w}}}\,(\mathbf{I}_\rho + \mathbf{I}_\alpha) & \mathbf{I}_c\,\dot{\mathbf{w}} \\ -\dot{\mathbf{w}}^{\mathrm{T}}\,\mathbf{I}_\alpha^{'} & 0 \end{bmatrix}, \tag{43}$$

the expression in Eq. (41) can be put in the form

$$\delta K = -\int_{l_o} \left\{ \delta\mathbf{u}_{\mathrm{G}}{}^{\mathrm{T}} A_\rho\,\ddot{\mathbf{u}}_{\mathrm{G}} + \delta\mathbf{w}^{w\mathrm{T}} \left[\mathbf{I}_\rho^1\,\ddot{\mathbf{w}}^w + \mathbf{I}_\rho^2\,\dot{\mathbf{w}}^w \right] \right\} \mathrm{d}l\,. \tag{44}$$

4 Beam kinematics

In this work, the corotational framework introduced by Rankin and Nour-Omid [34,36], and further developed Battini and Pacoste [4] is fully adopted.

The definition of the corotational two noded-beam element, described in this section, involves several coordinate systems, see Fig. 3. First a global reference system is defined by the triad of unit orthogonal vectors $\mathbf{e}_j$ $(j = 1,2,3)$. Next, a local system which continuously rotates and translates with the element is selected. The orthonormal basis vectors of the local system are denoted by $\mathbf{r}_j$ $(j = 1,2,3)$. In the initial (undeformed) configuration, the local system is defined by the orthonormal triad $\mathbf{e}_j^o$. In addition, $\mathbf{t}_j^1$ and $\mathbf{t}_j^2$ $(j = 1,2,3)$, denote two unit triads rigidly attached to nodes 1 and 2. The origin of each unit triad (except the global one $\mathbf{e}_j$) coincides with the centroid of the cross-section.

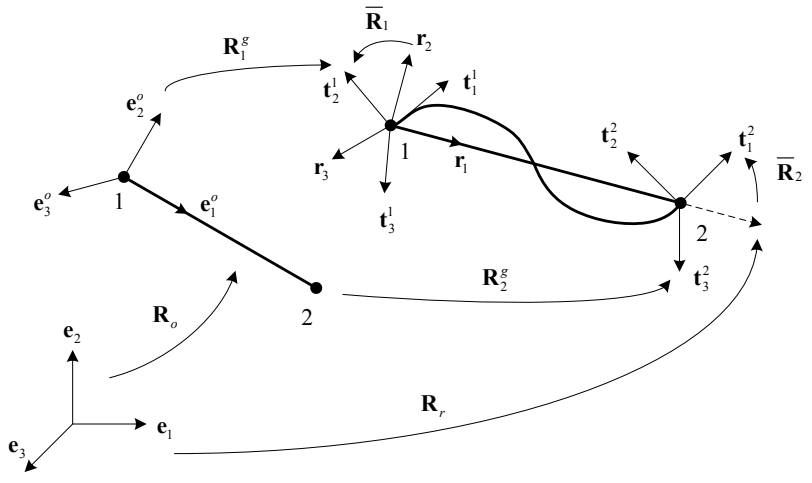

Fig. 3. Beam kinematics and the coordinate systems

According to the main idea of the corotational formulation, the motion of the element from the initial to the final deformed configuration is split into a rigid body component and a deformational part. The

rigid body motion consists of a rigid translation and rotation of the local element frame. The origin of the local system is taken at node 1 and thus the rigid translation is defined by $\mathbf{u}_1^g$, the translation of the cross-section centroid at node 1. Here and in the sequel, superscript g indicates quantities expressed in the global reference system. The rigid rotation is such that the new orientation of the local reference system is defined by an orthogonal matrix $\mathbf{R}_r$, given by

$$\mathbf{R}_r = [\,\mathbf{r}_1\ \mathbf{r}_2\ \mathbf{r}_3\,]\,. \tag{45}$$

The first coordinate axis of the local system is defined by the line connecting nodes 1 and 2 of the element. Consequently, $\mathbf{r}_1$ is given by

$$\mathbf{r}_1 = \frac{\mathbf{x}_2^g + \mathbf{u}_2^g - \mathbf{x}_1^g - \mathbf{u}_1^g}{l_n}\,, \tag{46}$$

with $\mathbf{x}_i^g$ $(i = 1,2)$ denoting the nodal coordinates in the initial undeformed configuration and l_n denoting the current length of the beam, i.e.

$$l_n = \|\mathbf{x}_2^g + \mathbf{u}_2^g - \mathbf{x}_1^g - \mathbf{u}_1^g\|\,. \tag{47}$$

The remaining two axes are determined with the help of an auxiliary vector $\mathbf{p}$. In the initial configuration, $\mathbf{p}$ is directed along the local $\mathbf{e}_2^o$ direction, whereas in the deformed configuration its orientation is obtained from

$$\mathbf{p} = \frac{1}{2}\,(\mathbf{p}_1 + \mathbf{p}_2)\,, \quad \mathbf{p}_i = \mathbf{R}_i^g\,\mathbf{R}_o\,[0\ 1\ 0]^{\mathrm{T}} \quad (i = 1,2)\,, \tag{48}$$

where $\mathbf{R}_1^g$ and $\mathbf{R}_2^g$ are the orthogonal matrices used to specify the orientation of the nodal triads $\mathbf{t}_j^1$ and $\mathbf{t}_j^2$ respectively, and $\mathbf{R}_o$ specifies the orientation of the local frame in the initial configuration, i.e. $\mathbf{R}_o = [\mathbf{e}_1^o\ \mathbf{e}_2^o\ \mathbf{e}_3^o]$. The unit vectors $\mathbf{r}_2$ and $\mathbf{r}_3$ are then computed by the following vector products

$$\mathbf{r}_3 = \frac{\mathbf{r}_1 \times \mathbf{p}}{\|\mathbf{r}_1 \times \mathbf{p}\|}, \quad \mathbf{r}_2 = \mathbf{r}_3 \times \mathbf{r}_1\,, \tag{49}$$

resulting in the orthogonal matrix $\mathbf{R}_r$ (Eq. (45)) being completely determined.

The rigid motion previously described, is accompanied by local deformational displacements and rotations with respect to the local element axes. In this context, due to the particular choice of the local system, the local translations at node 1 are zero. Moreover, at node 2, the only non zero component is the translation along $\mathbf{r}_1$. This can easily be evaluated according to

$$\overline{u} = l_n - l_o\,, \tag{50}$$

with l_o denoting the length of the beam in the original undeformed configuration. Here and in the sequel, an overbar denotes a deformational kinematic quantity.

The global rotations at node i can be expressed in terms of the rigid rotation of the local axes, defined by $\mathbf{R}_r$, followed by a local rotation relative to these axes. The latter is defined by the orthogonal matrix $\overline{\mathbf{R}}_i$. Consequently, the orientation of the nodal triad $\mathbf{t}_j^i$ can be obtained by means of the product $\mathbf{R}_r\,\overline{\mathbf{R}}_i$. On the other hand, (see Fig. 3) this orientation can also be obtained through the product $\mathbf{R}_i^g\,\mathbf{R}_o$, which gives

$$\overline{\mathbf{R}}_i = \mathbf{R}_r^{\mathrm{T}}\,\mathbf{R}_i^g\,\mathbf{R}_o \quad (i = 1,2)\,. \tag{51}$$

The local rotations are then evaluated from

$$\overline{\boldsymbol{\theta}}_i = \log\left(\overline{\mathbf{R}}_i\right) \quad (i = 1,2)\,. \tag{52}$$

Due to the choice of the local coordinate system, the local nodal displacement vector $\mathbf{d}_l^w$ has only nine components and is given by

$$\mathbf{d}_l^w = \left[\, \overline{u} \;\; \overline{\boldsymbol{\theta}}_1^{\mathrm{T}} \;\; \overline{\boldsymbol{\theta}}_2^{\mathrm{T}} \;\; \alpha_1 \;\; \alpha_2 \,\right]^{\mathrm{T}}. \tag{53}$$

with α_i $(i = 1,2)$ denoting the additional warping degrees of freedom.

The variation of the local nodal displacement vector is

$$\delta\mathbf{d}_l^w = \left[\, \delta\overline{u} \;\; \delta\overline{\boldsymbol{\theta}}_1^{\mathrm{T}} \;\; \delta\overline{\boldsymbol{\theta}}_2^{\mathrm{T}} \;\; \delta\alpha_1 \;\; \delta\alpha_2 \,\right]^{\mathrm{T}}, \tag{54}$$

and the global counterpart is given by

$$\delta\mathbf{d}_g^w = \left[\, \delta\mathbf{u}_1^{g\mathrm{T}} \;\; \delta\mathbf{w}_1^{g\mathrm{T}} \;\; \delta\mathbf{u}_2^{g\mathrm{T}} \;\; \delta\mathbf{w}_2^{g\mathrm{T}} \;\; \delta\alpha_1 \;\; \delta\alpha_2 \,\right]^{\mathrm{T}}, \tag{55}$$

with $\delta\mathbf{w}_i^g$ $(i = 1,2)$ denoting spatial spin variables defined by

$$\delta\mathbf{R}_i^g = \widetilde{\delta\mathbf{w}_i^g}\,\mathbf{R}_i^g. \tag{56}$$

Since the warping is a deformational quantity, it remains constant during the transformation between the global and local system, see Eqs. (54) and (55).

Further, let $\delta\overline{\mathbf{w}}_i$ and $\delta\mathbf{w}_r^g$ denote the spatial spin variables defined by

$$\delta\overline{\mathbf{R}}_i = \widetilde{\delta\overline{\mathbf{w}}_i}\,\overline{\mathbf{R}}_i, \quad \delta\mathbf{R}_r = \widetilde{\delta\mathbf{w}_r^g}\,\mathbf{R}_r. \tag{57}$$

By taking the variation of Eq. (51), one obtains the following relation (see [4])

$$\delta\overline{\mathbf{w}}_i = \delta\mathbf{w}_i^e - \delta\mathbf{w}_r^e \quad (i = 1,2), \tag{58}$$

where use of Eq. (51) has been made along the fact that $\mathbf{R}_r$ transforms a vector and a tensor from global to local coordinates according to

$$\mathbf{x}^e = \mathbf{R}_r^{\mathrm{T}}\mathbf{x}^g, \quad \widetilde{\mathbf{x}^e} = \mathbf{R}_r^{\mathrm{T}}\widetilde{\mathbf{x}^g}\,\mathbf{R}_r. \tag{59}$$

Let consider only the global translational and rotational variables

$$\delta\mathbf{d}_g = \left[\, \delta\mathbf{u}_1^{g\mathrm{T}} \;\; \delta\mathbf{w}_1^{g\mathrm{T}} \;\; \delta\mathbf{u}_2^{g\mathrm{T}} \;\; \delta\mathbf{w}_2^{g\mathrm{T}} \,\right]^{\mathrm{T}}, \tag{60}$$

and let

$$\delta\mathbf{d}_g^e = \mathbf{E}^{\mathrm{T}}\,\delta\mathbf{d}_g, \quad \mathbf{E} = \begin{bmatrix} \mathbf{R}_r & \mathbf{0} & \mathbf{0} & \mathbf{0} \\ \mathbf{0} & \mathbf{R}_r & \mathbf{0} & \mathbf{0} \\ \mathbf{0} & \mathbf{0} & \mathbf{R}_r & \mathbf{0} \\ \mathbf{0} & \mathbf{0} & \mathbf{0} & \mathbf{R}_r \end{bmatrix}, \tag{61}$$

with $\mathbf{0}$ denoting the 3×3 zero matrix.

Using the chain rule, $\delta\overline{\mathbf{w}}_i$ is evaluated as

$$\delta\overline{\mathbf{w}}_i = \frac{\partial\overline{\mathbf{w}}_i}{\partial\mathbf{d}_g^e}\frac{\partial\mathbf{d}_g^e}{\partial\mathbf{d}_g}\,\delta\mathbf{d}_g = \frac{\partial\overline{\mathbf{w}}_i}{\partial\mathbf{d}_g^e}\,\mathbf{E}^{\mathrm{T}}\,\delta\mathbf{d}_g \quad (i = 1,2). \tag{62}$$

Then Eq. (58) can be rewritten as

$$\begin{bmatrix} \delta\overline{\mathbf{w}}_1 \\ \delta\overline{\mathbf{w}}_2 \end{bmatrix} = \left(\begin{bmatrix} \mathbf{0}\ \mathbf{I}\ \mathbf{0}\ \mathbf{0} \\ \mathbf{0}\ \mathbf{0}\ \mathbf{0}\ \mathbf{I} \end{bmatrix} - \begin{bmatrix} \mathbf{G}^{\mathrm{T}} \\ \mathbf{G}^{\mathrm{T}} \end{bmatrix} \right) \mathbf{E}^{\mathrm{T}}\,\delta\mathbf{d}_g = \mathbf{P}\mathbf{E}^{\mathrm{T}}\,\delta\mathbf{d}_g\,, \tag{63}$$

where the matrix $\mathbf{G}$ is defined by

$$\mathbf{G}^{\mathrm{T}} = \frac{\partial \mathbf{w}_r^e}{\partial \mathbf{d}_g^e}\,. \tag{64}$$

For the local coordinate system defined in Eqs. (46) - (49), the above equation yield to

$$\mathbf{G}^{\mathrm{T}} = \begin{bmatrix} 0 & 0 & \dfrac{\eta}{l_n} & \dfrac{\eta_{12}}{2} & -\dfrac{\eta_{11}}{2} & 0\ 0\ 0 & -\dfrac{\eta}{l_n} & \dfrac{\eta_{22}}{2} & -\dfrac{\eta_{21}}{2} & 0 \\ 0 & 0 & \dfrac{1}{l_n} & 0 & 0 & 0\ 0\ 0 & -\dfrac{1}{l_n} & 0 & 0 & 0 \\ 0 & -\dfrac{1}{l_n} & 0 & 0 & 0 & 0\ 0 & \dfrac{1}{l_n} & 0 & 0 & 0 & 0 \end{bmatrix}, \tag{65}$$

$$\eta = \frac{p_1}{p_2}\,, \quad \eta_{11} = \frac{p_{11}}{p_2}\,, \quad \eta_{12} = \frac{p_{12}}{p_2}\,, \quad \eta_{21} = \frac{p_{21}}{p_2}\,, \quad \eta_{22} = \frac{p_{22}}{p_2}\,, \tag{66}$$

where (see Eq. (48)) p_j and p_{ij} are the components of the vectors $\mathbf{R}_r^{\mathrm{T}}\,\mathbf{p}$ and $\mathbf{R}_r^{\mathrm{T}}\,\mathbf{p}_i$, respectively.

5 Inertia force vector and tangent dynamic matrix

5.1 Local beam kinematic description

The local motion of a beam cross-section from the initial (i.e. rotated but still undeformed) configuration to the current configuration is defined by $[\,\overline{u}_1\ \overline{u}_2\ \overline{u}_3\,]^{\mathrm{T}}$, the translation of the cross-section centroid G and $\overline{\boldsymbol{\theta}} = [\,\overline{\theta}_1\ \overline{\theta}_2\ \overline{\theta}_3\,]^{\mathrm{T}}$, the local rotation of the section (see Figs. 4 and 5) and α, the warping intensity (see Eq. (13)).

The main interest in the separation of the local deformation and the rigid body motion is that different assumptions can be made to represent the local displacements. Hence, linear interpolation is used for the axial displacement whereas cubic interpolations are used for the transverse displacements and for the axial rotation. Then, due to the particular choice of the local degrees of freedom, one has

$$\begin{bmatrix} \overline{u}_1 \\ \overline{u}_2 \\ \overline{u}_3 \\ \overline{\theta}_1 \\ \overline{\theta}_2 \\ \overline{\theta}_3 \\ \alpha \end{bmatrix} = \begin{bmatrix} N_2 & 0 & 0 & 0 & 0 & 0 & 0 & 0 & 0 \\ 0 & 0 & 0 & N_3 & 0 & 0 & N_4 & 0 & 0 \\ 0 & 0 & -N_3 & 0 & 0 & -N_4 & 0 & 0 & 0 \\ 0 & N_7 & 0 & 0 & N_8 & 0 & 0 & N_3 & N_4 \\ 0 & 0 & N_5 & 0 & 0 & N_6 & 0 & 0 & 0 \\ 0 & 0 & 0 & N_5 & 0 & 0 & N_6 & 0 & 0 \\ 0 & N_9 & 0 & 0 & -N_9 & 0 & 0 & N_5 & N_6 \end{bmatrix} \mathbf{d}_l^w\,, \tag{67}$$

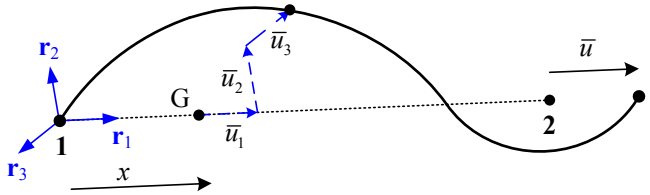

Fig. 4. Local beam configuration - Translation.

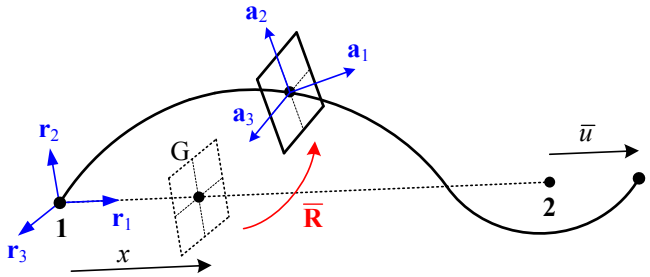

Fig. 5. Local beam configuration - Rotation.

where the local nodal displacement vector $\mathbf{d}_l^w$ is defined by Eq. (53).

The expressions of the interpolation functions are given by

$$
\begin{aligned}
&N_1 = 1 - \frac{x}{l_o}, \quad N_2 = 1 - N_1, \quad N_3 = x\left(1 - \frac{x}{l_o}\right)^2, \\
&N_4 = -\left(1 - \frac{x}{l_o}\right)\frac{x^2}{l_o}, \quad N_5 = \left(1 - \frac{3x}{l_o}\right)\left(1 - \frac{x}{l_o}\right), \quad N_6 = \left(\frac{3x}{l_o} - 2\right)\frac{x}{l_o}, \\
&N_7 = 1 - \frac{3x^2}{l_o^2} + \frac{2x^3}{l_o^3}, \quad N_8 = 1 - N_7, \quad N_9 = \frac{6x^2}{l_o^3} - \frac{6x}{l_o^2}.
\end{aligned}
$$

Let $\mathbf{u}_l = [0 \;\; \overline{u}_2 \;\; \overline{u}_3]^{\mathrm{T}}$ denotes the local transverse displacement vector. From Eq. (67), this vector is given by

$$
\mathbf{u}_l = \mathbf{P}_1 \begin{bmatrix} \overline{\boldsymbol{\theta}}_1 \\ \overline{\boldsymbol{\theta}}_2 \end{bmatrix}, \tag{68}
$$

with

$$
\mathbf{P}_1 = \begin{bmatrix} 0 & 0 & 0 & 0 & 0 & 0 \\ 0 & 0 & N_3 & 0 & 0 & N_4 \\ 0 & -N_3 & 0 & 0 & -N_4 & 0 \end{bmatrix}. \tag{69}
$$

From Eq. (67), the local rotation and the warping degree of freedom are given by

$$
\begin{bmatrix} \overline{\boldsymbol{\theta}} \\ \alpha \end{bmatrix} = \begin{bmatrix} \mathbf{P}_2 & \mathbf{P}_3 \\ \mathbf{P}_4 & \mathbf{P}_5 \end{bmatrix} \begin{bmatrix} \overline{\boldsymbol{\theta}}_1 \\ \overline{\boldsymbol{\theta}}_2 \\ \alpha_1 \\ \alpha_2 \end{bmatrix}, \tag{70}
$$

with

$$\mathbf{P}_2 = \begin{bmatrix} N_7 & 0 & 0 & N_8 & 0 & 0 \\ 0 & N_5 & 0 & 0 & N_6 & 0 \\ 0 & 0 & N_5 & 0 & 0 & N_6 \end{bmatrix}, \quad \mathbf{P}_3 = \begin{bmatrix} N_3 & N_4 \\ 0 & 0 \\ 0 & 0 \end{bmatrix}, \tag{71}$$
$$\mathbf{P}_4 = \begin{bmatrix} N_9 & 0 & 0 & -N_9 & 0 & 0 \end{bmatrix}, \quad \mathbf{P}_5 = \begin{bmatrix} N_5 & N_6 \end{bmatrix}.$$

5.2 Translational displacement variables

The position of the cross-section centroid in the global coordinate system is given by (see Fig. 4)

$$\mathrm{OG} = \mathbf{x}_\mathrm{G} = \mathbf{x}_1^g + \mathbf{u}_1^g + (x + \overline{u}_1)\,\mathbf{r}_1 + \overline{u}_2\mathbf{r}_2 + \overline{u}_3\mathbf{r}_3\,. \tag{72}$$

Using Eqs. (46), (50) and (67), the above relation can be put in the following form

$$\mathrm{OG} = N_1\mathbf{x}_1^g + N_2\mathbf{x}_2^g + N_1\mathbf{u}_1^g + N_2\mathbf{u}_2^g + \mathbf{R}_r\mathbf{u}_l\,, \tag{73}$$

with $\mathbf{u}_l$ as defined in Eq. (68).

Then by taking the variation of the above equation, the following expression is obtained

$$\delta\mathrm{OG} = \delta\mathbf{u} = \mathbf{N}\,\delta\mathbf{d}_g + \mathbf{R}_r\delta\mathbf{u}_l + \delta\mathbf{R}_r\mathbf{u}_l\,, \tag{74}$$

with $\mathbf{N} = \begin{bmatrix} N_1\mathbf{I} & \mathbf{0} & N_2\mathbf{I} & \mathbf{0} \end{bmatrix}$.
One interesting property of $\mathbf{N}$ is that

$$\mathbf{N} = \mathbf{R}_r\mathbf{N}\mathbf{E}^\mathrm{T}. \tag{75}$$

The variation $\delta\mathbf{R}_r$ is calculated

$$\delta\mathbf{R}_r = \mathbf{R}_r\,\widetilde{\delta\mathbf{w}_r^e}\,. \tag{76}$$

From Eqs. (61) and (64), $\delta\mathbf{w}_r^e$ is obtained as

$$\delta\mathbf{w}_r^e = \mathbf{G}^\mathrm{T}\mathbf{E}^\mathrm{T}\,\delta\mathbf{d}_g\,. \tag{77}$$

By taking the differentiation of Eq. (68), one obtains

$$\delta\mathbf{u}_l = \mathbf{P}_1 \begin{bmatrix} \delta\overline{\boldsymbol{\theta}}_1 \\ \delta\overline{\boldsymbol{\theta}}_2 \end{bmatrix}. \tag{78}$$

In the corotational approach, the local rotations at the nodes $\overline{\boldsymbol{\theta}}_i$ $(i = 1,2)$, defined in Eq. (52), are small and the operator $\mathbf{T}_s(\overline{\boldsymbol{\theta}}_i)$ is close to the identity matrix. Consequently, see Eq. (5), the following approximation is adopted

$$\delta\overline{\mathbf{w}}_i \approx \delta\overline{\boldsymbol{\theta}}_i\,. \tag{79}$$

Then, using Eqs. (63) and (79), the expression in (78) becomes

$$\delta\mathbf{u}_l \approx \mathbf{P}_1 \begin{bmatrix} \delta\overline{\mathbf{w}}_1 \\ \delta\overline{\mathbf{w}}_2 \end{bmatrix} = \mathbf{P}_1\,\mathbf{P}\,\mathbf{E}^\mathrm{T}\,\delta\mathbf{d}_g\,. \tag{80}$$

Inserting Eqs. (75) - (77) and (80) into Eq. (74), one obtains

$$\delta\mathbf{u} = \mathbf{R}_r \mathbf{H}_1 \mathbf{E}^{\mathrm{T}} \delta\mathbf{d}_g \,, \tag{81}$$

where

$$\mathbf{H}_1 = \mathbf{N} + \mathbf{P}_1 \mathbf{P} - \widetilde{\mathbf{u}}_l \mathbf{G}^{\mathrm{T}} \,. \tag{82}$$

Obviously, the translational velocity of the cross-section centroid is given as

$$\dot{\mathbf{u}} = \mathbf{R}_r \mathbf{H}_1 \mathbf{E}^{\mathrm{T}} \dot{\mathbf{d}}_g \,. \tag{83}$$

By taking the time derivative of the above equation, the expression of the translational acceleration reads as follows

$$\ddot{\mathbf{u}} = \mathbf{R}_r \mathbf{H}_1 \mathbf{E}^{\mathrm{T}} \ddot{\mathbf{d}}_g + \left(\dot{\mathbf{R}}_r \mathbf{H}_1 \mathbf{E}^{\mathrm{T}} + \mathbf{R}_r \dot{\mathbf{H}}_1 \mathbf{E}^{\mathrm{T}} + \mathbf{R}_r \mathbf{H}_1 \dot{\mathbf{E}}^{\mathrm{T}} \right) \dot{\mathbf{d}}_g \,, \tag{84}$$

with $\dot{\mathbf{H}}_1$ given in Appendix B.

By noting that $\dot{\mathbf{R}}_r = \mathbf{R}_r \widetilde{\dot{\mathbf{w}}_r^e}$ (see Eq. (76)), one has

$$\dot{\mathbf{E}} = \mathbf{E}\mathbf{E}_t \,, \quad \mathbf{E}_t = \begin{bmatrix} \widetilde{\dot{\mathbf{w}}_r^e} & \mathbf{0} & \mathbf{0} & \mathbf{0} \\ \mathbf{0} & \widetilde{\dot{\mathbf{w}}_r^e} & \mathbf{0} & \mathbf{0} \\ \mathbf{0} & \mathbf{0} & \widetilde{\dot{\mathbf{w}}_r^e} & \mathbf{0} \\ \mathbf{0} & \mathbf{0} & \mathbf{0} & \widetilde{\dot{\mathbf{w}}_r^e} \end{bmatrix} . \tag{85}$$

$\dot{\mathbf{w}}_r^e$ (see Eq. (77)) is calculated as

$$\dot{\mathbf{w}}_r^e = \mathbf{G}^{\mathrm{T}} \mathbf{E}^{\mathrm{T}} \dot{\mathbf{d}}_g \,. \tag{86}$$

By introducing the notation

$$\mathbf{C}_1 = \widetilde{\dot{\mathbf{w}}_r^e} \mathbf{H}_1 + \dot{\mathbf{H}}_1 - \mathbf{H}_1 \mathbf{E}_t \,, \tag{87}$$

Eq. (84) can be rewritten in a more compact form as

$$\ddot{\mathbf{u}} = \mathbf{R}_r \mathbf{H}_1 \mathbf{E}^{\mathrm{T}} \ddot{\mathbf{d}}_g + \mathbf{R}_r \mathbf{C}_1 \mathbf{E}^{\mathrm{T}} \dot{\mathbf{d}}_g \,. \tag{88}$$

5.3 Finite rotations and warping variables

Combining Eq. (70) with the approximation defined in Eq. (79), the local spatial spin and warping variables are calculated as follows

$$\delta\overline{\mathbf{w}} = \begin{bmatrix} \mathbf{P}_2 & \mathbf{P}_3 \end{bmatrix} \begin{bmatrix} \delta\overline{\mathbf{w}}_1 \\ \delta\overline{\mathbf{w}}_2 \\ \delta\alpha_1 \\ \delta\alpha_2 \end{bmatrix} , \quad \delta\alpha = \begin{bmatrix} \mathbf{P}_4 & \mathbf{P}_5 \end{bmatrix} \begin{bmatrix} \delta\overline{\mathbf{w}}_1 \\ \delta\overline{\mathbf{w}}_2 \\ \delta\alpha_1 \\ \delta\alpha_2 \end{bmatrix} . \tag{89}$$

Using Eq. (63), the above equation leads to

$$\delta\overline{\mathbf{w}} = \begin{bmatrix} \mathbf{P}_2 & \mathbf{P}_3 \end{bmatrix} \begin{bmatrix} \mathbf{P}\mathbf{E}^{\mathrm{T}} & \mathbf{0} \\ \mathbf{0} & \mathbf{I}_2 \end{bmatrix} \delta\mathbf{d}_g^w = \begin{bmatrix} \mathbf{P}_2\mathbf{P} & \mathbf{P}_3 \end{bmatrix} \mathbf{E}^{w\mathrm{T}} \delta\mathbf{d}_g^w , \tag{90}$$

$$\delta\alpha = \begin{bmatrix} \mathbf{P}_4 & \mathbf{P}_5 \end{bmatrix} \begin{bmatrix} \mathbf{P}\mathbf{E}^{\mathrm{T}} & \mathbf{0} \\ \mathbf{0} & \mathbf{I}_2 \end{bmatrix} \delta\mathbf{d}_g^w = \mathbf{H}_3 \mathbf{E}^{w\mathrm{T}} \delta\mathbf{d}_g^w , \tag{91}$$

where

$$\mathbf{E}^w = \begin{bmatrix} \mathbf{E} & \mathbf{0} \\ \mathbf{0} & \mathbf{I}_2 \end{bmatrix}, \quad \mathbf{I}_2 = \begin{bmatrix} 1 & 0 \\ 0 & 1 \end{bmatrix}, \quad \mathbf{H}_3 = \begin{bmatrix} \mathbf{P}_4\mathbf{P} & \mathbf{P}_5 \end{bmatrix}. \tag{92}$$

Using Eqs. (58) and (59), the spatial spin variables, associated to the global rotation of a cross-section, are evaluated using

$$\delta\mathbf{w} = \mathbf{R}_r \delta\mathbf{w}^e = \mathbf{R}_r \left(\delta\mathbf{w}_r^e + \delta\overline{\mathbf{w}} \right). \tag{93}$$

Using Eqs. (77) and (90), the above expression can be rewritten in as

$$\delta\mathbf{w} = \mathbf{R}_r \mathbf{H}_2 \mathbf{E}^{w\mathrm{T}} \delta\mathbf{d}_g^w , \tag{94}$$

with

$$\mathbf{H}_2 = \begin{bmatrix} \mathbf{P}_2\mathbf{P} + \mathbf{G}^{\mathrm{T}} & \mathbf{P}_3 \end{bmatrix}. \tag{95}$$

$\dot{\mathbf{w}}$ and $\dot{\alpha}$ are calculated with expressions similar to (91) and (94)

$$\dot{\mathbf{w}} = \mathbf{R}_r \mathbf{H}_2 \mathbf{E}^{w\mathrm{T}} \dot{\mathbf{d}}_g^w , \quad \dot{\alpha} = \mathbf{H}_3 \mathbf{E}^{w\mathrm{T}} \dot{\mathbf{d}}_g^w . \tag{96}$$

$\ddot{\mathbf{w}}$ is obtained by taking the time derivative of $\dot{\mathbf{w}}$

$$\ddot{\mathbf{w}} = \mathbf{R}_r \mathbf{H}_2 \mathbf{E}^{w\mathrm{T}} \ddot{\mathbf{d}}_g^w + \mathbf{R}_r \left(\widetilde{\dot{\mathbf{w}}_r^e} \mathbf{H}_2 + \dot{\mathbf{H}}_2 - \mathbf{H}_2 \mathbf{E}_t^w \right) \mathbf{E}^{w\mathrm{T}} \dot{\mathbf{d}}_g^w , \tag{97}$$

with $\dot{\mathbf{H}}_2$ given in Appendix B and

$$\mathbf{E}_t^w = \begin{bmatrix} \mathbf{E}_t & \mathbf{0} \\ \mathbf{0} & \mathbf{0}_2 \end{bmatrix}. \tag{98}$$

By noting that

$$\mathbf{P}_4\mathbf{P} = \begin{bmatrix} 0 & 0 & 0 & N_9 & 0 & 0 & 0 & 0 & 0 & -N_9 & 0 & 0 \end{bmatrix}, \tag{99}$$

and by taking the time derivative of $\dot{\alpha}$, the expression of $\ddot{\alpha}$ is obtained

$$\ddot{\alpha} = \mathbf{H}_3 \mathbf{E}^{w\mathrm{T}} \ddot{\mathbf{d}}_g^w - \mathbf{H}_3 \mathbf{E}_t^w \mathbf{E}^{w\mathrm{T}} \dot{\mathbf{d}}_g^w . \tag{100}$$

Introducing Eqs. (91),(94),(96),(97), and (100) into Eq. (42), one obtains

$$\delta\mathbf{w}^w = \begin{bmatrix} \mathbf{R}_r & \mathbf{0} \\ \mathbf{0} & 1 \end{bmatrix} \begin{bmatrix} \mathbf{H}_2 \\ \mathbf{H}_3 \end{bmatrix} \mathbf{E}^{w\mathrm{T}} \delta\mathbf{d}_g^w = \mathbf{R}_r^w \mathbf{H}_2^w \mathbf{E}^{w\mathrm{T}} \delta\mathbf{d}_g^w , \tag{101}$$

$$\dot{\mathbf{w}}^w = \mathbf{R}_r^w \, \mathbf{H}_2^w \, \mathbf{E}^{w\mathrm{T}} \, \dot{\mathbf{d}}_g^w \,, \tag{102}$$

$$\ddot{\mathbf{w}}^w = \mathbf{R}_r^w \, \mathbf{H}_2^w \, \mathbf{E}^{w\mathrm{T}} \, \ddot{\mathbf{d}}_g^w + \mathbf{R}_r^w \, \mathbf{C}_2 \, \mathbf{E}^{w\mathrm{T}} \, \dot{\mathbf{d}}_g^w \,, \tag{103}$$

where

$$\mathbf{C}_2 = \begin{bmatrix} \widetilde{\dot{\mathbf{w}}_r^e} \, \mathbf{H}_2 + \dot{\mathbf{H}}_2 - \mathbf{H}_2 \, \mathbf{E}_t^w \\ -\mathbf{H}_3 \, \mathbf{E}_t^w \end{bmatrix} . \tag{104}$$

5.4 Inertia force vector and tangent dynamic matrix

By inserting the expressions of $\delta\mathbf{u}$ and $\delta\mathbf{w}^w$ given in Eqs. (81) and (101) into Eq. (44), the inertia force vector is obtained as

$$\mathbf{f}_{\mathrm{k}}^w = \mathbf{E}^w \left\{ \begin{bmatrix} \int_{l_o} \mathbf{H}_1^{\mathrm{T}} \, \mathbf{R}_r^{\mathrm{T}} \, A_\rho \, \ddot{\mathbf{u}} \mathrm{d}l \\ \mathbf{0} \end{bmatrix} + \int_{l_o} \mathbf{H}_2^{w\mathrm{T}} \, \mathbf{R}_r^{w\mathrm{T}} \left[\mathbf{I}_\rho^1 \, \ddot{\mathbf{w}}^w + \mathbf{I}_\rho^2 \, \dot{\mathbf{w}}^w \right] \mathrm{d}l \right\} . \tag{105}$$

As shown in the above equation, the inertia force vector depends on $\mathbf{d}_g^w, \dot{\mathbf{d}}_g^w$ and $\ddot{\mathbf{d}}_g^w$. Hence, linearization of this force vector is evaluated as follows

$$\Delta\mathbf{f}_{\mathrm{k}}^w = \mathbf{M}\Delta\ddot{\mathbf{d}}_g^w + \mathbf{C}_{\mathrm{k}}\Delta\dot{\mathbf{d}}_g^w + \mathbf{K}_{\mathrm{k}}\Delta\mathbf{d}_g^w \,. \tag{106}$$

Some authors [7, 17] proposed to keep only the mass matrix $\mathbf{M}$, and to eliminate the gyroscopic $\mathbf{C}_{\mathrm{k}}$ and centrifugal $\mathbf{K}_{\mathrm{k}}$ dynamic matrices. However, in [29], extensive numerical studies have shown that it is advantageous to retain also the gyroscopic matrix as it enhances the computational efficiency. The same approach is used here. The centrifugal matrix, whose derivation is complicated and would give rise to a lengthy mathematical expression, is neglected. Therefore, the iterative scheme of the present formulation is implemented with the following approximative linearization

$$\Delta\mathbf{f}_{\mathrm{k}}^w \approx \mathbf{M}\Delta\ddot{\mathbf{d}}_g^w + \mathbf{C}_{\mathrm{k}}\Delta\dot{\mathbf{d}}_g^w \,. \tag{107}$$

From the expressions (88), (102) and (103), the following linearizations are derived

$$\begin{aligned} \Delta\ddot{\mathbf{u}} &= \mathbf{R}_r \left[\mathbf{H}_1 \, \mathbf{E}^{\mathrm{T}} \, \Delta\ddot{\mathbf{d}}_g + \mathbf{C}_1 \, \mathbf{E}^{\mathrm{T}} \, \Delta\dot{\mathbf{d}}_g + (\frac{\partial \mathbf{C}_1}{\partial \dot{\mathbf{d}}_g} \Delta\dot{\mathbf{d}}_g) \, \mathbf{E}^{\mathrm{T}} \, \dot{\mathbf{d}}_g \right] + f(\Delta\mathbf{d}_g) \\ &= \mathbf{R}_r \left[\mathbf{H}_1 \, \mathbf{E}^{\mathrm{T}} \, \Delta\ddot{\mathbf{d}}_g + (\mathbf{C}_1 + \mathbf{C}_3) \, \mathbf{E}^{\mathrm{T}} \, \Delta\dot{\mathbf{d}}_g \right] + f(\Delta\mathbf{d}_g) \,, \end{aligned} \tag{108}$$

$$\Delta\dot{\mathbf{w}}^w = \mathbf{R}_r^w \, \mathbf{H}_2^w \, \mathbf{E}^{w\mathrm{T}} \, \Delta\dot{\mathbf{d}}_g^w + f(\Delta\mathbf{d}_g^w) \,, \tag{109}$$

$$\begin{aligned} \Delta\ddot{\mathbf{w}}^w &= \mathbf{R}_r^w \left[\mathbf{H}_2^w \, \mathbf{E}^{w\mathrm{T}} \, \Delta\ddot{\mathbf{d}}_g^w + \mathbf{C}_2 \, \mathbf{E}^{w\mathrm{T}} \, \Delta\dot{\mathbf{d}}_g^w + (\frac{\partial \mathbf{C}_2}{\partial \dot{\mathbf{d}}_g^w} \Delta\dot{\mathbf{d}}_g^w) \, \mathbf{E}^{w\mathrm{T}} \, \dot{\mathbf{d}}_g^w \right] + f(\Delta\mathbf{d}_g^w) \\ &= \mathbf{R}_r^w \left[\mathbf{H}_2^w \, \mathbf{E}^{w\mathrm{T}} \, \Delta\ddot{\mathbf{d}}_g^w + (\mathbf{C}_2 + \mathbf{C}_4) \, \mathbf{E}^{w\mathrm{T}} \, \Delta\dot{\mathbf{d}}_g^w \right] + f(\Delta\mathbf{d}_g^w) \,, \end{aligned} \tag{110}$$

with $\mathbf{C}_3$ and $\mathbf{C}_4$ given in Appendix C.

Using the above linearizations, the expression of the mass matrix $\mathbf{M}$ is obtained as

$$\begin{aligned}\mathbf{M} &= \mathbf{E}^w \left\{ \begin{bmatrix} \int_{l_o} \mathbf{H}_1^{\mathrm{T}} A_\rho \, \mathbf{H}_1 \, \mathrm{d}l & \mathbf{0} \\ \mathbf{0} & \mathbf{0} \end{bmatrix} + \int_{l_o} \mathbf{H}_2^{w\mathrm{T}} \, \mathbf{R}_r^{w\mathrm{T}} \, \mathbf{I}_\rho^1 \, \mathbf{R}_r^w \, \mathbf{H}_2^w \, \mathrm{d}l \right\} \mathbf{E}^{w\mathrm{T}} \\ &= \mathbf{E}^w \, \mathbf{M}^e \, \mathbf{E}^{w\mathrm{T}} . \end{aligned} \tag{111}$$

Regarding the gyroscopic matrix $\mathbf{C}_{\mathrm{k}}$, the following intermediate variation is used

$$\begin{aligned}\frac{\partial \mathbf{I}_\rho^2 \dot{\mathbf{w}}^w}{\partial \dot{\mathbf{w}}^w} \Delta \dot{\mathbf{w}}^w &= \begin{bmatrix} \widetilde{\dot{\mathbf{w}}} \, (\mathbf{I}_\rho + \mathbf{I}_\alpha) \Delta \dot{\mathbf{w}} + \widetilde{\Delta \dot{\mathbf{w}}} \, (\mathbf{I}_\rho + \mathbf{I}_\alpha) \dot{\mathbf{w}} + \mathbf{I}_c \, (\Delta \dot{\mathbf{w}} \, \dot{\alpha} + \dot{\mathbf{w}} \Delta \dot{\alpha}) \\ -\Delta \dot{\mathbf{w}}^{\mathrm{T}} \, \mathbf{I}_\alpha^{'} \, \dot{\mathbf{w}} - \dot{\mathbf{w}}^{\mathrm{T}} \, \mathbf{I}_\alpha^{'} \, \Delta \dot{\mathbf{w}} \end{bmatrix} \\ &= \begin{bmatrix} \widetilde{\dot{\mathbf{w}}} \, (\mathbf{I}_\rho + \mathbf{I}_\alpha) & \mathbf{I}_c \, \dot{\mathbf{w}} \\ -\dot{\mathbf{w}}^{\mathrm{T}} \, \mathbf{I}_\alpha^{'} & 0 \end{bmatrix} \Delta \dot{\mathbf{w}}^w + \begin{bmatrix} \widetilde{(\mathbf{I}_\rho + \mathbf{I}_\alpha) \dot{\mathbf{w}}} & + \mathbf{I}_c \, \dot{\alpha} & \mathbf{0} \\ -\dot{\mathbf{w}}^{\mathrm{T}} \, \mathbf{I}_\alpha^{'\mathrm{T}} & & 0 \end{bmatrix} \Delta \dot{\mathbf{w}}^w \\ &= \left(\mathbf{I}_\rho^2 + \mathbf{I}_\rho^3 \right) \Delta \dot{\mathbf{w}}^w . \end{aligned} \tag{112}$$

Finally, the gyroscopic matrix $\mathbf{C}_{\mathrm{k}}$ is calculated from

$$\begin{aligned}\mathbf{C}_{\mathrm{k}} = & \mathbf{E}^w \left\{ \begin{bmatrix} \int_{l_o} \mathbf{H}_1^{\mathrm{T}} A_\rho \, (\mathbf{C}_1 + \mathbf{C}_3) \, \mathrm{d}l & \mathbf{0} \\ \mathbf{0} & \mathbf{0} \end{bmatrix} + \int_{l_o} \mathbf{H}_2^{w\mathrm{T}} \, \mathbf{R}_r^{w\mathrm{T}} \, \mathbf{I}_\rho^1 \, \mathbf{R}_r^w \, (\mathbf{C}_2 + \mathbf{C}_4) \, \mathrm{d}l \right. \\ & \left. + \int_{l_o} \mathbf{H}_2^{w\mathrm{T}} \, \mathbf{R}_r^{w\mathrm{T}} \, \left(\mathbf{I}_\rho^2 + \mathbf{I}_\rho^3 \right) \, \mathbf{R}_r^w \, \mathbf{H}_2^w \, \mathrm{d}l \right\} \mathbf{E}^{w\mathrm{T}} = \mathbf{E}^w \, \mathbf{C}_{\mathrm{k}}^e \, \mathbf{E}^{w\mathrm{T}} . \end{aligned} \tag{113}$$

In this work, the warping deformations and the eccentricity of the shear center have been taken into account in deriving the inertial terms, see Eq. (13). Consequently, several additional terms have been introduced in the expressions of the inertia force vector and the tangent (mass and gyroscopic) matrices. The importance of these terms can be discussed. In the five numerical examples presented in Section 7, it has been found, as expected, that the warping deformations in the dynamic terms have a negligible contribution to the response and can be omitted. This is done by setting $I_\omega = 0$ in Eqs. (19) and (20).

The eccentricity of the shear center with respect to the centroid generates extra dynamic terms whose importance has been investigated. It appears that for slender beams (Examples 7.1, 7.2 and 7.4), these terms do not affect the results and can be therefore neglected. But as it will be shown in Example 7.5, they may have a significant contribution for short beams.

If $I_\omega = y_c = z_c = 0$ is adopted, then the expression of the inertia force vector in Eq. (105) can be simplified as

$$\mathbf{f}_{\mathrm{k}}^w = \mathbf{E}^w \left\{ \begin{bmatrix} \int_{l_o} \mathbf{H}_1^{\mathrm{T}} \, \mathbf{R}_r^{\mathrm{T}} \, A_\rho \, \ddot{\mathbf{u}} \mathrm{d}l \\ \mathbf{0} \end{bmatrix} + \int_{l_o} \mathbf{H}_2^{\mathrm{T}} \, \mathbf{R}_r^{\mathrm{T}} \, \left[\mathbf{I}_\rho \, \ddot{\mathbf{w}} + \widetilde{\ddot{\mathbf{w}}} \, \mathbf{I}_\rho \, \dot{\mathbf{w}} \right] \mathrm{d}l \right\} , \tag{114}$$

and similar simplifications apply also for the expressions of the mass and gyroscopic matrices.

6 Internal force vector and tangent stiffness matrix

The purpose of this section is to present briefly the derivation of the inertial force vector and the tangent stiffness matrix. A complete description can be found in [4].

The local nodal displacements and rotations defined in Eq. (53) are extracted from the global degrees of freedom using Eqs. (50), (51) and (52).

The local internal force vector $\mathbf{f}_{\mathrm{l}}^{w}$ and the local tangent stiffness matrix $\mathbf{K}_{\mathrm{l}}^{w}$ associated with $\delta\mathbf{d}_{l}^{w}$ (see Eq. (54)) are derived using the same local beam kinematic description as in 5.1. However, to incorporate the bending shear deformations, the Hermitian shape functions for the transverse displacements are slightly modified as suggested in the Interdependent Interpolation Element (IIE) [37]. The Maple codes for $\mathbf{f}_{\mathrm{l}}^{w}$ and $\mathbf{K}_{\mathrm{l}}^{w}$ are given in Appendix A. A low order of geometrical nonlinearity is introduced through a shallow arch strain description and the Wagner term.

The global internal force vector $\mathbf{f}_{\mathrm{g}}^{w}$ and the global tangent stiffness matrix $\mathbf{K}_{\mathrm{g}}^{w}$ associated with $\delta\mathbf{d}_{g}^{w}$ (see Eq. (55)) are obtained through a change of variables based on the transformation matrix $\mathbf{B}^{w}$ defined by

$$\delta\mathbf{d}_{l}^{w} = \mathbf{B}^{w}\,\delta\mathbf{d}_{g}^{w}\,. \tag{115}$$

By equating the internal virtual work in both the global and local systems, the expression of the global internal force vector $\mathbf{f}_{\mathrm{g}}^{w}$ is obtained as

$$\mathbf{f}_{\mathrm{g}}^{w} = \mathbf{B}^{w\mathrm{T}}\mathbf{f}_{\mathrm{l}}^{w}\,. \tag{116}$$

By taking the variations of Eq. (116), the expression of the global tangent stiffness matrix $\mathbf{K}_{\mathrm{g}}^{w}$ is obtained

$$\mathbf{K}_{\mathrm{g}}^{w} = \mathbf{B}^{w\mathrm{T}}\mathbf{K}_{\mathrm{l}}^{w}\mathbf{B}^{w} + \left.\frac{\partial(\mathbf{B}^{w\mathrm{T}}\mathbf{f}_{\mathrm{l}}^{w})}{\partial\mathbf{d}_{g}^{w}}\right|_{\mathbf{f}_{\mathrm{l}}^{w}}. \tag{117}$$

The expressions of $\mathbf{f}_{\mathrm{g}}^{w}$ and $\mathbf{K}_{\mathrm{g}}^{w}$ are given in [4].

7 Numerical examples

The purpose of the five numerical examples presented in this section is to assess the accuracy of the proposed corotational dynamic formulation for beam with thin-walled cross-section. For that, additional 3D-solid analyses are performed with the commercial finite element program Abaqus.

Besides, the influence of the warping deformations (I_{ω}) and the shear center eccentricity (y_c, z_c) in the dynamic terms of the corotational formulation is also studied. In all the examples, and as expected, the same results have been obtained with and without I_{ω} in the inertia terms. In Examples 7.1, 7.2 and 7.4, which consists of slender beams, the same results have been obtained with $y_c = z_c = 0$. However, for the short beam in Example 7.5, different results are obtained with and without account for the eccentricity of the shear center.

Regarding the time integration method, the HHT α method with $\alpha = -0.05$ is used in this work. This energy-dissipative method, which is implemented in several commercial FEM programs (Abaqus, Lusas) and was employed by many authors [7, 10, 26], limits the influence of high frequencies by introducing a numerical damping. However, a numerical damping gives also a dissipation of the total energy, which can affect long time analyses. It can be noted that for beam structures, more robust alternatives to the HHT α method have been proposed in the literature [22].

In the present work, at the beginning of each time step, the predictor proposed by Crisfield [11] for the particular case of linear inertia force vector and further developed for the general case by the authors [29], is adopted. The idea of this predictor is to use the tangent operator at the time instant t_n to predict the values at the time instant t_{n+1}.

Damping is not considered. The following convergence criterion is adopted: the norm of the residual vector must be less than the prescribed tolerance $\varepsilon_f = 10^{-5}$.

The following material properties are used for all the five examples: $E = 210$ GPa, $\nu = 0.33$ and $\rho = 7850$ kg/m^3. All the dimensions in the figures are in meter.

7.1 Example 1: Cantilever beam with a T cross-section

The nonlinear dynamic behavior of a cantilever beam with a T cross-section, see Fig. 6, is investigated. The eccentricity of the shear center is $y_c = 0.046$ m. At the left end, the beam is clamped and all degrees of freedom, including warping, are set to zero. At the point O of the right end section, two time-varying loads are applied: $F_y^{\mathrm{O}} = -50F$, $F_z^{\mathrm{O}} = 25F$. The time evolution of F is given in Fig. 7.

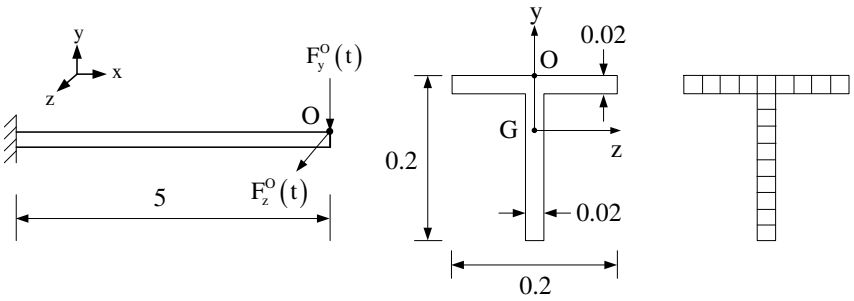

Fig. 6. Cantilever beam with T cross-section : geometrical data.

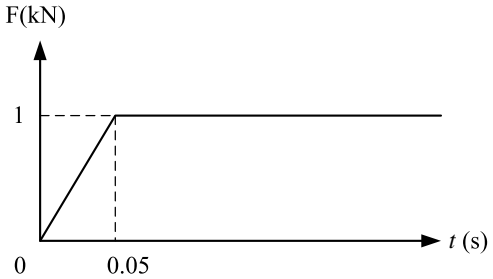

Fig. 7. Cantilever beam with T cross-section - Loading history.

The cantilever is modeled using 40 corotational beam elements. Besides, the commercial finite element software Abaqus is employed considering both beam and 3D-solid elements.

For the beam analysis, 80 B31OS elements are used. The beam element B31OS has seven degrees of freedom at each node. The additional degree of freedom represents the warping of the beam cross-section. Linear interpolations are used for all variables. For the 3D-solid analysis, the mesh consists of $18 \cdot 160 = 2880$ isoparametric 20 node elements (see Fig. 6). All analyses are performed with a time step $\Delta t = 10^{-3}$ s.

The displacements of the right end centroid G are depicted in Figs. 8, 9, and 10. A very good agreement in the predictions of both the corotational beam element and Abaqus 3D-solid analyses is obtained. However, large discrepancies in the predictions of both Abaqus beam and 3D-solid models can be observed, especially in Fig. 8.

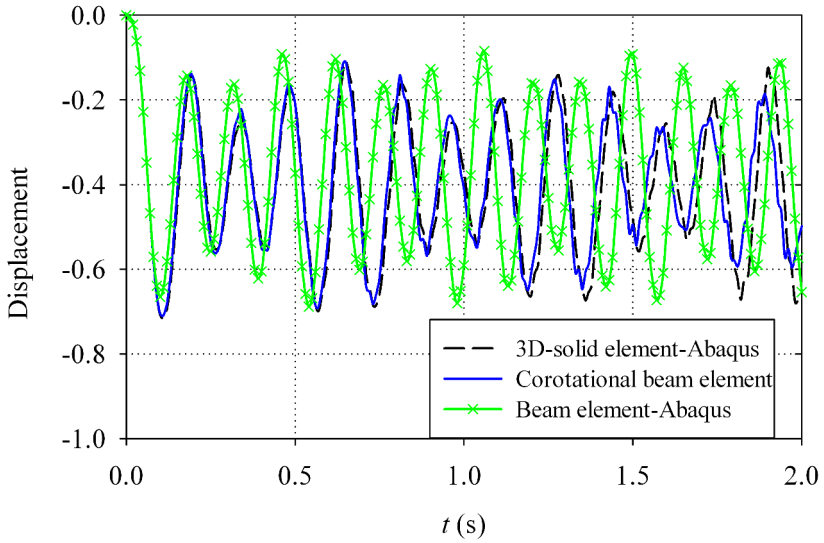

Fig. 8. Cantilever beam with T cross-section - Time evolution of the displacement u_y of point G.

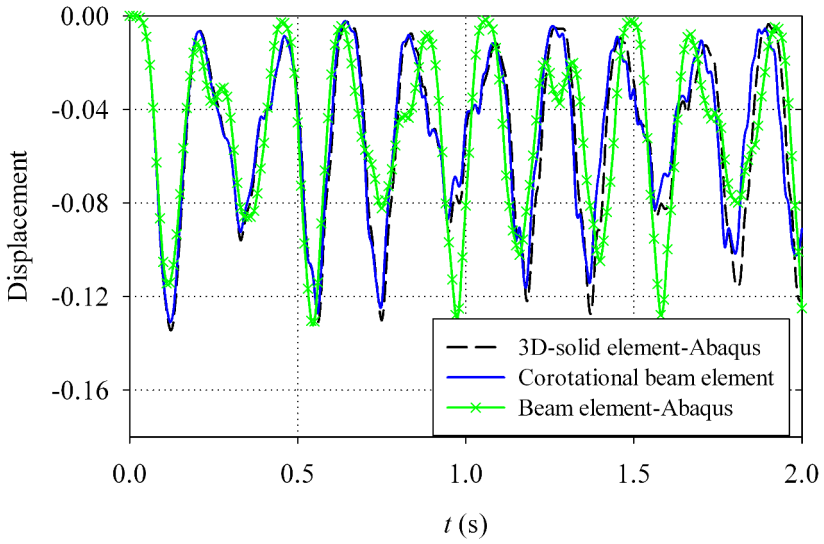

Fig. 9. Cantilever beam with T cross-section - Time evolution of the displacement u_x of point G.

A small but increasing phase lead can be observed between the results obtained with the corotational beam element and those obtained with the solid analysis. To investigate this aspect, the problem has been run for a time period of 7 s. The results are shown in Fig. 11. It can be observed that after 7 s the phase lead remains negligible. In fact, this increasing phase lead is due to a small difference in the estimation of natural frequencies between the two models.

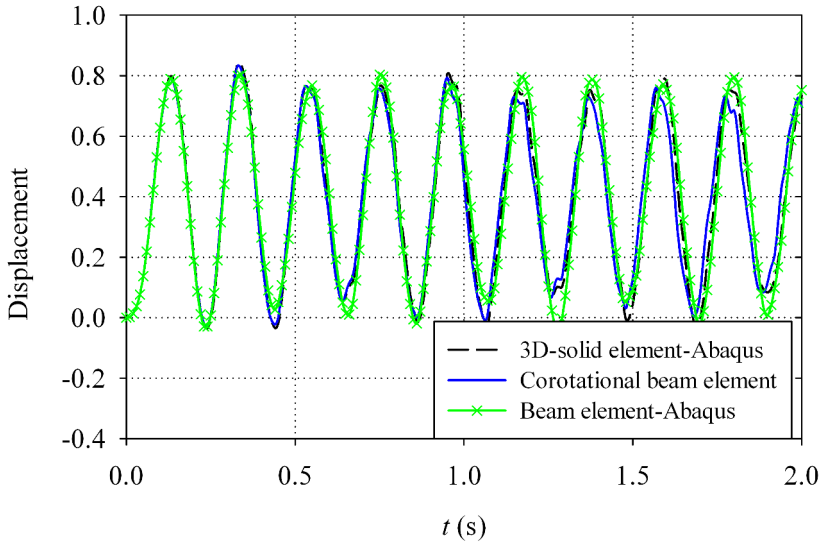

Fig. 10. Cantilever beam with T cross-section - Time evolution of the displacement u_z of point G.

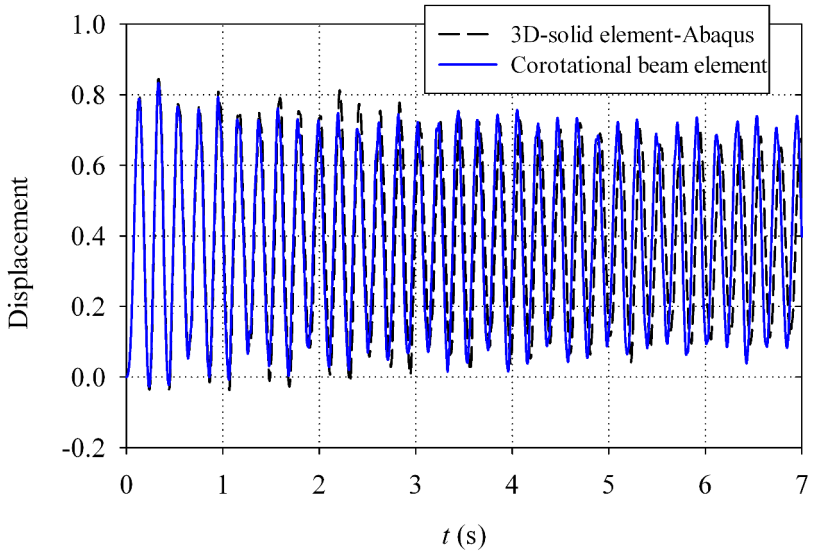

Fig. 11. Cantilever beam with T cross-section - Time evolution of the displacement u_z of point G for 7 s.

7.2 Example 2: Cantilever beam with an U cross-section

The second example, depicted in Fig. 12, is a cantilever beam with an U cross-section. The eccentricity of the shear center is given by $z_c = -0.060$ m. The beam is subjected to a dynamic concentrated load at the right end. The load, see Fig. 13, is applied at point O and acts only during $0 \leq t(\text{s}) \leq 0.6$. Thereafter the cantilever undergoes free vibration.

The cantilever is modeled using 40 corotational beam elements. For the 3D-solid analysis using Abaqus the mesh consists of $22 \cdot 225 = 4950$ isoparametric 20 node elements (see Fig. 12). Moreover, the beam is modeled with 40 Abaqus beam elements B31OS. All analyses are performed with a time step $\Delta t = 5 \cdot 10^{-4}$

s.

The time evolution of the displacements of point A at the right end are depicted in Figs. 14, 15 and 16. The results obtained with the corotational beam element are in a good agreement with those provided by Abaqus 3D-solid analysis. Again, large discrepancies between the predictions of Abaqus beam and

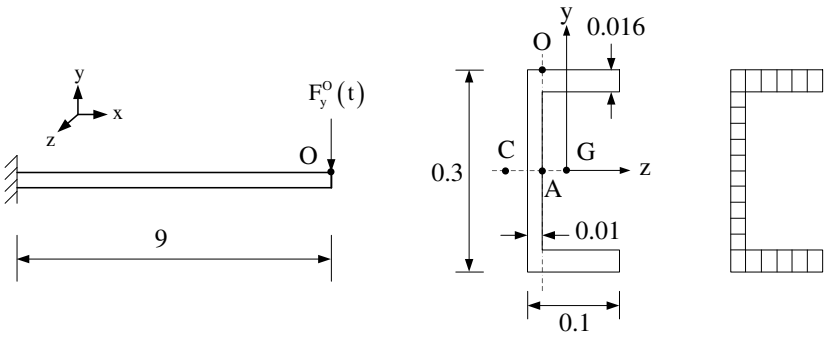

Fig. 12. Cantilever beam with U cross-section : geometrical data.

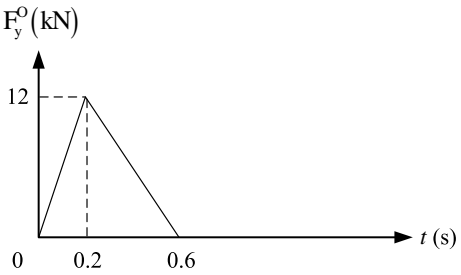

Fig. 13. Cantilever beam with U cross-section - Loading history.

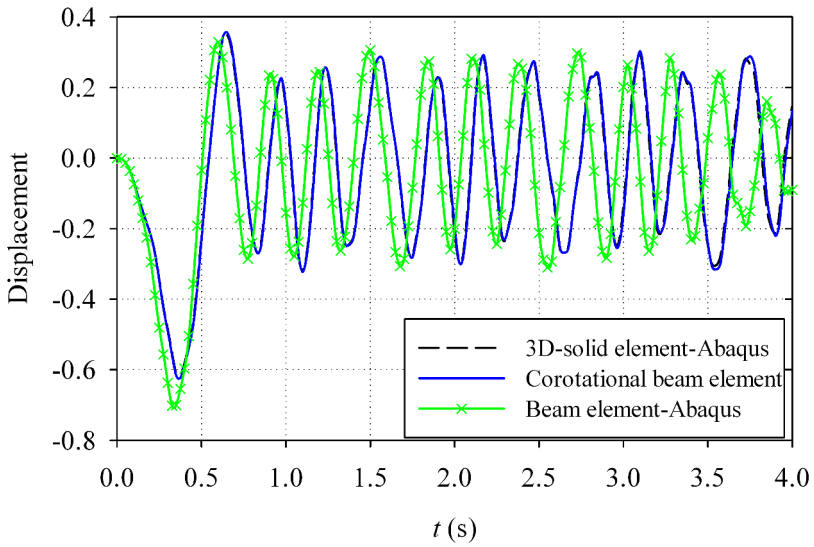

Fig. 14. Cantilever beam with U cross-section - Time evolution of the displacement u_y of point A.

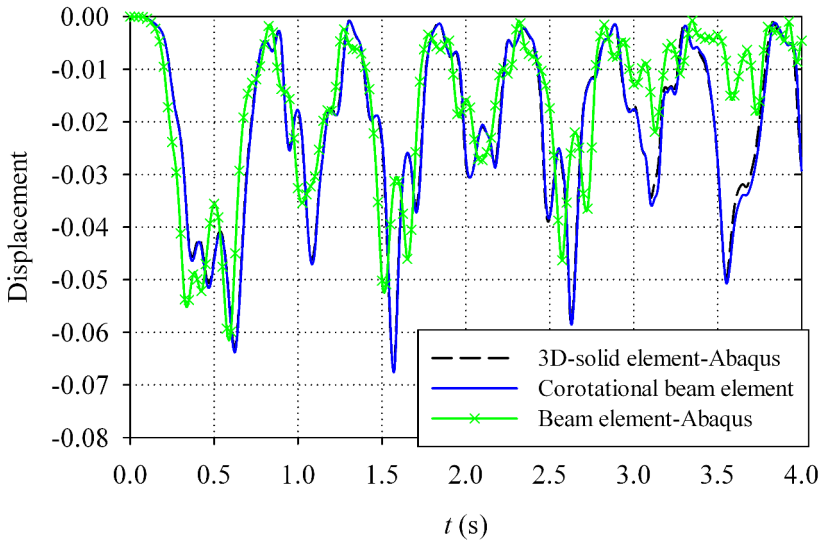

Fig. 15. Cantilever beam with U cross-section - Time evolution of the displacement u_x of point A.

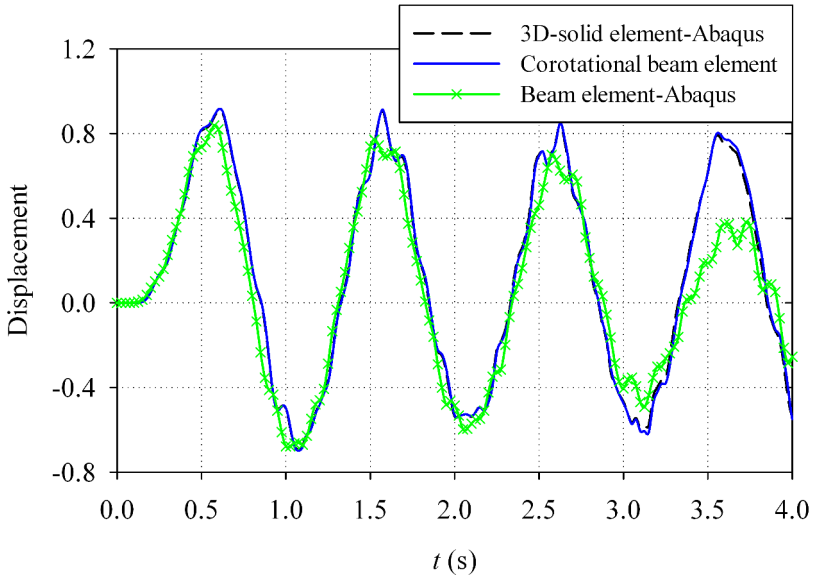

Fig. 16. Cantilever beam with U cross-section - Time evolution of the displacement u_z of point A.

3D-solid models can be seen.

In order to assess the stability of the HHT α method when combined with the new beam element, this numerical example is run for a time period $t = 20$ s (40000 time increments). The time evolution of the total energy is depicted in Fig. 17. The results show that no numerical instability has appeared during the time period under consideration. The dissipation of energy between $t = 0.6$ s and $t = 4$ s is about 2%. At the end of the analysis (after 40000 time increments), the total energy is equal to 48% of the energy at $t = 0.6$ s.

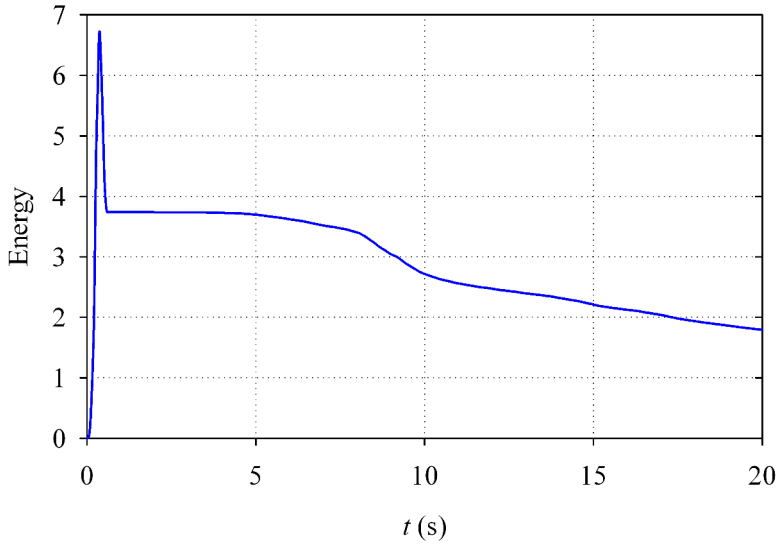

Fig. 17. Cantilever beam with U cross-section - Time evolution of the total energy.

7.3 Example 3: Cantilever beam with an I cross-section

The third example concerns a cantilever beam with an I cross-section, see Fig. 18. The beam is set into motion by four dynamic concentrated loads applied at the cross-section centroid A and at point O. The time-varying loads, applied at point A, are: $F_y^{\mathrm{A}} = 20F$, $F_z^{\mathrm{A}} = -10F$. The time-varying loads, applied at point O, are: $F_y^{\mathrm{O}} = -10F$, $F_z^{\mathrm{O}} = 5F$. The time evolution of F is given in Fig. 19.

Both the corotational beam element, Abaqus beam element B31OS and Abaqus 3D-solid element are used to simulate the nonlinear dynamic behavior of the beam. All analyzes are performed with a time step $\Delta t = 10^{-4}$ s. The displacements of the cross-section centroid G at the right end are depicted in Figs. 20, 21 and 22. The results, obtained with 20 corotational beam elements are in a good agreement with the ones provided by the 3D-solid model. The 3D-solid model adopts a mesh with $18 \cdot 100 = 1800$ isoparametric 20 node elements (see Fig. 18). It can be noted that in this case (bisymmetric cross-section), the beam model with 20 B31OS elements gives good results in comparison with the 3D-solid one. Therefore, it seems that the discrepancies observed in the first two examples could be attributed to the approach adopted in Abaqus to introduce the eccentricity of the shear center. In order to assess the stability of the HHT α method when

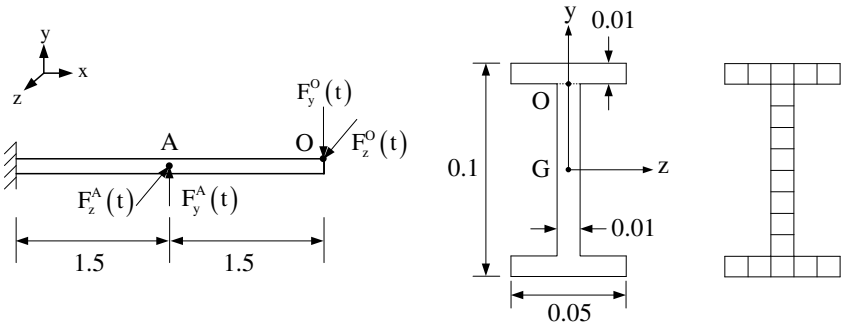

Fig. 18. Cantilever beam with I cross-section : geometrical data.

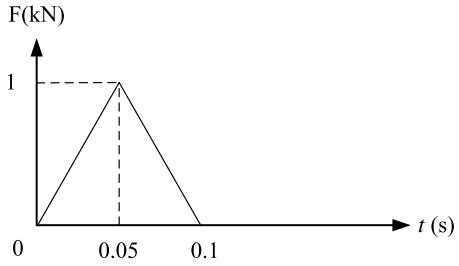

Fig. 19. Cantilever beam with I cross-section - Loading history.

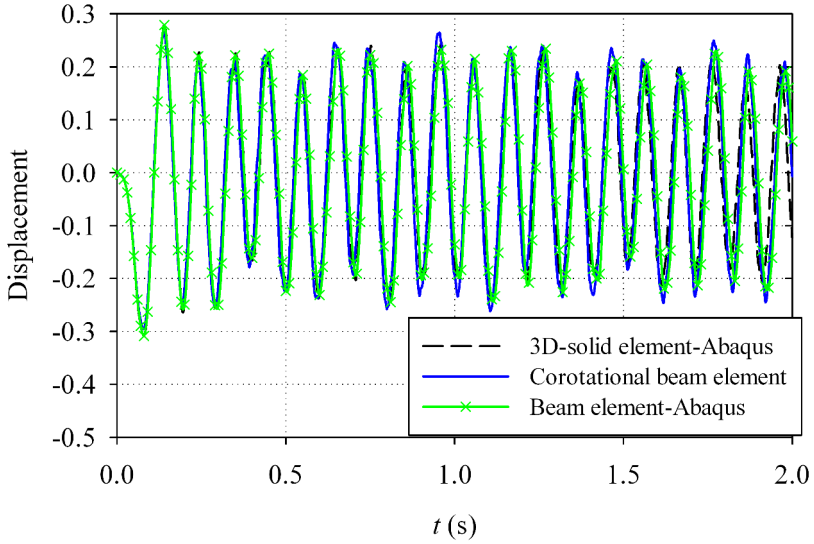

Fig. 20. Cantilever beam with I cross-section - Time evolution of the displacement u_y of point G.

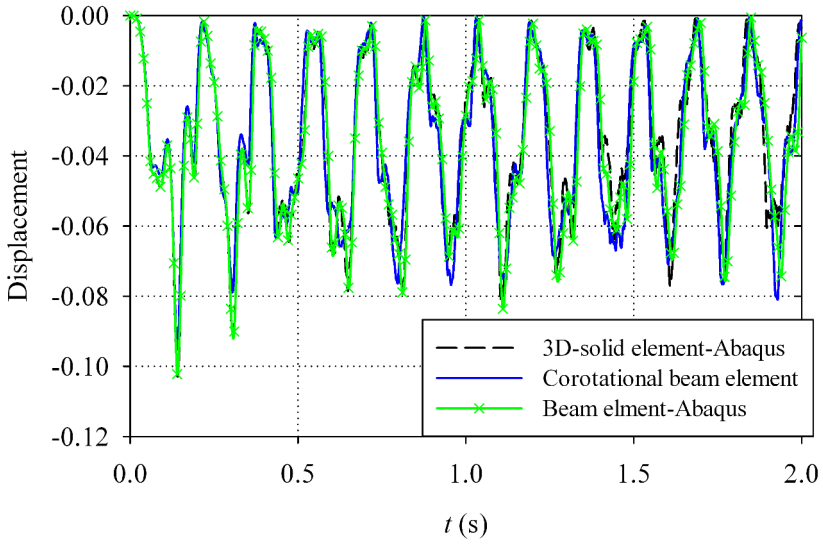

Fig. 21. Cantilever beam with I cross-section - Time evolution of the displacement u_x of point G.

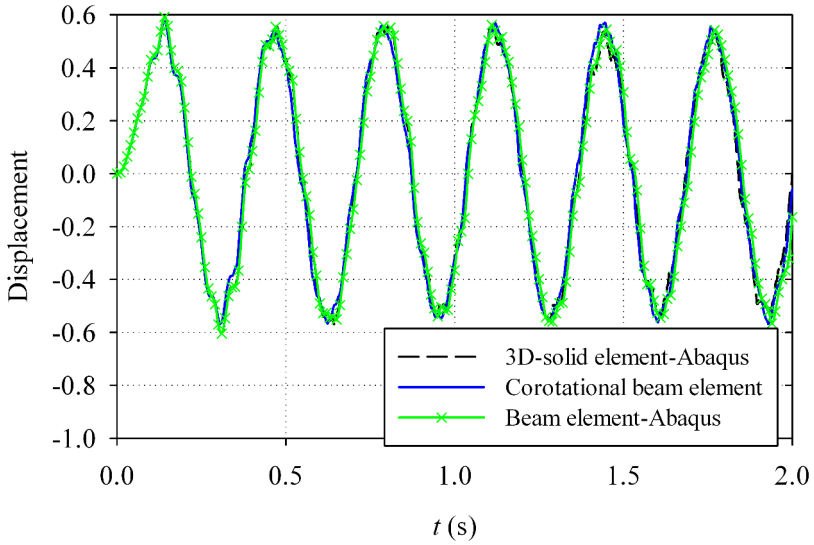

Fig. 22. Cantilever beam with I cross-section - Time evolution of the displacement u_z of point G.

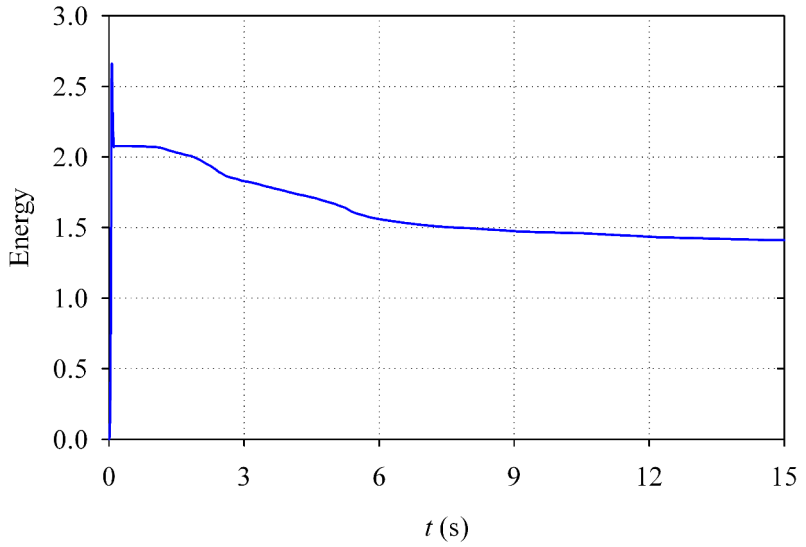

Fig. 23. Cantilever beam with C cross-section - Time evolution of the total energy.

combined with the new beam element, this numerical example is run for a time period $t = 15$ s (150000 time increments). The time evolution of the total energy is depicted in Fig. 23. The results shows that no numerical instability has appeared during the time period under consideration. The dissipation of energy between $t = 0.1$ s and $t = 2$ s is about 5%. At the end of the analysis (after 150000 time increments), the total energy is equal to 68% of the energy at $t = 0.1$ s.

7.4 Example 4: Cantilever beam with a L cross-section

In this example, a cantilever beam with a L cross-section is analyzed (see Fig. 24). The eccentricity of the shear center is given by $y_c = -0.054$ m and $z_c = -0.03$ m. The beam is subjected to two sinusoidal concentrated loads applied at points A and B. The time-varying loads are: $F_y^{\mathrm{A}} = -F_z^{\mathrm{B}} = F_o \sin(\omega t)$, with $F_o = -35$ kN and $\omega = 5$ rad/s.

The nonlinear dynamic behavior of the beam is investigated using both the corotational beam element and Abaqus 3D-solid analysis. The time step is $\Delta t = 2.5 \cdot 10^{-3}$ s. The displacements of point A are depicted in Figs. 25, 26 and 27. The results, obtained with 40 corotational beam elements, are in a good agreement with the ones provided by the 3D-solid model. The 3D-solid model adopts a mesh with $17 \cdot 84 = 1428$ isoparametric 20 node elements (see Fig. 24).

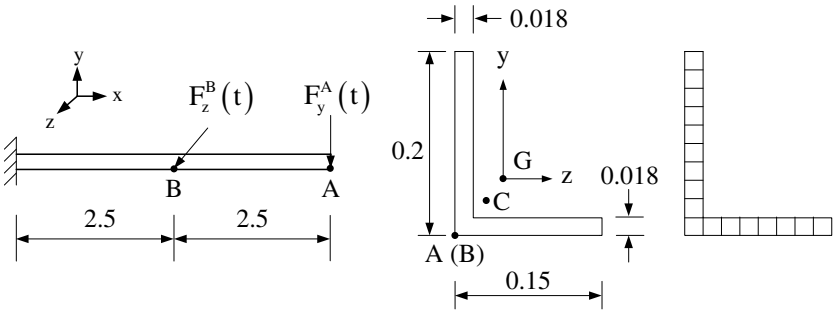

Fig. 24. Cantilever beam with L cross-section : geometrical data.

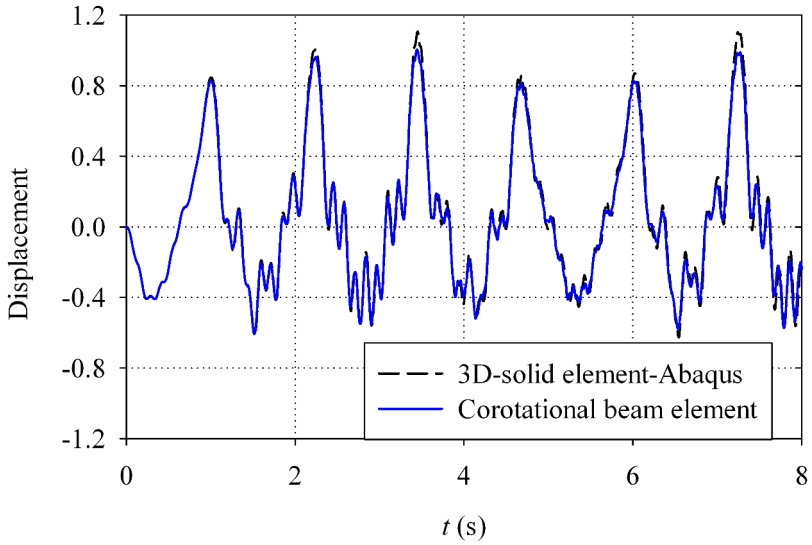

Fig. 25. Cantilever beam with L cross-section - Time evolution of the displacement u_y of point G.

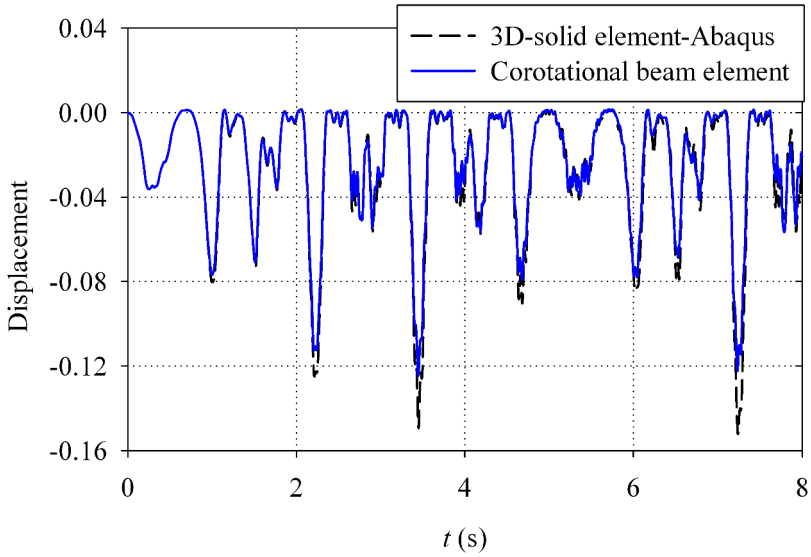

Fig. 26. Cantilever beam with L cross-section - Time evolution of the displacement u_x of point G.

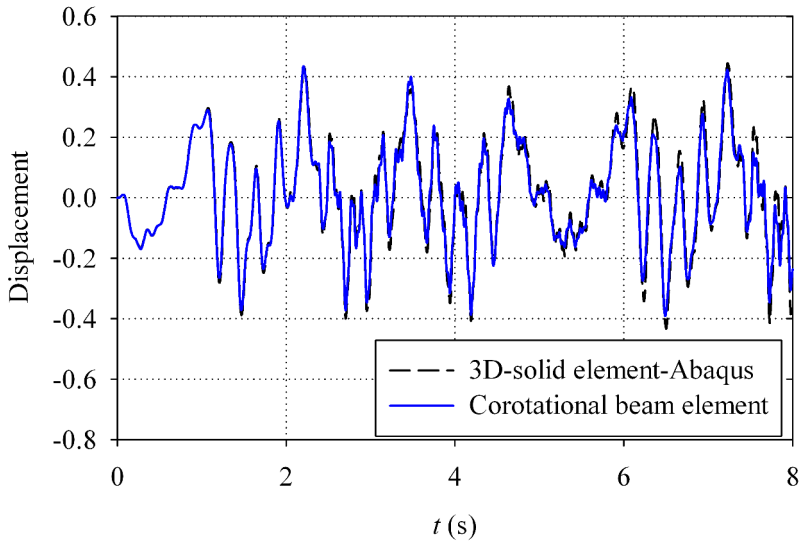

Fig. 27. Cantilever beam with L cross-section - Time evolution of the displacement u_z of point G.

7.5 Example 5: Short cantilever beam with an U cross-section

The aim of the last numerical example is not only to assess the performance of the present formulation, but also to highlight the influence of the eccentricity of the shear center on the inertia terms. In fact, for the examples 7.1, 7.2 and 7.4), the latter does not affect the numerical results and can be neglected by replacing $y_c = z_c = 0$ in Eqs. (105), (111) and (113). But, this example will show a case when the contribution of the eccentricity of the shear center is important.

The cantilever beam with an U cross-section, see Fig. 28, is analysed. The eccentricity of the shear center is given by $z_c = -0.138$ m. The beam is subjected to two out-of-plane time-varying concentrated loads,

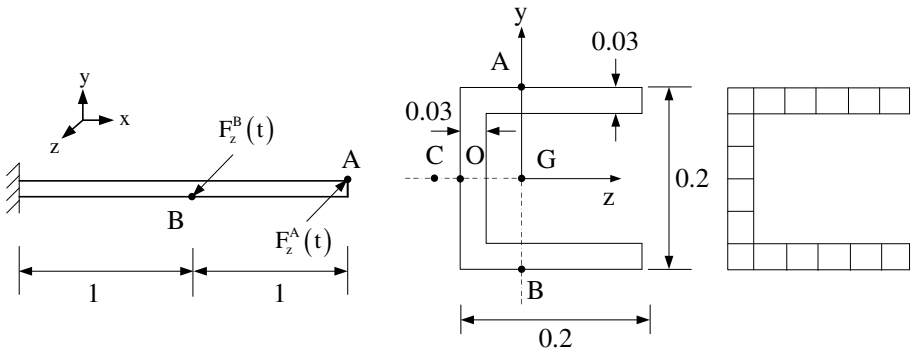

Fig. 28. Cantilever beam with U cross-section : geometrical data.

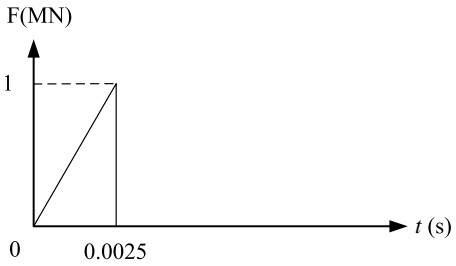

Fig. 29. Cantilever beam with U cross-section - Loading history.

one at the middle and one at the right end. The time-varying load applied at point A is $F_z^{\mathrm{A}} = -4F$. The time-varying load applied at point B is $F_z^{\mathrm{B}} = 2F$. The time evolution of F is given in Fig. 29.

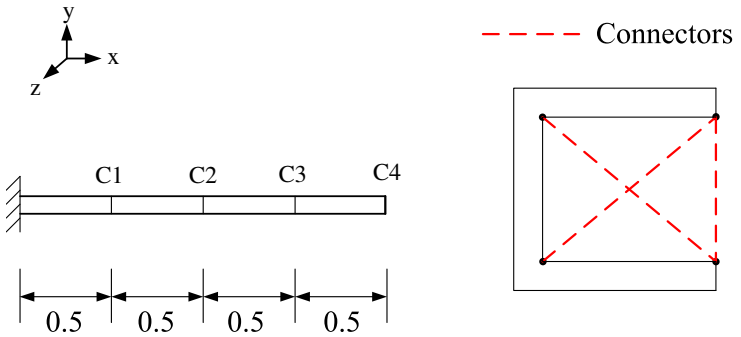

Fig. 30. Cantilever beam with U cross-section : Connectors in the 3D-solid model.

Two different corotational beam models with 40 elements are employed. In the first one, the warping deformations and the eccentricity of the shear center are incorporated in the inertia terms while in the second one the same are neglected.

The solid mesh consists of $16 \cdot 60 = 960$ isoparametric 20 node elements. For the 3D-solid model, four connectors are added at sections C1-C4 along the beam (see Fig. 30) in order to avoid in-plane deformations of the flanges. The connector between 2 nodes maintains the distance of these nodes during the

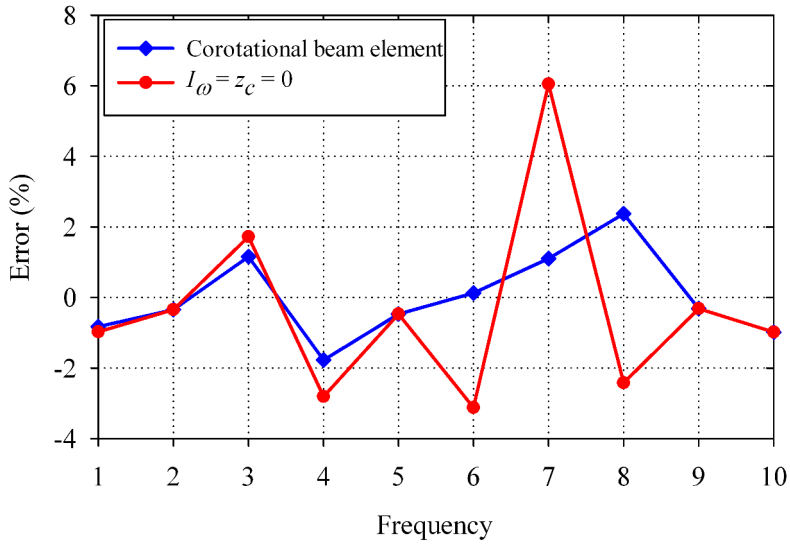

Fig. 31. Cantilever beam with U cross-section - Natural frequency analysis.

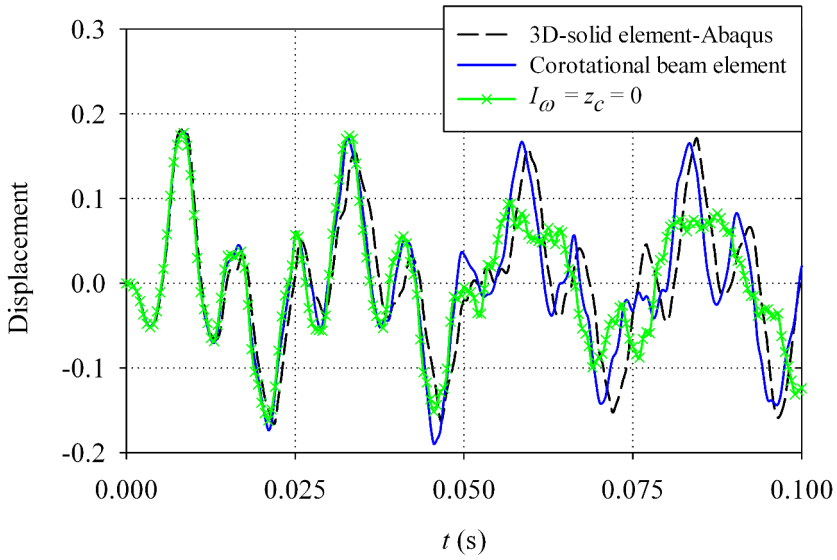

Fig. 32. Cantilever beam with U cross-section - Time evolution of the displacement u_y of point O.

analysis.

The first ten linear natural frequencies of the cantilever are calculated with all the models. For the beam models, linearized version of the corotational formulation is used. The difference between the i^{th} natural frequency given by a beam model and by the 3D-solid model is calculated as follow

$$Error^i = \left(\frac{Fre^i_{Beam}}{Fre^i_{Solid}} - 1 \right) \cdot 100\% \tag{118}$$

The results, depicted in Fig. 31, show that, for the pure bending modes $2^{\text{nd}}, 5^{\text{th}}, 10^{\text{th}}$ and the axial mode 9^{th},

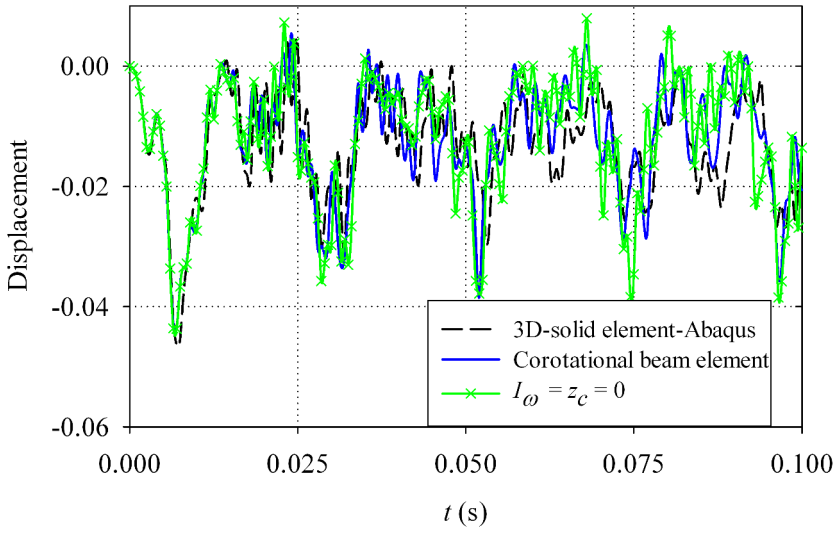

Fig. 33. Cantilever beam with U cross-section - Time evolution of the displacement u_x of point O.

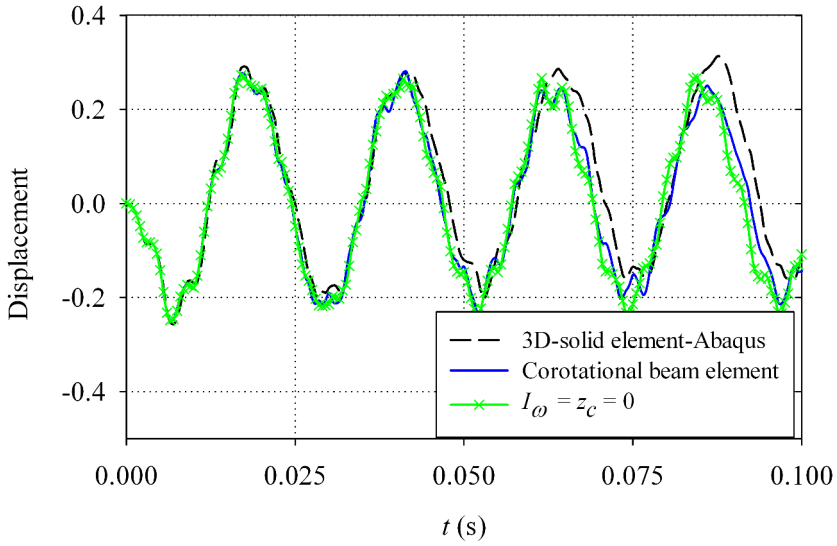

Fig. 34. Cantilever beam with U cross-section - Time evolution of the displacement u_z of point O.

the warping deformations and the eccentricity of the shear center do not effect the frequencies. However, for the torsion-bending modes, the frequencies are better estimated by the beam element which incorporated the warping deformations and the eccentricity of the shear center. The differences between this beam analysis and the 3D-solid one remain smaller than 2.5%. But, when $I_\omega = z_c = 0$, the differences can reach 6%.

The nonlinear behavior of the cantilever due to the time-varying loads are investigated. All analyzes are performed with a time step $\Delta t = 5 \cdot 10^{-5}$ s. The time evolution of the displacements of point O at the right end are depicted in Figs. 32, 33 and 34. A very good agreement between the corotational beam and Abaqus 3D-solid analysis is obtained. However, when $I_\omega = z_c = 0$, large discrepancies between the beam and 3D-solid analysis can be noted, especially in Fig. 32.

One further interesting aspect is related to the computational cost of the proposed corotational beam formulation. Since this element has been implemented in Matlab, it is not possible to perform any comparison against Abaqus. However, in [30], the computational cost of the dynamic corotational formulation with six degrees of freedom at each node was compared against the total Lagrangian formulation proposed by Simo and Vu-Quoc [38]. It was found that both elements demand the same computational time but the corotational formulation requires significantly less number of elements to reach the same level of accuracy. If the warping deformations and the eccentricity of the shear center are ignored in the dynamic terms, then the present beam element is a straightforward extension of the beam element with 6 degrees of freedom per node presented in [30]. It can be also observed that the additional warping degrees of freedom do not modify the corotational framework. Consequently, the computational efficiency is not affected. Accounting for the warping deformations and the eccentricity of the shear centre in the dynamic terms leads to an increase in computation time by about 7 %.

8 Conclusion

In this paper, a corotational dynamic formulation for nonlinear analysis of beams with arbitrary thin-walled cross-sections was developed. The formulation is an extension of the one proposed by the authors in [30]. The same kinematic assumptions were used to derive the static and dynamic terms. Hence, the element has seven degrees of freedom at each node and cubic shape functions are used to interpolate local transverse displacements and axial rotations.

The warping deformations and the shear center eccentricity were fully taken into account in the derivation of the dynamic terms. This leads to additional terms in the expressions of the inertia force vector and the tangent (mass and gyroscopic) dynamic matrices.

Five 3D beam problems, with different thin-walled cross-sections and load pattern, were analysed. The predictions of the proposed formulation were compared against the numerical results obtained with both Abaqus beam element and 3D-solid analyses. For all the examples, a very good agreement between the results obtained with the corotational beam element and the 3D-solid element was obtained. Besides, the numerical results also showed that the warping deformations have a negligible influence in the dynamic terms and could be omitted. However, the additional dynamic terms due to the shear center eccentricity cannot always be neglected. In fact, it seems that for slender beams, the same numerical results are obtained with or without these terms. However, for short beams, the numerical results seem to be improved if the shear center eccentricity is considered.

Finally, the thin-walled beam formulation presented in this paper is limited to beams with homogeneous cross-sections. One interesting future work is to consider the case of thin-walled laminated composite beams. Here, one advantage of the corotational method is that the corotational framework is not affected and only the local formulation needs to be modified.

Appendix A Local elastic force vector and tangent stiffness matrix

```
>with(linalg):
>
> N3:=x*(1-x/L)^2:
> N4:=x^2*(x/L-1)/L:
> N7:=1-3*(x/L)^2+2*(x/L)^3:
> N8:=1-N7:
> t1:=N7*t11+N3*a1+N8*t12+N4*a2:
> dt1:=diff(t1,x):
> ddt1:=diff(dt1,x):
```

```
>
> Omegay:=E*Iyy/(G*A*ky*L):
> muy:=1/(1+12*Omegay):
> N32:=muy*x*(6*Omegay*(1-x/L)+(1-x/L)^2):
> N42:=muy*x*(6*Omegay*(x/L-1)-x/L+x^2/L^2):
> N52:=muy*(1+12*Omegay-12*Omegay*x/L-4*x/L+3*x^2/L^2):
> N62:=muy*(12*Omegay*x/L-2*x/L+3*x^2/L^2):
>
> u2:=N32*t31+N42*t32:
> du2:=diff(u2,x):
> t3:=N52*t31+N62*t32:
> dt3:=diff(t3,x):
>
> Omegaz:=E*Izz/(G*A*kz*L):
> muz:=1/(1+12*Omegaz):
> N33:=muz*x*(6*Omegaz*(1-x/L)+(1-x/L)^2):
> N43:=muz*x*(6*Omegaz*(x/L-1)-x/L+x^2/L^2):
> N53:=muz*(1+12*Omegaz-12*Omegaz*x/L-4*x/L+3*x^2/L^2):
> N63:=muz*(12*Omegaz*x/L-2*x/L+3*x^2/L^2):
>
> u3:=-N33*t21-N43*t22:
> du3:=diff(u3,x):
> t2:=N53*t21+N63*t22:
> dt2:=diff(t2,x):

> g12:=du2-t3:
> g13:=du3+t2:
> k2:=-dt3+c3*ddt1:
> k3:=dt2-c2*ddt1:
>
> eps:=u/L+1/2/L*int(du2^2+du3^2+Io/A*dt1^2,x=0..L):
> Phi1:=A*eps^2+Iyy*Ky^2+Izz*Kz^2+1/4*(Ir4-Io^2/A)*dV^4+Iw*ddV^2:
> Phi2:=2*Iyz*k2*k3+Iyr*k2*dt1^2+Izr*k3*dt1^2+Iwr*ddt1*dt1^2:
> Phi3:=A*(ky*g12^2+kz*g13^2)+J*dV^2:
>
> Phi:=1/2*int(E*Phi1+E*Phi2+G*Phi3,x=0..L):
> fl:=grad(Phi,[u,t11,t21,t31,a1,t12,t22,t32,a2]):
> kl:=hessian(Phi,[u,t11,t21,t31,a1,t12,t22,t32,a2]):
```

Appendix B Expressions of $\dot{\mathbf{H}}_1$ and $\dot{\mathbf{H}}_2$

By the definitions (see Eqs. (82) and (95)), one has

$$\mathbf{H}_1 = \mathbf{N} + \mathbf{P}_1 \mathbf{P} - \widetilde{\mathbf{u}_l} \mathbf{G}^{\mathrm{T}}, \tag{119}$$

$$\mathbf{H}_2 = \left[\mathbf{P}_2 \mathbf{P} + \mathbf{G}^{\mathrm{T}} \;\; \mathbf{P}_3 \right]. \tag{120}$$

The variations of the above relations read

$$\delta \mathbf{H}_1 = \mathbf{P}_1 \, \delta \mathbf{P} - \widetilde{\delta \mathbf{u}_l} \, \mathbf{G}^{\mathrm{T}} - \widetilde{\mathbf{u}_l} \, \delta \mathbf{G}^{\mathrm{T}}, \tag{121}$$

$$\delta \mathbf{H}_2 = \left[\delta (\mathbf{P}_2 \mathbf{P} + \mathbf{G}^{\mathrm{T}}) \;\; \mathbf{0} \right], \tag{122}$$

where $\mathbf{u}_l$ are the local transverse displacements assumed to be small. Therefore, the last term in Eq. (121) is neglected.
By using the expressions of the matrices $\mathbf{P}_1$, $\mathbf{P}_2$, $\mathbf{G}$ and $\mathbf{P}$, one obtains

$$\mathbf{P}_1\mathbf{P} = \begin{bmatrix} 0 & 0 & 0 & 0 & 0 & 0 & 0 & 0 & 0 & 0 & 0 & 0 \\ 0 & \frac{N_{10}}{l_n} & 0 & 0 & 0 & N_3 & 0 & \frac{-N_{10}}{l_n} & 0 & 0 & 0 & N_4 \\ 0 & 0 & \frac{N_{10}}{l_n} & 0 & -N_3 & 0 & 0 & 0 & \frac{-N_{10}}{l_n} & 0 & -N_4 & 0 \end{bmatrix}, \tag{123}$$

$$\mathbf{P}_2\mathbf{P}+\mathbf{G}^{\mathrm{T}} = \begin{bmatrix} 0 & 0 & 0 & N_7 & 0 & 0 & 0 & 0 & 0 & N_8 & 0 & 0 \\ 0 & 0 & \frac{-N_{11}}{l_n} & 0 & N_5 & 0 & 0 & 0 & \frac{N_{11}}{l_n} & 0 & N_6 & 0 \\ 0 & \frac{N_{11}}{l_n} & 0 & 0 & 0 & N_5 & 0 & \frac{-N_{11}}{l_n} & 0 & 0 & 0 & N_6 \end{bmatrix}, \tag{124}$$

with $N_{10} = N_3 + N_4$ and $N_{11} = N_5 + N_6 - 1$.
Referring first to the current length of the beam element l_n, the variation of Eq. (47) gives

$$\delta l_n = \mathbf{r}\,\delta\mathbf{d}_g, \quad \mathbf{r} = \begin{bmatrix} -\mathbf{r}_1^{\mathrm{T}} & \mathbf{0}_{[1\times3]} & \mathbf{r}_1^{\mathrm{T}} & \mathbf{0}_{[1\times3]} \end{bmatrix}, \tag{125}$$

when $\mathbf{r}_1$ is defined in Eq. (46).
It is straightforward to obtain

$$\delta(\mathbf{P}_1\mathbf{P}) = \frac{N_{10}}{l_n^2}\mathbf{A}_1\,\mathbf{r}\,\delta\mathbf{d}_g, \tag{126}$$

$$\delta(\mathbf{P}_2\mathbf{P}+\mathbf{G}^{\mathrm{T}}) = \frac{N_{11}}{l_n^2}\mathbf{A}_2\,\mathbf{r}\,\delta\mathbf{d}_g, \tag{127}$$

with

$$\mathbf{A}_1 = \begin{bmatrix} 0 & 0 & 0 & 0 & 0 & 0 & 0 & 0 & 0 & 0 & 0 & 0 \\ 0 & -1 & 0 & 0 & 0 & 0 & 1 & 0 & 0 & 0 & 0 & 0 \\ 0 & 0 & -1 & 0 & 0 & 0 & 0 & 0 & 1 & 0 & 0 & 0 \end{bmatrix}, \tag{128}$$

$$\mathbf{A}_2 = \begin{bmatrix} 0 & 0 & 0 & 0 & 0 & 0 & 0 & 0 & 0 & 0 & 0 & 0 \\ 0 & 0 & 1 & 0 & 0 & 0 & 0 & 0 & -1 & 0 & 0 & 0 \\ 0 & -1 & 0 & 0 & 0 & 0 & 0 & 1 & 0 & 0 & 0 & 0 \end{bmatrix}. \tag{129}$$

By inserting Eqs. (126) and (127) into Eqs. (121) and (122), the variations of $\mathbf{H}_1$, $\mathbf{H}_2$ are obtained as

$$\delta\mathbf{H}_1 = \frac{N_{10}}{l_n^2}\mathbf{A}_1\,\mathbf{r}\,\delta\mathbf{d}_g - \widetilde{\delta\mathbf{u}_l}\,\mathbf{G}^{\mathrm{T}}, \tag{130}$$

$$\delta\mathbf{H}_2 = \frac{N_{11}}{l_n^2}\begin{bmatrix} \mathbf{A}_2\,\mathbf{r}\,\delta\mathbf{d}_g & \mathbf{0} \end{bmatrix}. \tag{131}$$

Finally, one has

$$\dot{\mathbf{H}}_1 = \frac{N_{10}}{l_n^2}\mathbf{A}_1\,\mathbf{r}\,\dot{\mathbf{d}}_g - \widetilde{\dot{\mathbf{u}}}_l\,\mathbf{G}^{\mathrm{T}}, \tag{132}$$

$$\dot{\mathbf{H}}_2 = \frac{N_{11}}{l_n^2}\begin{bmatrix} \mathbf{A}_2\,\mathbf{r}\,\dot{\mathbf{d}}_g & \mathbf{0} \end{bmatrix}. \tag{133}$$

Appendix C Expressions of $\mathbf{C}_3$ and $\mathbf{C}_4$

By the definitions (see Eqs. (108) and (110)), one has

$$\mathbf{C}_3\,\mathbf{E}^{\mathrm{T}}\,\Delta\dot{\mathbf{d}}_g = (\frac{\partial \mathbf{C}_1}{\partial \dot{\mathbf{d}}_g}\Delta\dot{\mathbf{d}}_g)\,\mathbf{E}^{\mathrm{T}}\,\dot{\mathbf{d}}_g\,, \tag{134}$$

$$\mathbf{C}_4\,\mathbf{E}^{w\mathrm{T}}\,\Delta\dot{\mathbf{d}}_g^w = (\frac{\partial \mathbf{C}_2}{\partial \dot{\mathbf{d}}_g^w}\Delta\dot{\mathbf{d}}_g^w)\,\mathbf{E}^{w\mathrm{T}}\,\dot{\mathbf{d}}_g^w\,, \tag{135}$$

where $\mathbf{C}_1$ and $\mathbf{C}_2$ are given by Eqs. (87) and (104), respectively.
Eqs. (134) and (135) can be rewritten as

$$\mathbf{C}_3\,\mathbf{E}^{\mathrm{T}}\,\Delta\dot{\mathbf{d}}_g = \left(\widetilde{\Delta\dot{\mathbf{w}}_r^e}\,\mathbf{H}_1 + \Delta\dot{\mathbf{H}}_1 - \mathbf{H}_1\,\Delta\mathbf{E}_t\right)\mathbf{E}^{\mathrm{T}}\,\dot{\mathbf{d}}_g\,, \tag{136}$$

$$\mathbf{C}_4\,\mathbf{E}^{w\mathrm{T}}\,\Delta\dot{\mathbf{d}}_g^w = \begin{bmatrix} \widetilde{\Delta\dot{\mathbf{w}}_r^e}\,\mathbf{H}_2 + \Delta\dot{\mathbf{H}}_2 - \mathbf{H}_2\,\Delta\mathbf{E}_t^w \\ -\mathbf{H}_3\,\Delta\mathbf{E}_t^w \end{bmatrix}\mathbf{E}^{w\mathrm{T}}\,\dot{\mathbf{d}}_g^w\,. \tag{137}$$

It should be noted that only the variations with respect to $\dot{\mathbf{d}}_g$ and $\dot{\mathbf{d}}_g^w$ are considered.
Using Eq. (77), the first terms in Eqs. (136) and (137) can be rewritten as

$$\widetilde{\Delta\dot{\mathbf{w}}_r^e}\,\mathbf{h}_i = -\widetilde{\mathbf{h}}_i\,\Delta\dot{\mathbf{w}}_r^e = -\widetilde{\mathbf{h}}_i\,\mathbf{G}^{\mathrm{T}}\,\mathbf{E}^{\mathrm{T}}\,\Delta\dot{\mathbf{d}}_g \quad (i=1,2)\,, \tag{138}$$

with

$$\mathbf{h}_1 = \mathbf{H}_1\,\dot{\mathbf{d}}_g^e\,, \quad \mathbf{h}_2 = \mathbf{H}_2\,\mathbf{E}^{w\mathrm{T}}\,\dot{\mathbf{d}}_g^w\,. \tag{139}$$

By noting that (see Eqs. (61), (80) and (86))

$$\dot{\mathbf{w}}_r^e = \mathbf{G}^{\mathrm{T}}\,\dot{\mathbf{d}}_g^e\,, \quad \Delta\dot{\mathbf{u}}_l = \mathbf{P}_1\,\mathbf{P}\,\mathbf{E}^{\mathrm{T}}\,\Delta\dot{\mathbf{d}}_g\,, \tag{140}$$

and using Eqs. (132) and (133), the following expressions are derived

$$\Delta\dot{\mathbf{H}}_1\,\mathbf{E}^{\mathrm{T}}\,\dot{\mathbf{d}}_g = \left(\frac{N_{10}}{l_n^2}\,\mathbf{A}_1\,\mathbf{r}\,\Delta\dot{\mathbf{d}}_g - \widetilde{\Delta\dot{\mathbf{u}}_l}\,\mathbf{G}^{\mathrm{T}}\right)\dot{\mathbf{d}}_g^e = \left(\frac{N_{10}}{l_n^2}\,\mathbf{A}_1\,\dot{\mathbf{d}}_g^e\,\mathbf{r}^e + \widetilde{\dot{\mathbf{w}}_r^e}\mathbf{P}_1\,\mathbf{P}\right)\mathbf{E}^{\mathrm{T}}\,\Delta\dot{\mathbf{d}}_g\,, \tag{141}$$

$$\Delta\dot{\mathbf{H}}_2\,\mathbf{E}^{\mathrm{w}\mathrm{T}}\,\dot{\mathbf{d}}_g^w = \frac{N_{11}}{l_n^2}\,\mathbf{A}_2\,\mathbf{r}\,\Delta\dot{\mathbf{d}}_g\,\mathbf{E}^{\mathrm{T}}\,\dot{\mathbf{d}}_g = \frac{N_{11}}{l_n^2}\,\mathbf{A}_2\,\dot{\mathbf{d}}_g^e\,\mathbf{r}^e\,\mathbf{E}^{\mathrm{T}}\,\Delta\dot{\mathbf{d}}_g\,, \tag{142}$$

in which

$$\mathbf{r}^e = \mathbf{r}\,\mathbf{E} = \left[\,[-1\,0\,0]\;\;\mathbf{0}_{[1\times3]}\;\;[1\,0\,0]\;\;\mathbf{0}_{[1\times3]}\,\right]. \tag{143}$$

Using the expressions of $\mathbf{H}_2$ and $\mathbf{H}_3$ given by (91) and (95), the following relations are derived

$$\mathbf{H}_2\,\Delta\mathbf{E}_t^w\,\mathbf{E}^{w\mathrm{T}}\,\dot{\mathbf{d}}_g^w = \left(\mathbf{P}_2\,\mathbf{P} + \mathbf{G}^{\mathrm{T}}\right)\Delta\mathbf{E}_t\,\mathbf{E}^{\mathrm{T}}\,\dot{\mathbf{d}}_g\,, \tag{144}$$

$$\mathbf{H}_3\,\Delta\mathbf{E}_t^w\,\mathbf{E}^{w\mathrm{T}}\,\dot{\mathbf{d}}_g^w = \mathbf{P}_4\,\mathbf{P}\,\Delta\mathbf{E}_t\,\mathbf{E}^{\mathrm{T}}\,\dot{\mathbf{d}}_g\,. \tag{145}$$

Using Eq. (85), the following expression is obtained

$$\Delta\mathbf{E}_t\,\mathbf{E}^{\mathrm{T}}\,\dot{\mathbf{d}}_g = \Delta\mathbf{E}_t\,\dot{\mathbf{d}}_g^e = -\mathbf{F}_1\,\Delta\dot{\mathbf{w}}_r^e = -\mathbf{F}_1\,\mathbf{G}^{\mathrm{T}}\,\mathbf{E}^{\mathrm{T}}\,\Delta\dot{\mathbf{d}}_g\,, \tag{146}$$

with

$$\mathbf{F}_1 = [\,\widetilde{\dot{\mathbf{u}}_1^e}^{\mathrm{T}}\,\widetilde{\dot{\mathbf{w}}_1^e}^{\mathrm{T}}\,\widetilde{\dot{\mathbf{u}}_2^e}^{\mathrm{T}}\,\widetilde{\dot{\mathbf{w}}_2^e}^{\mathrm{T}}\,]^{\mathrm{T}}. \tag{147}$$

Finally, the expressions of $\mathbf{C}_3$ and $\mathbf{C}_4$ are evaluated as

$$\mathbf{C}_3 = -\widetilde{\mathbf{h}}_1 \mathbf{G}^{\mathrm{T}} + \left(\frac{N_{10}}{l_n^2} \mathbf{A}_1 \dot{\mathbf{d}}_g^e \mathbf{r}^e + \widetilde{\dot{\mathbf{w}}}_r^e \mathbf{P}_1 \mathbf{P} \right) + \mathbf{H}_1 \mathbf{F}_1 \mathbf{G}^{\mathrm{T}}, \tag{148}$$

$$\mathbf{C}_4 = \begin{bmatrix} \widetilde{\mathbf{h}}_2 \mathbf{G}^{\mathrm{T}} + \dfrac{N_{11}}{l_n^2} \mathbf{A}_2 \dot{\mathbf{d}}_g^e \mathbf{r}^e + \left(\mathbf{P}_2 \mathbf{P} + \mathbf{G}^{\mathrm{T}} \right) \mathbf{F}_1 \mathbf{G}^{\mathrm{T}} & \mathbf{0} \\ \mathbf{P}_4 \mathbf{P} \mathbf{F}_1 \mathbf{G}^{\mathrm{T}} & \mathbf{0} \end{bmatrix}. \tag{149}$$

References

[1] R. Grutmann, R. Sauer, W. Wagner, Theory and numerics of three-dimensional beams with elastoplastic behaviour, Int. J. Num. Methods. Engrg., Vol. 48, 1675-1702 (2000).

[2] J. Argyris, An excursion into large rotations, Comput. Methods Appl. Mech. Engrg., Vol. 32, 85-155 (1982).

[3] K.J. Bathe, E. Ramm, Wilson E.L., Finite element formulations for large deformation dynamic analysis, Int. J. Num. Methods. Engrg., Vol. 9, 353-386 (1975).

[4] J.-M. Battini, C. Pacoste, Co-rotational beam elements with warping effects in instability problems, Comput. Methods Appl. Mech. Engrg., Vol. 191, 1755-1789 (2002).

[5] K. Behdinan, M.C Stylianou, B. Tabarrok, Co-rotational dynamic analysis of flexible beams, Comput. Methods Appl. Mech. Engrg., Vol. 154, 151-161 (1998).

[6] P. Betsch, P. Steinmann, Constrained dynamics of geometrically exact beams, Comput. Mech., Vol. 31, 49-59 (2003).

[7] A. Cardona, M. Geradin, A beam finite element non-linear theory with finite rotations, Int. J. Num. Methods. Engrg., Vol. 26, 2403-2438 (1988).

[8] M.A. Crisfield, J. Shi, An energy conserving co-rotational procedure for non-linear dynamics with finite elements, Nonlinear Dynamics, Vol. 9, 37-52 (1996).

[9] M.A. Crisfield, G.F. Moita, A unified co-rotational framework for solids shells and beams, Int. J. Solids Struct., Vol. 33, 29692992 (1996).

[10] M.A. Crisfield, U. Galvanetto, G. Jelenić, Dynamics of 3-D co-rotational beams, Comput. Mech., Vol. 20, 507-519 (1997).

[11] M.A. Crisfield, Non-Linear Finite Element Analysis of Solids and Structures, Volume 2: Advanced Topics, Wiley, Chischester (1997).

[12] H.A. Elkaranshawy, M.A. Dokainish, Corotational finite element analysis of planar flexible multibody systems, Comput. Struct., Vol. 54, No.5, 881-890 (1995).

[13] U. Galvanetto, M.A. Crisfield, An energy conserving co-rotational procedure for dynamics of planar beam structures, Int. J. Num. Methods. Engrg., Vol. 39, 2265-2282 (1996).

[14] M. Geradin, A. Cardona, Kinematics and dynamics of rigid and flexible mechanisms using finite elements and quaternion algebra, Comput. Mech., Vol. 4, 115-135 (1989).

[15] M. Geradin, A. Cardona, Flexible multibody dynamics : A finite element approach, 120-127. Wiley, Chischester (2001).

[16] K.M. Hsiao, R.T. Yang, A co-rotational formulation for nonlinear dynamic analysis of curved Euler beam, Comput. Struct. , Vol. 54, No.6, 1091-1097 (1995).

[17] K.M. Hsiao, J.Y. Lin, W.Y. Lin, A consistent co-rotational finite element formulation for geometrically nonlinear dynamics analysis of 3-D beams, Comput. Methods Appl. Mech. Engrg., Vol. 169, 1-18 (1999).

[18] K.M. Hsiao, W.Y. Lin, R.H. Chen, Geometrically non-linear dynamic analysis of thin-walled beams, Proc. World Congress Engrg., Vol. II (2009).

[19] A. Ibrahimbegović, F. Frey, I. Kožar, Computational aspects of vector-like parameterization of three-dimensional finite rotations, Int. J. Num. Methods. Engrg., Vol. 38, 3653-3673 (1995).

[20] A. Ibrahimbegović, On the choice of finite rotation parameters, Comput. Methods Appl. Mech. Engrg., Vol. 149, 49-71 (1997).

[21] A. Ibrahimbegović, M.A. Mikdad, Finite rotations in dynamics of beams and implicit time-stepping schemes, Int. J. Num. Methods. Engrg., Vol. 41, 781-814 (1998).

[22] A. Ibrahimbegović, S. Mamouri, Energy conserving/decaying implicit time-stepping scheme for nonlinear dynamics of three-dimensional beams undergoing finite rotations, Comput. Methods Appl. Mech. Engrg., Vol. 191, 4241-4258 (2002).

[23] M. Iura, S.N. Atluri, Dynamic analysis of finitely stretched and rotated three-dimensional space-curved beams, Comput. Struct., Vol. 29, 875-889 (1988).

[24] M. Iura, S.N. Atluri, Dynamic analysis of planar flexible beams with finite rotations by using inertial and rotating frames, Comput. Struct., Vol. 55, No.3, 453-462 (1995).

[25] G. Jelenić, M.A. Crisfield, Interpolation of rotational variables in nonlinear dynamics of 3D beams, Int. J. Num. Methods. Engrg., Vol. 43, 1193-1222 (1998).

[26] G. Jelenić, M.A. Crisfield, Geometrically exact 3D beam theory: implementation of a strain-invariant element for stactics and dynamics, Comput. Methods Appl. Mech. Engrg., Vol. 171, 141-171 (1999).

[27] S. Krenk, Non-Linear Modeling And Analysis Of Solids And Structures, 47-75, Cambridge University Press, New York (2009).

[28] T.-N. Le, J.-M. Battini, M. Hjiaj, Efficient formulation for dynamics of corotational 2D beams, Comput. Mech., Vol. 48, No. 2, 153-161 (2011).

[29] T.-N. Le, J.-M. Battini, M. Hjiaj, Dynamics of 3D beam elements in a corotational context: A comparative study of established and new formulations, Finite Elem. Anal. Des., Vol. 61, 97-111 (2012).

[30] T.-N. Le, J.-M. Battini, M. Hjiaj, A consistent 3D corotational beam element for nonlinear dynamic analysis of flexible structures, Comput. Methods Appl. Mech. Engrg., accepted (2013).

[31] E.V. Lens, A. Cardona, A nonlinear beam element formulation in the framework of an energy preserving time integration scheme for constrained multibody systems dynamics, Comput. Struct. , Vol. 86, 47-63 (2008).

[32] J. Mäkinen, Total Lagrangian Reissner's geometrically exact beam element without singularities, Int. J. Num. Methods. Engrg., Vol. 70, 1009-1048 (2007).

[33] N. Masuda, T. Nishiwaki, M. Minaaawa, Nonlinear dynamic analysis of frame structures, Comput. Struct., Vol. 27, No.1, 103-110 (1987).

[34] B. Nour-Omid, C.C. Rankin, Finite rotation analysis and consistent linearization using projectors, Comput. Methods Appl. Mech. Engrg., Vol. 93, 353-384 1991.

[35] C. Oran, A. Kassimali, Large deformations of framed structures under static and dynamic loads, Comput. Struct., Vol. 6, 539-547 (1976).

[36] C.C. Rankin, B. Nour-Omid, The use of projectors to improve finite element performance, Comput. Struct., Vol. 30, 257-267 (1988).

[37] J.N. Reddy, On locking-free shear deformable beam finite elements, Comput. Methods Appl. Mech. Engrg., Vol. 149, 113-132 (1997).

[38] J.C. Simo, L. Vu-Quoc, On the dynamics in space of rods undergoing large motions - A geometrically exact approach, Comput. Methods Appl. Mech. Engrg., Vol. 66, 125-161 (1988).

[39] Q. Xue, J.L Meek, Dynamic response and instability of frame structures, Comput. Methods Appl. Mech. Engrg., Vol. 190, 5233-5242 (2001).

[40] E. Zupan, M. Saje, D. Zupan, Quaternion-based dynamics of geometrically nonlinear spatial beams using the RungeKutta method, Finite Elem. Anal. Des., Vol. 54, 48-60 (2012).

[41] E. Zupan, M. Saje, D. Zupan, Dynamics of spatial beams in quaternion description based on the Newmark integration scheme, Comput. Mech., Vol. 51, 47-64 (2013).

Résumé en français: Eléments de poutre corotationnels pour l'analyse dynamique non-linéaire des structures à barres.

1 Introduction

1.1 Motivation

Les structures flexibles à barres sont utilisées dans de nombreuses applications, parmi lesquelles on peut citer les hélices d'avion, les pales d'éolienne, les plates-formes offshores... Il n'est pas rare que ces structures subissent de grands déplacements et de grandes rotations. Néanmoins dans la plupart des cas pratiques qui relèvent du Génie Civil, les déformations restent petites. La simulation du comportement dynamique non-linéaire de ces structures est généralement réalisée à l'aide d'éléments finis de poutre. Plusieurs formulations d'élément poutre pour l'analyse dynamique non-linéaire de ces structures ont été proposées dans la littérature. On distingue clairement deux groupes d'éléments: ceux qui sont formulé dans un contexte lagrangien total classique (voir [44, 46] pour le cas 2D, et [11, 25, 28, 29, 36, 47] pour le cas 3D) et ceux qui adoptent le cadre corotationnel.

Bien que cette dernière soit également une formulation lagrangienne totale, l'idée centrale de cette approche est de décomposer le mouvement de l'élément en un mouvement de type corps rigide et un mouvement en petites perturbations (déformations pures). Au cours du mouvement de corps rigide, un système de coordonnées locales, fixé à l'élément, se déplace et tourne avec ce dernier. Les déformations sont mesurées dans ce système local. Cette approche a été adoptée par plusieurs auteurs qui ont développé des éléments de poutre et de coque pour l'analyse statique et dynamique non-linéaire des structures [2, 6, 9, 13–17, 21, 23, 27, 37, 39, 40, 48]. En analyse statique non-linéaire, cette approche permet de simplifier les calculs des forces élastiques dans les modèles éléments finis en grands déplacements/rotations. Plusieurs versions de la méthode corotationnelle ont été proposées dans la littérature. Celle utilisée dans ce travail a été proposée par Rankin et Nour-Omid [38, 42], puis développée par Battini et Pacoste [8]. De nombreux travaux basés sur cette approche ont été effectués pendant ces dernières années. Plusieurs éléments de poutre efficaces 2D et 3D, dédiés à la simulation du comportement géométriquement non-linéaire des structures à barres de section arbitraire, ont été développés par la Division of Structural Engineering and Bridges (KTH-Stockholm) et par le Structural Engineering Research Group (INSA de Rennes) [1, 2, 5, 8, 41]. Les structures peuvent avoir une section solide ou à paroi mince.

Le principal intérêt de la méthode corotationnelle est qu'avec un choix approprié de la longueur de l'élément, les déplacements dans le repère local restent petits. Le gain en termes de calcul est clair. Ainsi, les calculs dans ce repère corotationnel se font sur base de la théorie de l'élasticité linéaire, ou éventuellement, de la mécanique matériellement linéaire.

Pour l'analyse statique non-linéaire des systèmes de poutres par approche corotationnelle, plusieurs formulations locales ont été proposées par Battini et Pacoste [8] et Alsafadie et al. [1]. Les résultats d'une étude comparative portant sur les performances de plusieurs formulations de poutre 3D (voir [1]) ont montré que les formulations locales basées sur des interpolations cubiques sont efficaces et plus précises que celles qui utilisent des interpolations linéaires. Cependant, en dynamique, nous devons traiter les termes d'inertie qui sont compliqués à établir. Cela est particulièrement vrai pour la formulation corotationnelle des éléments de poutre de type Bernoulli. Cette difficulté, explicitement reconnue dans [13], a été un frein au développement d'éléments finis corotationnel pour l'analyse dynamique non-linéaire. Les différents auteurs qui ont travaillé sur ce sujet se sont résignés à abandonner une écriture cohérente des termes d'inertie. Ainsi plusieurs approches ont été proposées, toutes conduisant à une formulation "incohérente" (inconsistent).

Pour l'analyse dynamique non-linéaire en 2D, plusieurs auteurs [37, 39, 48] ont adopté une matrice de masse diagonale sans vérifier la précision de cette approximation. Iura et Atluri [27] ont suggéré de simplement utiliser un modèle de poutre de Timoshenko dont la matrice de masse est constante conduisant ainsi à une simplification considérable de l'expression des termes d'inertie. Behdinan et al. [9] ont proposé une formulation dynamique corotationnelle 2D où les interpolations cubiques ont été utilisées pour les déplacements globaux, ce qui n'est pas cohérent avec l'idée centrale de la méthode corotationnelle

[38]. Pour l'analyse dynamique 3D, Crisfield et al. [13] ont proposé d'utiliser une matrice de masse de Timoshenko constante tout en adoptant des interpolations cubiques pour établir l'expression du vecteur force interne et de la matrice de rigidité tangente. Cette combinaison n'est pas cohérente même si l'on peut noter que des résultats satisfaisants peuvent être obtenus avec un grand nombre d'éléments. Hsiao et al. [21] ont présenté une formulation corotationnelle de poutre 3D. Toutefois, l'approche corotationnelle adoptée dans [21] est différente de celle proposée par Nour-Omid et al.[38]. Une analyse approfondie de l'état de l'art révèle l'absence d'une formulation cohérente d'un élément fini de poutre corotationnelle en dynamique non-linéaire. L'objectif premier de ce travail est de proposer des éléments finis de poutre (2D et 3D) corotationnelle pour l'analyse dynamique non-linéaire et d'évaluer les performances de ces éléments.

Il est important de noter que les éléments finis de poutre 3D ne sont pas une simple extension des éléments finis de poutre 2D développés dans ce travail. La raison principale est la nature complexe de grandes rotations. Plus précisément, les grandes rotations sont non-commutatives et non-additives. Elles ne peuvent donc pas être traitées de la même façon que les translations et exigent des procédures adpatées. Plusieurs possibilités pour paramétrer les grandes rotations ont été proposées dans la litérature [11, 25, 47]. Chaque paramétrisation a ses avantages et ses inconvénients, et le choix d'une approche efficace est toujours un aspect central de la formulation.

1.2 Objectifs

L'objectif principal est d'étendre l'usage des éléments finis de poutre corotationnelle (2D et 3D) à l'analyse dynamique non-linéaire. Nous proposons 3 éléments finis de poutre (2D et 3D) corotationnelle pour l'analyse dynamique géométriquement non-linéaire des structures à barres. Tous les éléments finis proposés considèrent des interpolations cubiques pour l'ensemble des termes (statiques et dynamiques) assurant ainsi la cohérence des formulations proposées. Les contributions originales de ce travail sont collectées dans quatres articles.

Dans le premier article [31], un élément de poutre 2D corotationnelle est développé pour la dynamique non-linéaire. Afin de prendre en compte correctement les effets d'inertie, les interpolations cubiques sont adoptées non seulement pour établir l'expression des termes élastiques, mais aussi pour obtenir les termes d'inertie. Plusieurs exemples numériques sont ensuite analysés afin de comparer la précision de la nouvelle formulation par rapport aux deux formulations classiques dans lesquelles la matrice de masse linéaire de Timoshenko et la matrice de masse diagonale sont utilisées.

Bien que l'efficacité des interpolations cubiques a été démontrée dans [1, 31], force est de constater l'usage quasi systématique des interpolations linéaires pour établir l'expression du vecteur force de l'inertie et de la matrice d'inertie tangente des éléments finis de poutre corotationnelle 3D en dynamique. Notre second objectif est, comme pour le cas 2D, de développer de manière cohérente un élément fini de poutre corotationnelle 3D pour l'analyse dynamique non-linéaire. Cependant, cette tâche n'est pas triviale. Une difficulté provient de la nature complexe des grandes rotations et son interaction avec les schémas d'intégration temporelle. Ainsi avant de développer l'élément de poutre 3D à proprement dit, la paramétrisation des grandes rotations et les procédures de mise à jour associées (update algorithms) sont soigneusement étudiées. Sur base d'une étude bibliographique approfondie, nous développons quatre formulations de poutre en dynamique non-linéaire qui sont basées sur trois paramétrisations différentes des rotations. Les trois premières formulations sont prises dans la littérature. La dernière est originale et utilise trois des quatre paramètres d'Euler (quaternion) comme variables de rotation. Pour toutes ces approches, les calculs théoriques ainsi que les implémentations pratiques sont donnés en détail. Les points communs et les différences entre les quatre formulations sont mis en évidence. Six exemples numériques ont été analysés afin de comparer ces quatre formulations en termes de précision numérique et d'efficacité de calcul. En ce qui concerne l'efficacité, plusieurs prédicteurs et possibilités de simplifier la matrice d'inertie tangente sont testés. Ce travail est présenté dans le deuxième article [32].

Pour chacune de ces formulations, le vecteur des forces internes et la matrice de rigidité tangente sont

établis dans un contexte lagrangien total.

Dans la troisième partie de ce travail, un élément est développé pour l'analyse des poutres avec des sections solides. De manière similaire au cas 2D, les interpolations cubiques locales sont utilisées pour dériver à la fois les termes internes et l'inertie. Cette approche permet d'assurer la cohérence de la formulation. Afin de simplifier les calculs, une approximation des rotations locales est adoptée dans les calculs des termes d'inertie. Pour améliorer l'efficacité de la procédure itérative, le terme moins importante dans la matrice d'inertie tangente est ignoré. Quatre exemples numériques sont ensuite analysés dans le but de comparer les performances de la nouvelle formulation. Les résultats obtenu sont comparés à deux autres approches. La première est semblable à celle présentée ci-dessus, mais des interpolations linéaires locales sont utilisées pour établir seulement les termes dynamiques. Le but est d'évaluer l'influence du choix des interpolations locales sur les termes dynamiques. La deuxième approche est la formulation lagrangienne totale classique proposé par Simo et Vu-Quoc [45–47]. Ce travail est présenté dans le troisième article [33].

Enfin, l'élément de poutre 3D précédent est étendu aux poutres avec des sections arbitraires à parois minces. A cet effet, les déformations de gauchissement et l'excentricité du centre de cisaillement sont prises en compte. Afin d'introduire les déformations de gauchissement, la description cinématique proposée par Gruttmann et al. [20] est adoptée. Par conséquent, l'élément de poutre possède 14 degrés de liberté, 7 par nœud. En ce qui concerne les termes de déformations statiques, c-à-d le vecteur force interne et la matrice de rigidité tangente, l'élément de poutre corotationnelle développé par Battini et Pacoste [8] est adopté. Toutefois, afin d'introduire les déformations de cisaillement de flexion, les fonctions d'Hermite cubiques sont modifiées comme suggéré dans la fomulation d'Interdependent Interpolation Element (IIE) [43]. Quatre exemples numériques sont analysés pour évaluer la précision de la nouvelle formulation en comparant les résultats qu'elle fournit à ceux obtenus avec un modéle EF volumique (Abaqus). Ce travail est présenté dans le quatrième article [34].

2 Formulation corotationnelle de l'élément de poutre 2D

L'approche corotationnelle est une méthode bien connue pour formuler des éléments finis non-linéaires de poutre efficaces. L'idée principale est de décomposer le mouvement de l'élément en deux parties: un mouvement de corps rigide et un mouvement en petites perturbations (déformations pures). Au cours du mouvement de corps rigide, un système de coordonnées locales, fixé à l'élément, se déplace et tourne avec ce dernier. Les déformations sont mesurées dans ce système local. Le principal intérêt de cette approche est la possibilité d'utiliser différentes formulations locales.

Dans l'article [31], les auteurs ont proposé une nouvelle formulation corotationnelle. L'originalité réside dans l'usage d'interpolations cubiques locales à la fois pour obtenir les termes élastiques, mais aussi pour établir les termes d'inertie. A travers quatre exemples numériques, l'efficacité de la formulation est évaluée en comparant les résultats obtenus avec cette dernière à ceux obtenus à l'aide de deux autres formulations corotationnelles basées sur la matrice de masse de Timoshenko et la matrice de masse diagonale. Il est démontré que la présente formulation fournit des résultats précis avec un nombre réduit d'éléments.

2.1 Cinématique de l'élément de poutre corotationnel

La cinématique d'un élément de poutre corotationnelle à deux nœuds est représenté à la Fig. 2.1. Le nœud 1 est pris comme l'origine du système des coordonnées local (x_l, z_l). L'axe x_l coïncide avec la droite reliant les deux nœuds de l'élément. Par suite du choix du système local, le vecteur des déplacements locaux est

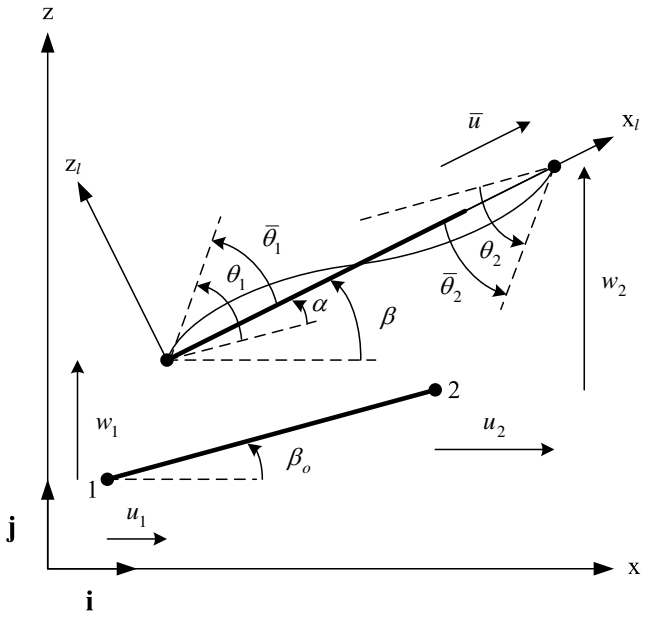

Fig. 1. Cinématique de la poutre.

défini par

$$\overline{\mathbf{q}} = [\, \overline{u} \quad \overline{\theta}_1 \quad \overline{\theta}_2 \,]^{\mathrm{T}} , \tag{1}$$

tandis que le vecteur des déplacements globaux est défini par

$$\mathbf{q} = [\, u_1 \quad w_1 \quad \theta_1 \quad u_2 \quad w_2 \quad \theta_2 \,]^{\mathrm{T}} , \tag{2}$$

La relation entre la variation du vecteur des déplacements globaux et celle du vecteur des déplacements locaux est donnée par la matrice de transformation $\mathbf{B}$

$$\delta\overline{\mathbf{q}} = \mathbf{B}\,\delta\mathbf{q} . \tag{3}$$

2.2 Vecteur force élastique et matrice de rigidité tangente

En égalant le travail virtuel exprimé dans les systèmes d'axes local et global, la relation entre le vecteur forces locales $\mathbf{f}_l$ et le vecteur forces globales $\mathbf{f}_g$ est donnée par l'expression:

$$V = \delta\mathbf{q}^{\mathrm{T}}\mathbf{f}_g = \delta\overline{\mathbf{q}}^{\mathrm{T}}\mathbf{f}_l = \delta\mathbf{q}^{\mathrm{T}}\mathbf{B}^{\mathrm{T}}\mathbf{f}_l . \tag{4}$$

Eq. (4) devant être valable quelque soit la variation $\delta\mathbf{q}$, il s'en suit:

$$\mathbf{f}_g = \mathbf{B}^{\mathrm{T}}\mathbf{f}_l , \quad \text{with} \quad \mathbf{f}_l = [\, N \quad M_1 \quad M_2 \,]^{\mathrm{T}} . \tag{5}$$

La matrice de rigidité tangente globale est définie par:

$$\delta\mathbf{f}_g = \mathbf{K}_g\,\delta\mathbf{q} . \tag{6}$$

En calculant la variation de l'équation (5), nous obtenons la matrice de rigidité globale

$$\mathbf{K}_g = \mathbf{B}^{\mathrm{T}}\mathbf{K}_l\mathbf{B} + \frac{\mathbf{z}\,\mathbf{z}^{\mathrm{T}}}{l_n}N + \frac{1}{l_n^2}(\mathbf{r}\,\mathbf{z}^{\mathrm{T}} + \mathbf{z}\,\mathbf{r}^{\mathrm{T}})(M_1 + M_2) . \tag{7}$$

Le vecteur forces élastiques locales $\mathbf{f}_l$ et la matrice de rigidité tangente locale $\mathbf{K}_l$, qui est définie par $\delta\mathbf{f}_l = \mathbf{K}_l\,\delta\overline{\mathbf{q}}$, dépendent de la formulation locale. Dans cette formulation locale, les fonctions d'interpolation de l'Interdependent Interpolation Element (IIE), proposées dans [43], ont été utilisées conjointement à une théorie des poutres en arc à profondeur faible. Le développement de l'IIE est basée sur la solution exacte sous la forme homogène des équations d'équilibre d'une poutre de Timoshenko. Par conséquent, l'IIE conserve non seulement la précision inhérente à l'interpolation cubique, mais comprend également la déformation de cisaillement. Les expressions de $\mathbf{f}_l$, $\mathbf{K}_l$ ont ensuite été calculées à l'aide de Maple. Le code est donné dans [31].

2.3 Vecteur force d'inertie et matrice d'inertie tangente

L'énergie cinétique K d'un élément de poutre est donnée par

$$K = \frac{1}{2}\rho\left\{\int_{l_o} A(\dot{u}_{\mathrm{G}}^2 + \dot{w}_{\mathrm{G}}^2)\mathrm{d}l + \int_{l_o} I\,\dot{\theta}^2\mathrm{d}l\right\}, \tag{8}$$

où

- ρ est la masse volumique,
- u_{G} , w_{G} sont les déplacements globaux du centre de gravité de la section,
- θ est la rotation globale de la section.

Sur base des relations géométriques décrivant la cinématique de la poutre corotationnelle et des fonctions de forme cubiques locales, les vitesses $\dot{u}_{\mathrm{G}}, \dot{w}_{\mathrm{G}}, \dot{\theta}$, sont interpolées à partir des vitesses nodales $\dot{\mathbf{q}}$ et l'expression exacte de l'énergie cinétique de K est alors obtenue. En prenant Ω égal à 0, on retombe sur la poutre de Bernoulli [43]. Des études numériques effectuées par l'auteur ont montré que cette simplification ne modifie pas les résultats numériques.

En outre, l'énergie cinétique peut s'écrire sous la forme suivante

$$K = \frac{1}{2}\,\dot{\mathbf{q}}^{\mathrm{T}}\,\mathbf{M}\,\dot{\mathbf{q}} = \frac{1}{2}\dot{\mathbf{q}}^{\mathrm{T}}\,\mathbf{T}^{\mathrm{T}}\,\mathbf{M}_l\,\mathbf{T}\,\dot{\mathbf{q}}\,, \tag{9}$$

où $\mathbf{T}$ est la matrice de rotation. Par conséquent, l'expression de la matrice locale $\mathbf{M}_l$ peut être déterminée. À ce stade, deux simplifications sont introduites dans l'expression de la matrice de masse local. Le déplacement local w est supposé petit et donc les termes contenant w^2 sont négligés. En outre, l'approximation $l_n = l_o$ est considérée (hypothèse des petites déformations axiales). Ces simplifications conduisent à une matrice de masse local fonction uniquement de $\overline{\theta}_1$ et $\overline{\theta}_2$.

Le vecteur force d'inertie est calculé à partir de l'énergie cinétique à l'aide de l'équation de mouvement de Lagrange. A partir de l'expression de l'énergie cinétique, l'expression de $\mathbf{f}_K$ est obtenue

$$\begin{aligned}\mathbf{f}_K = \mathbf{M}\,\ddot{\mathbf{q}} + \left\{\mathbf{M}_\beta\left(\frac{\mathbf{z}^{\mathrm{T}}}{l_n}\dot{\mathbf{q}}\right) + \mathbf{M}_{\overline{\theta}_1}(\mathbf{b}_2^{\mathrm{T}}\dot{\mathbf{q}}) + \mathbf{M}_{\overline{\theta}_2}(\mathbf{b}_3^{\mathrm{T}}\dot{\mathbf{q}})\right\}\dot{\mathbf{q}} \\ - \left(\frac{1}{2}\dot{\mathbf{q}}^{\mathrm{T}}\mathbf{M}_\beta\dot{\mathbf{q}}\right)\frac{\mathbf{z}}{l_n} - \left(\frac{1}{2}\dot{\mathbf{q}}^{\mathrm{T}}\mathbf{M}_{\overline{\theta}_1}\dot{\mathbf{q}}\right)\mathbf{b}_2 - \left(\frac{1}{2}\dot{\mathbf{q}}^{\mathrm{T}}\mathbf{M}_{\overline{\theta}_2}\dot{\mathbf{q}}\right)\mathbf{b}_3\,,\end{aligned} \tag{10}$$

où $\mathbf{M}_\beta = \dfrac{\partial\mathbf{M}}{\partial\beta}$, $\mathbf{M}_{\overline{\theta}_1} = \dfrac{\partial\mathbf{M}}{\partial\overline{\theta}_1}$, $\mathbf{M}_{\overline{\theta}_2} = \dfrac{\partial\mathbf{M}}{\partial\overline{\theta}_2}$.

2.4 Exemple numérique

Dans l'article [31], quatre exemples numériques ont été analysés. Le but de ces quatre exemples est d'évaluer les performances de la nouvelle formulation corotationnelle en dynamique non-linéaire. En par-

ticulier, les résultats obtenues avec cette nouvelle formulation sont comparées à ceux obtenus avec les deux formulations classiques, proposées dans la littérature, dans lesquelles la matrice de masse diagonale et la matrice de masse de Timoshenko sont utilisées.

Dans cette section, un des quatre exemples est repris. Le comportement dynamique d'une poutre console soumise à une force sinusoïdale $P = P_o \sin(wt)$ est analysé. La longueur de la poutre est $L = 10$ m. La hauteur et la largeur de la section transversale sont respectivement $a = 0.25$ m et $e = 0.5$ m. L'amplitude et la fréquence de la force appliquée à l'extrémité libre sont $P_o = 10$ MN et $w = 50$ rad/s. Le module élastique E est égal à 210 GPa, tandis que la masse volumique ρ est prise égale à 7850 kg/m^3.

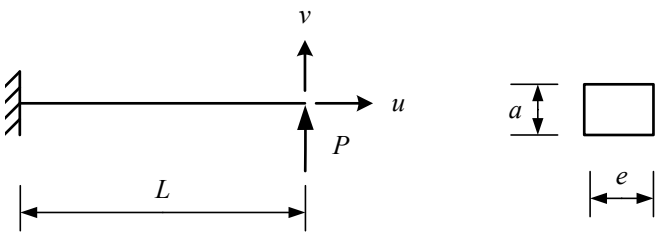

Fig. 2. Poutre console: Données géométriques.

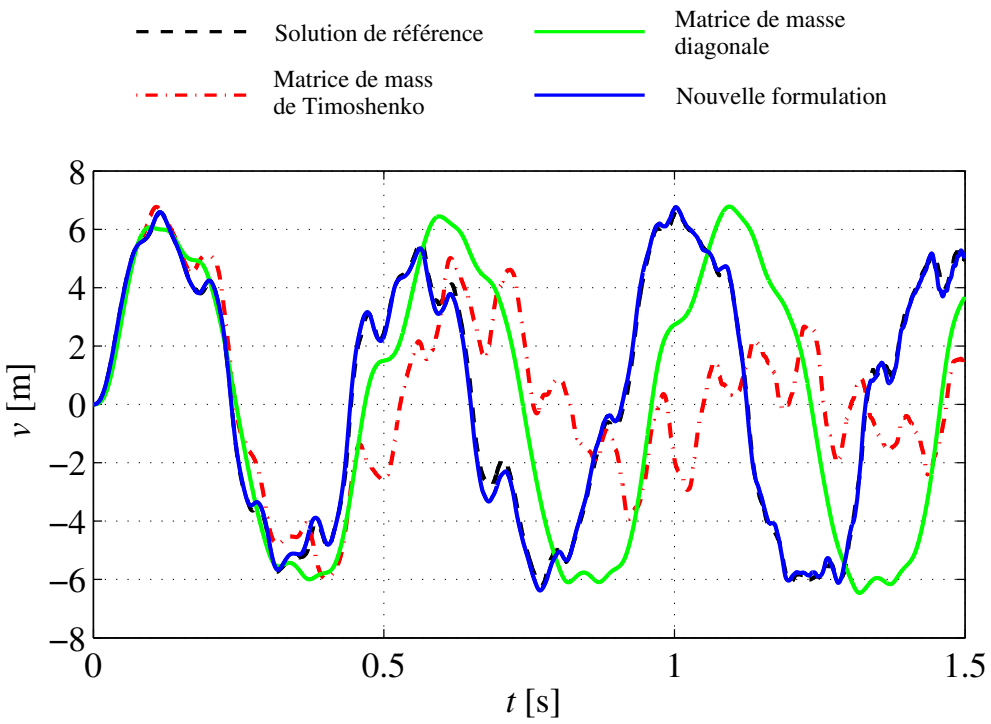

Fig. 3. Poutre console - Evolution temporelle du déplacement vertical.

Les résultats donnés par les trois formulations ont été comparés à une solution de référence. Cette solution, obtenue avec un grand nombre d'éléments, est identique pour les trois formulations dynamiques considérées. La solution de référence a également été comparée aux résultats fournis par Abaqus (formulation lagrangienne totale) et des résultats identiques ont été obtenus.

Pour le problème considéré, la solution de référence, obtenue avec 48 éléments, et les résultats fournis par les trois formulations avec seulement 3 éléments sont présentés à la Fig. 3. Le pas du temps Δt est pris égal

à 10^{-4} s. On peut observer que la nouvelle formulation produit des résultats qui sont en très bon accord avec la solution de référence. Tandis que, les résultats obtenus avec les deux autres approches sont assez éloignés de la solution de référence pour le domaine temporel considéré.

Le résultat de cet exemple montre également que la nouvelle formulation, basée sur des interpolations cubiques locales, est plus efficace que les autres formulations, qui reposent sur des interpolations linéaires locales (la matrice de masse de Timoshenko) et la matrice de masse diagonale. Cet avantage peut être attribué à une meilleure représentation des déplacements locaux dans les termes d'inertie.

3 Grandes rotations en dynamique

L'extension d'une formulation de poutre de 2D en 3D n'est pas une tâche triviale. La difficulté est principalement due à la nature complexe de grandes rotations. Plus précisément, les grandes rotations sont non-commutatives et non-additives, donc elles ne peuvent pas être traitées de la même manière que les translations. En conséquence, la méthode classique de Newmark ne peut pas être directement appliquée aux grandes rotations. Cette méthode doit être reformulée selon le paramétrage des grandes rotations retenu.

Plusieurs aspects des grandes rotations en dynamique ont été étudiés dans [32]. Le premier aspect concerne la paramétrisation des grandes rotations. Plusieurs possibilités pour paramétrer des grandes rotations peuvent être trouvés dans [3, 11, 12, 19, 30]. Dans [32] le tenseur de rotation, le vecteur de rotation et les paramètres d'Euler ont été étudiés.

Un second aspect important est lié à la fois aux méthodes de Newmark pour les grandes rotations ainsi que l'efficacité de la procédure itérative. Deux algorithmes de Newmark proposés dans la littérature ont retenus notre attention. Le premier a été proposé par Simo et Vu-Quoc [47], les équations de Newmark ont été écrites en utilisant le vecteur matériel incrémental de rotation , la vitesse angulaire matérielle et l'accélération angulaire matérielle. Dans la seconde approche, introduite par Cardona et Geradin [11], l'algorithme classique de Newmark a été appliqué au vecteur incrémental de rotation et ses dérivés temporelles. Par conséquent, la procédure de mise à jour des rotations a une forme similaire à celle des déplacements. En ce qui concerne l'efficacité de la procédure itérative, plusieurs prédicteurs et différentes possibilités de simplifier la matrice d'inertie tangente ont été également testés.

Afin de comparer ces paramétrages et les méthodes de Newmark associées, quatre formulations dynamiques non-linéaires ont été étudiés dans [32]. Pour toutes ces formulations, les calculs théoriques sont donnés en détail. Les points communs et les différences entre ces quatre formulations sont soulignés. Par ailleurs, afin d'évaluer la performance de ces quatre formulations en termes de précision numérique et d'efficacité, six exemples ont été analysés.

L'objectif de cette section est de présenter un bref résumé de ces aspects.

3.1 Grandes rotations

La rotation d'un vecteur de la position $\mathbf{x}_o$ à la position $\mathbf{x}$ peut être représentée par une matrice de rotation $\mathbf{R}$

$$\mathbf{x} = \mathbf{R}\,\mathbf{x}_o\,. \tag{11}$$

La variation spatiale de la matrice de rotation est calculée comme suit

$$\delta\mathbf{R} = \widetilde{\delta\mathbf{w}}\mathbf{R}, \tag{12}$$

où $\delta\mathbf{w}$ est un vecteur contenant les variables spatiales de spin. La notation $\widetilde{\mathbf{x}}$ désigne la matrix anti-symétrique du vecteur $\mathbf{x}$.

La matrice de rotation $\mathbf{R}$ est une matrice orthogonale comprenant neuf composantes. Toutefois, en raison de la condition d'orthonormalité, la matrice de rotation $\mathbf{R}$ peut être paramétrée en utilisant seulement trois paramètres indépendants. Une possibilité est d'utiliser le vecteur de rotation défini par:

$$\boldsymbol{\theta} = \theta\,\mathbf{n}, \tag{13}$$

où $\mathbf{n}$ est un vecteur unitaire définissant l'axe de rotation et $\theta = (\boldsymbol{\theta}^{\mathrm{T}}\boldsymbol{\theta})^{1/2}$ est l'angle de rotation.

Une autre possibilité de paramétrer la matrice de rotation est d'utiliser les paramètres d'Euler (ou quaternions), qui en introduisant un facteur d'échelle 2 donne:

$$\mathbf{q} = 2\sin\frac{\theta}{2}\,\mathbf{n}. \tag{14}$$

Ce paramétrage ne nécessite que trois paramètres $\mathbf{q}$ (voir Eq. (14)) au lieu de quatre $(\mathbf{q}, q_o)$ comme souvent proposé dans la littérature.

Si les paramètres du vecteur de rotation ou les paramètres d'Euler sont utilisés (voir [6, 40]), les rotations deviennent additives et sont simplement mises à jour à chaque itération de la même manière que les déplacements de translation. Toutefois, l'angle de rotation est limitée à 2π avec le vecteur de rotation et π dans le cas des paramètres d'Euler. Dans de nombreuses analyses dynamiques, les angles des rotations peuvent excéder ces deux limites. Afin de remédier à cet inconvénient, Cardona et Geradin [11], Ibrahimbegović [24] et Battini [7] ont introduit la notion du vecteur de rotation incrémental et les paramètres d'Euler incrémentaux. Les mises à jour additives s'appliquent toujours à l'intérieur de chaque incrément. Les amplitudes des rotations sont seulement limitées à chaque incrément, ce qui ne pose aucun problème en pratique.

3.2 Intégration temporelle de grandes rotations

3.2.1 Méthode de Newmark

Dans [47], Simo et Vu-Quoc ont proposé d'appliquer directement l'algorithme de Newmark classique aux vitesses angulaires matérielles, accélération angulaires matérielles et au vecteur de rotation matériel incrémental. L'algorithme est donnée par

$$\boldsymbol{\Theta}_{n+1} = h\dot{\boldsymbol{\omega}}_n + h^2\left[(\frac{1}{2}-\beta)\ddot{\boldsymbol{\omega}}_n + \beta\,\ddot{\boldsymbol{\omega}}_{n+1}\right], \tag{15}$$

$$\dot{\boldsymbol{\omega}}_{n+1} = \dot{\boldsymbol{\omega}}_n + h\left[(1-\gamma)\ddot{\boldsymbol{\omega}}_n + \gamma\ddot{\boldsymbol{\omega}}_{n+1}\right]. \tag{16}$$

Cette méthode d'intégration temporelle de Newmark est adoptée dans [13, 26, 28, 29, 50]. Ibrahimbegović et Mikdad [25] ont reformulé cette méthode en utilisant les formes spatiales.

Cardona et Geradin, dans [11], ont proposé d'utiliser d'une autre manière la méthode de Newmark pour les grandes rotations. Les dérivés temporelles du vecteur de rotation incrémental sont utilisées à la place de la vitesse angulaire et de l'accélération angulaire. Par conséquent, la propriété additive du vecteur de rotation spatial incrémental peut être utilisée et la procédure de mise à jour de Newmark classique pour les translations est également appliquée aux variables de rotation. Dans ce cas, l'algorithme est donnée par:

$$\boldsymbol{\theta}_{n+1} = h\dot{\boldsymbol{\theta}}_n + h^2\left[(\frac{1}{2}-\beta)\ddot{\boldsymbol{\theta}}_n + \beta\,\ddot{\boldsymbol{\theta}}_{n+1}\right], \tag{17}$$

$$\dot{\boldsymbol{\theta}}_{n+1} = \dot{\boldsymbol{\theta}}_n + h\left[(1-\gamma)\ddot{\boldsymbol{\theta}}_n + \gamma\ddot{\boldsymbol{\theta}}_{n+1}\right]. \tag{18}$$

3.2.2 *Prédicteurs pour la procédure itérative*

Dans l'analyse dynamique non-linéaire des structures, les déplacements (translations et rotations), les vitesses et les accélérations doivent être calculées à chaque pas de temps. Pour ces trois inconnues, la méthode de Newmark fournit seulement deux relations. Ainsi, il est nécessaire de faire une hypothèse sur l'une des trois variables en t_{n+1}. Un mauvais prédicteur peut causer l'augmentation du nombre d'itérations et, dans certains cas, la divergence de la procédure itérative. Dans [32], quatre prédicteurs proposés dans la littérature ont été implémentés et testés:

- Pred. 1: les déplacements et les rotations en t_n sont pris comme valeurs initiales pour la solution en t_{n+1}.
- Pred. 2: les accélérations de translations et de rotations sont prises égale à zero au démarrage de la procédure itérative en t_{n+1}.
- Pred. 3: on suppose que les accélérations de translations et de rotations en t_{n+1} sont égales à celles en t_n.
- Pred. 4: on suppose que l'opérateur tangent est constant entre t_n et t_{n+1}. Ce prédicteur a été proposé par Crisfield [12] pour le cas d'un vecteur de force d'inertie linéaire et développé ensuite dans [32] pour un vecteur de force d'inertie quelconque.

3.2.3 *Matrice d'inertie tangente*

L'équation non-linéaire de mouvement est résolue en utilisant la méthode itérative de Newton-Raphson. Ainsi, la linéarisation du vecteur force d'inertie doit être calculée:

$$\Delta \mathbf{f}_k = \mathbf{M}\Delta\ddot{\mathbf{d}} + \mathbf{C}_k\Delta\dot{\mathbf{d}} + \mathbf{K}_k\Delta\mathbf{d}\,, \tag{19}$$

où $\mathbf{K}_k$, $\mathbf{C}_k$ et $\mathbf{M}$ désignent respectivement la matrice centrifuge, la matrice gyroscopique et la matrice de masse.

Dans plusieurs cas, une linéarisation exacte de la force d'inertie est difficile à obtenir. Afin de remédier à ce problème et de réduire le temps de calcul, Geradin et Cardona [11, 19] ont recommandé de ne garder que la matrice de masse et de négliger les matrices gyroscopique et centrifuge.

Dans [32], nous avons évalué différentes simplifications de la relation (19). Les trois cas suivants ont été testés: la matrice d'inertie tangente exacte (c-à-d les matrices de masse, gyroscopiques et centrifuges), la matrice de masse seule (comme proposé dans [11, 19]), et les termes de masse et gyroscopique (la nouvelle proposition).

3.3 *Comparaison des formulations dynamiques*

Quatre formulations d'élément de poutre 3D pour la dynamique non-linéaire ont été comparées dans [32].s Pour chaque formulation, le vecteur force d'inertie et la matrice d'inertie tangente ont été obtenus dans un contexte lagrangien total et calculé en utilisant deux points de Gauss. Le vecteur des efforts internes a été obtenu en utilisant la méthode corotationnelle. La première formulation a été proposée par Simo et Vu-Quoc [47] et utilise les variables de spin spatiales (Var. Spin. Spat). Une modification du calcul des quantités de rotation aux points de Gauss a été introduit afin d'obtenir une plus grande efficacité. La seconde formulation, développée par Ibrahimbegović et Mikdad dans [25], est basée sur le vecteur de rotation incrémental (V. Rot. Inc. 1). La troisième, également basée sur le vecteur de rotation incrémental (V. Rot. Inc. 2), a été proposée par Cardona et Geradin [11]. Elle a été reformulée en utilisant la forme spatiale du vecteur de rotation incrémental au lieu de la forme matérielle. La quatrième formulation fait usage de trois des quatre paramètres d'Euler (Euler Inc.) comme les variables de rotation. Cette idée a été introduite par Battini [7] pour l'analyse statique, puis développée dans [32] pour l'analyse dynamique.

En ce qui concerne les termes statiques, c'est à dire le vecteur force interne et la matrice de rigidité tangente, l'élément local *t3d* développés par Battini et Pacoste [7, 8] a été employé.

Table 1. Quatre formulations dynamiques non-linéaire.

Formulation	Variables de rotation	Méthode d'intégration temporelle
Simo & Vu-Quoc [47]	Variables de spin spatiales	Simo & Vu-Quoc
Ibrahimbegović & Mikdad [25]	Vecteur de rotation incrémental	
Cardona & Geradin [11]		Cardona & Geradin
Nouvelle formulation [32]	Paramètres d'Euler incrémental	

3.4 Exemple numérique

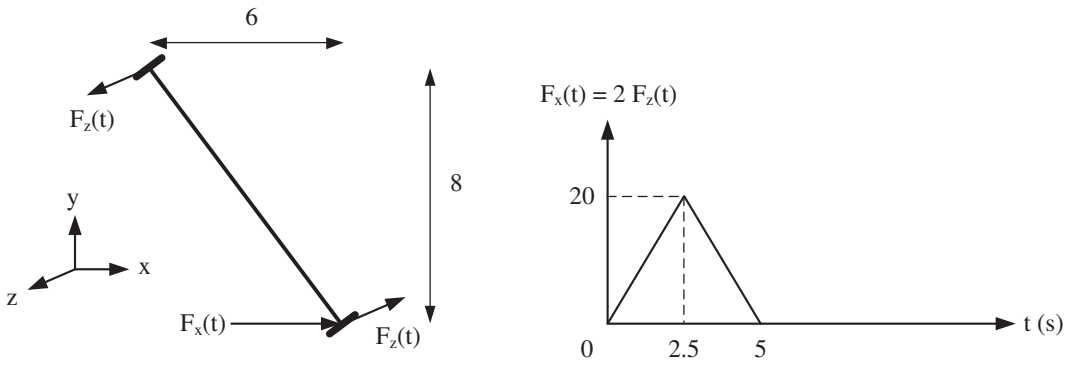

Fig. 4. Données du problème.

Cet exemple, proposé par Ibrahimbegović et Mikdad [25], analyse le mouvement d'une poutre flexible avec disques rigides attachés aux extrémités. La configuration initiale est donnée à la Fig. 4. La masse par unité de longueur de la poutre et la matrice des moments d'inertie de la section transversale dans la configuration initiale sont $A_\rho = 1, \mathbf{J}_\rho = \mathrm{diag}(20, 10, 10)$, respectivement. Les autres propriétés du matériau sont $EA = GA = 10^4, EI = GJ = 500$. Les disques ont une masse ponctuelle $M = 10.0$ et une matrice d'inertie $\mathbf{J}_\rho = \mathrm{diag}(200.0, 100.0, 100.0)$. Le système est mis en mouvement par l'application d'un couple de forces hors du plan $F_z(t)$ et une force dans le plan $F_x(t)$ avec $F_x(t) = 2F_z(t)$. La poutre a été discrétisée en utilisant 10 éléments et les disques ont été modélisés avec des éléments nodaux. Dans cet exemple, toutes les quantités sont sans unité.

L'exemple a été analysé à l'aide des quatre formulations dynamiques. Le pas de temps $\Delta t = 0.10$ s a été choisi et les évolutions temporelles des déplacements de l'extrémité basse de la poutre sont présentées à la Fig. 5. Puisque toutes les formulations donnent les mêmes résultats numériques, les courbes présentées pourraient être obtenues avec toutes les formulations discutées.

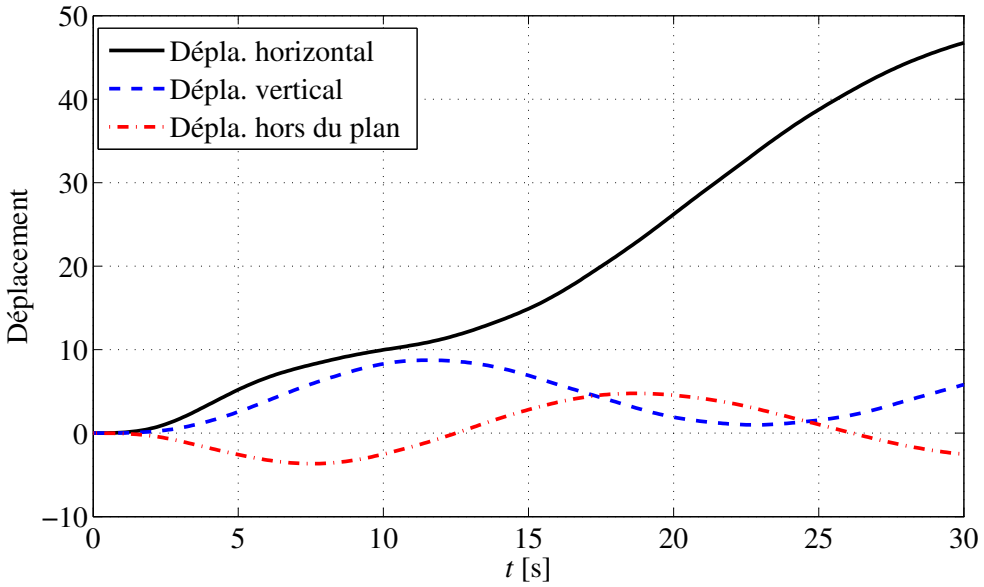

Fig. 5. Évolution temporelle de l'extrémité à droite.

3.4.1 Choix du préditeur

Quatre prédicteurs ont été comparés avec différents pas de temps. Les matrices d'inertie tangentes exactes ont été utilisées. Le nombre d'itérations total pour chaque formulations est donné dans au tableau 2.

Table 2. Nombre d'itérations.

		Pred. 1	Pred. 2	Pred. 3	Pred. 4
Var. Spin. Spat.	$\Delta t = 0.25$ s	479	363	363	357
	$\Delta t = 0.10$ s	1181	902	901	878
V. Rot. Inc.1	$\Delta t = 0.25$ s	479	363	363	357
	$\Delta t = 0.10$ s	1181	902	901	877
V. Rot. Inc.2	$\Delta t = 0.25$ s	479	363	363	357
	$\Delta t = 0.10$ s	1181	902	897	877
Euler Inc.	$\Delta t = 0.25$ s	479	363	363	357
	$\Delta t = 0.10$ s	1181	902	897	877

Pour toutes les formulations, Pred. 4 a fourni la meilleure performance. Le nombre d'itérations est le plus bas. Cela peut s'expliquer par le fait que Pred. 4 suppose la linéarité du système au cours du pas de temps. C'est souvent une bonne approximation, en particulier avec de petits pas de temps. Dans la suite, seulement Pred. 4 a été utilisé dans les calculs numériques.

3.4.2 Choix de la matrice tangente et comparison des quatre formulations

Pour chaque formulation, la matrice d'inertie tangente exacte, et la matrice simplifiée proposée par l'auteur (Simpl. 1) et celle proposée par Geradin et Cardona (Simpl. 2) ont été testés. Le temps de calcul et le nombre d'itérations total (entre parenthèses) pour chaque formulations sont donnés au tableau 3.

Table 3. Performance numérique.

	Var. Spin. Spat.	V. Rot. Inc.1	V. Rot. Inc.2	Euler Inc.
Exacte	19.5 (878)	21.9 (877)	25.1 (877)	22.5 (877)
Simpl. 1	19.2 (885)	20.2 (882)	20.0 (881)	18.6 (881)
Simpl. 2	22.8 (1150)	23.8 (1140)	21.8 (1144)	21.1 (1154)

D'après les résultats numériques, on peut conclure que:

- Pour les deux premières formulations, Simpl. 2 est la plus lente. Elle a conduit à une augmentation du nombre d'itérations d'environ 25 % à 38 % par rapport à la matrice exacte. En effet, pour ces formulations, les matrices tangentes ne nécessitent pas beaucoup de temps de calcul, donc le temps de calcul pris par la simplification ne peut pas compenser celui nécessaire aux itérations supplémentaires. D'après les résultats, il était assez difficile de faire un choix entre la matrice d'inertie tangente exacte et Simpl. 1. La différence en termes de coût de temps de calcul entre ces deux matrices est petite. L'auteur recommande d'utiliser la matrice tangente exacte avec ces deux formulations.
- Pour les deux dernières formulations, il est recommandé d'utiliser Simpl. 1 qui réduit le temps de calcul d'environ 25 % par rapport à la matrice exacte et d'environ 15 % par rapport à Simpl. 2.
- La formulation basée sur les paramètres d'Euler spatiaux avec Simpl. 1 semble être la plus performante.

3.4.3 Influence du pas de temps

Les résultats précédents ont montré que la formulation basée sur les paramètres d'Euler spatiaux avec Simpl. 1 est la plus rapide. Cependant, l'exemple a été résolu avec un seul pas de temps. Pour avoir une vue plus complète, l'exemple a été recalculé avec de différents pas de temps. Les formulations Var. Spin. Spat. et V. Rot. Inc.1 ont été mises en œuvre avec la matrice d'inertie tangente exacte. Les deux autres formulations ont été mises en œuvre avec Simpl. 1.

Les résultats sont présentés au tableau 4. Ils montrent que la taille du pas de temps n'a pas d'incidence sur la hiérarchie entre les formulations.

Table 4. Performances numériques avec des pas du temps variés.

	Var. Spin. Spat.	V. Rot. Inc.1	V. Rot. Inc.2	Euler Inc.
$\Delta t = 0.1$ s	19.5 (878)	21.9 (877)	20.0 (881)	18.6 (881)
$\Delta t = 0.5$ s	5.7 (239)	5.9 (237)	5.3 (239)	4.9 (239)

4 Éléments de poutre corotationnels 3D avec une section transversale solide

Le but de cette section est de présenter les principaux résultats du troisième article [33]. Dans cet article, un nouvel élément de poutre a été développé. La nouveauté de cet élément est que la description cinématique corotationnelle a été utilisée pour obtenir non seulement le vecteur force interne et la matrice de rigidité tangente, mais aussi le vecteur force d'inertie et la matrice d'inertie tangente. Les mêmes interpolations cubiques locales ont été adoptées pour calculer à la fois les termes d'inertie et les termes internes. Ce faisant, les expressions complexes des termes d'inertie ont été considérablement simplifiées grâce à une approximation sur les rotations locales. Pour améliorer l'efficacité de la procédure itérative, le terme le moins important de la matrice d'inertie tangente a été ignoré. Quatre exemples numériques ont été étudiés dans le but de comparer les performances de la nouvelle formulation vis-à-vis des deux autres approches. La première approche est similaire à celle présentée ci-dessous, sauf que les termes dynamiques sont calculés

sur base d'interpolations linéaires locales alors que les termes internes sont calculés à l'aide de fonctions interpolations cubiques. Le but est d'évaluer l'influence du choix du degré des interpolations locales sur les termes dynamiques. La deuxième approche est une formulation lagrangienne totale classique proposée par Simo et Vu-Quoc [45–47].

4.1 Cinématique de poutre

La méthode corotationnelle introduite par Nour-Omid et Rankin [38], et développée par Pacoste et Eriksson [41] et Battini et Pacoste [8] est adoptée. L'idée principale de la méthode corotationnelle est de décomposer le mouvement de l'élément en deux parties: un mouvement de corps rigide et un mouvement en petites perturbations. Au cours du mouvement corps rigide, un système de coordonnées locales, fixé à l'élément, se déplace et tourne avec ce dernier. Le mouvement du corps rigide est constitué d'une translation et d'une rotation rigides de l'élément. L'origine du système local est prise au nœud 1. Le premier axe de coordonnées du système local est défini par la ligne reliant les nœuds 1 et 2 de l'élément.

Le mouvement de corps rigide décrit précédemment, est accompagné d'un movement local en petites perturbations. Grâce au choix du système de coordonnées local, le vecteur des déplacements nodaux locaux $\mathbf{d}_l$ ne dispose que de sept éléments et est donnée par:

$$\mathbf{d}_l = \left[\bar{u} \;\; \bar{\boldsymbol{\theta}}_1^{\mathrm{T}} \;\; \bar{\boldsymbol{\theta}}_2^{\mathrm{T}} \right]^{\mathrm{T}} . \tag{20}$$

La variation de ce vecteur est donnée par:

$$\delta\mathbf{d}_l = \left[\delta\bar{u} \;\; \delta\bar{\boldsymbol{\theta}}_1^{\mathrm{T}} \;\; \delta\bar{\boldsymbol{\theta}}_2^{\mathrm{T}} \right]^{\mathrm{T}} , \tag{21}$$

et la variation du vecteur des déplacements nodaux globaux est donnée par:

$$\delta\mathbf{d}_g = \left[\delta\mathbf{u}_1^{g\mathrm{T}} \;\; \delta\mathbf{w}_1^{g\mathrm{T}} \;\; \delta\mathbf{u}_2^{g\mathrm{T}} \;\; \delta\mathbf{w}_2^{g\mathrm{T}} \right]^{\mathrm{T}} , \tag{22}$$

où $\delta\mathbf{w}_i^g \;\; (i = 1,2)$ désigne le vecteur des variables de spin spatiales comme définies dans Eq. (12).

La relation entre les variations des déplacements locaux et globaux est définie par une matrice de transformation $\mathbf{B}$

$$\delta\mathbf{d}_l = \mathbf{B}\,\delta\mathbf{d}_g . \tag{23}$$

4.2 Vecteur force interne et matrice de rigidité tangente

Dans cette nouvelle formulation, les interpolations cubiques locales et la théorie de poutre en arc à profondeur faible sont adoptées pour calculer le vecteur force interne local $\mathbf{f}_l$ et la matrice de rigidité tangente local $\mathbf{K}_l$ associé à $\delta\mathbf{d}_l$. Les codes de Maple pour $\mathbf{f}_l$ et $\mathbf{K}_l$ sont donnés dans [8].

En égalant le travail interne virtuel dans les deux systèmes global et local, l'expression du vecteur force interne global $\mathbf{f}_g$ est obtenue par:

$$\mathbf{f}_g = \mathbf{B}^{\mathrm{T}}\mathbf{f}_l . \tag{24}$$

En prenant les variations de Eq. (24), l'expression de la matrice de rigidité globale tangente $\mathbf{K}_g$ est obtenu

$$\mathbf{K}_g = \mathbf{B}^{\mathrm{T}}\mathbf{K}_l\mathbf{B} + \left.\frac{\partial(\mathbf{B}^{\mathrm{T}}\mathbf{f}_l)}{\partial\mathbf{d}_g}\right|_{\mathbf{f}_l} . \tag{25}$$

4.3 Vecteur force d'inertie et matrice d'inertie tangente

Dans cette section, nous résumons les étapes permettant d'établir les expressions du vecteur force d'inertie et de la matrice d'inertie tangente présentée dans [33]. La nouveauté de cette approche est que la même description cinématique corotationnelle est adoptée pour formuler à la fois les termes d'inertie et les termes internes. Cette approche assure la cohérence de la formulation. Comme déjà mentionné, cette formulation dynamique corotationnelle 3D est l'extension de la celle en 2D proposée dans [31].

En utilisant le centre de gravité de la section transversale comme point de référence, la variation de l'énergie cinétique peut être exprimée comme suit (voir [19])

$$\delta K = -\int_{l_o} \left\{ \delta \mathbf{u}^{\mathrm{T}} A_\rho \ddot{\mathbf{u}} + \delta \mathbf{w}^{\mathrm{T}} \left[\mathbf{I}_\rho \dot{\mathbf{w}} + \widetilde{\dot{\mathbf{w}}} \mathbf{I}_\rho \dot{\mathbf{w}} \right] \right\} \mathrm{d}l \,, \tag{26}$$

où $\dot{\mathbf{u}}$, $\dot{\mathbf{w}}$ sont respectivement la vitesse de translation et la vitesse angulaire de la section transversale et $\mathbf{I}_\rho$ est la matrice des moments d'inertie spatiaux.

Sur base des relations géométriques et des interpolations cubiques locales, les variations $\delta\mathbf{u}, \delta\mathbf{w}$ sont calculées à partir du vecteur des déplacements nodaux globaux $\mathbf{d}_g$.

Le vecteur force d'inertie est ensuite déterminé à partir de la relation suivante

$$\delta K = -\mathbf{f}_k^{\mathrm{T}} \delta \mathbf{d}_g \,. \tag{27}$$

Toutefois, dans l'approche corotationnelle, les rotations locales au niveau des nœuds $\overline{\boldsymbol{\theta}}_i$ $(i = 1,2)$ peuvent être considérées comme petites. Par conséquent, l'approximation suivante est introduite dans la dérivation de l'expression du vecteur $\mathbf{f}_k$

$$\delta \overline{\mathbf{w}}_i \approx \delta \overline{\boldsymbol{\theta}}_i \,. \tag{28}$$

Finalement, l'expression du vecteur force d'inertie est obtenue sous la forme:

$$\mathbf{f}_k = \mathbf{E} \left[\int_{l_o} \left\{ \mathbf{H}_1^{\mathrm{T}} \mathbf{R}_r^{\mathrm{T}} A_\rho \ddot{\mathbf{u}} + \mathbf{H}_2^{\mathrm{T}} \mathbf{R}_r^{\mathrm{T}} \left[\mathbf{I}_\rho \dot{\mathbf{w}} + \widetilde{\dot{\mathbf{w}}} \mathbf{I}_\rho \dot{\mathbf{w}} \right] \right\} \mathrm{d}l \right] . \tag{29}$$

Ensuite, une procédure itérative est mise en œuvre en tronquant l'expression de $\Delta\mathbf{f}_k$

$$\Delta \mathbf{f}_k \approx \mathbf{M} \Delta \ddot{\mathbf{d}}_g + \mathbf{C}_k \Delta \dot{\mathbf{d}}_g \,. \tag{30}$$

Les expressions de la matrice de masse $\mathbf{M}$ et de la matrice gyroscopique $\mathbf{C}_k$ sont données par

$$\mathbf{M} = \mathbf{E} \left\{ \int_{l_o} \left(\mathbf{H}_1^{\mathrm{T}} A_\rho \, \mathbf{H}_1 + \mathbf{H}_2^{\mathrm{T}} \mathbf{I}_\rho^e \, \mathbf{H}_2 \right) \mathrm{d}l \right\} \mathbf{E}^{\mathrm{T}} = \mathbf{E} \, \mathbf{M}^e \, \mathbf{E}^{\mathrm{T}} , \tag{31}$$

$$\begin{aligned} \mathbf{C}_k = \mathbf{E} \Bigg\{ & \int_{l_o} \mathbf{H}_1^{\mathrm{T}} A_\rho \, (\mathbf{C}_1 + \mathbf{C}_3) \, \mathrm{d}l + \int_{l_o} \mathbf{H}_2^{\mathrm{T}} \mathbf{I}_\rho^e \, (\mathbf{C}_2 + \mathbf{C}_4) \, \mathrm{d}l \\ & + \int_{l_o} \mathbf{H}_2^{\mathrm{T}} \left(\widetilde{\mathbf{w}^e} \mathbf{I}_\rho^e - \widetilde{\mathbf{I}_\rho^e \mathbf{w}^e} \right) \mathbf{H}_2 \mathrm{d}l \Bigg\} \mathbf{E}^{\mathrm{T}} = \mathbf{E} \, \mathbf{C}_k^e \, \mathbf{E}^{\mathrm{T}} . \end{aligned} \tag{32}$$

4.4 Exemple numérique

Cet exemple classique, proposé par Simo et Vu-Quoc [47], a été fréquemment pris pour valider les formulations dynamiques non-linéaires [21, 25, 29, 36]. Une poutre cantilever à 90^o, soumis à une force hors plan

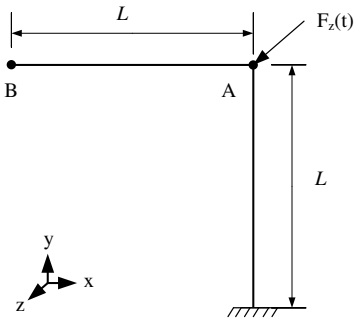

Fig. 6. Données géométriques.

(voir Fig. 6) est analysée. Chaque partie de la poutre a une longueur $L = 10$. Les propriétés du matériau sont $GA = EA = 10^6$, $GJ = EI = 10^3$. La masse par unité de longueur et la matrice des moments d'inertie sont $A_\rho = 1$ et $\mathbf{J}_\rho = \text{diag}(20, 10, 10)$, respectivement. La variation de la force est donnée à la Fig. 7. Dans cet exemple, tous les quantités sont sans unité.

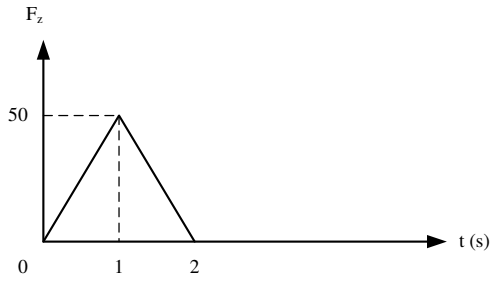

Fig. 7. Chargement.

L'analyse dynamique de cet exemple a été réalisée en utilisant trois formulations différentes: la nouvelle approche corotationnelle, l'approche corotationnelle linéaire et la formulation lagragienne totale de Simo et Vu-Quoc [45–47]. L'approche corotationnelle linéaire est similaire à la nouvelle formulation, mais les interpolations cubiques ont été remplacées par des interpolations linéaires dans le développement des termes d'inertie. On peut noter que ces interpolations linéaires impliquent $\mathbf{u}_l = \mathbf{0}_{3\times 1}$ ce qui simplifie de manière substantielle les calculs.

Les trois formulations ont été programmées avec Matlab. Le même niveau d'optimisation dans la construction des matrices tangentes et des vecteurs force a été soigneusement assuré.

Les résultats donnés par ces trois formulations dynamiques sont comparés à une solution de référence. Cette dernière est obtenue en augmentant le nombre d'éléments jusqu'à ce que les trois formulations dynamiques convergent vers le même résultat.

L'évolution temporelle du déplacement hors du plan du nœud A est présentée à la Fig. 8. La solution de référence a été obtenue avec un total de 20 éléments de poutre (10 éléments par tronçon), tandis que les résultats des trois formulations ont été obtenus en utilisant seulement 4 éléments (2 éléments par tronçon). Les calculs ont été réalisés avec $\Delta t = 0.25$ s. Avec seulement 4 éléments de poutre, l'approche corotationnelle cubique fournit quasi les mêmes résultats que la solution de référence. Les résultats obtenus avec l'approche corotationnelle linéaire sont assez proches de la solution de référence. Cependant, les résultats obtenus avec la formulation de Simo et Vu-Quoc sont assez éloignés de la solution de référence, ce qui est évidemment dû à la nature linéaire de l'interpolation.

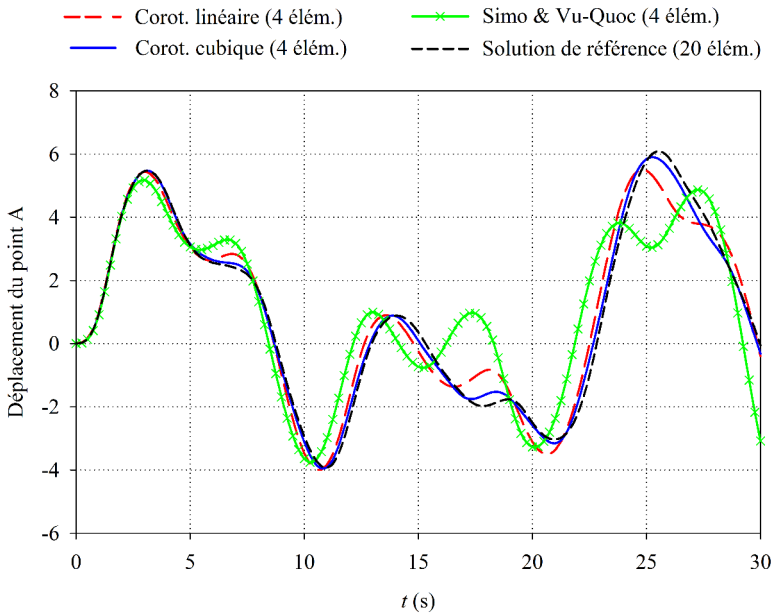

Fig. 8. Évolution temporelle du déplacement hors du plan du point A.

Les temps de calcul et le nombre total d'itérations requises pour chaque formulation sont donnés au tableau 5. Avec le même nombre d'éléments, l'approche corotationnelle linéaire est la plus rapide et la méthode corotationnelle cubique est la plus lente. Ce résultat est cohérent car plusieurs termes d'inertie disparaissent lorsque les interpolations locales sont linéaires. En outre, dans l'approche corotationnelle linéaire, le vecteur force d'inertie et la matrice d'inertie tangente ont été intégrés en utilisant deux points de Gauss, tandis que trois points de Gauss ont été nécessaires pour la formulation corotationnelle cubique.

Table 5. Temps de calcul (nombre total d'itérations).

Nombre d'élément	Corot. linéaire	Corot. cubique	Simo & Vu-Quoc
4	3.66 (633)	5.31 (637)	4.59 (521)
20	19.84 (636)	25.61 (612)	22.90 (517)

Cet exemple montre qu'avec un maillage grossier, les formulation de Simo et Vu-Quoc à deux nœuds et la formulation corotationnelle linéaire donnent des résultats moins précis que l'approche corotationnelle cubique. Cela démontre l'importance d'une description précise des déformations dans les termes dynamiques, ce qui n'est pas possible avec des interpolations linéaires. Avec un maillage fin, toutes les formulations donnent les mêmes résultats.

5 Élément de poutre corotationnel avec une section transversale à paroi mince

Dans la littérature, plusieurs formulations de poutre 3D ont été proposées pour l'analyse dynamique non-linéaire des structures flexibles [4, 9–11, 13–18, 21–23, 25–29, 31, 33, 35–37, 39, 47–50]. Toutefois, le nombre de formulations qui traitent de la dynamique non-linéaire des poutres avec des sections à parois minces est très limité [22].

Dans [34], une nouvelle formulation dynamique pour l'analyse non-linéaire des poutres avec des sections à parois minces a été proposée. En fait, cette nouvelle formulation est l'extension de celle développée

dans [33] en prenant en compte les déformations de gauchissement et l'excentricité du centre de cisaillement. Par conséquent, la méthode corotationnelle a été utilisée pour dériver à la fois les termes internes et d'inertie. Pour une description cinématique locale, l'interpolation linéaire a été adoptée pour le déplacement axial, alors qu'une interpolation cubique a été utilisée pour les déplacements transversaux et la rotation axiale.

Afin d'introduire les déformations de gauchissement, la description cinématique proposée par Gruttmann et al. [20] a été adoptée. Par conséquent, l'élément de poutre possède sept degrés de liberté à chaque nœud. Il est important de souligner que la cinématique adoptée génère plusieurs termes supplémentaires dans les expressions des vecteurs de force d'inertie et la matrice d'inertie tangente. Les contributions de ces termes au comportement dynamique non-linéaire ont ensuite été étudiés sur base d'exemples numériques. En ce qui concerne les termes de déformation statiques, c-à-d le vecteur force interne et la matrice de rigidité tangente, l'élément de poutre corotationnel développé par Battini et Pacoste [8] a été adopté. Toutefois, afin d'introduire les déformations de cisaillement de flexion, les fonctions d'Hermite cubiques ont été modifiées comme suggéré dans la formulation d'Interdepent Interpolation Element (IIE) [43]. Quatre exemples numériques ont été analysés pour évaluer la précision de la nouvelle formulation en comparant les résultats qu'elle fournit à ceux obtenus à l'aide d'un modèle EF volumique (Abaqus).

5.1 Énergie cinétique

La description cinématique proposée par Gruttmann et al. [20] est adoptée et brièvement présentée (voir Fig. 9). Une poutre avec une section transversale arbitraire est considérée. G et C sont le centre de gravité et

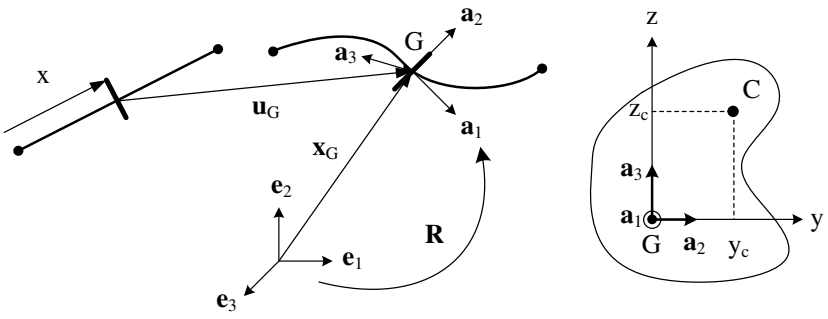

Fig. 9. Configurations initiale et actuelle de la poutre

le centre de cisaillement de la section transversale. $\mathbf{e}_i$ et $\mathbf{a}_i$ $(i = 1,2,3)$ désignent respectivement le système de coordonnées globales et le système de coordonnées attachées à la section. La relation qui lie les deux systèmes de coordonnées est définie par:

$$\mathbf{a}_i = \mathbf{R}\,\mathbf{e}_i\,. \tag{33}$$

La position d'un point arbitraire P dans la configuration actuelle, $\mathbf{x}_P(x,y,z)$, est donnée par

$$\mathbf{x}_P(x,y,z) = \mathbf{x}_G(x) + y\,\mathbf{a}_2(x) + z\,\mathbf{a}_3(x) + \alpha(x)\,\overline{\omega}(y,z)\,\mathbf{a}_1(x)\,, \tag{34}$$

avec $\mathbf{x}_G$ désignant le vecteur position de G dans la configuration actuelle.
La fonction de gauchissement $\overline{\omega}(y,z)$ est définie par la théorie de la torsion de Saint-Venant et se réfère au centre de gravité G.

En prenant la dérivée temporelle de l'expression ci-dessus, on obtient la composante de la vitesse du point P:

$$\dot{\mathbf{u}}_P = \dot{\mathbf{u}}_G + \mathbf{R}\,(-\widetilde{\mathbf{X}}\,\dot{\boldsymbol{\omega}} - \alpha\,\widetilde{\mathbf{n}_{\overline{\omega}}}\,\dot{\boldsymbol{\omega}} + \dot{\alpha}\,\mathbf{n}_{\overline{\omega}})\,, \tag{35}$$

avec $\mathbf{X} = [0 \ y \ z]^{\mathrm{T}}$ et $\mathbf{n}_{\overline{\omega}} = [\overline{\omega} \ 0 \ 0]^{\mathrm{T}}$.

L'énergie cinétique de la poutre est alors calculée à l'aide de:

$$K = \frac{1}{2} \int_V \rho \ \dot{\mathbf{u}}_{\mathrm{P}}^{\mathrm{T}} \ \dot{\mathbf{u}}_{\mathrm{P}} \ \mathrm{d}V \,. \tag{36}$$

Après quelques calculs, la forme spatiale de l'énergie cinétique est obtenue comme suit:

$$K = \frac{1}{2} \int_{l_o} \left[\dot{\mathbf{u}}_{\mathrm{G}}^{\mathrm{T}} A_\rho \, \dot{\mathbf{u}}_{\mathrm{G}} + \dot{\mathbf{w}}^{\mathrm{T}} \mathbf{I}_\rho \, \dot{\mathbf{w}} \right] \mathrm{d}l + \frac{1}{2} \int_{l_o} \left[\dot{\mathbf{w}}^{\mathrm{T}} \mathbf{I}_\alpha \, \dot{\mathbf{w}} - 2 \, \dot{\mathbf{w}}^{\mathrm{T}} \mathbf{I}_b \, \dot{\alpha} + J_{\overline{\omega}} \, \dot{\alpha}^2 \right] \mathrm{d}l, \tag{37}$$

où $\mathbf{I}_\rho, \mathbf{I}_{\overline{\omega}}, \mathbf{I}_a, \mathbf{I}_b, \mathbf{I}_\alpha, J_{\overline{\omega}}$ sont les moments d'inertie de la section.

En comparant Eq. (37) avec l'énergie cinétique d'une poutre avec une section transversale solide, il apparait que la seconde intégrale dans Eq. (37) est l'énergie cinétique supplémentaire dûe aux déformations de gauchissement et à l'excentricité du centre de cisaillement par rapport au centre de gravité.

Après plusieurs calculs analytiques [34], la variation de l'énergie cinétique est obtenue comme suit:

$$\delta K = - \int_{l_o} \left\{ \delta \mathbf{u}_{\mathrm{G}}{}^{\mathrm{T}} A_\rho \ddot{\mathbf{u}}_{\mathrm{G}} + \delta \mathbf{w}^{w\mathrm{T}} \left[\mathbf{I}_\rho^1 \ddot{\mathbf{w}}^w + \mathbf{I}_\rho^2 \dot{\mathbf{w}}^w \right] \right\} \mathrm{d}l \,, \tag{38}$$

avec

$$\delta \mathbf{w}^w = \begin{bmatrix} \delta \mathbf{w} \\ \\ \delta \alpha \end{bmatrix}, \quad \dot{\mathbf{w}}^w = \begin{bmatrix} \dot{\mathbf{w}} \\ \\ \dot{\alpha} \end{bmatrix}, \quad \ddot{\mathbf{w}}^w = \begin{bmatrix} \ddot{\mathbf{w}} \\ \\ \ddot{\alpha} \end{bmatrix}, \tag{39}$$

$$\mathbf{I}_\rho^1 = \begin{bmatrix} (\mathbf{I}_\rho + \mathbf{I}_\alpha) & -\mathbf{I}_b \\ \\ -\mathbf{I}_b^{\mathrm{T}} & J_{\overline{\omega}} \end{bmatrix}, \quad \mathbf{I}_\rho^2 = \begin{bmatrix} \widetilde{\dot{\mathbf{w}}} \, (\mathbf{I}_\rho + \mathbf{I}_\alpha) & \mathbf{I}_c \, \dot{\mathbf{w}} \\ \\ -\dot{\mathbf{w}}^{\mathrm{T}} \, \mathbf{I}_\alpha{}' & 0 \end{bmatrix}. \tag{40}$$

5.2 Cinématique de poutre

La cinématique de poutre corotationnelle, adoptée ici, est similaire à celle donnée dans la section 4.1. La seule différence est que, pour tenir compte des effets de gauchissement, un degré de liberté supplémentaire (gauchissement) $\alpha_i \ (i = 1,2)$ est introduit à chaque nœuds de l'élément. Le vecteur déplacement local devient ainsi:

$$\mathbf{d}_l^w = \left[\overline{u} \ \overline{\boldsymbol{\theta}}_1^{\mathrm{T}} \ \overline{\boldsymbol{\theta}}_2^{\mathrm{T}} \ \alpha_1 \ \alpha_2 \right]^{\mathrm{T}}. \tag{41}$$

Cependant, puisque le gauchissement est en soi une quantité de déformation, ces degrés de liberté supplémentaires restent constants au cours des changements des systèmes de coordonnées. Ainsi, la variation $\delta \mathbf{d}_g$ est réécrite comme suit:

$$\delta \mathbf{d}_g^w = \left[\delta \mathbf{u}_1^{g\mathrm{T}} \ \delta \mathbf{w}_1^{g\mathrm{T}} \ \delta \mathbf{u}_2^{g\mathrm{T}} \ \delta \mathbf{w}_2^{g\mathrm{T}} \ \delta \alpha_1 \ \delta \alpha_2 \right]^{\mathrm{T}}. \tag{42}$$

5.3 Vecteur force interne et matrice de rigidité tangente

En égalant le travail interne virtuel dans les deux systèmes global et local, l'expression du vecteur force interne global $\mathbf{f}_g^w$ est obtenue à l'aide de:

$$\mathbf{f}_g^w = \mathbf{B}^{w\mathrm{T}} \mathbf{f}_l^w \,. \tag{43}$$

En prenant les variations de Eq. (43), l'expression de la matrice de rigidité globale tangente $\mathbf{K}_g$ est obtenue

$$\mathbf{K}_g^w = \mathbf{B}^{w\mathrm{T}} \mathbf{K}_l^w \mathbf{B}^w + \left. \frac{\partial (\mathbf{B}^{w\mathrm{T}} \mathbf{f}_l^w)}{\partial \mathbf{d}_g^w} \right|_{\mathbf{f}_l^w} . \tag{44}$$

Les expressions du vecteur force interne local $\mathbf{f}_l^w$ et de la matrice de rigidité tangente locale $\mathbf{K}_l^w$ associée à $\delta \mathbf{d}_l^w$ sont établies en utilisant les fonctions de forme cubiques et la théorie de poutre en arc à profondeur faible. Toutefois, afin de tenir compte des déformations de cisaillement de flexion, les fonctions de forme d'Hermite pour les déplacements transversaux sont légèrement modifiées comme suggéré dans la formulation d'Interdependent Interpolation Element (IIE) [43]. De plus, l'hypothèse de Vlasov est adoptée et les termes non-linéaires dans l'expression des courbures sont négligés. Une non-linéarité géométrique d'ordre réduit est introduite grâce à une description de poutre en arc à profondeur faible et le terme de Wagner. Les codes de Maple pour $\mathbf{f}_l^w$ et $\mathbf{K}_l^w$ sont donnés dans [34].

5.4 Vecteur force d'inertie et matrice d'inertie tangente

En utilisant l'expression de la variation de l'énergie cinétique donnée par Eq.(38), l'expression du vecteur force d'inertie est obtenue à partir de la relation suivante:

$$\delta K = -\mathbf{f}_k^{w\mathrm{T}} \delta \mathbf{d}_g^w . \tag{45}$$

À l'aide des relations géométriques et des interpolations cubiques locales, les variations $\delta \mathbf{u}$ and $\delta \mathbf{w}^w$ sont calculées à partir du vecteur des déplacements nodaux globaux $\mathbf{d}_g^w$. En utilisant la même approximation que celle donnée par Eq.(28), nous obtenons l'expression du vecteur force d'inertie:

$$\mathbf{f}_k^w = \mathbf{E}^w \left\{ \begin{bmatrix} \int_{l_o} \mathbf{H}_1^{\mathrm{T}} \mathbf{R}_r^{\mathrm{T}} A_\rho \ddot{\mathbf{u}} \mathrm{d}l \\ \mathbf{0} \end{bmatrix} + \int_{l_o} \mathbf{H}_2^{w\mathrm{T}} \mathbf{R}_r^{w\mathrm{T}} \left[\mathbf{I}_\rho^1 \ddot{\mathbf{w}}^w + \mathbf{I}_\rho^2 \dot{\mathbf{w}}^w \right] \mathrm{d}l \right\} . \tag{46}$$

Seuls deux termes de l'expression du vecteur force d'inertie linéarisée sont retenus pour la procédure itérative:

$$\Delta \mathbf{f}_k^w \approx \mathbf{M} \Delta \ddot{\mathbf{d}}_g^w + \mathbf{C}_k \Delta \dot{\mathbf{d}}_g^w . \tag{47}$$

L'expression de la matrice de masse $\mathbf{M}$ est:

$$\begin{aligned} \mathbf{M} &= \mathbf{E}^w \left\{ \begin{bmatrix} \int_{l_o} \mathbf{H}_1^{\mathrm{T}} A_\rho \mathbf{H}_1 \, \mathrm{d}l & \mathbf{0} \\ \mathbf{0} & \mathbf{0} \end{bmatrix} + \int_{l_o} \mathbf{H}_2^{w\mathrm{T}} \mathbf{R}_r^{w\mathrm{T}} \mathbf{I}_\rho^1 \mathbf{R}_r^w \mathbf{H}_2^w \mathrm{d}l \right\} \mathbf{E}^{w\mathrm{T}} \\ &= \mathbf{E}^w \mathbf{M}^e \mathbf{E}^{w\mathrm{T}} . \end{aligned} \tag{48}$$

et la matrice gyroscopique $\mathbf{C}_k$ est calculée à l'aide de:

$$\begin{aligned} \mathbf{C}_k =& \mathbf{E}^w \left\{ \begin{bmatrix} \int_{l_o} \mathbf{H}_1^{\mathrm{T}} A_\rho \, (\mathbf{C}_1 + \mathbf{C}_3) \, \mathrm{d}l & \mathbf{0} \\ \mathbf{0} & \mathbf{0} \end{bmatrix} + \int_{l_o} \mathbf{H}_2^{w\mathrm{T}} \mathbf{R}_r^{w\mathrm{T}} \mathbf{I}_\rho^1 \mathbf{R}_r^w \, (\mathbf{C}_2 + \mathbf{C}_4) \, \mathrm{d}l \right. \\ &\left. + \int_{l_o} \mathbf{H}_2^{w\mathrm{T}} \mathbf{R}_r^{w\mathrm{T}} \left(\mathbf{I}_\rho^2 + \mathbf{I}_\rho^3 \right) \mathbf{R}_r^w \mathbf{H}_2^w \mathrm{d}l \right\} \mathbf{E}^{w\mathrm{T}} = \mathbf{E}^w \mathbf{C}_k^e \mathbf{E}^{w\mathrm{T}} , \end{aligned} \tag{49}$$

où

$$\mathbf{I}_{\rho}^{3} = \begin{bmatrix} \widetilde{(\mathbf{I}_{\rho} + \mathbf{I}_{\alpha})}\dot{\mathbf{w}} + \mathbf{I}_{c}\,\dot{\alpha} & \mathbf{0} \\ -\dot{\mathbf{w}}^{\mathrm{T}}\,\mathbf{I}_{\alpha}^{\prime\mathrm{T}} & 0 \end{bmatrix}. \tag{50}$$

Le gauchissement et l'excentricité du centre de cisaillement ont été pris en compte dans l'établissement des termes d'inertie, voir Eq. (35). En conséquence, plusieurs termes supplémentaires ont été introduits dans les expressions du vecteur force d'inertie et des matrices de masse et gyroscopique. L'importance de ces termes ont été discutés dans [34] à travers plusieurs exemples numériques. Il a été constaté que les déformations de gauchissement apparaissant dans les termes dynamiques ont une contribution négligeable sur les résultats numériques et pourraient être omises. Ceci est fait en considérant $I_{\omega} = 0$.

L'excentricité du centre de cisaillement par rapport au centre de gravité génère des termes dynamiques supplémentaires dont l'importance a également été étudiée. Il est apparu que pour des poutres minces, ces termes n'ont pas d'incidence sur les résultats et peuvent être donc négligés. Toutefois, ces derniers peuvent avoir une influence significative pour les poutres courtes.

Si $I_{\omega} = y_c = z_c = 0$ est adoptée, l'expression du vecteur force d'inertie dans Eq. (46) peut être simplifiée comme suit:

$$\mathbf{f}_{k}^{w} = \mathbf{E}^{w} \left\{ \begin{bmatrix} \int_{l_o} \mathbf{H}_{1}^{\mathrm{T}}\,\mathbf{R}_{r}^{\mathrm{T}}\,A_{\rho}\ddot{\mathbf{u}}\mathrm{d}l \\ \mathbf{0} \end{bmatrix} + \int_{l_o} \mathbf{H}_{2}^{\mathrm{T}}\,\mathbf{R}_{r}^{\mathrm{T}} \left[\mathbf{I}_{\rho}\ddot{\mathbf{w}} + \widetilde{\dot{\mathbf{w}}}\mathbf{I}_{\rho}\dot{\mathbf{w}} \right] \mathrm{d}l \right\}. \tag{51}$$

Des simplifications similaires peuvent également s'appliquer aux expressions des matrices de masse et gyroscopique.

5.5 Exemple numérique

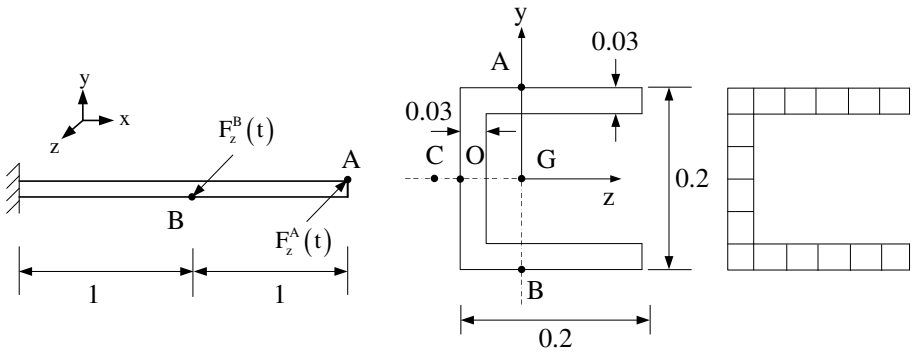

Fig. 10. Données géométriques.

Une poutre console avec une section transversale en U (voir Fig. 10) a été analysée. L'excentricité du centre de cisaillement est donnée par $z_c = -0.138$ m.

La poutre est soumise à deux forces concentrées hors du plan, l'une au milieu et l'autre à l'extrémité droite. La force appliquée au point A est $F_z^{\mathrm{A}} = -4F$. La force appliquée au point B est $F_z^{\mathrm{B}} = 2F$. L'évolution temporelle de F est donnée à la Fig. 11. L'objectif de cet exemple n'est pas seulement d'évaluer la performance de la nouvelle formulation, mais aussi de mettre en évidence l'influence de l'excentricité du centre de cisaillement sur le comportement dynamique de la poutre. En fait, pour les deux premiers exemples

dans [34], celui-ci n'a pas d'incidence sur les résultats numériques et pouvait être négligé en remplaçant $y_c = z_c = 0$ dans Eqs. (46), (48) et (49). Le présent exemple montre que la contribution de l'excentricité du centre de cisaillement est importante.

Les propriétés du matériau suivantes ont été utilisées: $E = 210$ GPa, $\nu = 0,33$ et $\rho = 7850$ kg/m^3. Toutes les dimensions données à la Fig. 10 sont en mètre.

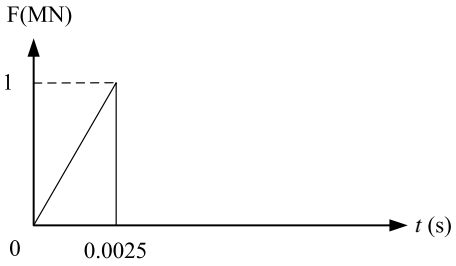

Fig. 11. Chargement.

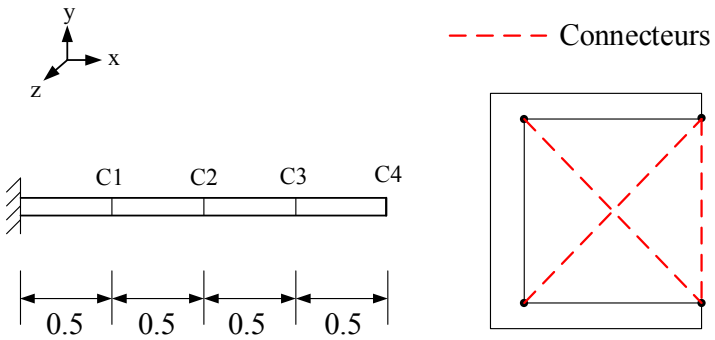

Fig. 12. Connecteurs dans le modèle volumique 3D.

Deux modèles différents de poutre corotationnels avec 40 éléments ont été utilisés. Dans le premier, les déformations de gauchissement et l'excentricité du centre de cisaillement ont été prises en compte dans les termes d'inertie tandis que dans le second, ils ont été négligées.

Les résultats sont comparés à un modèle éléments finis volumiques Abaqus. La poutre est maillée à l'aide de $(6+4+6)\cdot 60 = 960$ éléments isoparamétriques à 20 nœuds. Pour le modèle volumique 3D, quatre connecteurs ont été ajoutés le long de la poutre au niveau des sections C1-C4 (voir Fig.12) afin d'éviter des déformations dans le plan des semelles (hypothèse de section rigide dans son plan). Le connecteur entre 2 nœuds a maintenu la distance entre ces nœuds lors de l'analyse.

Toutes les analyses ont été réalisées avec un pas de temps $\Delta t = 5 \cdot 10^{-5}$ s. L'évolution temporelle des déplacements du point O à l'extrémité droite est présentée à la Fig. 13. Un très bon accord entre l'élément de poutre corotationnel et l'analyse solide 3D de l'Abaqus a été obtenu. Cependant, quand $I_\omega = z_c = 0$, des écarts importants entre les deux modèles sont observés.

Cet exemple montre que le nouvel élément peut être utilisé pour analyser le comportement dynamique non-linéaire des poutres avec des sections arbitraires et que les termes dynamiques supplémentaires dûs

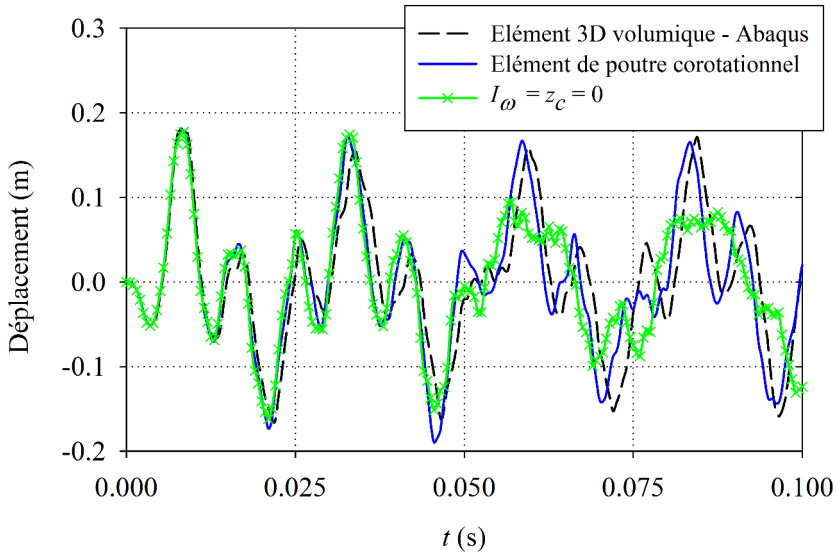

Fig. 13. Évolution temporelle du déplacement u_y du point O.

à l'excentricité du centre de cisaillement ne peuvent pas toujours être négligés. Dans certains cas, les résultats numériques semblent être améliorés si l'excentricité du centre de cisaillement est prise en compte.

6 Conclusions

L'objectif principal de cette recherche a été de développer des formulations de poutre efficaces pour la dynamique non-linéaire des structures flexibles en utilisant la méthode corotationnelle. Plusieurs formulations de poutre 2D et 3D (section pleine et section arbitraire à parois minces) ont été proposées et testées.

Formulation de poutre 2D

Une formulation de poutre corotationnelle cohérente a été proposée pour l'analyse dynamique non-linéaire en 2D. La même description cinématique corotationnelle a été adoptée pour toutes les deux parties statiques et dynamiques. Par ailleurs, afin de tenir compte de l'effet d'inertie dû aux déplacements transversaux locaux, les interpolations cubiques locales étaient non seulement adoptées pour développer les expressions des termes élastiques, mais aussi pour établir les termes d'inertie.

Cette nouvelle formulation a été comparée avec deux formulations classiques dans lesquelles la matrice de masse de Timoshenko et la matrices de masse diagonale sont utilisées. Plusieurs exemples numériques ont montré que la nouvelle formulation est plus efficace que les deux formulations classiques. En effet, tous les résultats ont indiqué que la nouvelle formulation a consommé plus de temps de calcul, mais permet de réduire significativement le nombre d'éléments. Cet avantage est dû à une meilleure représentation des déplacements locaux dans les termes d'inertie.

Grandes rotations en dynamique

La matrice de rotation, le vecteur de rotation incrémental et les paramètres d'Euler incrémentaux ont été adoptées pour paramétrer les grandes rotations. Quatre formulations dynamiques basées sur ces paramé-

trages ont été comparées. Les trois premières formulations ont été prises dans la littérature [11, 25, 47]. La dernière était originale. Dans ces formulations, la méthode corotationnelle a été utilisée pour développer les expressions des forces internes et les matrices de rigidité tangentes, tandis que les termes dynamiques ont été formulées dans un contexte lagrangien total. Les points communs et les différences entre les formulations ont été mis en évidence. De nombreux exemples numériques ont été analysés afin d'évaluer la précision numérique et l'efficacité des formulations. De plus, plusieurs prédicteurs pour la procédure itérative et diverses possibilités de simplifier la matrice d'inertie tangente ont été testés.

Les résultats numériques ont montré que:

- Pour la programmation, la nouvelle formulation et celle proposée par Cardona et Geradin [11] étaient les plus simples. La méthode de Newmark classique est utilisée à la fois pour les translations et les rotations. Aucune quantités supplémentaires doivent être sauvegardées à chaque point de Gauss.
- Pour toutes les formulations, le prédicteur proposé par Crisfield dans [12] et ensuite développé par l'auteur [31] est le plus efficace.
- Pour chaque formulation, le choix de la matrice d'inertie tangente a significativement affecté l'efficacité de calcul. Pour les deux premières formulations, le meilleur choix est d'adopter la matrice d'inertie tangente exacte. Pour les deux dernières, il valait mieux ne prendre que les matrices de masse et gyroscopique.
- Toutes les formulations ont donné les mêmes résultats numériques, mais la formulation proposée a été légèrement plus efficace que les autres au niveau du temps de calcul.

Formulation de poutre 3D avec une section transversale solide

Un élément de poutre corotationnel 3D cohérent pour la dynamique non-linéaire des structures flexibles a été présenté. En comparaison avec les autres formulations trouvées dans la littérature, la nouveauté de la formulation est que la cinématique corotationnelle est utilisée pour établir tous de l'équation de la dynamique. En outre, les fonctions d'interpolation cubique locales ont été utilisées. Le vecteur force d'inertie et la matrice d'inertie tangente ont été obtenus grâce à l'introduction d'une approximation des rotations locales. Pour améliorer l'efficacité de la procédure itérative, une matrice d'inertie tangente approximative a été adoptée.

Quatre exemples numériques ont été considérés pour comparer la nouvelle formulation par rapport aux deux autres approches. La première approche, appelée "approche corotationnelle linéaire", découle de la nouvelle formulation en remplaçant, dans les termes d'inertie, les interpolations cubiques par des interpolations linéaires. La deuxième approche est une formulation lagrangienne totale proposée par Simo et Vu-Quoc [45–47]. Cette approche peut être mise en œuvre avec différents nombres de nœuds. Afin d'assurer une comparaison valable des formulations, l'approche de Simo et Vu-Quoc a été implémentée avec deux nœuds, ce qui corresponds à une interpolation linéaire pour toutes les variables globales.

Sur base de l'analyse de ces exemples, les conclusions suivantes peuvent être tirées

- Toutes les formulations ont donné les mêmes résultats avec un maillage fin.
- Comme prévu, avec un maillage grossier, la formulation à deux nœuds de Simo et Vu-Quoc et la formulation corotationnelle linéaire ont donné des résultats moins précis comparés à ceux obtenus avec l'approche corotationnelle cubique. Ceci a démontré l'importance d'une description précise des déformations locales dans les termes dynamiques, ce qui n'était pas possible avec des interpolations linéaires.
- L'approche corotationnelle linéaire est plus rapide que l'approche corotationnelle cubique. Ce résultat était attendu parce que plusieurs termes d'inertie disparaissent lorsque l'on adopte des interpolations linéaires locales ont été adoptées. En outre, dans l'approche corotationnelle linéaire, le vecteur force d'inertie et la matrice d'inertie tangente ont été intégrés en utilisant deux points de Gauss, tandis que

pour les termes dynamiques de la formulation corotationnelle cubique, trois points de Gauss ont été utilisés.

- La formulation corotationnelle cubique est un peu plus lent que les formulations linéaires (environ 12 %).

On peut conclure que la nouvelle formulation corotationnelle dynamique basée sur les interpolations cubiques locales a des résultats avec une précision suffisante pour un nombre d'éléments relativement faible par rapport aux formulations linéaires.

Formulation de poutre 3D avec une section transversale à paroi mince

Une formulation corotationnelle pour l'analyse dynamique non-linéaire des poutres avec des sections arbitraires à parois minces a été développée. Cette formulation est une extension de celle proposée dans [33]. L'élément a sept degrés de liberté à chaque nœud. De plus, les fonctions de forme cubiques ont été utilisées pour interpoler les déplacements transversaux locaux et les rotations axiales.

Le gauchissement et l'excentricité du centre de cisaillement ont été pris en compte dans le calcul des termes dynamiques. Cela a introduit des termes supplémentaires dans les expressions du vecteur force d'inertie et des matrices de masse et gyroscopique.

Quatre problèmes de poutre 3D, avec différentes sections à parois minces et conditions de chargement, ont été analysés. Les prédictions de la formulation proposée ont été comparées aux résultats numériques obtenus avec les éléments de poutre (Abaqus) et un modèle d'élément fini volumique (Abaqus). Pour tous les exemples, on a obtenu un très bon accord entre les résultats obtenus avec l'élément de poutre corotationnel et le modèle d'élément fini volumique. Par ailleurs, les résultats numériques ont également montré que les déformations de gauchissement ont eu une influence négligeable sur les termes dynamiques et peuvent être omises. Toutefois, les termes dynamiques supplémentaires dus à l'excentricité du centre de cisaillement ne peuvent pas toujours être négligés. En fait, il semble que pour les poutres minces, les mêmes résultats numériques ont été obtenus avec ou sans ces termes. Toutefois, pour les poutres courtes, les résultats numériques semblent être améliorés si l'excentricité du centre de cisaillement est prise en compte.

References

[1] R. Alsafadie, J.-M. Battini, M. Hjiaj, and H. Somja. A comparative study of displacement and mixed-based corotational finite element formulations for elasto-plastic three-dimensional beam analysis. *Engerg. Computs*, 28:939–982, 2011.

[2] R. Alsafadie, M. Hjiaj, and J.-M. Battini. Corotational mixed finite element formulation for thin-walled beams with generic cross-section. *Comput. Methods Appl. Mech. Engrg.*, 199:3197–3212, 2010.

[3] J. Argyris. An excursion into large rotations. *Comput. Methods Appl. Mech. Engrg.*, 32:85–155, 1982.

[4] K.J. Bathe, E. Ramm, and E.L. Wilson. Finite element formulations for large deformation dynamic analysis. *Int. J. Num. Methods. Engrg.*, 9:353–386, 1975.

[5] J.-M. Battini. *Co-rotational beam elements in instability problems*. Phd thesis, KTH Royal Institute of Technology, Stockholm, SWEDEN, 2002.

[6] J.-M. Battini. A modified corotational framework for triangular shell elements. *Comput. Methods Appl. Mech. Engrg.*, 196:1905–1914, 2007.

[7] J.-M. Battini. Large rotations and nodal moments in corotational elements. *CMES*, 33(1):1–15, 2008.

[8] J.-M. Battini and C. Pacoste. Co-rotational beam elements with warping effects in instability problems. *Comput. Methods Appl. Mech. Engrg.*, 191:1755–1789, 2002.

[9] K. Behdinan, M.C. Stylianou, and B. Tabarrok. Co-rotational dynamic analysis of flexible beams. *Comput. Methods Appl. Mech. Engrg.*, 154:151–161, 1998.
[10] P. Betsch and P. Steinmann. Constrained dynamics of geometrically exact beams. *Comput. Mech.*, 31:49–59, 2003.
[11] A. Cardano and M. Geradin. A beam finite element non-linear theory with finite rotations. *Int. J. Num. Methods. Engrg.*, 26:2403–2438, 1988.
[12] M.A. Crisfield. *Non-Linear Finite Element Analysis of Solids and Structures: Advanced Topics*. John Wiley & Sons, Inc., New York, NY, USA, 1st edition, 1997.
[13] M.A. Crisfield, U. Galvanetto, and G. Jelenić. Dynamics of 3-d co-rotational beams. *Comput. Mech.*, 20:507–519, 1997.
[14] M.A. Crisfield and G.F. Moita. A unified co-rotational framework for solids shells and beams. *Int. J. Solids Struct.*, 33:2969–2992, 1996.
[15] M.A. Crisfield and J. Shi. An energy conserving co-rotational procedure for non-linear dynamics with finite elements. *Nonlinear Dynamics*, 9:37–52, 1996.
[16] H.A. Elkaranshawy and M.A. Dokainish. Corotational finite element analysis of planar flexible multibody systems. *Comput. Struct.*, 54(5):881–890, 1995.
[17] U. Galvanetto and M.A. Crisfield. An energy conserving co-rotational procedure for dynamics of planar beam structures. *Int. J. Num. Methods. Engrg.*, 39:2265–2282, 1996.
[18] M. Geradin and A. Cardona. Kinematics and dynamics of rigid and flexible mechanisms using finite elements and quaternion algebra. *Comput. Mech.*, 4:115–135, 1989.
[19] M. Geradin and A. Cardona. *Flexible multibody dynamics: a finite element approach*. John Wiley, 2001.
[20] R. Gruttmann, R. Sauer, and R. Wagner. Theory and numerics of three-dimensional beams with elastoplastic behavior. *Int. J. Num. Meth. Engng.*, 48:1675–1702, 2000.
[21] K.M. Hsiao, J.Y. Lin, and W.Y. Lin. A consistent co-rotational finite element formulation for geometrically nonlinear dynamic analysis of 3-d beams. *Comput. Methods Appl. Mech. Engrg*, 169:1–18, 1999.
[22] K.M. Hsiao, W.Y. Lin, and R.H. Chen. Geometrically non-linear dynamic analysis of thin-walled beams. *Proc. World Congress Engrg.*, II, 2009.
[23] K.M. Hsiao and R.T. Yang. A co-rotational formulation for nonlinear dynamic analysis of curved euler beam. *Comput. Struct.*, 54(6):1091–1097, 1995.
[24] A. Ibrahimbegović. On the choice of finite rotation parameters. *Comput. Methods Appl. Mech. Engrg.*, 149:49–71, 1997.
[25] A. Ibrahimbegović and M.A. Mikdad. Finite rotations in dynamics of beams and implicit time-stepping schemes. *Int. J. Num. Methods. Engrg.*, 41:781–814, 1998.
[26] M. Iura and S.N. Atluri. Dynamic analysis of finitely stretched and rotated three-dimensional space-curved beams. *Comput. Struct.*, 29:875–889, 1988.
[27] M. Iura and S.N. Atluri. Dynamic analysis of planar flexible beams with finite rotations by using inertial and rotating frames. *Comput. Struct.*, 55(3):453–462, 1995.
[28] G. Jelenić and M.A. Crisfield. Interpolation of rotational variables in nonlinear dynamics of 3d beams. *Int. J. Num. Methods. Engrg.*, 43:1193–1222, 1998.
[29] G. Jelenić and M.A. Crisfield. Geometrically exact 3d beam theory: implementation of a strain-invariant element for stactics and dynamics. *Comput. Methods Appl. Mech. Engrg.*, 171:141–171, 1999.
[30] S. Krenk. *Non-linear modeling and analysis of solids and structures*. Cambridge University Press, 2009.
[31] T.-N. Le, J.-M. Battini, and M. Hjiaj. Efficient formulation for dynamics of corotational 2d beams. *Comput. Mech.*, 48(2):153–161, 2011.
[32] T.-N. Le, J.-M. Battini, and M. Hjiaj. Dynamics of 3d beam elements in a corotational context: A comparative study of established and new formulations. *Finite Elem. Anal. Des.*, 61:97–111, 2012.
[33] T.-N. Le, J.-M. Battini, and M. Hjiaj. A consistent 3d corotational beam element for nonlinear dynamic analysis of flexible structures. *Comput. Methods Appl. Mech. Engrg.*, accepted, 2013.
[34] T.-N. Le, J.-M. Battini, and M. Hjiaj. Corotational formulation for nonlinear dynamics of beams with

arbitrary thin-walled cross-sections. *Comput. Struct.*, accepted, 2013.

[35] E.V. Lens and A. Cardona. A nonlinear beam element formulation in the framework of an energy preserving time integration scheme for constrained multibody systems dynamics. *Comput. Struct.*, 86:47–63, 2008.

[36] J. Mäkinen. Total lagrangian reissner's geometrically exact beam element without singularities. *Int. J. Num. Methods. Engrg.*, 70:1009–1048, 2007.

[37] N. Masuda, T. Nishiwaki, and M. Minaaawa. Nonlinear dynamic analysis of frame structures. *Comput. Struct.*, 27(1):103–110, 1987.

[38] B. Nour-Omid and C.C. Rankin. Finite rotation analysis and consistent linearization using projectors. *Comput. Methods Appl. Mech. Engrg.*, 93:353–384, 1991.

[39] C. Oran and A. Kassimali. Large deformations of framed structures under static and dynamic loads. *Comput. Struct.*, 6:539–547, 1976.

[40] C. Pacoste. Corotational flat facet triangular elements for shell instability analysis. *Comput. Methods Appl. Mech. Engrg.*, 156:75–110, 1998.

[41] C. Pacoste and A. Eriksson. Beam elements in instability problems. *Comput. Methods Appl. Mech. Engrg.*, 144:163–197, 1997.

[42] C.C. Rankin and B. Nour-Omid. The use of projectors to improve finite element performance. *Comput. Struct.*, 30:257–267, 1988.

[43] J.N. Reddy. On locking-free shear deformable beam finite elements. *Comput. Methods Appl. Mech. Engrg.*, 149:113–132, 1997.

[44] I. Sheinman. Dynamic large-displacement analysis of curved beams involving shear deformation. *Int. J. Solids Structures*, 16:1037–1049, 1980.

[45] J.C. Simo. A finite strain beam formulation. the three-dimensional dynamic problem. part i. *Comput. Methods Appl. Mech. Engrg.*, 49:55–70, 1985.

[46] J.C. Simo and L. Vu-Quoc. On the dynamics of flexible beams under large overall motions - the plane case: Part i. *J. Appl. Mech. ASME*, 53:849–863, 1986.

[47] J.C. Simo and L. Vu-Quoc. On the dynamics in space of rods undergoing large motions - a geometrically exact approach. *Comput. Methods Appl. Mech. Engrg.*, 66:125–161, 1988.

[48] Q. Xue and J.L. Meek. Dynamic response and instability of frame structures. *Comput. Methods Appl. Mech. Engrg.*, 190:5233–5242, 2001.

[49] E. Zupan, M. Saje, and D. Zupan. Quaternion-based dynamics of geometrically nonlinear spatial beams using the Runge – Kutta method. *Finite Elem. Anal. Des.*, 54:48–60, 2012.

[50] E. Zupan, M. Saje, and D. Zupan. Dynamics of spatial beams in quaternion description based on the newmark integration scheme. *Comput. Mech.*, 51:47–64, 2013.

INSA de RENNES
Service des Formations

AVIS DU JURY SUR LA REPRODUCTION DE LA THESE SOUTENUE

Titre de la thèse:
Nonlinear dynamics of flexible structures using corotational beam elements

Nom Prénom de l'auteur : LE THANH NAM

Membres du jury :
- Madame PANDOLFI Anna
- Monsieur KOUHIA Reijo
- Monsieur BATTINI Jean-Marc
- Monsieur ROMERO Ignacio
- Monsieur HJIAJ Mohammed
- Monsieur COMBESCURE Alain
- Monsieur STAINIER Laurent
- Monsieur IZZUDDIN Bassam

Président du jury : A COMBESCURE

Date de la soutenance : 18 Octobre 2013

Reproduction de la these soutenue

☒ Thèse pouvant être reproduite en l'état
☐ Thèse pouvant être reproduite après corrections suggérées

Fait à Rennes, le 18 Octobre 2013

Signature du président de jury

Le Directeur,

M'hamed DRISSI

Résumé

L'objectif de cette thèse est de proposer des éléments finis poutres corotationnels 2D et 3D pour l'analyse du comportement dynamique non-linéaire des structures à barres. La contribution majeure de cette thèse est l'utilisation de fonctions d'interpolations cubiques à la fois pour la détermination de l'expression des efforts internes mais aussi celle des termes d'inertie. En négligeant le carré du déplacement transversal dans le repère local, une expression analytique des termes dynamiques en 2D est obtenue. Sur base d'une étude comparative approfondie sur la paramétrisation des rotations et les algorithmes d'intégration temporelle et d'une approximation des rotations locales, nous proposons deux éléments finis poutre 3D précis et robustes. Contrairement au premier, le second élément 3D prend en compte les déformations de gauchissement et l'excentricité du centre de cisaillement. Les diverses comparaisons réalisées démontrent la pertinence des formulations proposées.

Abstract

The purpose of this thesis is to propose several corotational beam formulations for both 2D and 3D nonlinear dynamic analyse of flexible structures. The main novelty of these formulations is that the cubic interpolation functions are used to derive not only the internal force vector and the tangent stiffness matrix but also the inertial force vector and the dynamic matrix. By neglecting the quadratic terms of the local transversal displacements, closed-form expressions for the inertial terms are obtained for 2D problems. Based on an extensive comparative study of the parameterizations of the finite rotations and the time stepping method, and by adopting an approximation of the local rotations, two consistent and effective beam formulations for 3D dynamics are developed. In contrast with the first formulation, the second one takes into account the warping deformations and the shear center eccentricity. The accuracy of these formulations is demonstrated through several numerical examples.

N° d'ordre : 13ISAR 25 / D13 - 25

Institut National des Sciences Appliquées de Rennes
20, Avenue des Buttes de Coëmes • CS 70839 • F-35708 Rennes Cedex
Tel : 02 23 23 82 00 - Fax : 02 23 23 83 96